# Synthesis and characterization of polysaccharide-silica composite aerogels for thermal superinsulation.

Arnaud Demilecamps

HAL Id: tel-01279456

https://pastel.hal.science/tel-01279456

Submitted on 26 Feb 2016

École doctorale n° 364 : Sciences fondamentales et appliquées

# Doctorat ParisTech

# T H È S E

**pour obtenir le grade de docteur délivré par**

# l'École nationale supérieure des mines de Paris

**Spécialité " Science et génie des matériaux "**

*présentée et soutenue publiquement par*

## Arnaud DEMILECAMPS

le 7 juillet 2015

## Synthesis and characterization of polysaccharide-silica composite aerogels for thermal superinsulation

## Synthèse et caractérisation d'aérogels composites à base de polysaccharides et de silice pour la superisolation thermique

Directeurs de thèse :

**Tatiana Budtova**
**Arnaud Rigacci**

**Jury**

**Mme Irina Smirnova**, Professeur, Technische Universität Hamburg — Rapporteur

**Mme Sylvie Etienne-Calas**, Maître de Conférences – HDR, Université Montpellier — Rapporteur

**M. Herbert Sixta**, Professeur, Aalto University — Examinateur

**M. Matthias Koebel**, Docteur, Swiss Federal Laboratories for Materials Science and Technology — Examinateur

**M. Arnaud Rigacci**, Docteur HDR, PERSEE MinesParisTech — Examinateur

**Mme Tatiana Budtova**, Docteur HDR, CEMEF Mines ParisTech — Examinateur

T
H
È
S
E

# Remerciements

# Table of contents

# Abreviations List

wt%: weight percent

$\rho_{bulk}$ (g/cm$^3$): bulk density

$\rho_{skeletal}$ (g/cm$^3$): skeletal (or solid) density

$\varepsilon$ (%): porosity

$S_{BET}$ (m²/g): specific surface area

E (MPa): Young modulus

$\sigma_{yield}$ (MPa): yield stress

$\sigma^*$ (MPa): stress at break

$\varepsilon_{yield}$ (%): yield strain

$\varepsilon_d$ (%): densification strain

$\varepsilon^*$ (%) maximal strain at break

$W_{40\%}$ (kJ/m$^3$): absorbed energy from 0 to 40% strain

$\lambda$ (W.m-1.K-1): total or effective thermal conductivity

$\eta$ (Pa.s): viscosity

[$\eta$] (mL/g): intrinsic viscosity

G' (Pa): elastic modulus

G'' (Pa): viscous modulus

CA: cellulose acetate

DMSO: dimethylsulfoxide

EMIMAc: 1-ethyl-3-methylimidazolium acetate

BET: method of Brunauer-Emmett-Teller for specific surface area

BJH: method of Barrett, Joyner and Halenda for pore size distribution

EDS: Energy-dispersive X-ray spectroscopy

SEM: Scanning Electron Microscope

DE : Degree of Esterification of pectins

$H_m$ : mass uptake in a humid environment

Hv: volume contraction of a sample submitted to humidity

$\theta_{H2O}$: water contact angle

PEDS: Polyethoxydisiloxane

HMDZ: Hexamethyldisilazane

HMDSO: Hexamethyldisiloxane

# Résumé du travail de thèse

Dans un contexte où l'environnement est au cœur des préoccupations générales, et alors que les ressources de combustibles fossiles diminuent, limiter l'impact de l'humanité sur le climat est l'un des défis majeurs du XXI$^{\text{ème}}$ siècle. Le chauffage et la climatisation des bâtiments sont responsables des émissions de $CO_2$ les plus importantes en Europe, et comptent pour près de 40% de la consommation énergétique globale. Améliorer l'efficacité énergétique des constructions existantes est indispensable afin d'économiser l'énergie de chauffage et de réduire les émissions de $CO_2$ atmosphériques pour les prochaines décennies. L'accomplissement de cet objectif passe par l'élaboration de solutions d'isolation thermique plus efficaces. De plus, l'utilisation de meilleurs matériaux isolants pourrait même permettre l'obtention d'une performance accrue pour des matériaux plus fins. Dans les régions où le prix par rapport à la surface habitable est élevé, un tel gain d'espace serait économiquement significatif. Parallèlement, de nombreux secteurs nécessitent des matériaux super-isolants, tels l'électroménager et l'industrie des transports (ce qui inclut le transport d'énergie). Pour l'électroménager, l'isolation des réfrigérateurs et des congélateurs joue un rôle important, tandis que l'industrie des transports nécessite une bonne isolation pour les containers et les camions réfrigérés.

En guise d'illustration, nous pouvons citer la réglementation française (RT 2012) qui requiert que tout bâtiment neuf possède une résistance thermique $R$ (définie par le rapport entre l'épaisseur de la couche isolante et sa conductivité thermique $\lambda$) supérieure à 4 m².K.W$^{-1}$ pour les murs et à 8 m².K.W$^{-1}$ pour les combles. Les conductivités thermiques des matériaux couramment utilisés comme isolants thermiques, ainsi que les épaisseurs correspondantes permettant d'atteindre une résistance thermique de 4 m².K.W$^{-1}$ sont présentées dans le tableau 1. Un matériau est considéré comme superisolant s'il présente une conductivité thermique inférieure à celle de l'air, avec $\lambda_{\text{air}} = 0.025$ W.m$^{-1}$.K$^{-1}$ en conditions ambiantes. Suite aux avancées récentes en sciences des matériaux, cette limite est descendue à 0.020 W.m$^{-1}$.K$^{-1}$

Les matériaux superisolants peuvent être divisés en deux catégories: les panneaux d'isolation sous vide (PIV), et les super-isolants à pression ambiante (SIPA). Pour ces derniers, leurs propriétés d'isolation exceptionnelles sont dues à leur capacité à confiner l'air à l'intérieur de mésopores (ce phénomène physique est appelé l'effet Knudsen).

**Table 1: Conductivités thermiques et épaisseurs requises pour obtenir une résistance R de 4 m².K.W$^{-1}$ pour des matériaux isolants communément utilisés par l'industrie du bâtiment.**

| Type d'isolation | Matériau | $\lambda$ (W.m$^{-1}$K$^{-1}$) | Epaisseur (cm) |
|---|---|---|---|
| **Isolation classique** | Laine minérale | 0.035 | 14 |
| | Laine de verre | 0.040 | 16 |
| | Polystyrene expansé | 0.032 | 13 |
| | Mousse polyurethane | 0.026-0.030 | 10.4 - 12 |
| **Superisolation** | Aérogels organiques | 0.013-0.020 | 5.2 - 8 |
| | Aerogels de silice | 0.013 | 5.2 |
| | Panneaux d'isolation sous vide (PIV) | 0.007 | 3 |

Parmi les matériaux à pression ambiante utilisés pour améliorer la performance énergétique des systèmes d'isolation, les aérogels de silice sont les plus connus et les plus développés. Les aérogels de silice présentent des densités apparentes relativement faibles (avec des $\lambda$ avoisinant les 0.013 W.m$^{-1}$.K$^{-1}$ en conditions ambiantes). Cependant l'utilisation à grande échelle des aérogels de silice est encore limitée à ce jour et ce, pour différentes raisons. Premièrement, les aérogels de silice sont des matériaux fragiles et cassants, ayant tendance à libérer des poussières nanostructurées.

Deuxièmement, le procédé d'élaboration des aérogels de silice est long et coûteux à la fois du fait du prix élevé des précurseurs de silice et des spécificités du procédé de séchage au $CO_2$ supercritique. De plus ce procédé d'élaboration n'est pas continu. Une procédure de séchage à pression ambiante a été développée à la fin du 20ème siècle grâce à un traitement chimique des gels de silice; elle aboutit à des « grains » de silice de quelques millimètres de diamètre après un simple séchage évaporatif. Ce développement a été utilisé pour produire des lits granulaires et des « blankets » superisolants (dont la cohésion est assurée par un mat fibreux non tissé) commercialisés respectivement par les sociétés Cabot et Aspen Aerogels. Cependant ces matériaux posent toujours un problème lié à une émission de poussières très conséquente.

A ce jour, des aérogels organiques à base de polyuréthane sont en cours de développement industriel par BASF (produit Slentite™ de $\lambda = 0.016$ W.m$^{-1}$.K$^{-1}$) qui devrait inaugurer sa ligne de production pilote pour 2015. Cependant la chimie du polyuréthane implique le recours à des matières toxiques. Par conséquent, de nouveaux aérogels, non-toxiques, présentant des coûts acceptables par le marché, mécaniquement résistants et aux propriétés superisolantes demeurent nécessaires.

Dans ce cadre, les polysaccharides sont des matériaux biosourcés qui semblent être des candidats prometteurs pour renforcer ou, à terme, se substituer aux aérogels de silice. Les premiers aérogels à base de polysaccharides ont été synthétisés il y a environ 10 ans ; ces matériaux n'existent encore qu'à l'échelle laboratoire. La cellulose, l'amidon, les alginates ou la pectine sont désormais connus pour former des aérogels après dissolution du polymère dans un solvant approprié suivi d'un séchage au $CO_2$ supercritique. Ces matériaux ultraporeux, appelés « bio-aérogels », présentent des masses volumiques apparentes de 0.1-0.2 g.cm$^{-3}$, des surfaces spécifiques - assez élevées - autour de 200 - 400 m$^2$.g$^{-1}$ et sont mécaniquement plus résistants que les aérogels de silice (ils présentent un large domaine de déformation plastique jusqu'à 60-80% avant effondrement de la structure poreuse).

A ce jour, très peu d'études des propriétés thermiques des bio-aérogels sont disponibles, et seuls trois exemples de bio-aérogels superisolants thermiques ont été rapportés: l'aéropectine obtenue par dissolution et coagulation puis séchage au $CO_2$ supercritique à partir d'une solution aqueuse de pectine, dont la conductvité thermique atteint 0.016-0.020 W.m$^{-1}$K$^{-1}$ en conditions ambiantes (Rudaz et al., 2014); un aérogel de cellulose à base de nanofibres carboxylées en surface, avec une conductivité de 0.018 W.m$^{-1}$K$^{-1}$ (Kobayashi et al, 2014) ; et un aérogel à base d'amidon atteignant 0.024 W.m$^{-1}$K$^{-1}$ (Glenn et al., 1999). Pour les aérogels à base de cellulose préparés par dissolution-coagulation, la distribution de taille de pores s'étale de quelques dizaines de nm à plusieurs microns, ce qui nuit à leur niveau de conductivité. En ce qui concerne les aérogels à base de nanofibres de cellulose, la préparation des nanocelluloses est en elle-même un procédé énergivore, car elle résulte d'une suspension diluée de nanofibrilles dans l'eau, cette dernière ne pouvant être éliminée aisément.

L'une des voies potentielles pour l'élaboration de matériaux superisolants à partir de bio-aérogels est le « remplissage » des plus gros pores d'une matrice polysaccharide par une phase de silice nanostructurée, phase plus isolante que l'air qui s'y trouve. La contribution de la phase gazeuse à la conductivité thermique devrait dans ce cas être considérablement réduite grâce à la présence de silice superisolante au sein des pores du réseau de polysaccharide. Le réseau cellulosique pourrait alors agir comme renfort mécanique pour la phase de silice générée in situ. Il sera parallèlement nécessaire, afin d'assurer des propriétés superisolantes, de limiter l'augmentation de densité de tels matériaux composites de par l'adjonction significative de matière.

L'objectif de la thèse est d'élaborer des aérogels composites polysaccharide-silice dotés de propriétés thermiques superisolantes, puis d'établir les relations structure-propriétés permettant d'accroître la connaissance de ce nouveau type de matériaux. Pour cela, nous étudierons deux polysaccharides connus comme précurseurs de bio-aérogels : la cellulose et la pectine. Deux procédés visant à obtenir ces composites ont été étudiés dans le cadre de ce travail :

- Le mélange direct, dans un solvant commun, du polysaccharide et d'un précurseur de silice, suivi de la gélification simultanée des deux phases. Les aérogels composites ont alors été obtenus par séchage au $CO_2$ supercritique. Ce procédé est appelé méthode « one-pot ».

- L'imprégnation par un sol de silice d'une matrice polysaccharide poreuse imprégnée de solvant ; le gel de slice est alors formé *in situ* dans la porosité de la matrice par synthèse sol-gel en catalyse basique. Les composites ont été ensuite séchés au $CO_2$ supercritique. Ce procédé ayant donné les résultats plus prometteurs, une hydrophobisation des phases organique et inorganique a été réalisée afin de diminuer la sensibilité des aérogels à l'humidité ambiante. Ces aérogels hydrophobisés ont également permis d'obtenir des xérogels composites par séchage évaporatif à pression atmosphérique.

Ces travaux ont été réalisés dans le cadre du projet européen AEROCOINs (Aerogel-Based Composite/Hybrid Nanomaterials for Cost-Effective Building Super-Insulation Systems). Ce projet a réuni neuf partenaires industriels et académiques, avec pour objectif la réalisation de matériaux superisolants monolithiques à partir d'aérogels de silice renforcés synthétisés au moindre coût possible.

Les partenaires impliqués dans le projet AEROCOINs et leurs principales tâches respectives sont brièvement présentés ainsi :

Coordination du projet:

Fundación Tecnalia research & innovation (TECNALIA), Bilbao, Espagne

Synthèse des matériaux:

- Centres CEMEF et PERSEE de MINES ParisTech, Sophia Antipolis, France
- Swiss federal laboratories for materials testing and research (EMPA), Zurich, Suisse
- Fundación Tecnalia research & innovation (TECNALIA), Bilbao, Espagne

Séchage supercritique:

- SEPAREX, SA, Nancy, France

Fournisseur de précurseurs de silice, polyethoxydisiloxane (PEDS):

- PCAS, Longjumeau, France

Caracterisation des matériaux, étude des propriétés thermo-mécaniques, analyse de cycle de vie et modélisation du séchage :

- Technical University of Lòdz (TUL), Varsovie, Pologne
- Technical Research Centre of Finland (VTT), Helsinki, Finlande
- Bavarian Center for Applied Energy Research (ZAE), Würzburg, Allemagne
- ACCIONA infraestructuras, Madrid, Espagne.

Le présent manuscrit se divise en six chapitres comme suit.

## Chapitre I: Etat de l'art

Ce chapitre décrit tout d'abord les propriétés et les procédés de mise en forme des deux polysaccharides étudiés dans nos travaux : la cellulose et la pectine. Le procédé de synthèse sol-gel utilisé pour l'élaboration des aérogels est présenté, ainsi que le procédé général d'élaboration des bio-aérogels. Les propriétés de ces matériaux, en particulier en termes de conductivité thermique sont exposées. Les trois techniques utilisées pour le séchage des gels, à savoir le séchage supercritique, la lyophilisation et le séchage à pression ambiante sont décrites en détails. Quelques exemples de techniques d'hydrophobisation connues pour les aérogels de silice sont présentés. Enfin, l'état de l'art concernant les composites et les hybrides à base de cellulose et de silice est établi.

## Chapitre II: Matériel et méthodes

Le second chapitre est dédié à la description des matériaux et procédures expérimentales utilisés au cours des travaux. Les détails de la synthèse des bio-aérogels et de leurs composites élaborés avec la silice sont présentés, ainsi que les techniques de séchage utilisés.

La caractérisation des solutions, gels et aérogels a été réalisée en utilisant une vaste gamme de techniques complémentaires. Le comportement en solution des mélanges cellulose-silicate de sodium a été étudié par mesures en rhéologie dynamique. La densité apparente et la morphologie des matériaux ont été examinées respectivement par pycnométrie à poudre et microscopie électronique à balayage (MEB). La composition chimique des composites a été analysée par spectroscopie infrarouge ainsi que par analyse élémentaire et spectroscopie de diffraction d'énergie (EDS). L'adsorption d'azote à 77 K a été utilisée pour l'évaluation de la surface spécifique des matériaux poreux grâce à la méthode de Brunauer, Emmet and Teller (BET). Les propriétés mécaniques des bio-aérogels et de leurs composites avec la silice ont été étudiées par compression uniaxiale. Enfin, les deux techniques de caractérisation de la conductivité thermique utilisées sont présentées.

## Chapitre III: Aérogels composites cellulose-silice via une synthèse "one-pot".

Dans ce chapitre nous étudions la préparation d'aérogels composites cellulose-silice à partir du mélange direct en solution de cellulose et d'un précurseur de silice, ici le silicate de sodium ($Na_2SiO_3$). Pour assurer un mélange homogène des solutions initiales, un solvant commun aux deux systèmes a dû être utilisé. La cellulose n'étant pas solubles dans les solvants classiques, la solution la plus simple est d'utiliser une solution de cellulose dissoute en milieu alcalin (eau-NaOH 8%wt) et de mélanger cette solution avec une solution alcaline de silicate de sodium. Le mélange ainsi obtenu se solidifie rapidement à température ambiante ; la coagulation a été réalisée dans un bain acide (HCl). Le comportement rhéologique des mélanges de cellulose et de silicate de sodium a été étudié par mesures en rhéologie dynamique pour différentes proportions de cellulose/silicate de sodium et en fonction de la température. Le fort effet déstabilisant du silicate de sodium sur les solutions de cellulose-NaOH a ainsi été mis en évidence.

Le séchage au $CO_2$ supercritique des gels a donné les aérogels composites. Les matériaux obtenus avaient des densités comprises entre 0,1 et 0,25 g.cm$^{-3}$. La microscopie électronique à balayage a montré que les pores de l'aérocellulose étaient remplis par des particules micrométriques de silice. La diminution significative de la surface spécifique observée en présence de ces particules

démontre leur non-porosité. La conductivité thermique des composites a augmenté de 0.035-0.040 $W.m^{-1}.K^{-1}$ pour l'aérocellulose pure à 0,045-0,050 $W.m^{-1}.K^{-1}$ pour les composites, car les particules de silice ont augmenté la contribution du squelette solide du composite à la conductivité thermique. Enfin, le module d'Young a augmenté de 20MPa pour l'aérocellulose pure à 30-40MPa pour les composites, montrant que les particules de silice avaient un effet de renfort mécanique sur le composite. Ce procédé « one-pot » s'est donc montré inefficace pour l'élaboration de composites nanostructurés, car les deux matériaux ne peuvent être mélangés que dans une gamme restreinte de concentrations, et ces conditions ne permettent pas la formation d'une structure d'aérogel de silice.

## Chapitre IV: Aérogels composites cellulose-silice obtenus par de imprégnation de matrices cellulosiques poreuses par un sol de polyethoxydisiloxane.

Le quatrième chapitre traite de la préparation de composites cellulose-silice par imprégnation d'un réseau tridimensionnel de cellulose coagulée (alcogel) avec un sol de polyethoxydisiloxane (PEDS). L'objectif ciblé est l'obtention d'un composite constitué d'un réseau interpénétré de cellulose et de silice, suivie de l'étude de ses propriétés thermomécaniques.

Des aérogels légers, monolithiques et mécaniquement résistants peuvent être obtenus par imprégnation de cellulose coagulée par une solution de PEDS, suivie par une immersion dans une solution de catalyseur $NH_4OH$ dans un mélange eau/éthanol, une étape d'échange de solvant puis un séchage supercritique. L'imprégnation peut être réalisée soit par simple diffusion moléculaire, soit par un procédé dit « par flux forcé » où le PEDS est forcé de circuler dans la porosité de la cellulose par l'application d'une différence de pression. Le but de l'imprégnation forcée est une réduction significative du temps nécessaire à l'imprégnation, de 7 heures pour la diffusion moléculaire à une vingtaine de minutes pour l'imprégnation par flux forcé. Une analyse par spectroscopie à diffraction d'énergie des rayons X et au MEB ont permis d'observer la structure et la distribution de la phase silice formée au sein de la matrice cellulosique.

L'analyse par BET a confirmé la formation de silice nanostructurée à l'intérieur de la matrice cellulosique: la surface spécifique a augmenté de $\approx 300$ $m^2.g^{-1}$ pour l'aérocellulose de référence à 750-800 $m^2.g^{-1}$ pour les composites. La conductivité thermique en conditions ambiantes a diminué de 0,033 $W.m^{-1}.K^{-1}$ pour l'aerocellulose à 0,027 $W.m^{-1}.K^{-1}$ pour les aérogels composites grâce aux propriétés superisolantes de l'aérogel de silice, démontrant ainsi la validité de la méthode d'imprégnation pour obtenir des composites nanostructurés aux performances thermiques accrues. Les aérogels composites ont été renforcés mécaniquement par rapport aux aérogels de silice de référence : le module d'Young a augmenté d'un facteur 3-4 et la déformation à la rupture était de 60% pour les composites contre 4-10% pour la référence.

## Chapitre V: Aérogels et xerogels composites cellulose-silice hydrophobes.

A cause de l'importante sensibilité à l'humidité des phases de cellulose et de silice en l'absence de traitement hydrophobant, les aérogels composites cellulose-silice perdent leurs propriétés thermo-mécaniques avec le temps, ce qui limite fortement leur application à la superisolation pour l'industrie du bâtiment. Ce chapitre est donc focalisé sur l'obtention de composites cellulose-silice entièrement hydrophobés. Une cellulose chimiquement modifiée, la tritylcellulose, a été synthétisée comme base pour des alcogels cellulosiques, qui ont été ensuite imprégnés par le PEDS selon la méthode décrite au Chapitre IV. La phase silice est hydrophobisée par un traitement du composite à l'hexamethyldisilazane (HMDZ) et les échantillons sont séchés au $CO_2$ supercritique.

Les aérogels obtenus sont résistants à l'humidité, la reprise hydrique massique a été réduite de 10% pour un composite non hydrophobe à 1-3% et des angles de contact avec l'eau de 133° ont été obtenus. Les composites sont finement structurés, présentant des surfaces spécifiques de 600-800 $m^2.g^{-1}$. La présence de la phase silice dans la porosité de la tritylcellulose a renforcé le matériau mais l'a rendu plus cassant. Cependant les propriétés mécaniques des composites étaient bien meilleures que celles des aérogels de silice. Des aérogels superisolants ont été obtenus, leur conductivité thermique étant de 0.021-0.022 $W.m^{-1}.K^{-1}$.

Un développement à long terme pour les composites cellulose-silice entièrement hydrophobés est l'obtention de matériaux superisolants séchés à pression ambiante. Nous avons donc étudié les propriétés de ces xérogels composites tritylcellulose-silice, et comparé leurs propriétés à celles des aérogels composites.

La densité apparente des xérogels à base de tritylcellulose et de composites tritylcellulose-silice est notablement supérieure à celle des aérogels correspondants du fait d'une forte contraction au séchage évaporatif. En revanche l'effet cohésif de la phase cellulosique au sein du composite permet d'obtenir des xérogels monolithiques, bien que présentant des fissures macroscopiques. Cette densification importante indique que les xérogels de tritylcellulose ne sont pas encore adaptés à des applications pour l'isolation thermique. L'hydrophobicité des xérogels est maintenue, comme le montrent des angles de contact avec l'eau de 120-148°.

## Chapitre VI: Aeropectine et aerogels composites aeropectine-silice.

Dans le sixième et dernier chapitre, un autre polysaccharide, la pectine, est étudié comme renfort mécanique pour les aérogels de silice. Premièrement, les propriétés des aérogels basés sur la pectine réticulée par les ions calcium sont étudiées. La pectine est un déchet peu coûteux provenant de l'industrie agro-alimentaire ; elle peut former des gels après dissolution dans l'eau par réticulation avec les ions divalents come les ions calcium ($Ca^{2+}$). Le séchage au $CO_2$ supercritique permet d'obtenir des matériaux nanostructurés et ultra-légers. L'influence de la concentration de pectine, du pH de gélification et de la densité de l'aéropectine sur sa conductivité thermique ont été étudiés.

Des composites pectine-silice ont été préparés en utilisant la stratégie déjà développée pour es composites cellulose-silice. Les aérogels composites ont été étudiés en termes de morphologie, surface spécifique, et densité apparente. L'hydrophobisation de surface des composites a été réalisée à l'aide de trois agents d'hydrophobisation bien connus pour la silice.

Un rapport molaire d'environ 0.22 entre les ions calcium et les groupements acide carboxyliques, et un pH de 6-8 a donné les aérogels avec la plus faible densité. Pour l'aéropectine une dépendance linéaire de la conductivité thermique avec la densité a été observée, avec des valeurs de conductivité de 0.013 à 0.022 $W.m^{-1}.K^{-1}$ pour des densités de 0.03-0.10 $g.cm^{-3}$. La morphologie des aérogels composites observée au MEB s'apparente à un fin réseau de nanofibres de pectine couvertes par l'aérogel de silice. La surface spécifique des aérogels a augmenté de 200-300 $m^2.g^{-1}$ pour la pectine pure à 800-850 $m^2.g^{-1}$ pour les composites. La conductivité des composites pectine-silice est restée dans le domaine 0.015-0.022 $W.m^{-1}.K^{-1}$. Les aéropectines sont capables de se déformer à 80% sans casser. L'hydrophobisation de la phase silice des composites a donné des angles de contact de 135° et a permis de réduire la reprise massique en eau à 5-6% au lieu de 20% pour l'aéropectine pure.

## Conclusions et perspectives:

Au cours de cette thèse nous avons étudié des matériaux composites à base de polysaccharides et de silice et obtenu des propriétés prometteuses pour l'isolation thermique. Le mélange en solution de cellulose et de silice ne permet pas d'élaborer des composites nanostructurés. En revanche il est possible d'obtenir un réseau interpénétré de cellulose et de silice par imprégnation d'une matrice cellulosique par un précurseur de silice, suivie de la synthèse in-situ de l'aérogel de silice dans la porosité de la cellulose. Imprégner la cellulose en forçant la circulation du précurseur de silice dans la matrice cellulosique via un gradient de pression permet de diminuer considérablement le temps d'imprégnation.

Les aérogels composites ainsi obtenus ont une conductivité thermique réduite comparé à l'aérocellulose pure ; le composite est également bien plus résistant en compression que l'aérogel de silice. L'utilisation d'une cellulose hydrophobisée comme matrice d'imprégnation a permis d'obtenir des aérogels entièrement hydrophobes et donc capables de résister aux conditions d'humidité auxquelles les matériaux d'isolation sont soumis en usage. Enfin, la pectine, nouveau polysaccharide utilisé pour la production de bio-aérogels, présente des propriétés thermiques superisolantes remarquables, que ce soit seule ou en composite avec la silice.

Ces matériaux extrêmement poreux peuvent en outre être employés pour d'autres domaines que l'industrie du bâtiment, telle l'isolation pour l'industrie du transport et de l'électroménager ; leur grande porosité peut également convenir à des applications pour la libération contrôlée de médicaments ou la récupération de déchets organiques.

## References:

Glenn, G. M., & Stern, D. J. (1999). *U.S. Patent No. 5,958,589*. Washington, DC: U.S. Patent and Trademark Office.

Kobayashi, Y., Saito, T., & Isogai, A. (2014). Aerogels with 3D Ordered Nanofiber Skeletons of Liquid-Crystalline Nanocellulose Derivatives as Tough and Transparent Insulators, *Angewandte Chemie*, *126*(39), 10562-10565.

Rudaz, C., Courson, R., Bonnet, L., Calas-Etienne, S., Sallée, H., & Budtova, T. (2014); Aeropectin: Fully Biomass-Based Mechanically Strong and Thermal Superinsulating Aerogel, *Biomacromolecules*, *15*(6), 2188-2195.

# Introduction

In a context of growing environmental awareness and decreasing fossil fuel resources, lowering the impact of mankind on Earth climate is among the greatest challenges of the XXI$^{st}$ century. Heating and cooling of buildings is responsible for the largest $CO_2$ emissions in Europe, and represents 40% of the total energy consumption. Improving the energy efficiency of existing buildings is thus required to save energy and lower $CO_2$ emissions in the coming decades. To achieve this, more efficient thermal insulation solutions are required. Moreover, the use of better insulating materials could allow a better insulation performance with thinner materials. Moreover, in the areas where the price per habitable surface is high, the space gain would be economically significant. In the same way, another important set of sectors requiring thermal super-insulating materials is appliances and transport industries (including transport of energy). In appliances, the insulation of refrigerators and freezers plays a major role, whereas in the transport industry, the insulation concerns reefer containers and refrigerated trucks.

As an example, the French thermal regulation (RT 2012) requires for all new buildings to possess a thermal resistance $R$ (defined as the ratio between insulation panel thickness and its thermal conductivity $\lambda$) above 4 m².K.W$^{-1}$ for walls and above 8 m².K.W$^{-1}$ for attics. The thermal conductivities of common insulation materials and the thickness required for reaching a thermal resistance of 4 m².K.W$^{-1}$ is presented in table I.2. A material was historically considered superinsulating if its thermal conductivity is lower that the conductivity of air, with $\lambda_{air} = 0.025$ W.m$^{-1}$.K$^{-1}$ in ambient conditions. Nowadays, because of growing improvements in materials science, this limit has been decreased within the main players to 0.020 W.m$^{-1}$.K$^{-1}$.

Superinsulating materials can be divided in two categories: vacuum insulation panels (VIP), and ambient pressure insulating materials. For the latter, their exceptional insulation properties come from their ability to reduce drastically the gaseous contribution to the thermal transfer by confining air inside small pores (physical mechanisms known as Knudsen effect).

**Table 1: Typical thermal conductivities and thickness required to have R = 4 m².K.W$^{-1}$ for common insulation materials used in the building industry**

| Type of insulation | Material | $\lambda$ (W.m$^{-1}$K$^{-1}$) | Thickness (cm) |
|---|---|---|---|
| **Conventional insulation** | Mineral wool | 0.035 | 14 |
| | Glass Wool | 0.040 | 16 |
| | Expanded polystyrene | 0.032 | 13 |
| | Polyurethane foams | 0.026-0.030 | 10.4 - 12 |
| **Superinsulation** | Organic aerogels | 0.013-0.020 | 5.2 - 8 |
| | Silica aerogels | 0.013 | 5.2 |
| | Vacuum insulation panels (VIP) | 0.007 | 3 |

Among ambient pressure materials used to improve the energy performance of insulation systems, silica aerogels are the most developed. Silica aerogels show rather low density ($< 0.15$ g.cm$^{-3}$) and superinsulating thermal properties ($\lambda$ as low as 0.013 W.m$^{-1}$.K$^{-1}$ in ambient conditions). However, the larger-scale usage of silica aerogels is limited to this day, for several reasons. First, silica aerogels are very fragile, brittle materials, and have a tendency to release "dust". Second, the preparation process of silica aerogels is long and costly because of the high price of silica precursors and supercritical $CO_2$ drying process; in addition it is not a continuous process. A drying procedure at ambient pressure was developed at the beginning of the 21$^{st}$ century resulting in silica granules of few millimetres in diameter thanks to chemical treatments. This improvement was used for production of granular beds and so-called "blankets" (in which

cohesion is given by fibrous structures) commercialised respectively by Cabot and Aspen Aerogels. However, the problem of intense "dusting" remains. Besides organic (polyurethane) aerogels are under industrial development with strong advancements made by BASF (Slentite™ with thermal conductivity around 0.016 $W.m^{-1}.K^{-1}$, pilot line promised to be started in 2015). However, polyurethane chemistry is harsh. Thus there is still a need in non-toxic, cost-effective and mechanically robust aerogels with thermal super-insulating properties, i.e. an extremely low thermal conductivity in room conditions.

Polysaccharides are bio-sourced polymers which appear to be suitable candidates either to reinforce or even replace silica aerogels. The first aerogels based on polysaccharides were synthesised around 10 years ago and still remain at the laboratory scale. Cellulose, starch, alginate or pectin have been reported to form aerogels after polymer dissolution in an appropriate solvent, followed by coagulation in a non-solvent and drying with supercritical (sc) $CO_2$. These ultraporous materials, called "bio-aerogels", have typical bulk densities of 0.1-0.2 $g.cm^{-3}$, quite high specific surface areas around 200 - 400 $m^2.g^{-1}$ and are mechanically stronger than silica-based aerogels (with a large plastic deformation region up to 60-80% strain before pore collapse).

Until now, there are very few studies of the thermal conductivity of bio-aerogels and only three examples of thermal super-insulating bio-aerogels are known: one is *Aeropectin* obtained via pectin dissolution-coagulation-drying with sc $CO_2$ route and presenting a thermal conductivity between 0.016 and 0.020 $W.m^{-1}K^{-1}$ in room conditions (Rudaz et al., 2014); the second is surface carboxylated nanofibrillated cellulose aerogel with the lowest thermal conductivity of 0.018 $W.m^{-1}.K^{-1}$ (Kobayashi et al., 2014) and finally, the lowest value of the thermal conductivity of starch aerogels (prepared, as Aeropectin, via dissolution-coagulation-drying with sc $CO_2$ route) were reported to be just below that of air, 0.024 $W.m^{-1}K^{-1}$ (Glenn et al., 1999). For cellulose-based aerogels prepared via dissolution-coagulation route the relatively large pore size distribution, from tens of nm to a few microns, is detrimental to their thermal insulation properties. As for nanofibrillated cellulose based aerogels, the preparation of nanocellulose itself is an energy consuming process because it results in a dilute suspension of nanofibrils dispersed in water the elimination of which is not straightforward and very costly.

One of the potential ways to make thermal superinsulating materials with bio-based aerogels could be by filling of the large pore in polysaccharide matrix by a nanostructured superinsulating silica phase, which should result in lower thermal conductivity compared to the pristine bio-aerogels. Theoretically, it is then expected that the conductivity of the gaseous phase, which represents about 60% of the total conductivity, would be significantly decreased due to the presence superinsulating silica aerogel matrix in the pores of the bio-aerogel network. Moreover, the fibrous polysaccharide network will act as reinforcement for the aerogel structure. Of course, to obtain at the end a superinsulating material, the density increase of the so-prepared composite must be controlled.

The goal of this thesis is to prepare polysaccharide-silica composite aerogels with thermal superinsulating properties and correlate their morphology and properties to improve the knowledge in this new domain. For this purpose, we focus the study on two polysaccharides that are known as starting materials for bio-aerogels: cellulose and pectin. Two different methods to obtain such composites were investigated in this study:

- Direct mixing, in a common solvent, of dissolved polysaccharide and silica precursor, followed by the simultaneous gelation of each phase. Composite aerogels were then obtained by supercritical $CO_2$ drying. This process was called "one-pot" method.

- Impregnation of a porous wet polysaccharide matrix by a silica sol; the silica gel is formed by sol-gel process inside the pores of the polysaccharide network. The wet composites were then dried with supercritical $CO_2$. Because this process gave the most promising results, hydrophobisation of both phases, organic and inorganic, was performed to decrease the sensitivity of composite aerogels to humidity uptake. Finally, the first composite xerogels were prepared on this basis via ambient drying.

The work was performed in the frame of the European project AEROCOINs (Aerogel-Based Composite/Hybrid Nanomaterials for Cost-Effective Building Super-Insulation Systems). This project united 9 partners from the academy and industry, with the objective of making monolithic superinsulating materials from mechanically reinforced silica aerogels at the lowest possible cost.

The partners involved in AEROCOINS and an overview of their main respective associated tasks within the project were as follows:

Project coordination:

Fundación Tecnalia research & innovation (TECNALIA), Bilbao, Spain

Synthesis of new materials:

- CEMEF and PERSEE centers from MINES ParisTech, Sophia Antipolis, France
- Swiss federal laboratories for materials testing and research (EMPA), Zurich, Switzerland
- Fundación Tecnalia research & innovation (TECNALIA), Bilbao, Spain

Supercritical drying:

- SEPAREX, SA, Nancy, France

Manufacturer and provider of polyethoxydisiloxane (PEDS) silica precursors:

- PCAS, Longjumeau, France

Materials characterization, assessment of thermo-mechanical properties, life cycle analysis (LCA) and modelling of drying:

- Technical University of Lòdz (TUL), Warsaw, Poland
- Technical Research Centre of Finland (VTT), Helsinki, Finland
- Bavarian Center for Applied Energy Research (ZAE), Würzburg, Germany
- ACCIONA infraestructuras, Madrid, Spain.

The present manuscript is divided in six chapters:

## Chapter I: State of the art

This chapter describes first the properties and processing of the two polysaccharides used in this work: cellulose and pectin. The sol-gel synthesis process used to synthesize silica aerogels is presented, as well as the general synthesis processes for bio-aerogels. Their properties, with the focus on thermal insulation, are discussed. The three techniques used to obtained dry porous materials from the initial "wet" gels, i.e. supercritical drying, freeze-drying and ambient pressure drying are also described in details. We also present a few examples of the common techniques used to make hydrophobic silica aerogels. Finally, the state of the art in the domain of cellulose-silica composite and hybrid materials is reviewed.

## Chapter II: Materials and methods

The second chapter is dedicated to the description of the materials and experimental procedures used in the work. The synthesis of bio-aerogels and polysaccharide-silica composites is detailed, as well as the drying methods used.

The characterization of solutions, gels and aerogels was performed using a wide array of complementary techniques. The solution behavior of cellulose-silica mixtures is studied by dynamic rheology measurements. For the morphological characterization of the materials, powder pycnometry and scanning electron microscopy (SEM) are used. The chemical nature of the composites is surveyed using FTIR spectroscopy as well as elemental analysis and energy diffractive spectroscopy (EDS). Nitrogen adsorption at 77 K was used to evaluate the specific surface area of the materials by the Brunauer, Emmet and Teller (BET) method. The mechanical properties of the bio-aerogels and their composites with silica are studied by uniaxial compression measurements. Finally, the two techniques used to evaluate thermal conductivity of aerogel samples are reviewed.

## Chapter III: Cellulose-silica composite aerogels through "one-pot" synthesis.

In this chapter, we study the preparation of cellulose-silica composites from direct mixing of cellulose and silica precursor solutions. To ensure homogeneous mixing of the initial solutions, a common solvent for both systems and thus of the corresponding silica sol has to be identified. Because cellulose is not soluble in classical solvents, the only "easy" option was to use cellulose dissolved in alkaline media (water-8%wt NaOH) and mix it with an alkaline sodium silicate solution. The resulting mixture quickly solidifies at ambient temperature, it was then coagulated in an acid bath. The behavior of the cellulose-sodium silicate mixture is studied by dynamic rheological measurements for different cellulose/silicate proportions and as a function of temperature.

Supercritical $CO_2$ drying of the wet gels gave the composite aerogels. The materials are characterized in terms of bulk density, specific surface area and their morphology is examined by scanning electron microscopy (SEM). The Young modulus of the composites is evaluated by sound velocity measurements. Finally, the thermal conductivity of one-pot cellulose-silica composites was studied by hot-wire method. The morphology and thermal properties of freeze-dried one-pot samples is also characterized.

# Chapter IV: Cellulose-silica composite aerogels from impregnation of cellulose porous matrices with polyethoxydisiloxane sol.

The fourth chapter deals with the preparation of cellulose-silica composite by the impregnation of a cellulose alcogel (coagulated cellulose tridimensional network) with a silica sol. Polyethoxydisiloxane (PEDS) in ethanol is used as the silica precursor. The goal of this work was to obtain a composite made of an interpenetrated network of nanostructured cellulose and silica and study its thermo-mechanical properties.

Strong, light and monolithic crack-free cellulose-silica composite aerogels are prepared by impregnation of wet coagulated cellulose with PEDS solution, followed by immersion of the sample in a water/ethanol $NH_4OH$ catalyst solution, solvent exchange, and supercritical drying. The impregnation can be performed either by molecular diffusion or by a forced flow process where the silica sol is forced to penetrate inside the cellulose matrix due to a pressure difference. The goal of forced flow impregnation method is to significantly reduce processing times as compared to impregnation driven by simple molecular diffusion. Energy diffractive spectroscopy and SEM analysis are performed to compare silica spatial distribution in both series of samples. Bulk density, porosity, specific surface area, thermal conductivity and mechanical properties of cellulose-silica composites are evaluated and compared to those of the corresponding "pure" aerogels.

# Chapter V: Hydrophobic cellulose-silica composite aerogels and xerogels

Due to high sensitivity to humidity, cellulose-silica composites are prone to losing their properties (notably porosity and thermal conductivity) with time, which can be a hindrance to their applications for the superinsulation of buildings. This chapter is thus focused on the preparation of fully hydrophobic cellulose-silica composite aerogels. We synthesize chemically modified cellulose, tritylcellulose, as the basis of cellulosic alcogels, which were impregnated with PEDS with the same methods as described in chapter IV. The silica phase is hydrophobized by treatment of the composite with hexamethyldisilazane (HMDZ) and the samples are dried with supercritical $CO_2$. Additionally to the characterization of materials in terms of bulk density, specific surface area, morphology and thermo-mechanical properties, the water contact angle and the evolution of mass and volume of samples placed in extreme humidity conditions are studied to assess their hydrophobicity level.

A long-term development prospect of fully hydrophobized cellulose-silica composites is the preparation of ambient-dried superinsulating materials. Thus we investigate the properties of tritylcellulose-silica composite xerogels, i.e. gels dried at ambient pressure, and compare their properties to those of the corresponding aerogels.

# Chapter VI: Aeropectin and aeropectin-silica composite aerogels.

In the sixth and final chapter, another polysaccharide, pectin, is studied as a reinforcing material for silica aerogels. First, the properties of aerogels based on cross-linked pectin were investigated. Pectin, an inexpensive waste from food industry can form gels in aqueous solution by reticulation by divalent ions such as $Ca^{2+}$. Further coagulation and drying with supercritical $CO_2$ gives nanostructured ultralight materials. The influence of pectin concentration, gelation pH and of the amount of calcium ions on aeropectin density and thermal conductivity is studied.

Pectin-silica composites are prepared using the same strategy as developed for cellulose-silica route. The composite aerogel are studied in terms of morphology, specific surface area, and bulk density. The surface hydrophobization of the silica phase of the composites was studied using three well-known silica hydrophobizing agents to allow the composites to handle ambient humidity without losing their thermo-mechanical properties.

## Conclusion and prospects

Finally, we draw conclusions about the superinsulating materials studied in the thesis. We discuss the possibilities of further works and the array of potential applications for nanostructured interpenetrated polysaccharide-silica hybrid aerogels.

## References:

Glenn, G. M., & Stern, D. J. (1999). *U.S. Patent No. 5,958,589*. Washington, DC: U.S. Patent and Trademark Office.

Kobayashi, Y., Saito, T., & Isogai, A. (2014). Aerogels with 3D Ordered Nanofiber Skeletons of Liquid-Crystalline Nanocellulose Derivatives as Tough and Transparent Insulators, *Angewandte Chemie*, *126*(39), 10562-10565.

Rudaz, C., Courson, R., Bonnet, L., Calas-Etienne, S., Sallée, H., & Budtova, T. (2014) ; Aeropectin: Fully Biomass-Based Mechanically Strong and Thermal Superinsulating Aerogel, *Biomacromolecules*, *15*(6), 2188-2195.

# Communications and publications from this work

**Articles:**

Demilecamps, A., Reichenauer, G., Rigacci, A., & Budtova, T. (2014). Cellulose–silica composite aerogels from "one-pot" synthesis. *Cellulose*, *21*(4), 2625-2636.

Demilecamps, A., Beauger, C., Hildenbrand, C., Rigacci, A., & Budtova, T. (2015). Cellulose-silica aerogels. *Carbohydrate Polymers 122 (2015) 293–300*.

**Oral communications at international conferences:**

A.DEMILECAMPS, T. BUDTOVA, A. RIGACCI

"Cellulose-silica hybrid aerogels from "one-pot" synthesis", European Polymer Federation conference, Pisa, Italy, 16-21 June 2013.

A.DEMILECAMPS, M.ALVES, C.BEAUGER, C. HILDENBRAND, G. REICHENAUER, M. WIENER, A. RIGACCI, T. BUDTOVA

"Cellulose-silica hybrid aerogels" 3rd EPNOE International Polysaccharide Conference, Nice, France, 21-24 October 2013.

C. RUDAZ, A. DEMILECAMPS, C. HILDENBRAND, C. BEAUGER, A. RIGACCI, T. BUDTOVA

"Bio-aerogels and their hybrids", High Performance Thermal Insulation (HPI) 2013 - Towards Near Zero Energy Buildings, Wurzburg, Germany, 27-28 november, 2013

C. RUDAZ, A. DEMILECAMPS, S. CALAS-ETIENNE, R. COURSON, L. BONNET, H. SALLEE, G. REICHENAUER, M. WIENER, A. RIGACCI, T. BUDTOVA

« Nanostructuration of cellulose aerogels and their organic-inorganic hybrids", 247th ACS national meeting, Dallas, USA, March 16-20, 2014.

A. DEMILECAMPS, C. RUDAZ, C. HILDENBRAND, A. RIGACCI, T. BUDTOVA

"New thermal superinsulating materials from pectin based bio-aerogels", 12th International Conference on Nanostructured Materials (NANO-12), Moscow, Russia, 13-18 June 2014.

A. DEMILECAMPS, G. POUR, M. ALVES, A. RIGACCI, G. REICHENAUER, T. BUDTOVA

"Nanostructured organic-inorganic cellulose-based aerogels for thermal superinsulation", 11th French-Romania conference on polymers, Piteşti, Romania, 27-29 august 2014

C. RUDAZ, A. DEMILECAMPS, A. RIGACCI, T. BUDTOVA

« Pectin and pectin-silica aerogels: new promising thermal super-insulating materials » International Seminar on AEROGELS – 2014, Properties-Manufacture-Applications, Hamburg, Germany, 6-7 october 2014

C. RUDAZ, A. DEMILECAMPS, G. POUR, M. ALVES, A. RIGACCI, H. SALLEE, G.REICHENAUER, T. BUDTOVA

"Bio-based aerogels: a new generation of thermal super-insulating materials", Japanese European workshop "Cellulose and Functional Polysaccharides", Berlin, Germany, 14 16 october 2014.

C. RUDAZ, A. DEMILECAMPS, G. POUR, M. ALVES, A. RIGACCI, H. SALLEE, G. REICHENAUER, T. BUDTOVA

"Bio-based aerogels: a new generation of thermal super-insulating materials", EMN (Energy, Materials, nanotechnology) meeting on Polymer, Orlando, USA, 7-10 january 2015.

# Chapter I:
# State of the art:

*Cellulose, pectin and silica aerogels and their composites: preparation, morphology, and applications for thermal insulation*

## Introduction

This chapter will focus on the state of the art on bio-aerogels based on two polysaccharides used in this work, cellulose and pectin, and also on main characteristics of silica aerogels and cellulose-silica hybrid and composite materials.

The first part focuses on cellulose, the most abundant polysaccharide on Earth. After reviewing the general properties of cellulose, we will focus on the different techniques used to dissolve and process cellulose. The water-NaOH and ionic liquids, "green" solvents for cellulose, will be examined in details. The two major existing industrial processes for cellulose forming, Viscose and Lyocell, will also be presented.

The second part is centered on pectin. Pectin is a polysaccharide, constituent of plant cell walls. It is extracted from various plants, particularly fruits peel and seeds. The major interest of pectins is its gelling properties, used in applications targeting the food industry: we will present two mechanisms of pectin gelation, acid-based and calcium binding.

Our third part will be focused on aerogels. These extremely light materials have a large array of very interesting properties, such as high porosity and low thermal conductivity in ambient conditions. After a review of the main modes of preparation of aerogels, we will give some details about the most notable aerogel materials: silica aerogels. Two main families of silica aerogel precursors will be presented: sodium silicate and silica alcoxyde derivatives (called alcoxysilanes). Obtaining hydrophobic materials was an important step for the industrial-scale applications of silica aerogels, thus we will discuss the main routes reported for the hydrophobization of $SiO_2$ aerogels.

A new class of aerogels is polysaccharide-based aerogels, also known as bio-aerogels. We will show two very promising examples of this brand new class of materials, aerogels from cellulose and pectin.

Finally, cellulose-silica hybrid and composite materials will be reviewed in the fourth part. Although most literature on cellulose-silica hybrids aims at covering cellulose fibers with silica particles or films, some cellulose-silica composite aerogels were obtained in recent years.

# Introduction

Ce chapitre dresse l'état de l'art sur les bio-aerogels en se basant sur les deux polysaccharides utilisés dans cette thèse : la cellulose et la pectine, ainsi que sur les caractéristiques principales des aérogels de silice et des composites ou hybrides à base de cellulose et de silice.

La première partie se concentrera sur la cellulose, le polysaccharide naturel le plus abondant sur Terre. Après avoir passé en revue les propriétés générales de la cellulose, nous nous intéresserons aux différentes techniques utilisées pour la dissolution et la mise en forme de cette dernière. En particulier, les solvants eau-NaOH et liquides ioniques, solvants « verts » de la cellulose, seront étudiés en détails. Nous présenterons également les deux procédés Viscose et Lyocell, procédés majeurs de mise en forme industrielle de la cellulose.

La deuxième partie sera centrée sur la pectine. La pectine est un polysaccharide, constituant des parois des cellules végétales. Elle est extraite de différentes plantes, en particulier des écorces et pépins de fruits. Le principal intérêt de la pectine réside dans ses propriétés gélifiantes, utilisées dans de nombreuses applications par l'indutrie agro-alimentaire. Deux mécanismes de gélification de la pectine, l'un en milieu acide et le second via la réticulation par des ions calcium, seront présentés.

Notre troisième partie sera consacrée aux aérogels. Ces matériaux extrêmement légers possèdent une large gamme de propriétés très intéressantes, parmi lesquelles une grande porosité et une extrêmement faible conductivité thermique dès la pression ambiante. Après avoir examiné les différentes méthodes conduisant à la préparation des aérogels, nous donnerons plus de détails au sujet des aérogels les plus connus : les aérogels de silice. Deux types de précurseurs siliciques seront présentés : le silicate de sodium et les dérivés d'alcoxydes de silice (appelés alcoxysilanes). L'obtention de matériaux hydrophobes a été l'un des principaux challenges pour la production à échelle industrielle des aérogels de silice, nous discuterons donc des différentes voies connues pour l'hydrophobisation de ces aérogels.

Très récemment, un nouveau type d'aérogel est apparu. Il est constitué par les aérogels à base de polysaccharides, également appelés bio-aérogels. Deux exemples de cette toute nouvelle classe de matériaux seront présentés, l'Aerocellulose et l'Aéropectine.

Enfin, en quatrième partie nous nous intéresserons aux hybrides ou composites à base de cellulose et de silice. Bien que l'essentiel de la littérature scientifique soit focalisée sur la fonctionnalisation des fibres de cellulose par des particules ou des films de silice, plusieurs articles récents mentionnent des aérogels composites ou hybrides à base de cellulose et de silice.

# 1. Cellulose: structure and properties

## 1.1. Structure of cellulose

### 1.1.1. Origin

Cellulose is the most abundant natural polymer on Earth, and accounts for more than 50% of biomass, with more than 140 billion tons produced per year through photosynthesis (Klemm et al., 2005). It is a key part of plant cell walls and can be extracted from various sources, such as cotton, wood, or flax. Cellulose content in plant fibres varies from 10% to 99% depending on the source (Table I.1). The degree of polymerization, (DP), also depends on the cellulose origin. Some bacteria such as *Acetobacter xylinum* are also able to produce cellulose (so-called bacterial cellulose) of very high degree of polymerization of several thousands (Hestrin and Schramm, 1954).

Table I.1: Average cellulose content in different cellulose sources (Klemm, 1998 ; Krassig, 1993)

| Cellulose source | Wt% cellulose |
|---|---|
| Corn | 15-20 |
| Wood pulp | 40-50 |
| Cotton | 95-99 |
| Straw, flax, hemp | 70-80 |
| Bacterial cellulose | 99 |

### 1.1.2. Chemical structure and organization

The morphology of cellulose fibers is presented on figure I.1. Macrofibrils, of a length of 1-2 mm and 60-360µm diameter are the main structural unit of the cell walls (Lerouxel et al., 2006). They are constituted of agglomerated cellulose microfibrils, 2-20 µm in diameter depending on the cellulose source. Each microfibril is made of elementary cellulose fibrils containing six glucose chains linked together by hydrogen bonds. Elementary fibrils dimensions are around 1-10µm in length and 10 nm in diameter (figure I.1) (Klemm et al, 1998).
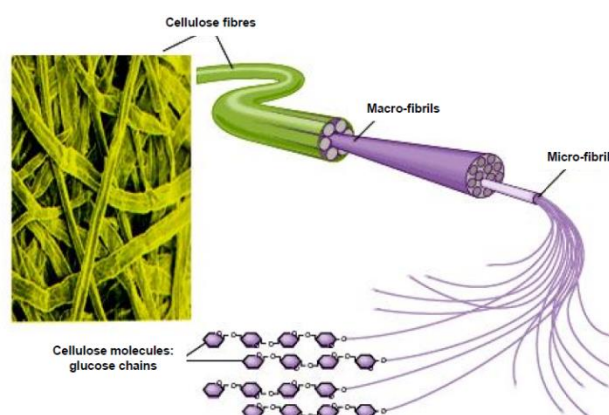


Figure I.1: Schematic view of the structure of cellulose fibers

Polysaccharides are long chains of saccharide (sugar) molecules. Their general formula is $(C_x(H_2O)_y)_n$ where n is the degree of polymerization.

Cellulose is a linear polysaccharide consisting of anhydroglucopyranose units (AGU) linked through β-(1-4) glycosidic bonds. Two AGU molecules make cellobiose, the repeating unit of cellulose (figure I.2). The molar mass of an AGU unit is 162 g.mol$^{-1}$. The degree of polymerization (DP) of cellulose, calculated from the number of anhydroglucopyranose units in the chain can vary from 100 to several trousands depending on the cellulose source.
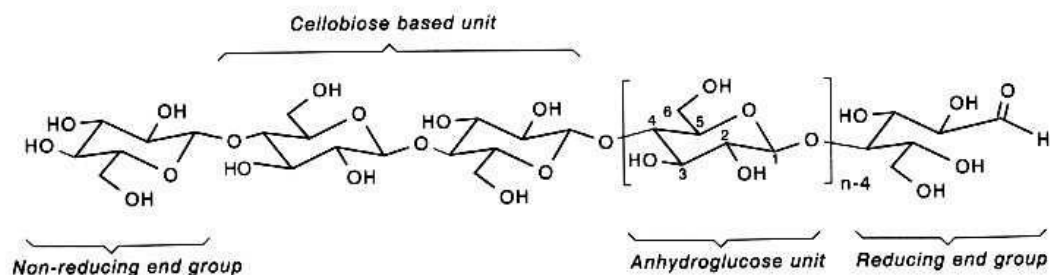


**Figure I.2: Chemical structure of cellulose chains (Klemm et al, 1998)**

Glucose rings adopt a "chair" conformation, where hydroxyl groups on carbons $C_2$, $C_3$ and $CH_2OH$ group on $C_6$ are in axial position, while hydrogen atoms are in equatorial position. This configuration favors the formation of inter- and intra- molecular hydrogen bonds between cellulose chains (Nishiyama, 2002).

Cellulose adopts a semi-crystalline structure. Four main polymorphs have been discovered and studied: cellulose I, II, III and IV (O'Sullivan, 1997). Celulose I is the native form of cellulose, and two coexisting crystalline structures were identified by $^{13}C$ NMR (Atalla, 1984). Cellulose $I_\alpha$ is triclinic and contains one cellulose chain per crystalline lattice while cellulose $I_\beta$ is monoclinic and has two chains per lattice. The proportion between the two depends on the cellulose source (Sugiyama, 1991). Cellulose II is a more stable form obtained through a treatment in alkaline media (called mercerization) or by cellulose dissolution followed by precipitation (aka regeneration) in a non-solvent (Sarko, 1974). The crystal lattice is monoclinic with two antiparallel chains.
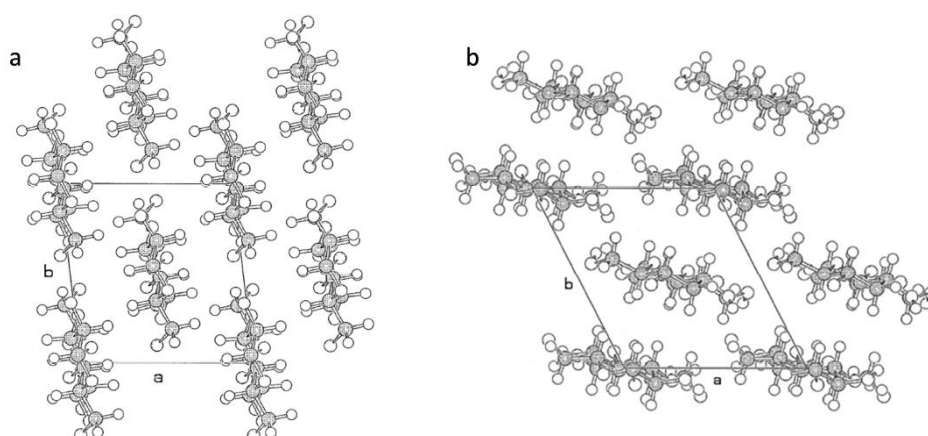


**Figure I.3: Molecular chains arrangements in (a) cellulose $I_\beta$ and (b) cellulose II (Zugenmaier, 2001, reprinted with permission from Elsevier)**

An intramolecular hydrogen bond forms between the OH on $C_6$ on one chain and the oxygen atom on the $C_3$ of another (fig. I.3). Intermolecular hydrogen bonds for cellulose I (see fig I.3 a) are formed between –OH of $C_3$ and the hydrogen on $C_5$, and another between –OH of $C_6$ and

–OH of $C_2$. These interactions give cellulose I a structure in layers, holding together through Van der Waals interactions (Zugenmaier, 2001).

In cellulose II, hydrogen bond structure is modified because of the change in chains orientation. The position of the –OH group on $C_6$ is now reversed as compared to cellulose I, that is *gauche* to the oxygen on $C_5$ and *trans* to the oxygen on $C_4$. Thus there are less intramolecular H-bonds, as the interaction between –OH of $C_6$ and –OH of $C_2$ is now formed between two neighboring chains instead of being intramolecular (figure I.4). The result is stronger bonds between molecular layers, and thus a greater stability of cellulose II as compared to cellulose I (Lagan, Nishiyama and Chanzy, 1999).
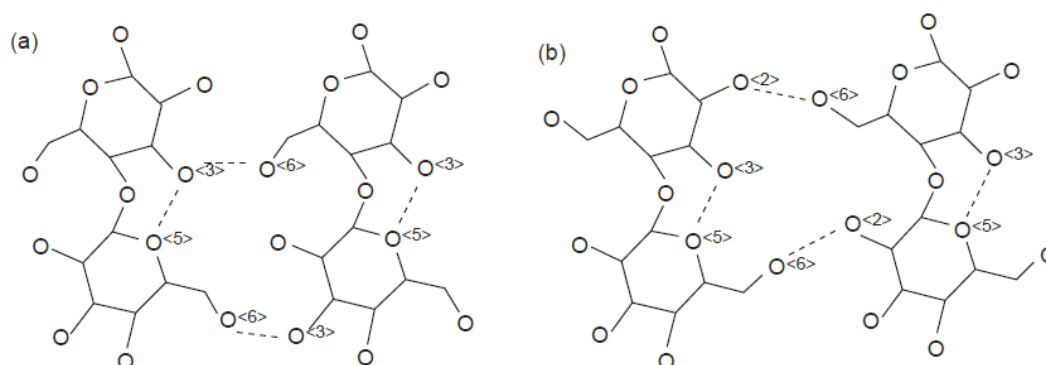


**Figure I.4: Hydrogen bonding structure of (a) cellulose I and (b) cellulose II (reproduced from O'Sullivan 1997, with permission from Springer)**

Cellulose III is obtained by alkaline treatment of cellulose I and II (giving polymorphs $III_I$ and $III_{II}$ respectively) in liquid ammonia or other amines such as ethylenediamine (Sarko, Southwick and Hayashi, 1976). Cellulose IV can be obtained by a heat treatment of cellulose III (Gardiner and Sarko, 1985).

## 1.2. Dissolution and processing of cellulose

### 1.2.1. Solvents for cellulose dissolution

Cellulose cannot melt, since it degrades before reaching its melting point (Stamm, 1956). Cellulose processing is challenging: the strong hydrogen bonds between chains give great stability to its solid form, rendering its dissolution uneasy in most common solvents. For instance, although the numerous hydroxyl functions make cellulose hydrophilic, it cannot be dissolved in water. Water interacts with cellulose by making the fibers "swell" through hydrogen bonds formed between water molecules and hydroxyl groups (Froix, 1975). There are, however, a handful of solvents able to break hydrogen bonds between chains and dissolve cellulose.

Solutions of lithium chloride in N,N Dimetylacetamide have been widely used to dissolve cellulose in an organic media, in order to perform chemical modifications (Dawsey and Mc Cormick, 1990). Cellulose treatment with concentrated alkaline solutions followed by derivatisation (cellulose xanthate) is known as a way of processing cellulose fibers since 1893 (viscose process). Cellulose has been shown to be soluble in NaOH-water solutions within a narrow range of temperatures and NaOH concentrations (Sobue, Kiessig and Hess, 1939). Hydrated N,N methylmorpholine oxide is the basic solvent for another industrial process, called Lyocell (Fink et al., 2001). Finally, a new category of cellulose solvent has attracted interest

over the last two decades: ionic liquids (Swaltowski, 2002). They are less toxic and flammable than most usual cellulose solvents, and allow dissolving cellulose in a wide range of concentrations (Gericke et al 2009; Sescousse et al., 2010). The most relevant solvents or categories of solvents will be presented in details in the following sections.

### 1.2.2.  Water/ sodium hydroxide

Cellulose dissolution in water/NaOH was studied since the 1930s. Sobue (Sobue, Kiessig and Hess, 1939) established the complete phase diagram of the cellulose-water-NaOH system (figure I.5). This work showed that complete dissolution of cellulose was possible in a limited range of temperatures (-10°C to -5°C) and NaOH concentrations (7-10% in weight). Cellulose solubility decreases when increasing the chain length, and cellulose of very high molecular weight cannot be dissolved anymore (Davidson, 1936).
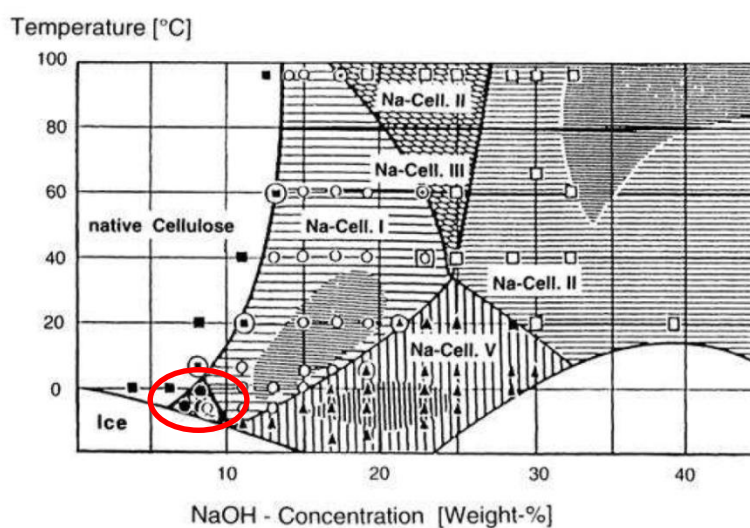


**Figure 1.5: Phase diagram of the water/NaOH/cellulose system (Sobue 1939) with dissolution region shown in red**

Dissolution of cellulose in aqueous NaOH was extensively studied since 80s. A group of Japanese researchers elaborated a method to treat native cellulose pulp with water vapor at high pressure and temperature to ease its dissolution in water-NaOH (Kamide and Okajima, 1987). They determined the main mechanisms involved through CP/MAS $^{13}$C NMR, infrared spectroscopy and X-ray diffraction (Kamide et al. 1987; Yamashiki et al., 1990; Kamide et al., 1992). The weakening of the $O_3$-H--$O_5$ and of $O_2$-H--$O_6$ intramolecular hydrogen bonds of cellulose was identified as the key factor for cellulose dissolution in the alkali solution. Swelling of cellulose (by vapor treatment or direct mixing with water) is a way to weaken the H-bonds. X-ray diffraction and $^{13}$C NMR showed that the disappearance of these hydrogen bonds partially destroyed the crystalline structure, creating new amorphous domains suitable for dissolution by sodium hydroxide.

Solubility of cellulose in water-NaOH varies greatly depending on the cellulose source, molecular weight, and the presence or not of lignin or hemicellulose. Isogai and Atalla dissolved cellulose from different sources and compositions in water/NaOH (Isogai and Atalla, 1998). Their dissolution process consisted in mixing cellulose powder or fibers with an 8-9%wt NaOH solution, freezing the system at -20°C, then thawing it at room temperature, followed by the addition of water to dilute NaOH to 5%wt. Final cellulose concentration was 2%wt. They

showed that while microcrystalline cellulose of low degree of polymerization was well soluble in these concentrations, higher molar mass cellulose such as cotton or kraft pulp were only partially dissolved. However, regenerated cellulose from other solvent systems, in the crystalline forms II and III, has better solubility. The presence of lignin along with cellulose decreases solubility, but hemicelluloses are of little influence.

Cellulose-NaOH solutions are essentially constituted of three parts: (1) free water molecules, (2) sodium hydroxide hydrates made of a core of $H_2O$ molecules bound to NaOH and a shell of amorphous water, and (3) NaOH hydrates bound to cellulose molecules (Yamashiki et al., 1988; Roy et al. 2001; Egal, Budtova and Navard, 2007). It was shown that at least 4 NaOH per anhydroglucose unit (AGU) are needed to dissolve cellulose. The dissolution of cellulose in water-NaOH does not change the amount of free water in the solution. Cellulose-water-NaOH solutions are thermodynamically instable. Rheological studies shown that micro-phase separation of cellulose occurs with time and temperature increase, leading to the formation of gels (Roy, Budtova and Navard, 2003). Time of gelation decreased when increasing cellulose concentration. The instability of cellulose-NaOH solution is problematic for processing, as the solutions cannot be stored for a too long time. The presence of other solutes along cellulose, such as lignin, can have a further destabilizing effect (Sescousse, Smacchia and Budtova, 2010).

Several additives have been studied in order to stabilize cellulose-NaOH solutions, notably urea and thiourea (Zhang et al. 2002; Cai et al., 2004; Zhou et al, 2006; Lu et al., 2011), and zinc oxide (Yang et al. 2011). These compounds were able to form hydrates with free water molecules, thus reducing the free water-cellulose interactions that lead to micro-phase separation and thus to cellulose gelation. Although these additives allowed an easier solvation of cellulose, the cellulose solubility limit was the same as for standard NaOH-cellulose solutions. Moreover, gelation was delayed by the action of the additives, but never suppressed. For example, time dependence of gelation for cellulose-NaOH-ZnO solutions follows a power law, but the addition of ZnO does not change significantly the scaling exponent, because the gelation mechanism of cellulose is not modified (Liu, Budtova and Navard, 2011). Stabilized cellulose-NaOH solutions were easier to use as the basis for regenerated cellulose objects such as membranes and fibers.

### 1.2.3. Viscose process

While direct dissolution of cellulose in water-NaOH is still mostly limited to lab-scale applications, modification of cellulose in alkali media is the basis of the major industrial process for cellulose processing: the viscose process, patented in 1893 (figure I.6).
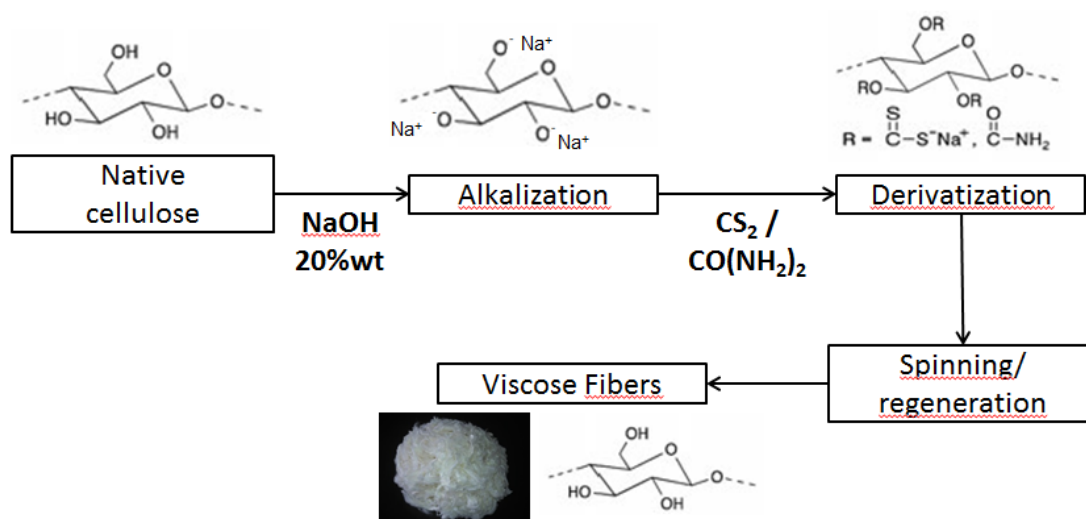
**Figure I.6: Overall scheme of the Viscose and Carbacell processes**

The first step is called mercerization: cellulose is swelled in concentrated NaOH (18-20%wt) to obtain cellulose in the alkaline form. A treatment with carbon disulfide forms cellulose xanthogenate, soluble in the alkali solution. Pure cellulose can then be "regenerated" from the highly viscous solution using an aqueous salt/acid bath. Different materials can be obtained depending on the application: spinning for fibers (Rayon fibers) or casting to obtain films. This process is still the major industrial source of man-made cellulose films and fibers, the latter with a production superior to 2.2 million tons per year (Klemm et al., 2005). However, this process is energy consuming and releases $H_2S$ and $CS_2$, very polluting gases. Cost-effective and less polluting procedures are now privileged when installing new cellulose processing units. The Carbacell process is an alternative using urea as substituent in replacement of $CS_2$, to form the alkali-soluble cellulose carbamate in xylene. After dissolution in concentrated NaOH the cellulose carbamate is spun and regenerated in an acid bath; then the substituent is eliminated by immersing the fibers in an alkali bath at high temperatures. The main advantage of this process is the stability of cellulose carbamate solutions, which can be stored for over one year without significant loss of product quality (Klemm 1998).

### 1.2.4. NMMO/ Lyocell process

An industrial alternative to the viscose process is called Lyocell process, developed by the Austrian company Lenzing (Fink et al., 2001). The basis for this process is the direct dissolution of cellulose in N-methyl morpholine oxide (NMMO) monohydrate between 80 and 120°C (figure I.7), which is possible without any cellulose functionalization. NMMO has the advantage of low toxicity, biodegradability and easy recycling during process. The Lyocell procedure is as follows:

(1) Cellulose dissolution in NMMO monohydrate.
(2) Spinning of the highly viscous cellulose solution into a precipitation bath.
(3) Coagulation of the cellulose fibers in the precipitation bath.
(4) Washing, drying and post-treatment of cellulose fibers.
(5) Recycling of NMMO from regeneration bath and washing residues.
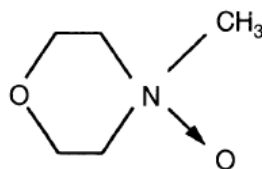
**Figure I.7: Chemical structure of N-methyl morpholine-N oxyde**

The dissolution of cellulose in tertiary amines has been first studied in 1939 (Graenacher & Sallmann, 1939). The preparation of regenerated objects from cellulose coagulated from cellulose-NMMO solutions was extensively studied by Chanzy (Chanzy et al., 1980; Chanzy et al., 1982). Due to the strong polarity of the N-O bond, NMMO is highly hydrophilic and forms strong hydrogen bonds. It is able to break cellulose hydrogen bonds and forms new H-bonds binding with cellulose and the solvent (Harmon et al., 1992). The presence of water in the system is essential to dissolve cellulose; however complete cellulose dissolution is only possible between 13%wt and 17%wt water content. Too low water ratio requires very high temperatures for dissolution, while when water content is higher than 17%wt, cellulose is swollen but not dissolved; at a water content over 35%wt there is no more specific interactions between cellulose and the solvent (Cussinat and Navard, 2006). A water rate of 13.3%wt has been identified as the optimal value for cellulose dissolution.

It is well known that side reactions occur in the cellulose-water-NMMO ternary system (Rosenau et al., 2001). Decomposition of NMMO generates several harmful effects for the Lyocell process, such as unnecessary losses of solvent, release of toxic or explosive compounds, unwanted coloration of cellulose, or even its degradation.

Lyocell fibers can be formed from a broad range of different cellulose sources. They display high strength and stability; however they have a tendency to fibrillate easily, due to a high crystallization ratio and the high orientation of the cellulose chains in the non-crystalline regions (Lenz, 1992). It is possible to modulate Lyocell fibers properties (notably strength and elasticity) and to limit side-effects of chemical degradation of NMMO through the use of various additives, depending on the targeted application (Chanzy et al. 1990).

### 1.2.5. Ionic liquids

Ionic liquids are organic salts with a melting point lower than 100°C, therefore liquid at ambient temperature. Most of them that are dissolving cellulose are quaternary ammonium compounds (figure 1.8). Their properties are extremely interesting for the dissolution of cellulose: high polarity, non-flammability, very high chemical and thermal stability (up to 400°C) and low vapor pressure. There is a large variety of ionic liquids, and their properties can be finely tuned by changing the nature of ammonium substituents, or the counter-anions.
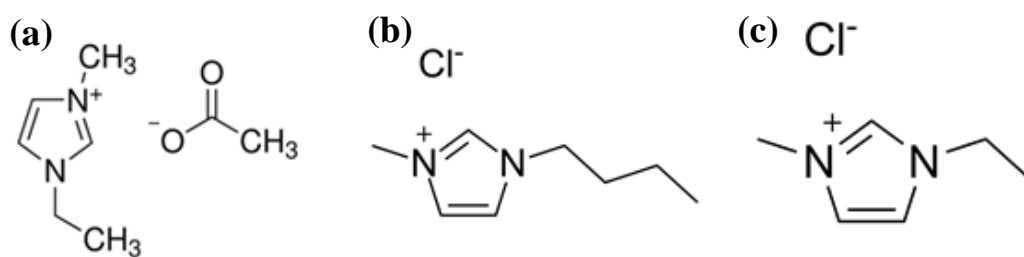
**Figure I.8: Chemical structure of a few ionic liquids commonly used to dissolve cellulose: (a) 1-ethyl-3-methylimidazolium acetate (EMIMAc); (b) 1-butyl-3-methylimidazolium chloride (BMIMCl) (c) 1-ethyl-3-methylimidazolium chloride (EMIMCl).**

The cellulose dissolution capacity in liquid ammonium salts was first reported by Graenacher (Graenacher, 1934) but at that time the dissolution could only take place at temperatures superior to 100°C and the solvent system was not well known. It was not until 2002 that the potential usage of a variety of ionic liquids to dissolve cellulose was studied for various imidazolium based compounds such as BMIMCl, where cellulose could be dissolved at concentrations up to 25%wt (Swaltowski, 2002; El Seoud, 2007).

Solvation mechanism, while not perfectly understood as of today, was investigated by several NMR techniques ($^1$H, $^{13}$C, $^{35/37}$Cl) (Remsing et al., 2006; Zhang et al., 2005; Feng and Chen 2008). Non-hydrated anions can act as electron donors, forming strong hydrogen bonds with the hydrogen atoms on cellulose hydroxyl groups, disrupting the interactions between glucose units. The ammonium cations provide hydrogen atoms acting as electron acceptors, forming new H-bonds with the oxygen atoms of cellulose hydroxyl groups (figure 1.9). In the case of EMIMAc the 1-ethyl-3-methylimidazolium acetate cation appears to form H-bonds preferentially on oxygen atoms with less steric hindrance (Zhang et al., 2010).
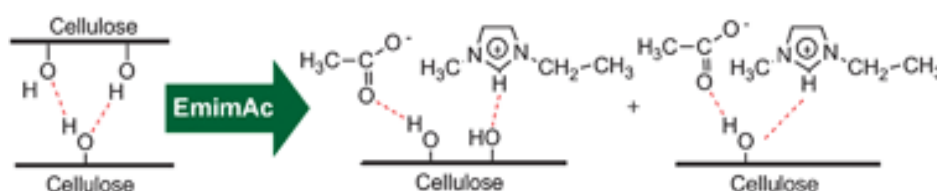


**Figure I.9: Mechanism suggested by (Zhang et al., 2010) for cellulose dissolution in EMIMAc. Reproduced with permission from the Royal Society of Chemistry.**

The understanding of the rheological behavior of cellulose/ionic liquids systems is extremely important for their use in cellulose processing and/or chemical derivatization. The properties of solutions of cellulose in BIMMCl, EMIMAc (Gericke et al 2009; Sescousse et al., 2010) and AMIMCl (Kuang et al., 2008) were thoroughly investigated in the dilute and semi-dilute regimes. Solution viscosity predictably increases with cellulose molecular mass and concentration. For cellulose-BIMMCl and cellulose-EMIMAc, a Newtonian behavior was observed over at least two decades of shear rates. In the case of AMIMCl-cellulose solution, a shear-thinning behavior was reported. It was observed that the intrinsic viscosity of cellulose-IL solutions decreases with increasing temperature, showing a decrease of the thermodynamic quality of the solvent (therefore a potential decrease in solubility). The very high viscosity of ionic liquid systems compared to more traditional solvents can be a hindrance for cellulose processing at high concentrations. The use of organic co-solvents, for example DMSO, is a possibility to lower the system viscosity and limit the overall costs (Le, Rudaz and Budtova, 2014)

The use of ionic liquids provides new opportunities for cellulose forming. Regenerated cellulose objects from ionic liquid solutions such as fibers (Kosan et al. 2008), membranes and films (Cao et al., 2010) or porous materials (Sescousse, Gavillon, & Budtova, 2011; Tsioptsias et al., 2008) were studied in recent years. Ionic liquids also proved themselves to be an interesting media for various cellulose chemical modifications, such as etherification, esterification or silylation (Kölher, Liebert and Heinze 2008; Heinze et al., 2008; Gericke, Fardim and Heinze, 2012).

When using ionic liquids as cellulose solvents, several drawbacks have to be kept in mind. First, the purity of ionic liquids is a concern: even small amounts of impurities can hinder the physical and chemical properties of ionic liquids (Seddon, Stark and Torres, 2000). The presence of impurities can make the recycling of ionic liquids more difficult (Keil, Kick and König, 2012). Commercial EMIMAc in particular, has a purity of 90-95%. The purification techniques have improved over the past years, allowing obtaining ionic liquids with purities over 98-99%. The often high hydrophilicity of ionic liquids means they tend to absorb moisture from the air in high quantities. The presence of water may play an important role on various IL properties, although rheological measurements shown that cellulose dissolution at low concentrations was still possible at a water content up to 15% in EMIMAc (Le, Sescousse, and Budtova, 2011). Secondly, side reactions can occur with ionic liquids when dissolving cellulose or proceeding to chemical modifications. For example, acetylation of cellulose by EMIMAc may happen, generating unwanted by-products (Ebner, 2008; Karatzos, 2011).

Finally, ionic liquids are costly materials, and this is probably the main obstacle to the democratization of their usage, particularly at industrial scale where the new IL/cellulose systems face competition from the well-established Viscose or even Lyocell processes.

## 2. Pectin: structure and properties

### 2.1. General properties of pectins

#### 2.1.1. Origin and molecular structure

Pectins are found in most plants. They are a primary constituent of lamellae and primary plant cell walls, where they bring rigidity and cohesion between cells. They are found associated by physical or chemical bonds with other polysaccharides such as cellulose and hemicelluloses. Depending on the age of plants, pectins are found in two forms, protopectin, insoluble in water because it is linked to other cell components, and water-soluble pectic acid. Protopectin is gradually transformed into pectin by the action of enzymes such as pectinase and pectinesterase (Tilly, 2010). This ripening process diminishes the cohesion of cell walls as the lamellae break, and induces a softening of the fruit.

The pectin molecule is made of linear polymers of D-galacturonic acid linked by 1,4 glycosidic bonds (fig. I.10). The chain has a spiral configuration with a period of 3. Along the galacturonic acid chain several substituents are present: carboxylic acid functions are partially esterified by methanol. The percentage of methyl esterified groups in the pectin chain is called degree of methylation (DM) or degree of esterification (DE).
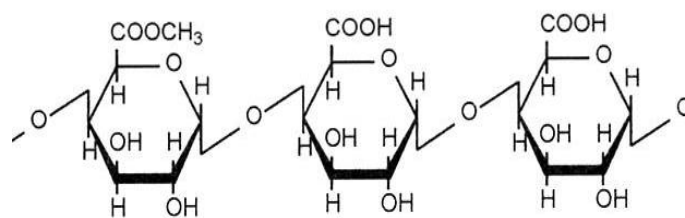
**Figure I.10: Molecular structure of pectin**

Pectin with DE > 50% are called high methylated (HM) pectins, while pectins with DE < 50% are called low methylated (LM) pectins. This factor has a great influence on pectin properties, notably its ability to form gels. The galacturonic acid function can also be amidated during the industrial processing of pectins. Pectin chains are also ramified by short lateral chains made of other polysaccharides (arabinanes, xylanes) attached to the C2 or C3 of the main chain. Deviations in the chain axis, also called "pectic elbows", are caused by inclusions of (r)-L rhamnose. These flexible zones play a role to help the formation of pectin gels (Sila et al., 2009). All commercially available pectins are extremely hydrophilic and readily dissolve in water.

### 2.1.2.    Extraction

The extraction of pectin is performed from waste from fruit juice industry. Apple pomace and citrus peel are the main sources due to their abundance and rich protopectin content. The source material is heated several hours in acidic conditions (pH is 1.5 to 3.5) to hydrolyze protopectin into pectic acid. The insoluble phase is filtered out, and pure pectin is precipitated with isopropanol. This fibrous precipitate is washed, pressed and grinded into a fine powder. The control of temperature, pH, and duration of heating allow tuning the degree of esterification of pectins. Extraction yields high molar mass, HM pectins with DE between 55 and 75%. To obtain LM pectins, de-esterification is done in alkaline or acidic conditions. Amidation of LM pectins can be done by alkaline treatment in an ammoniacal media (May, 1990).

## 2.2.    **Gelation of pectins**

### 2.2.1.    Gelation of high methylated pectins in acidic conditions

One of the most interesting property of pectin is its ability to form gels. Its main applications in the food industry take advantage of these properties, by using pectins as gelling agents or to increase viscosity. Two gelation mechanisms are distinguished: gelation through a combination of hydrogen bonds and hydrophobic interactions in acidic conditions (figure I.11), and cross-linking via electrostatic interactions with divalent ions such as $Ca^{2+}$ (see section 2.2.2).
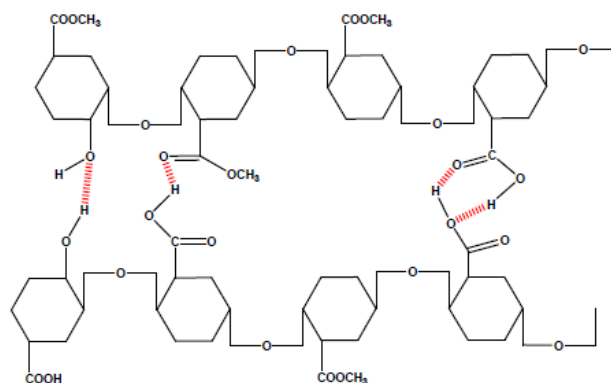
**Figure I.11: Gelling mechanism of HM pectins in acidic conditions (adapted from (Tilly, 2010)).**

In the first case, the gelation can be favored by the addition of sugars. Sugars act as dehydration agents, favoring the hydrogen bonding between chains, and stabilize junction zones by improving hydrophobic interactions (Oakenfull and Scott, 1984). Gelation of HM pectins is only possible when pH is lower than 3.5, when the carboxylic acid functions are protonated which diminishes electrostatic repulsions between chains. A lower degree of methylation increases the gelation time as well as the temperature required to form a gel.

### 2.2.2.  Gelation of pectins with $Ca^{2+}$ binding

The use of divalent cations to link LM pectin chains is the best known way to form pectin gels, and the most used in the food industry. The main mechanism of gelation involves electrostatic bonding of carboxylic moieties by calcium ions. The coordination mechanism is believed to be similar to that of alginate, called "egg-box" model (Grant et al., 1972) (figure I.12). In this model one calcium ion is participating to 9 coordination links between pectin molecules, involving carboxylic and hydroxyl functions. This structure can only exist in regions of the molecule containing only galacturonic monomers, no side chains or pectic elbows, and no esterified functions. The bonds are considered stable when there are at least seven consecutive galacturonic acid monomers (Powell et al, 1982). The egg-box model, while convenient, may not be a perfect description of pectin gelation mechanism: Braccini and Perez (Braccini and Pérez, 2001) simulated several dimers of polygalacturonic acid linked by calcium ions; they established that the calcium gelation occurred in two steps: dimerization through electrostatic interaction with calcium followed by chain aggregation with aging. The gelation of LM pectins also involves inter and intramolecular hydrogen bonding as well as hydrophobic interactions between methyl groups (Walkinshaw and Arnott, 1981).
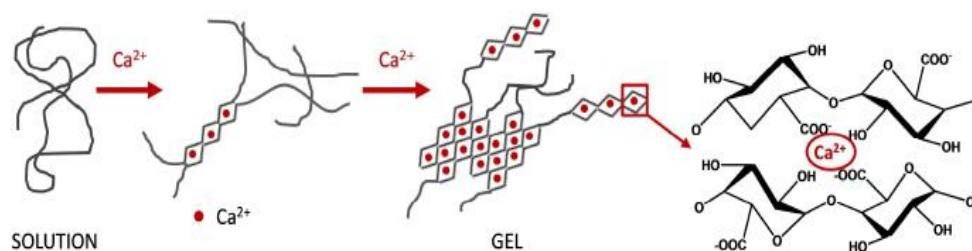


**Figure I.12: Gelling mechanism of LM pectins in the presence of calcium ions (adapted from (Tilly, 2010)).**

The calcium based gelation is generally faster when the DE is lower, because lower DE means a larger amount of free carboxyl groups. A lower DE will actually reduce the required quantity of calcium required for gelation, as the higher number of free carboxyls increases the probability of calcium binding. However, it is possible to gel pectins with higher DE by the action of calcium (Tibbits et al., 1998); in plant cell walls, HM pectins are coordinated by calcium ions. For the calcium binding to be effective, free carboxylic acid groups must be in the deprotonated form; this is achieved at relatively high pH values. If the pH is too high, the gels tend to be very rigid and brittle; the optimal pH value is in neutral conditions (6-8) (Capel et al., 2006; Garnier et al., 1992; Fraeye et al., 2010).

# 3. Silica and bio-based aerogels: properties and applications for thermal superinsulation

## 3.1. Generalities on drying methods

A "gel" is defined as a solid-liquid biphasic system, thermodynamically stable, made of a double interpenetrated tridimensional network, one solid and the other liquid. Aerogels can be considered as gels whose liquid phase was replaced by a gaseous phase, generally air, without too significant degradation (Phalippou and Kocon, 2005). The term "aerogel" was first employed by Kistler (Kistler, 1932) who reported the first synthesis of porous materials from gels dried without destruction of their initial porous structure, using supercritical (sc) drying. Aerogels typically show very high porosity (> 90%) and rather low density. The gel network can be formed either by polymerization of a precursor via sol-gel synthesis, or by physical interactions (such as electrostatic or hydrogen bonds between polymer chains or particles). These two types of gels are defined as "chemical gels" and "physical gels", respectively. There are currently three main drying routes to obtain dry materials: evaporative drying, freeze drying and supercritical drying (Pajonk, 1989).

During evaporative drying, the evaporating liquid forms liquid-vapour meniscus inside the gel porosity (figure I.13). This generates capillary forces, that can be described by the Young-Laplace equation (eq.I.1) The capillary pressure can be high enough to collapse the pores (because of their very small characteristic dimension), provoking cracks, densification and ultimate destruction of the network structure: the resulting materials may not be monolithic, are with high densities and a low porosity. For silica gels a method was developed to considerably reduce the capillary tension through chemical hydrophobization; this allowed obtaining materials with similar properties as for supercritically dried aerogels (so-called ambient dried silica aerogels). However, this chemical grafting does not allow to avoid fragmentation in most cases. This will be discussed in more details in section 3.1.4. In general, materials obtained through evaporative drying at ambient pressure can be called *xerogels*.
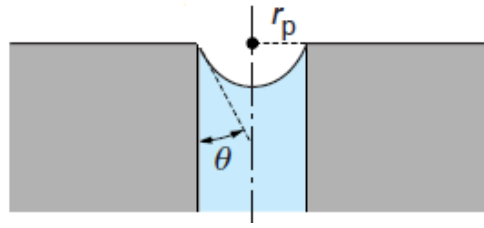
**Figure I.13: Liquid-gas interface within the gel pores during evaporative drying (adapted from Phalippou and Kocon, 2005).**

$$P_c = \frac{2\gamma cos\theta}{r_p}$$ (I.1)

with $P_c$ the capillary pressure inside the pores (Pa)
$\gamma$ the surface tension between the evaporating liquid and gas phase (N.m$^{-1}$).
$\theta$ the contact angle formed between the solid and the liquid (or meniscus angle in °)
$r_p$ the pore radius (m).

Freeze-drying consists of freezing the liquid inside the gel pores and then eliminating it by sublimation under vacuum (Pajonk et al., 1990; Scherer, 1993). As these conditions will provoke direct transition of the solvent from solid to gaseous state, liquid-gas meniscus is less likely to happen. However, the freezing of the solvent by itself can damage the pore structure as the rapid formation of solvent crystals generates strong pressure on the pore walls. Sublimation may not occur perfectly and liquid-gas menisci may form in non-ideal conditions. Generally, the fragile materials such as silica gels are cracked and/or powdered during this process. Because of the formation of large pores during the solvent freezing, freeze-dried gels usually have specific surface area lower than that of supercritically dried gels. Monolithic materials can be formed from more resistant polymeric or organic-inorganic composite gels. Freeze-dried materials are generally called *cryogels*.

Supercritical drying remains the method of choice for the preparation of aerogels. Nowadays supercritical $CO_2$ is the solvent most usually employed due to its very low critical temperature 31°C and its moderate critical pressure 73.7 bars (figure I.14).
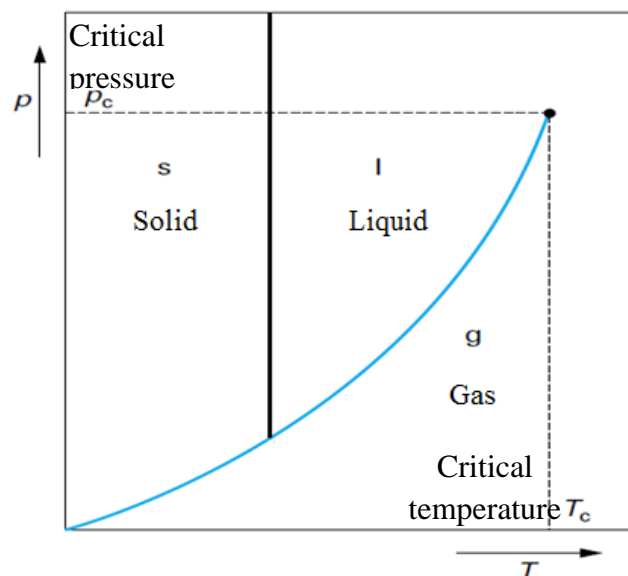


**Figure I.14: Phase diagram of a pure compound, adapted from (Phalippou and Kocon, 2005)**

Beyond its critical point, a fluid has intermediate properties, in-between those of a liquid and those of a gas. Starting from liquid $CO_2$ at low pressure, it is compressed and heated beyond its critical point; then it makes a solution with the liquid phase in the gel pores. To avoid occurrence of capillary tension, it is necessary to operate above the critical point of this "binary" mixture schematically composed of gelation solvent and $CO_2$. Depressurization of the sc phase (mostly $CO_2$ after sc extraction is complete) is performed until it is gaseous at ambient pressure. It must be isothermal (to avoid liquid/gaseous $CO_2$ menisci occurrence because of recondensation) and slow (to avoid fracturation and fragmentation because of very low permeability of the solid matrix). The gas is then extracted and replaced by air through simple molecular diffusion. In this way the liquid phase inside the pores is "extracted" without crossing the liquid-vapor curve (Perrut, 1999; Bisson et al. 2003). The use of supercritial fluids allows forming monolithic and crack-free aerogels presenting limited densification during drying step.
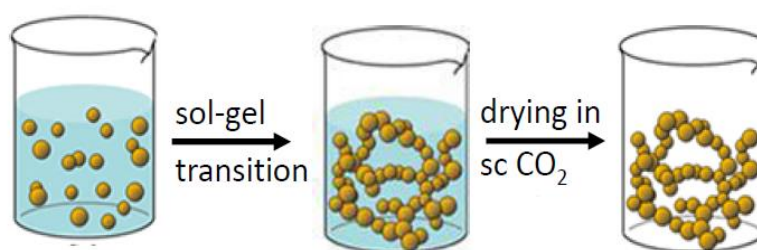


**Figure I.15: Schematic view of the preparation of an aerogel.**

Aerogels can be created from a large variety of organic and inorganic precursors. Inorganic aerogels are mostly synthesized from metal alcoxydes, whose general formula is $M(OR)_x(OH)_y$ with M a metallic or semi-metallic element (e.g. Si, Al, Ti, Zr) and $x + y = 4$. The case of silica gels from silica alcoxydes will be detailed in the following section. Organic aerogels can be made from several polymers, such as polyurethanes (Biesmans et al., 1998; Rigacci et al., 2004), resorcinol-formaldehyde (Pekkala et al., 1990; Mulik and Sotiriou-Leventis, 2011), or polysaccharides (see section 3.2).

Aerogels possess a large range of current and potential applications (Schmidt and Schwertfeger, 2008; Aergeter et al, 2011). A few examples are thermal and acoustic insulation, highly porous catalyst support, depollution through selective absorptions of organic fluids, fuel storage, controlled release of drugs or even space-dust collecting.

## 3.2. Silica-based aerogels

### 3.2.1. Sol-gel process and $SiO_2$ aerogel synthesis from alcoxysilanes

Preparation of silica aerogels starts from an alcoxysilane such as tetraethoxysilane (TEOS) in an organic solvent (very often the solvent is ethanol) (Rigacci and Pierre, 2008). The first step is the hydrolysis of the silane, which can be realized in acidic or basic conditions. Then polycondensation of the hydrolysed species occurs, following two mechanisms simultaneously: condensation of two silanols (Si-OH) groups is called oxolation, while condensation of a silanol on a siloxane (Si-OR) is called alcoxolation. The final texture of the gel can be varied a lot, depending on the synthesis parameters, such as the nature of the precursors, pH, reagent concentrations (Wagh et al. 1999; Pierre and Pajonk, 2002, Rao and Kalesh, 2003), temperature (Colby, Osaka and Mackenzie, 1986), water-to-alcoxyde molar ratio or presence of other

chemical entities (Sinkò, 2010). Gradually a $SiO_2$ tridimensional porous network is formed (Brinker and Scherer, 2013) (figure I.16).
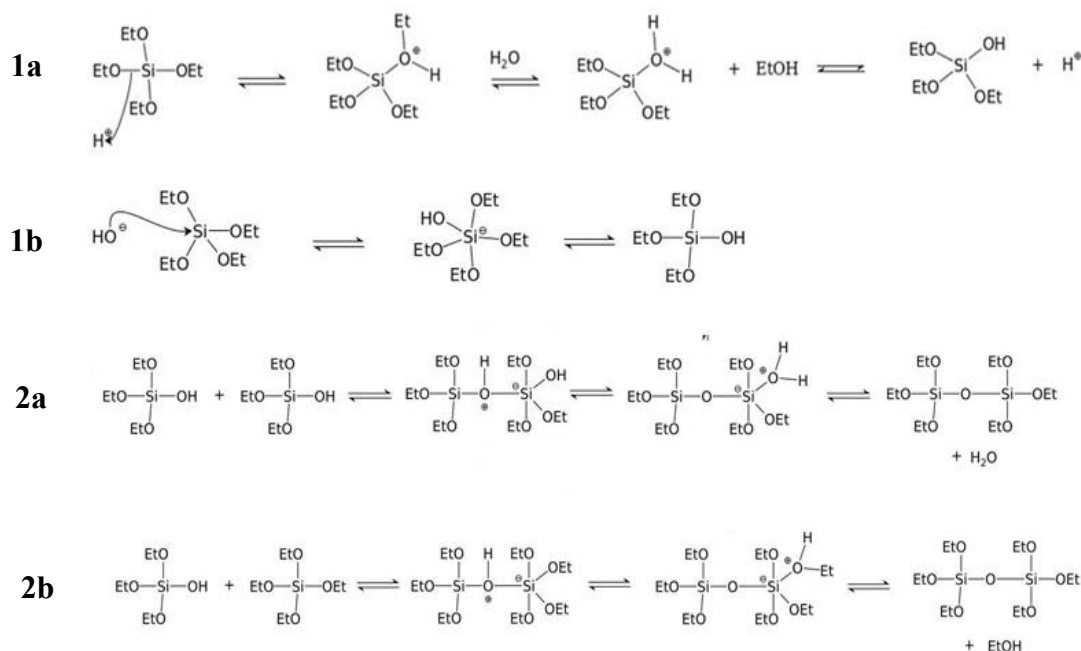


**Figure I.16: Reaction mechanisms of the different steps of the sol-gel synthesis of silica from TEOS. (1a) Hydrolysis in acid conditions; (1b) Hydrolysis in basic conditions; (2a) Condensation of two silanols groups (oxolation); (2b) condensation of a silanol group with a siloxane group (alcoxolation).**

Tilgner and Fisher determined the influence of catalysis type on gel texture (Tilgner and Fisher, 1995). With acid catalysis, hydrolysis is favoured on chain end groups, more accessible and thus easier to protonate. In this case the hydrolysis rate is faster than the condensation one. The result is linear entangled "polymeric" chains. Generally, these gels have lower mean pore sizes than with basic catalysis. Basic catalysis is a nucleophilic attack by $OH^-$ that favours the hydrolysis of silicium atoms with the highest partial charge. The condensation rate is then higher than the hydrolysis rate. Highly branched chains are obtained, and the gel is made of colloidal nanoparticle clusters. Porosity is mainly due to spacing between particles, and mean pore sizes are generally higher than those obtained with acid catalysis. Finally, Tilgner and Fisher investigated fluoride-catalysed formation of silica gels. The mechanism is analogous to basic catalysis, with fluoride anions ($F^-$) playing the role of nucleophile. The final structure of the gel is similar to that obtained in acid conditions with some characteristics coming from basic route.

Two-step processes can be used for a finer control of the gel nanostructuration. Acid-catalyzed pre-hydrolysis is immediately followed by basic (or fluoride) catalyzed polycondensation (Boonstra and Bernards, 1988). This process was used to synthesize the lightest silica aerogel ever made to date, with a bulk density of 0.003 g.cm$^{-3}$ (Kocon, Despetis and Phalippou, 1998).

The influence of water on TEOS based silica aerogel was studied in terms of molar ratio between water and TEOS (so-called hydrolysis ratio). It was determined (Rao and Parvathy, 1993) that an $H_2O$:TEOS molar ratio lower than 2 favorized the condensation reactions as compared to the hydrolysis, where at least a stoechiometric ratio is needed; if the water/alcoxyde ratio gets too high (> 12), the aerogels formed are denser, opaque and cracked.

The optimal water to alcoxyde molar ratio was evaluated between 4 and 10 for the obtention of crack-free and transparent aerogels, with porosities superior to 90% and bulk densities around 0.15 g.cm$^{-3}$ (figure I.17). It has to be kept in mind that the optimal water/alcoxyde molar ratio will vary depending on the silica precursor used.
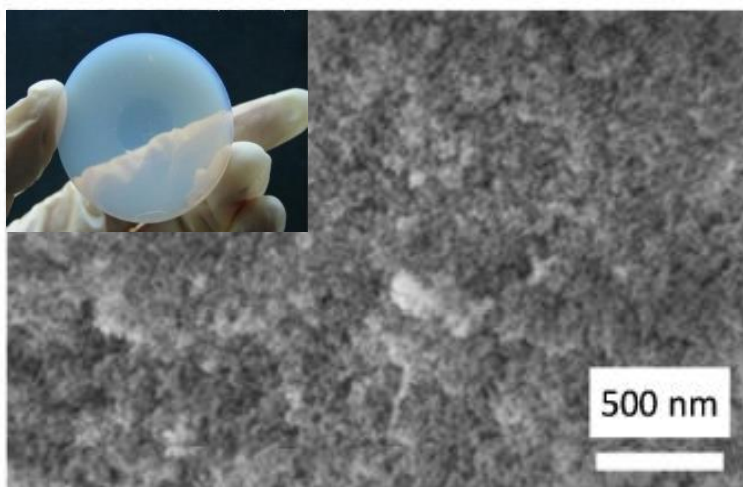


**Figure I.17: SEM micrograph showing the nanostructure of a typical silica aerogel, with a bulk density of 0.18 g.cm$^{-3}$ (Koebel, Rigacci and Achard, 2012) Inset: visual aspect of the aerogel after supercritical drying (courtesy of N. Diascorn, Centre PERSEE, Mines ParisTech.)**

Silica aerogels are highly porous. Overall the porosity of silica aerogels is generally higher than 90%, and their specific surface areas can range from 250 cm$^2$.g$^{-1}$ to more than 1000 cm$^2$.g$^{-1}$ (Zhou et al. 2007). Most silica aerogels are mesoporous materials, with pore size from 5 to 100 nm and an average pore diameter between 20 and 40 nm (fig.I.18).The characteristics of the porous networks such as pore size distribution, specific pore volume can be estimated by nitrogen adsorption (Reichnauer and Scherrer, 2001) or mercury porosimetry (Pirard et al. 1995) with different degree of accuracy, the latter permitting to characterize a significantly wider porous fraction than nitrogen-based technique.
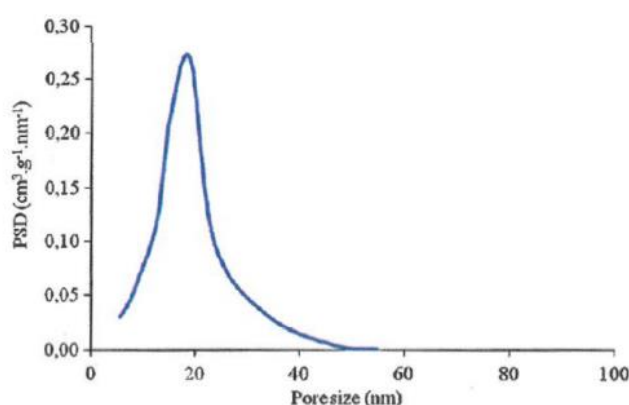


**Figure I.18: Pore size distribution of a 0.15 g.cm$^{-3}$ silica aerogel synthesized from TEOS, as obtained by non-intrusive mercury porosimetry (Pierre and Rigacci, 2011).**

The mechanical properties of pure silica aerogels are known to be poor: they are very brittle and crack easily. Their compressive strength, tensile strength and elastic modulus are low, and strongly dependent on aerogel density (Ma, Roberts, Jullien, Prévost and Scherrer, 2000). As a general rule, the elastic moduli (E) of aerogels exhibit power-law scaling with their densities with E ~ $\rho^m$, with 2.5 < m < 4.

The mechanical reinforcing of silica aerogels without loosing the very low level of thermal conductivity is thus a strategic concern for their large-scale use for massive application like thermal insulation. Several reinforcing methods for silica aerogels have been studied over the past years. They are the preparation of aerogel composites by dispersing fibers (e.g. Parmenter, 1998, Yang et al, 2011) directly inside the silica sol, or the synthesis of organic-inorganic hybrids from precursor containing polymerizable organic chains. Well-known examples of the later are Ormosils (standing for "organically modified silicates") (Mackenzie, 1994) or ceramers (Huang et al, 1985).

### 3.2.2.  Silica aerogels from sodium silicate

Sodium silicate ($Na_2SiO_3$), so-called waterglass, is the historical source of the very first silica aerogels made by Kistler in 1932. Sodium silicate is synthesized from reacting quartz sand with sodium hydroxide or carbonate at elevated pressures and temperatures. The abundance of these starting materials makes it a less expensive silica source. The highly polar nature of $Na_2SiO_3$ renders it easily soluble in water on the contrary of alkoxysilanes (Venkateswara Rao et al., 2011).

Two main chemical routes lead to silica aerogels from sodium silicate: both involve the acidification of $Na_2SiO_3$ into silicic acid, $H_2SiO_3$. The first route is the reaction in one step of the silicate with HCl or an organic acid. This method is fast but results in the formation of sodium salts, which must be washed away through long steps of washing and solvent exchange. The second method involves the acidification of an aqueous sodium silicate solution by passing on an ion-exchange column, a process that removes the sodium ions and thus prevents the formation of salts by-products. The polycondensation and subsequent gelation is catalyzed by adding a base to increase the pH from ~2 to 5-9 (Schfwerterger, Frank and Smith, 1998). A general reaction scheme of sodium silicate gelation is presented on figure I.19.
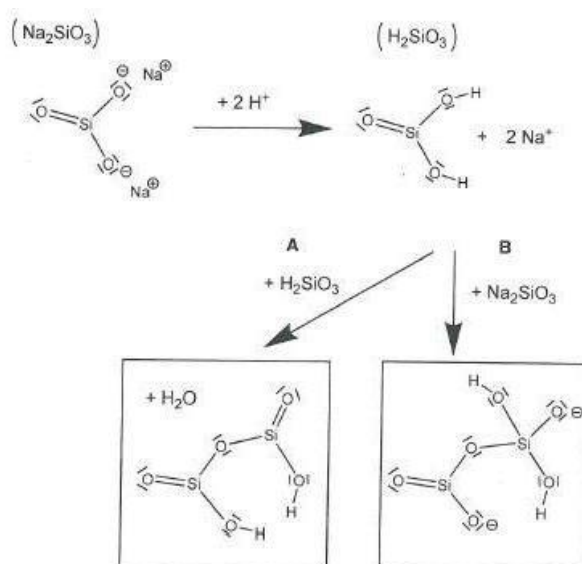


**Figure I.19: Reaction mechanism of the formation of silica from sodium silicate (adapted from Venkateswara Rao et al., 2011.)**

The simplified mechanism presented on fig. I.19 does not take into account the complex chemistry of sodium silicate, strongly dependent on pH. In sodium silicate alkaline solution (pH > 10), negatively charged silicate oligomers of various sizes between two and eight units coexist, and condensation is prevented because of electrostatic repulsion. When the pH is lower

than 4, neutrally charged silicic acid oligomers are the dominant species, which can condensate into small molecular clusters. The complete condensation of these clusters, and thus, sol gelation, is slowed down because partial re-dissolution of silicic species can occur through protonation of oxygen atoms. Moreover, negatively-charged silicium oxide groups are not present at low pH, which slows down the gelation because -Si-O$^-$ is a better nucleophile overall than -Si-OH. When gelation occurs at low pH, aerogels tend to be denser and have slightly lower porosity as compared to what is obtained in more neutral conditions. A pH value between 5 and 9 has been determined as an optimal value for sodium silicate gelation in the given conditions (Rao et al., 2008). Resulting silica aerogels had porosities around 95% and bulk densities lower than 0.1 g.cm$^{-3}$ (figure 1.20).
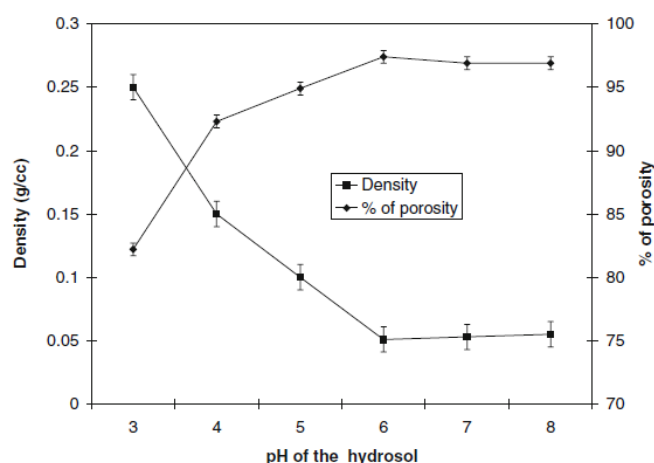


**Figure I.20: Influence of pH on the bulk density and porosity of silica aerogels from ion-exchanged sodium silicate solutions. (from Rao et al., 2008, reprinted with permission from Springer)**

The majority of sodium silicate-based aerogels are made now through the process of ion exchange, followed by basic catalysis. Many authors performed chemical modifications of the gel to obtain monolithic aerogels with hydrophobic properties via ambient drying (Hwang et al., 2007; Bhaghat et al, 2007). In terms of general properties, sodium silicate-based aero- and xerogels are similar to those of their silica alcoxydes counterparts.

In recent years sodium silicate has attracted renewed interest as a cheaper alternative to alcoxysilanes for the larger scale fabrication of silica aerogels. The parallel development of hydrophobization methods for silica gels allowed for the subcritical evaporative drying of silica aerogels, by definition less resource consuming than supercritical drying. This is why most of the recent research on sodium silicate-based aerogels focuses on ambient pressure dried materials.

### 3.2.3. Hydrophobization of silica aerogels

During the sol-gel process, some of the alcoxyde side-chains remain unreacted, or stay in the form of silanol functions ≡Si-OH. When hydroxyl groups are found at the pore surface of silica aerogel, they render the gel hydrophilic and interact with water vapours. In some cases silica aerogels can be very hygroscopic. Hydrophilicity induced by the silanol surface groups of pure silica aerogels can be a problem for several applications. First, as seen in section 3.1.1, an hydrophilic gel cannot be dried at ambient pressure, because of high surface tension leading to high capillary pressure and thus inducing pore collapse and densification during drying. Secondly, moisture sensitivity can be harmful for the long-term use of silica aerogel, as

properties will deteriorate over time when adsorbing water (Miner, 2004). As a consequence it is not surprising that a lot of research focuses on various chemical modification techniques to render silica aerogels hydrophobic (Anderson and Caroll, 2011).

To obtain hydrophobic silica aerogel, the polar hydroxyl groups must be replaced through chemical modification by apolar functions such as alkylsilanes ($\equiv$Si-CH$_3$). The structure of three common hemical modification agents is presented as an illustration on figure I.21.



MTMS          HMDSO          HMDZ
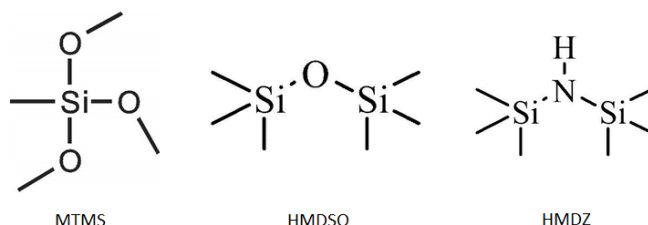
**Figure I.21: Chemical structure of three common hydrophobization agents used for the preparation of hydrophobic silica aero- and xerogels. From left to right: methyltrimetoxysilane (MTMS), hexamethyldisiloxane (HMDSO) and hexamethyldisilazane (HMDZ).**

Three main routes are reported for making hydrophobic silica aerogels. Vapor phase treatment can be used on dry aerogels: they are exposed to gaseous methanol at high temperatures (220-240 °C) (Lee et al., 1995). The effective replacement of Si-OH groups by Si-OCH$_3$ is visible by FTIR spectroscopy as the characteristic silanol peaks disappear over time; 10 to 40 hours of treatment are necessary. Among some obvious drawbacks of this method are the duration of treatment and double drying. Moreover the alcoxy groups can be re-hydrolyzed over time as the chemical process is reversible.

The co-precursor route is much more used and effective; it makes a large part of the literature on hydrophobic silica aerogels. The starting alcoxysilane is mixed in solution with another alcoxysilane with alkyl terminal chains, such as methyltrimethoxysilane (MTMS) (Schwertfeger et al., 1992). The sol-gel process and subsequent drying are then carried out, yielding a gel containing a certain apolar groups concentration. Several additional studies on MTMS were performed by Rao et al. (Rao and Pajonk, 2001; Rao et al. 2003). The hydrophobicity and transparency of tetramethoxysilane (TMOS)/MTMS aerogels was found to depend on the molar ratio between precursors: higher MTMS content gave better hydrophobicity but higher opacitybecause of the creation of large pores during the synthesis. Contact angles with water could go up to 140°. A good compromise aimed at applications for transparent insulating panels was an MTMS/TMOS molar ratio of 0.7 that gave 80% light transmittance at 750 nm, along with a contact angle of 110° stable in time (Rao, Pajonk and Haranath, 2001). A pure MTMS aerogel showing contact angles of 152° was synthesized by Baghat (Baghat et al., 2007).

MTMS derived aerogels also show good flexibility and elasticity: bendable silica aerogels have been obtained, either from pure MTMS (Rao et al., 2006; Hedge and Rao, 2007), or by using MTMS along with other alkylsilane precursors (Hayase et al., 2011). The flexible aerogels reported were able to sustain up to 60% elastic deformation and their Young moduli ranged from 0.034 to 0.13 MPa (figure I.22). Flexible gels were also achieved from mixing TMOS with vinyltrimethoxysilane, a co-precursor containing vinyl groups. This gel was further strengthened by adding bis [3-(triethoxysilyl) propyl] disulfide to the mixture, providing cross-

linking thanks to disulfide bridges, resulting in a fully elastic gel whose contact angle with water was 125° (Guo et al.,2009). While MTMS is one of the less expensive co-precursors available within this family, several other co-precursors containing perfluoroalkylsilanes (Zhou et al., 2007) or alkylsilanes (Rao and Kalesh 2004; Baghat and Rao 2006; Aravind, Niemeyer and Ratke, 2013) moieties were examined. An increase in the contact angle with water when the chain length of the co-precursor is increased was observed. In these cases, both supercritical and ambient drying can give highly porous materials, with densities lower than 0.1 g.cm$^{-3}$. The presence of a non-condensable apolar group in polysiloxane chains induces the formation of large pores during the sol-gel synthesis; thus the thermal conductivities of these materials are often higher than those of other silica aerogels (Maleki, Duares and Portugal, 2014).
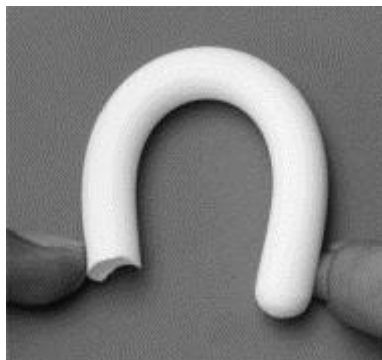


**Figure I.22: Bendable silica aerogel from MTMS derived gel, dried in supercritical CO$_2$. Molar ratio between MTMS:EtOH:H$_2$O was 1:35:8 (from Rao et al., 2006)**

Finally, another alternative is the surface silylation of the wet gel before drying (i.e. after gelation). In this method an already formed silica wet gel goes through solvent exchange and is immersed in a solution containing the functionalizing agent. The reaction is generally performed at mild temperatures between ambient and 100°C. This method is often chosen for the preparation of xerogels through ambient pressure drying. However, silylation processes can be long to complete because of the solvent exchange steps involved and the diffusion of the silylating agent in the mesoporosity of the gels. As opposite to the co-precursor method, in which hydrophobic groups are present in the bulk of the sample, the surface sililation only covers the pore walls with hydrophobic groups. The chemicals used for surface functionalization are often chloroalkylsilanes: trimethylchlorosilane (TMCS) is the best known, and has been used to obtain hydrophobized aerogel powders (Jeong et al, 2000) as well as monolithic materials (Wei et al., 2007). Hexamethyldisilazane (HMDZ) is another silylation agent (figure I.23) used in basic conditions. Aerogels treated with HMDZ in different organic solvents were reported (Shewale et al., 2008; Rao et al., 2005). They all showed very high contact angles with water around 140-160°. Hexamethyldisiloxane (HMDSO) can also functionalize gel surface with HCl catalysis (Bisson, 2004; Achard et al., 2007).
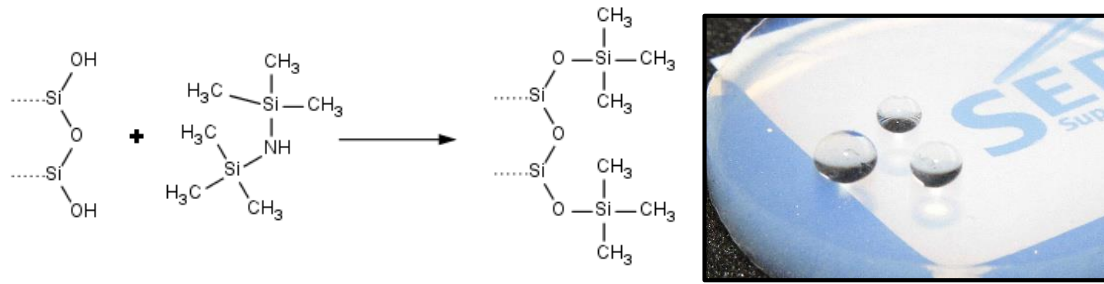
**Figure I.23: Silylation of silica aerogel surface with HMDZ and water droplets on the surface of an HMDZ-modified silica aerogel. Photo courtesy of SEPAREX S.A., Nancy, France.**

As the functionalization is performed on the already formed silica gel, most surface silylation is also applicable to sodium silicate based gels (Lee, Kim and Hyun, 2002; Shewale et al., 2009; Shi et al., 2006; Bangi et al. 2008). This is of particular interest for the large-scale application of silica aerogels, as the combination of ambient pressure drying and availability of sodium silicate makes it a rather inexpensive process. However, the steps of ion-exchange and solvent exchange remain time and energy consuming.

Rao et al. compared the effect of different modifying agents, as well as the co-precursor and surface silylation methods (Rao et al., 2003). They concluded that better hydrophobization was achieved with tri-alkyl compounds as compared to mono-alkylsilanes, as assessed by respective contact angles of 135° against 95°. They also observed that aerogels from the co-precursor method were more hydrophobic but less transparent than the silylated aerogels.

### 3.3. Thermal properties of aerogels: applications to superinsulation

#### 3.3.1. Heat transfer in aerogels

The remarkable thermal properties of aerogels were studied ever since Kistler synthesized the first silica aerogels in 1932. Silica aerogels in particular are the most popular superinsulating materials: the thermal conductivity of most silica aerogels is significantly lower than 0.025 $W.m^{-1}.K^{-1}$, the conductivity of air in ambient conditions, so-called "free air".

The heat transfer in aerogels can be described by the heat transfer equation and the Fourier Law which states that the heat flux density is proportional to the local temperature gradient and defines the thermal conductivity λ (equation I.2 and I.3) (Ebert, 2011).

$$\nabla \vec{q} + \Phi = \rho.c.\frac{\partial T}{\partial t} \qquad \text{(I.2)}$$

$$\vec{q} = -\lambda \nabla T \qquad \text{(I.3)}$$

with q the heat flux density, λ the thermal conductivity, ρ material bulk density, c its specific heat, Φ the heat source term describing the thermal radiation and T the local temperature. In the case of an isotropic aerogel, and if the heat transfer only depends on the temperature gradient, the heat transfer equation simplifies to eq. I.4:

$$\Delta T = \frac{\rho.c}{\lambda}.\frac{\partial T}{\partial t} \qquad \text{(I.4)}$$

in which case the thermal conductivity is a material property and do not depend on the experimental conditions of its determination.

The thermal transport in aerogels is made of three components: solid heat transfer along the aerogel backbone, gaseous conductivity from the gas inside the pore structure and radiative heat transfer. The effective conductivity can be simply deduced from the sum of all three contributions when thermal conditions and materials characteristics (optical thickness) permit to decorrelate thermal transferts by conduction and radiation (eq. I.4).

$$\lambda_{effective} = \lambda_{solid} + \lambda_{gas} + \lambda_{radiative}$$

(I.5)

A brief overview of each contribution will be presented in the following sections.

### 3.3.2. Solid thermal conductivity

The heat transfer through the aerogel backbone depends directly of the skeleton structure and connectivity, as well as its chemical composition. Heat transfer is mainly due to diffusing phonons within the chains of the aerogel backbone. The diffusion of phonons can be described with equation 6.

$$\lambda_{solid}(T) = G(\rho).\frac{1}{3}.\rho_0.c_v(T).l_{ph}(T).v_0(T)$$

(I.6)

with $\lambda_{solid}$ the solid thermal conductivity (W.m$^{-1}$.K$^{-1}$), $\rho_0$ the density of the backbone material (kg.m$^{-3}$), $c_v$ its specific heat at constant volume (J.kg$^{-1}$.K$^{-1}$), $l_{ph}$ the average mean free path of phonons (m) and $v_0$ the average velocity of the elastic waves within the backbone material (m.s$^{-1}$). G is a temperature independent geometric factor only depending on apparent density (Scheuerpflug et al. 1991).

At a given temperature, the thermal conductivity of the solid backbone only depends on the material apparent density $\rho_{app}$ following a power law; eq. 6 can thus be simplified:

$$\lambda_{solid} = C.\rho_{app}^{\alpha}$$

(I.7)

with $C$ a constant. The exponent factor alpha was determined to be around 1.5 for silica aerogels. (Fricke et al., 1992; Lu et al., 1993).

### 3.3.3. Gaseous thermal conductivity

Because of the very small size of pores in aerogel materials, the gas is confined in the porosity, and as a consequence the gas contribution is much lower than the conductivity of the free air (Knudsen effect). The gas confinement inside the pores is the main reason superinsulation can be achieved with ultraporous materials like aerogels. The heat transfer in the gas is characterized by the Knudsen number K$_n$:

$$K_n = \frac{l_g}{D}$$

(I.8)

with $D$ the pore diameter (m) and $l_g$ the free mean path of the air molecules

$l_g$ is determined by:

$$l_g = \frac{kT}{\sqrt{2}\pi d^2 P}$$

(I.9)

with $k$ the Boltzmann constant ($k=1.38.10^{-23}$ J.K$^{-1}$), T the temperature (K), $d$ the diameter of gas molecules ($d = 3.7.10^{-10}$ m for air), and P the pressure of gas (Pa). For air at 300 K and 1 bar, $l_g$ $\approx 70$ nm.

The gas heat transfer is described by:

$$\lambda_{gas} = \frac{\lambda_{g0}.\varepsilon}{1 + \alpha K_n} \tag{I.10}$$

with $\varepsilon$ the porosity, $\lambda_{g0}$ the thermal conductivity of free air, $\alpha$ a coefficient depending on the nature of the gas and the solid (i.e. interaction of gas with the pore walls).

When $D \gg l_g$, $K_n \ll 1$, which means that gas molecules are not confined and the majority of collisions happen between two gas molecules; in this case the gas thermal conductivity is equal to the free gas conductivity which is in case of air 0.025 W.m$^{-1}$.K$^{-1}$. When $D < l_g$, $K_n < 1$, which means that the majority of collisions happen between the gas molecules and the solid backbone. As a consequence, $l_{gas} < l_{g0}$. This phenomenon is called the Knudsen effect and gas is considered to bbe confined, as illustrated by figure I.24.
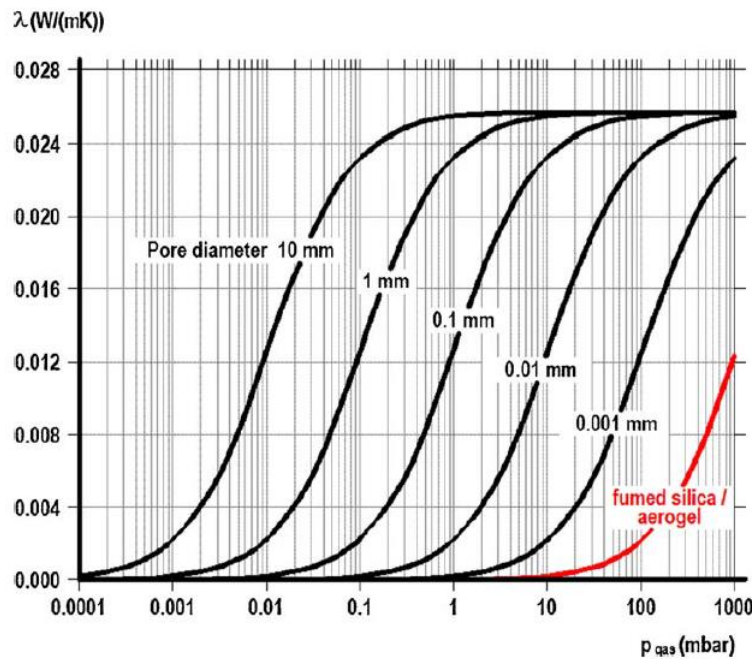


**Figure I.24 : Variation of the thermal conductivity of air contained in porous materials, as a function of pressure, plotted for different pore diameters. Reproduced from (Baetens et al., 2011), with permission from Elsevier.**

Because of the Knudsen effect, control of the aerogel pore sizes is extremely important to obtain superinsulating materials by significantly reducing the gas conductivity.

### 3.3.4. Radiative thermal conductivity

The radiative heat transfer in a material is dependent on its optical thickness $\tau$, representative on how often a photon with the mean free path $l_{pht}$ will interact with the material in a given distance $d$. We have $\tau = \dfrac{d}{l_{pht}}$. The radiative contribution to thermal transport can be expressed as:

$$\lambda_{radiative} = \frac{16}{3} n^2 . \sigma . \frac{T_r^3}{\rho . e_r} \tag{I.11}$$

with $\sigma$ the Stefan-Boltzmann constant, ($\sigma$ = 5.67.$10^{-8}$ W.m$^{-2}$.K$^{-4}$), $T_r$ the mean radiative temperature (K), $e_r$ the specific extinction coefficient (m$^{-1}$) and n the refractive index.

The so-called "radiative conductivity" is inversely proportional to material bulk density. To reduce the radiative transfer in silica aerogels, opacifiers can be loaded to reduce their optical thickness. Suitable opacifiers have high absorbing or light-scattering properties; carbon black or titanium dioxide are two respective examples (Kuhn et al.,1995; Lee et al., 1995).

### 3.3.5. Aerogels for thermal superinsulation

Thermal conductivity of some aerogels is significantly lower than 0.025 W.m$^{-1}$.K$^{-1}$, the conductivity of air, thus they really can be called superinsulating materials. These thermal insulation properties of aerogels make them suitable candidates for many fields of insulation applications, particularly the buildings sector where thin insulation is a very challenging issue.

Silica-based aerogels are considered to be very promising atmospheric pressure insulation materials. However, monolithic aerogel plates are generally fragile and it is difficult to produce crack-free plates of large size to address panel-based applications. Most of commercial applications use either aerogels granules, or "blankets" which have been considered for long like aerogel granules "linked" with fibers. Recently it was shown that such blankets had actually few real macropores as compared to granular beds, and that the macropores present were mostly due to small internal cracks (Diascorn, 2014). Some glazing solutions use monolithic translucent plates (fig. I.25.a).



**Figure I.25: Silica aerogel-based superinsulation materials aimed at various potential applications in the building domain. (a) Transparent aerogel glazing panel developed in the frame of the HILIT+ European project; (b) Aerogels blankets (here from the company Aspen Aerogels). (c) Render with dispersed aerogel granules developed by EMPA (Switzerland) and Fixit. Pictures taken from (Koebel et al., 2011 and Baetens et al., 2011), reproduced with permission from Springer and Elsevier respectively.**

Organic or quartz fibers are used in aerogel blankets to obtain more flexible and structurally resistant insulating materials for the retrofitting of walls (fig. I.29 b). Ambient pressure blankets started to be marketted, the better known are the Spaceloft® blankets produced by the north-american company Aspen. The main disavantage of aerogel blanket is their tendency to release quantities of thin powder: they require anti-dust protective equipment to be manipulated safely.

Aerogels granules are easy to manipulate. Cabot corporation is the main supplier of aerogels powdered or granular materials with its Nanogel® (now marketed as Lumira®) products. For

instance, they can be used to fill the space between two transparent panels to obtain translucent insulating windows, or dispersed in a solid matrix such as concrete or render (fig. I.29 c).

The main competition for aerogels in terms of superinsulation comes from vacuum insulation panels (VIP). Vacuum insulation panels are made of core of pressed mesoporous powder, generally fumed silica with IR opacifiers and short fibers, wrapped in a several layers of aluminum barrier foil. The material is evacuated below 1 hPa pressure and sealed, which effectively suppress the gas contribution to thermal conductivity, allowing VIPs to reach conductivities as low as 0.005 $W.m^{-1}.K^{-1}$. However, VIPs performances tend to decrease with time because of the loss of vacuum; VIP are also fragile and have to be handle delicately.

Finally, the price of silica aerogel-based materials is a real hindrance to their large scale development and applications. A current reference market price for a cubic meter of silica aerogel is on the order of 4,000 US$. With increasing commercialization, this value could drop below the 1,500 US$ mark by the year 2020 (Koebel et al., 2012).

## 3.4. Polysaccharide-based aerogels

Aerogels from polysaccharides have somewhat similar properties as compared to inorganic or other polymeric aerogels: they are highly porous and have low densities and quite high specific surface areas. They can be potentially used for numerous applications such as controlled drug release (Smirnova, 2011), catalysis (Quignard, 2008), or can be pyrolyzed to give carbon porous materials for electrochemical applications (White, 2009) like standard organic aerogels (e.g. resorcirnol-formaldehyde ones). In the following section we will only focus on aerogels from cellulose and pectin, as they are the materials of interest for the present study.

### 3.4.1. Cellulose aerogels

The general route to prepare cellulose aerogels based on cellulose II, often called "Aerocellulose", is summed up in figure I.26. This rather new type of aerogels was done by coagulating cellulose solutions in a non-solvent such as water or ethanol, followed by the standard drying with supercritical $CO_2$.
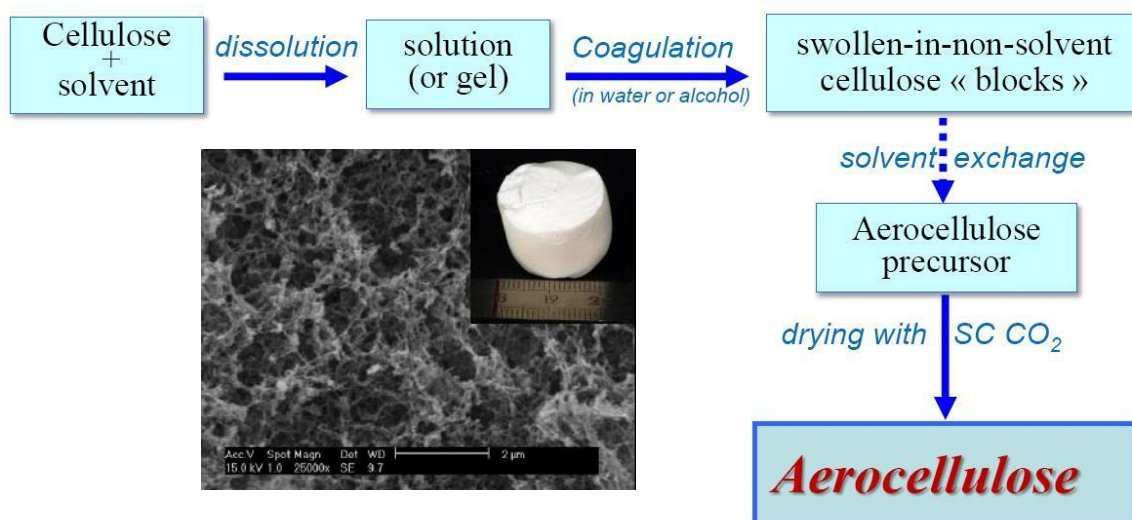


**Figure I.26: General preparation route of Aerocellulose. Inset: visual aspect and microstructure (as seen by SEM) of an aerocellulose made from 8%wtNaOH-water solution.**

Aerocellulose have been synthesized from a large variety of cellulose solvents. Aerogels with bulk densities ranging from 0.02 g.cm$^{-3}$ to 0.2 g.cm$^{-3}$ and specific surface areas ranging from 100-400 m².g$^{-1}$ were obtained from coagulated cellulose-NMMO solutions (Innerlohinger, 2006; Liebner et al., 2008). Water-NaOH or LiOH-cellulose solutions are thermodynamically unstable and spontaneously form gels over time or when increasing temperature. This property helps shaping Aerocellulose (Gavillon and Budtova, 2008; Cai et al., 2008). Ionic liquids are another direct cellulose solvent that can be used as the basis for elaborating aerocellulose (Aaltonen and Jauhainen, 2009; Sescousse et al., 2011; Tsioptsias et al., 2008; Deng et al., 2009).

Cellulose cryogels can also be obtained from freeze-drying of cellulose gels. Highly porous cellulose films were obtained from cellulose-calcium isocyanate solutions: cellulose could be dissolved in the salt hydrate at 110°C, and then a gel was formed by cooling the solution. The gels were freeze dried to obtain shock resistant porous films (Jin et al., 2004). Monolithic materials with bulk densities around 0.065 g.cm$^{-3}$ were obtained from supercritical and freeze drying, using the same cellulose dissolution method (Hoepfner, 2008).

Cellulose aerogels cited above are made of coagulated cellulose, in the crystalline form of cellulose II. However, cellulose I can also be used for making cellulose aerogels or cryogels, for example, from bacterial cellulose (Liebner et al., 2008), or from cellulose nanofibers dispersions (Kettunen, 2011; Cervin et al., 2012). Recently, an aerogel from surface-carboxylated cellulose nanofibers, dispersed in a nematic liquid crystalline order was reported. This new type of cellulosic gel was transparent, had good mechanical resistance and thermally superinsulating properties with a minimal conductivity in room conditions of 0.018 W.m$^{-1}$.K$^{-1}$ (Kobayashi, Saito and Isogai, 2014).

The nature of the solvent has a strong influence on the final morphology of aerocellulose. In the case of NaOH, LiOH, and calcium isocyanate, solutions are gelling and these gels are then coagulated; as a result a fibrous network of entangled "fibres" is formed. When NMMO or ionic liquids are the solvent, cellulose is directly coagulated in a non-solvent, resulting in a more nodular structure (figure I.27). The difference in phase separation mechanisms during the gel formation can explain the morphological differences in the final aerogels. In the case of spontaneous gelation of solution, a micro-phase separation occurs because of the thermodynamical instability of the solution; cellulose chains reorganize and self-associate. For cellulose-NMMO and cellulose-EMIMAc systems, coagulation happens in one step called spinodal decomposition, forming small spherical beads (Biganska and Navard, 2009).
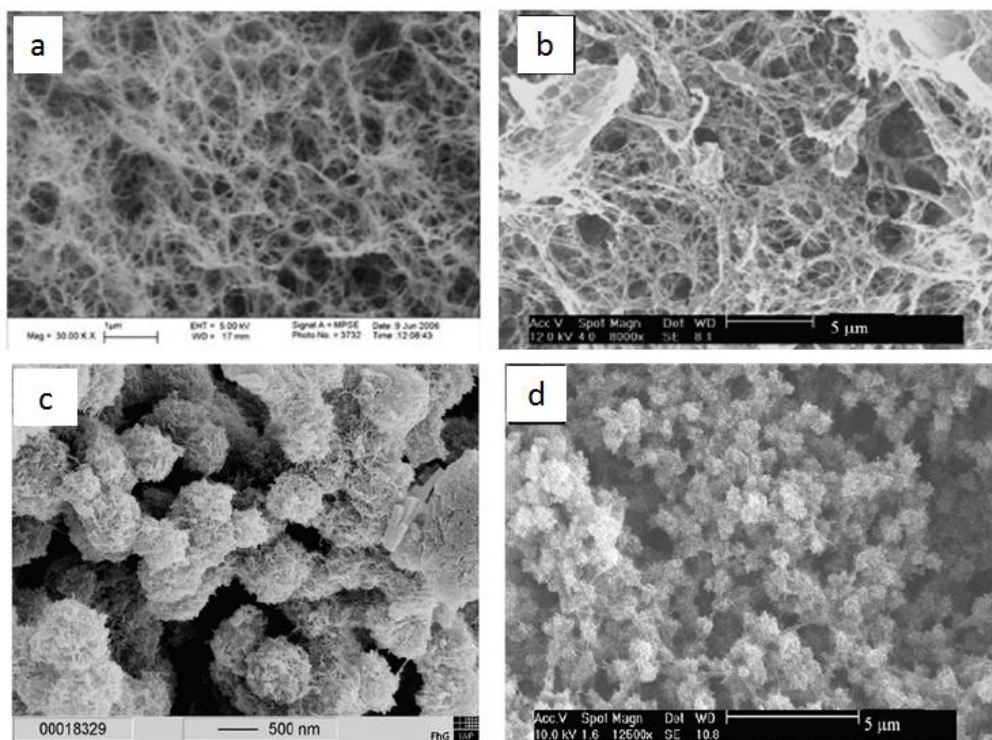
**Figure I.27: SEM images showing the morphology of aerocelluloses from different solvents. Fibrillar structures are observed in the case of cellulose gelled in (a) calcium isocyanate (Hoepfner 2008) and (b) Water-NaOH (Gavillon and Budtova, 2008), while nodular, hairy beads structure is observed for samples coagulated from (c) NMMO monohydrate (Gavillon and Budtova, 2008) and (d) ionic liquid ( EMIMAc) (Sescousse et al., 2011).**

Aerocellulose density is directly proportional to cellulose concentration in solution. Using cellulose of higher molar mass gives higher bulk density at equal concentration. The pore size distributions in aerocelluloses are wide, ranging from a few nanometers to a few microns.

Mechanical properties of aerocellulose were studied by uniaxial compression tests (Sescousse et al. 2011). Stress-strain curves were studied for aerocellulose from water-NaOH and ionic liquid solutions, to determine Young's modulus and yield stress. As for silica aerogels, the modulus depends directly on bulk density following a power law. The exponent factor for aerocellulose is around 3, which is similar to silica or resorcinol-formaldehyde (Pekala et al., 1990) aerogels and not to polymer foams, for which the exponent predicted by Gibbson and Ashby's model is 2 (Gibbson and Ashby, 1999).

Chemical cross-linking of cellulose derivatives such as cellulose acetate (Tan et al., 2001; Fisher et al., 2006) can also yield cellulosic aerogels. Cellulose acetate is cross-linked by isocyanates in acetone; pyrydin or dibutylin dilaurate are used as catalysts. Direct cross-linking of cellulose is also possible, for example by using epichlorhydrin (ECH) (Bai et al., 2006; Rudaz, 2013), or isocyanates. By varying the amount of cross-linker and the cellulose concentration, the structure of the aerogels can be controlled more precisely. Density and mechanical strength increase when increasing the cross-linker to glucose unit molar ratio. When cellulose is reticulated with isocyanates, thermal conductivities of 0.015 $W.m^{-1}.K^{-1}$ can be obtained on supercritically dried samples. However it is unlikely that such aergoels see large–scale development, as isocyanate are very toxic compounds. In the case of ECH-reticulated cellulose, an optimal molar ratio was identified as ECH/anhydroglucose unit = 0.5

(stoichiometric ratio): it resulted in the maximal specific surface area and the lowest thermal conductivity (0.026 $W.m^{-1}.K^{-1}$) for ECH-crosslinked cellulose samples (Rudaz, 2013).

### 3.4.2. Pectin aerogels

The first report on pectin aerogels or Aeropectin is rather recent (White et al., 2010): the goal was making porous carbon materials by pyrolysis of pectin aerogels. Two methods were used to produce pectin gels from citrus: thermal gelation by heating a pectin solution at 90 °C, and dissolving pectin in an acidic aqueous solution, then leaving it to gel at room temperature for 48 h. The gels were progressively solvent exchanged with ethanol and dried with supercritical $CO_2$. In the case of thermal gelation, a fine powder was obtained, while gelation in acid conditions yielded monolithic materials. The powders were denser than the monoliths (0.20 $g.cm^{-3}$ against 0.07 $g.cm^{-3}$, both for a pectin concentration in solution around 5%wt); observation of their structure by SEM (fig. I.28) showed that the structure of the monolithic aerogels was that of a fibrous nanostructured network, while the powders were made of more compact blocks. Specific surface areas were similar to other polysaccharide based materials, monolithic materials showed a specific surface area around 200 $m^2.g^{-1}$.
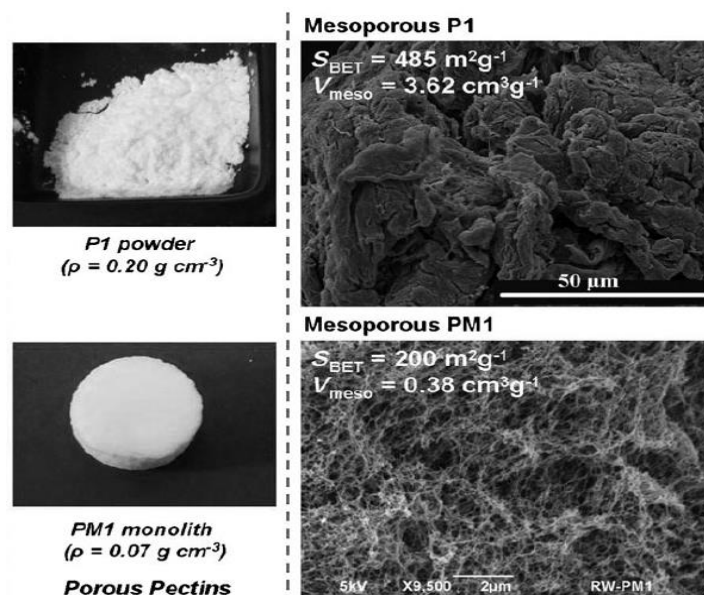


**Figure I.28: Visual aspect and SEM micrographs of powdered and monolithic aeropectins obtained by (White et al, 2010, reproduced with permission from John Wiley & Sons).**

Similar results were obtained by other authors (Garcìa-Gonzales et al. 2012). They obtained aeropectin with incorporated magnetic particles from 6%wt pectin aqueous solutions heated at 40-60°C; the pectin was coagulated by direct addition of ethanol to the mixture. Washing the gel with ethanol and supercritical $CO_2$ drying lead to aerogels with densities around 0.08 $g.cm^{-3}$ and specific surface areas around 250 $m^2.g^{-1}$. Pectin-clay biodegradable composite cryogels were obtained by (Chen et al. 2013). The authors investigated reticulation of pectins with monovalent ($Na^+$), bivalent ($Ca^{2+}$) and trivalent ($Al^{3+}$) cations, in the presence of montmorillonite. As expected, monovalent cations did not reticulate the pectin, while divalent and trivalent cations allowed the formation of gels. Increasing the valence of the cation lead to mechanically stronger gels; however, calcium had a better cross-linking ability than aluminium. The freeze dried pectin had bulk densities between 0.06 and 0.19 $g.cm^{-3}$ for pectin concentration in solution between 5 and 15%wt.The materials showed high biodegradability (around 40-57% of mass lost after 10 days in compost).

Finally, pectin aerogels showing thermal superinsulating properties (Rudaz et al. 2014) were reported for the very first time. The pectin aerogels were obtained from an acidic (pH < 1.5) apple or citrus pectin aqueous solutions gelled at room temperature for 48h, then submitted to gradual solvent exchange with ethanol and dried with supercritical $CO_2$. The obtained pectin aerogels had bulk densities between 0.05 to 0.20 g.cm$^{-3}$, specific surface areas around 200 m².g$^{-1}$ and compressive modulus between 4 and 18 MPa under uniaxial compression. Aeropectins were able to sustain up to 60% deformation before irreversible pore collapse. Their structure was alike the monolithic aeropectins obtained by White et al. in similar conditions: a nanostructured network of entangled fibers (fig. I.29). Finally, their thermal conductivity was 0.016 to 0.022 W.m$^{-1}$.K$^{-1}$, making them the first fully bio-based thermal superinsulating materials ever reported at the same time as nanocellulose aerogels (Kobayashi, Saito and Isogai, 2014).
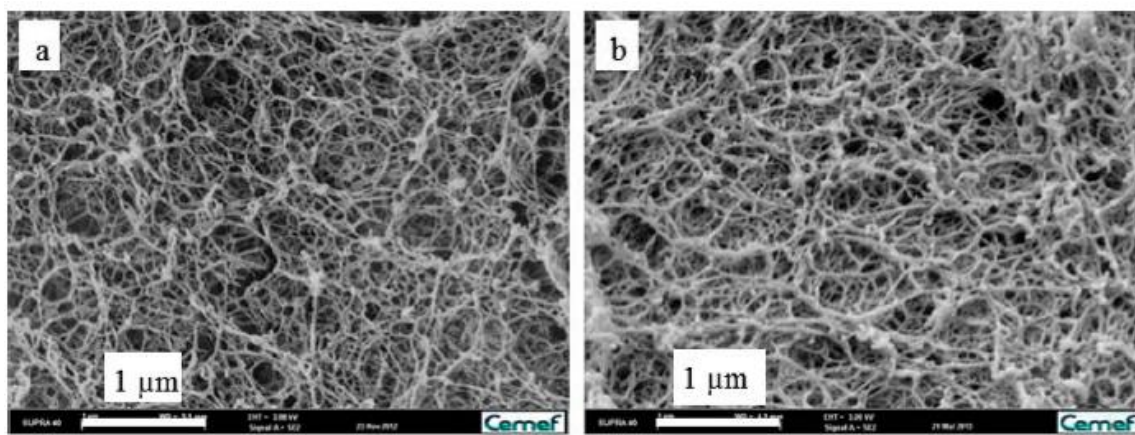


**Figure I.29: Aeropectins obtained by (Rudaz et al., 2014) from (a) apple pectin and (b) citrus pectin. Pectin initial concentration was 3%wt.**

## 4. Cellulose-silica hybrid and composite materials

### 4.1. Physical hybrids and composites

The present study aims at the preparation of new polysaccharide-silica composite aerogels with low thermal conductivity. The majority of literature about polysaccharide-silica composites focuses on cellulose-silica materials. Many studies are centered on the modification of cellulose fibers, mainly for application in the textile industry. In the past three years, cellulose-silica composite aerogels have been reported, in parallel with our studies: many possibilities are opened for highly porous aerogel composites, such as improved mechanical resistance or enhanced thermal insulation properties. The following section will detail the current properties and applications of silica modified cellulose fibers, as well as cellulose-silica composite aerogels.

#### 4.1.1. Surface modification of cellulose fibers with silica

In the case of "physical hybrids", silica was not chemically grafted on cellulose surface by a coupling agent. Silica is simply deposited on cellulose fibers surface, stabilized by the formation of hydrogen bonds or electrostatic interactions. Covalent bonds between cellulose and silica may be possible at the interface, even without chemical coupling: thermal treatments may allow the formation of such bonds as can be observed on wood treatment with

alcoxysilanes (Tingault, 2006). However, very few studies investigate the exact nature of cellulose-silica chemical interaction when specific chemical coupling is not involved.

Silica phase can be synthesized in situ by sol-gel process in the presence of cellulose fibers, resulting in silica nanoparticles deposited on fibers surface, or, in certain cases, a continuous silica film partially covering the cellulose fibers. Kulpinsky reported the preparation of silica modified cellulose fibers, obtained by using cellulose fibers from a cellulose-NMMO solution which were mixed with an aqueous dispersion of silica nanaoparticles (Kulpinsky, 2004). The modified fibers showed a slightly better elastic modulus but lower resistance to tearing. This work demonstrated the possibility of easily coating cellulose fibers with silica nanoparticles, with loadings up to 30%. Although Kulpinsky did not investigate the microstructure of his modified fibers, it is likely to be similar to what was obtained by Pinto et al. on similar materials (Pinto et al. 2008). They investigated two different routes to obtain the coated fibers: (1) synthesis in situ of silica from tetraethoxysilane (TEOS) with basic ($NH_4OH$) catalysis, in the presence of cellulose fibers, and (2) electrostatic bonding of negatively charged silica particles to positively charged cellulose surface by layer-by-layer polyelectrolyte adsorption (fig. I.30)
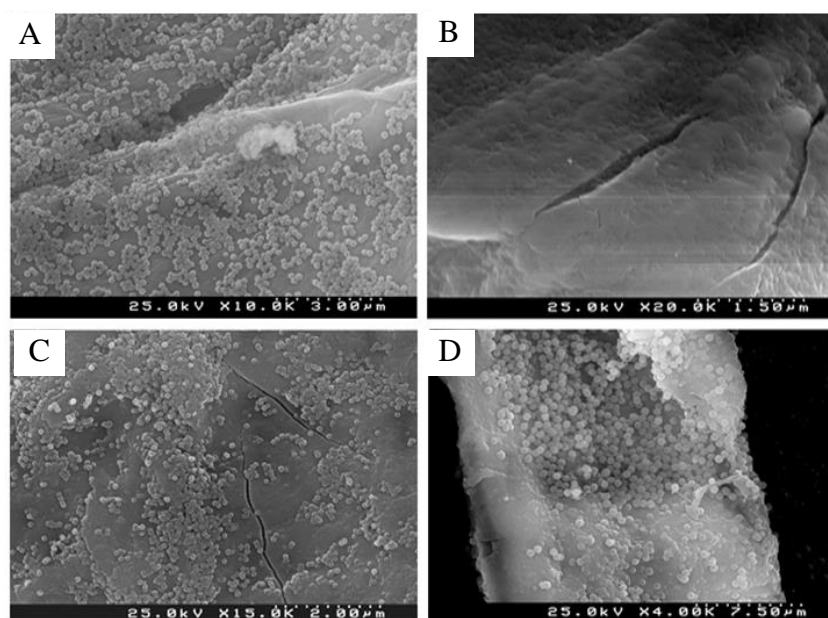


**Figure I.30: SEM pictures of cellulose fibers covered with silica nanoparticles (Pinto et al., 2008) obtained by (A) Layer by layer polyelectrolyte assembly; (B): [$NH_4OH$] = 0.06M; (C): [$NH_4OH$] = 0.2M and (D) [$NH_4OH$] = 2M. Reproduced with permission from Elsevier.**

As seen on SEM pictures (Figure 1.30), in both cases nanoparticles are scattered on the surface of cellulose fibers. In the case of in situ synthesis, it is easier to form a continuous film on cellulose surface, especially at low catalyst concentrations (0.06 M). Water uptake by these modified fibers, as measured after swelling in water at room temperature, was lower (26-40 wt% gain) than for untreated fibers (60 wt% gain).

Similar coated cellulose fibres can be obtained by acid-catalyzed formation of silica in the presence of cellulose fibers (Sequiera et al, 2007). The material degraded at 345°C against 305°C for the native cellulose pulp. Thermal conductivity of the treated fibers was investigated by the same authors (Sequiera, 2009): treated fibers had a thermal conductivity of 0.11 W/m.K, against 0.08 W/m.K for untreated cellulose. The presence of silica did improve fibre capacity

to withstand heat treatments, but not their thermal conductivity, probably because the obtained material was neither homogeneous and the silica phase was of high density.

### 4.1.2. Composite cellulose-silica aerogels

Many articles discuss the modification of the surface of cellulose fibres with silica, but very few consider combining cellulose aerogels with silica aerogels in the view of making interpenetrating networks. Such structures could prove particularly interesting for applications such as thermal insulation, controlled release or catalysis. Cellulose nanofibrils or cellulose aerogels have higher mechanical strength than pure silica aerogels, and thus could be used as a reinforcing matrix for nanostructured silica.

A cellulose alcogel obtained from an NMMO cellulose solution coagulated in ethanol, was impregnated by TEOS and/or chloropropyltrimethoxysilane (CPTMS) (Liebner et al.,2011) in acid conditions and then dried with supercritical $CO_2$ (fig. I.31).
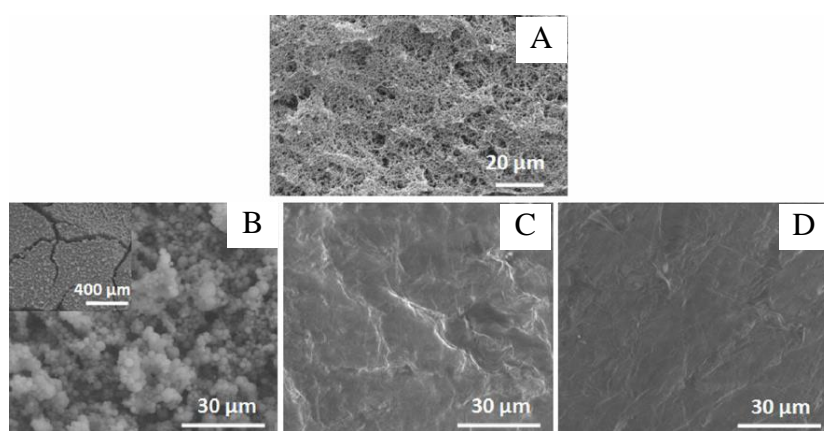


**Figure I.31: Aerogel from (A) pure cellulose and silica impregnated cellulose gels using (B) TEOS; (C) CPTS and (D) CPTS + TEOS. The catalyst used for silica formation was HCl 0.12M. From (Liebner, 2011), reproduced with permission from Springer.**

This study pointed out a few drawbacks of the direct synthesis of silica from TEOS within a porous cellulose matrix: cellulose degradation was observed due to the presence of strong acid necessary to catalyze the sol-gel process, and the diffusion of silica-based species within the porosity of cellulose was hindered by silica gel layer rapidly forming at the surface of the cellulose sample. Using CPTMS in conjunction with TEOS allowed to obtain more homogeneous materials. Specific surface area of the composite aerogels ranged from 220 to 290 m²/g.

Impregnation of cellulose alcogels from coagulation of a cellulose solution in aqueous NaOH was also reported by (Cai et al., 2012; Liu et al. 2014). In these studies, TEOS or sodium silicate ($Na_2SiO_3$) were respectively used as silica precursors. In the case of TEOS, the specific surface area of composite aerogel increased significantly, indicating the formation of nanostructured silica in the pores of cellulose. However, the presence of silica in the pores of cellulose matrix induced the increase of the thermal conductivity to 0.035-0.045 W/(m.K), and their mechanical properties slightly decreased as compared with those of neat aerocellulose. When sodium silicate was used for the impregnation, the specific surface area remained the same or even slightly decreased from 320 $m^2.g^{-1}$ for the neat Aerocellulose to 270 $m^2.g^{-1}$ for the composite aerogels, probably because of the formation of dense silica particles and not of an aerogel in the pores of cellulose matrix. Liu et al. did not report thermal conductivity of their composites.

Flexible hybrid aerogels were obtained starting from nanofibrillated cellulose, derived from wood pulp. Nanofibrils were put in suspension in ethanol in the presence of methyltrimethoxysilane (MTMS) and gels were dried with sc $CO_2$: bendable aerogel composites with a thermal conductivity from 0.015 to 0.025 $W.m^{-1}.K^{-1}$) were obtained (Hayase et al., 2014). The obtained composites showed high hydrophobicity, with water contact angles up to 150°.

Another type of "nanofibrillated" cellulose is bacterial cellulose produced by bacteria which make a network made of high molecular weight cellulose nanofibres. After washing out bacteria and substrate, a network of nanofibers dispersed in water or ethanol can be obtained. Although its production takes time, bacterial cellulose is a particularly interesting source for cellulose-silica nanostructured composites. Maeda et al. elaborated reinforced composite materials inspired by rice leaves (Maeda et al., 2006). Bacterial cellulose was impregnated with pre-hydrolyzed TEOS, and acid catalysis was used to yield $SiO_2$. Compression of the wet samples at 120°C and 1-2 MPa gave mechanically reinforced samples, with a Young modulus of 17.4 GPa against 11 GPa for pure bacterial cellulose counterpart. The same authors determined that a load of 8% wt in silica nanoparticles was optimal for the mechanical reinforcement of their composites (Maeda and Yano, 2008). The nanostructured morphology attainable when mixing bacterial cellulose and silica nanoparticles was observed by SEM (Barud et al., 2008).

Bacterial cellulose/silica composite cryogels with high specific surface area were recently reported by a Chinese team. Freeze-dried bacterial cellulose was impregnated by TEOS (Sai et al., 2013) and then freeze-dried again. By immersing wet bacterial cellulose in a sodium silicate solution, the same authors obtained comparable results with only one freeze-drying step (Sai et al., 2014). The specific surface area significantly increased in the presence of silica, from 129 $m^2/g$ for the neat freeze-dried bacterial cellulose to 800-900 $m^2/g$ for composite materials, demonstrating the formation of nanostructured silica aerogel in the porosity of cellulose (fig. I.32). Unfortunately, the thermal conductivity also increased with the increase of silica content from 0.030 for the neat bacterial cellulose to 0.033-0.037 $W.m^{-1}.K^{-1}$). A potential decrease of thermal conductivity of cellulosic matrix due to the impregnation of silica did not work probably because the increase of hybrid material overall density. The authors also performed hydrophobization of their composites by immersion in a MTMS sol, obtaining contact angles with water around 140° and high oil absorption capability.
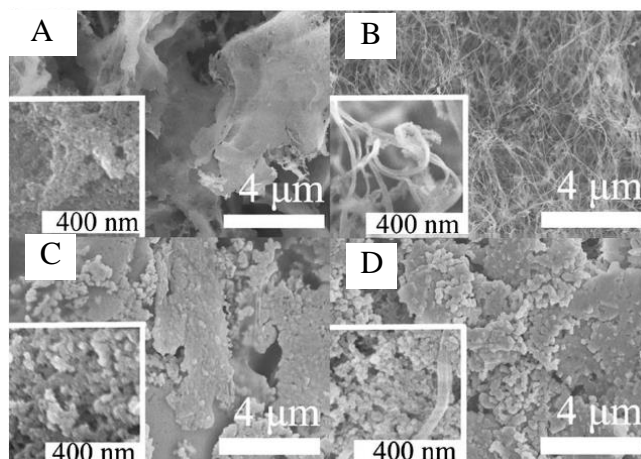


**Figure I.32: SEM micrographs of cellulose silica hybrid aerogels from (Sai et al., 2013), reproduced with permission from RSC. TEOS concentrations were 0.19M (A and B) and 0.168 (C and D).**

Table I.3 reviews the general properties of the major composite cellulose-silica aerogels reported in literature so far. The bulk densities, specific surface areas and thermal conductivities vary with cellulose and silica content. In the table we displayed for each parameter the overall range of values obtained by the respective authors.

**Table I.3: General properties of nanostructured cellulose silica composite aerogels**

| Cellulose source | Silica precursor | Bulk density $(g.cm^{-3})$ | Specific surface area $(cm^2.g^{-1})$ | Thermal conductivity $(W.m^{-1}K^{-1})$ | Reference |
|---|---|---|---|---|---|
| Cellulose dissolved in NMMO monohydrate and coagulated in ethanol | TEOS/CPTMS | n/a | 220-290 | n/a | Liebner et al, 2011 |
| **Cellulose dissolved in NaOH-urea-water and coagulated in ethanol** | TEOS | 0.35-0.58 | 400-650 | 0.025-0.045 | Cai et al., 2012 |
| Cellulose dissolved in LiOH/urea solution and coagulated in ethanol | Na$_2$SiO$_3$ | 0.202-0.228 | 271-341 | n/a | Liu et al., 2014 |
| **Nanofibrillated cellulose, water exchanged to ethanol** | MTMS | 0.020-0.186 | 525-732 | 0.015-0.024 | Hayase et al., 2014 |
| **Bacterial cellulose,** water exchanged to ethanol | TEOS | 0.020-0.200 | 180-900 | 0.033-0.037 | Sai et al., 2013 |
| **Bacterial cellulose,** water exchanged to ethanol | Na$_2$SiO$_3$ | 0.010-0.230 | 270-540 | 0.031-0.037 | Sai et al., 2014 |

## 4.2. Grafting of silica on cellulose: preparation of cellulose-silica chemical hybrids

Cellulose silica hybrid materials can be obtained by using reticulating agents with silanol functions, chemically grafted on cellulose chains. A possible application for such covalent hybrids is surface hydrophobization of textile cellulose fibers.

Cotton fibers functionalized with silica allowed the grafting of hexamethyltriethoxysilane (HMTES) on the fibers surface. The silica grafted to the fiber surface was synthesized from sodium silicate; the catalyst used for the reaction was citric acid. The C16 chains from HMTES permitted to attain a contact angle with water of 150° after synthesis (Liu et al., 2011). Thanks to the covalent bonding to the cellulose surface, the hydrophobic coating on the fibers was very stable with time, even after strong washing with water.
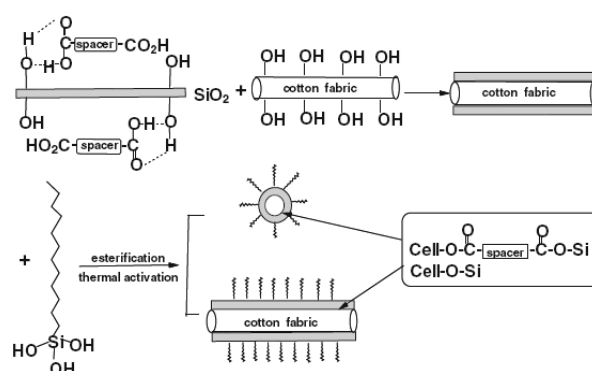
**Figure I.33: Cellulose fibers: coating with silica and hydrophobization process from (Liu et al., 2011), reprinted with permission from Springer.**

Omniphobic fibers, i.e fibers hydrophilic and lipophilic at the same time were also obtained by grafting of a silicium alcoxyde containing fluorocarbonated moieties, perfluorodecyltriethoxysilane (PFTTEOS) (Cunha et al., 2010). Similarly to the process used by Liu, the grafting of the PFTTEOS was made possible by prior modification of the cellulose fibers surface with a silane compound, 3-Isocyanopropyltriethoxysilane (ICPTEOS). Contact angles were reported as 140° with water, and 134° with dodecane.

Thermal stability of cellulose fibers can also be a concern; in this case, fully coating the cellulose by a homogeneous silica film significantly increases their thermal degradation temperature (Xie et al., 2009). To achieve this result, they used 2,4,6- tri[(2-Epihydrin-3-Bimethyl-Ammonium)propyl]-1,3,5-triazine Chloride (Tri-EBAC) as a reticulating agent: reticulation was ensured by the formation of amine bonds between the cross-linker, cellulose surface and TEOS. TEOS was then polycondensated to form a uniform silica layer around the cellulose fibres. A similar result could also be obtained directly from a cellulose-NMMO solution, using amidated polyhedral oligomeric silsesquioxanes (POSS-NH$_2$) as the cross-linker (Xie, Zhang and Lu, 2009).

## Conclusions

This introductive chapter had several goals. First, we briefly presented two polysaccharides used in the work, cellulose and pectin, as well as their solutions and gels .Then the nature and properties of aerogels, made from silica and the aforementioned polysaccharides, was explored. Finally, we studied the few cases of cellulose-silica composites and hybrids reported in the literature.

Cellulose is a linear polysaccharide made of anhydroglucopyranose units linked together by β 1.4 glycosidic bonds. It is the main constituent of plant cell walls. The cellulose molar mass and degree of crystallinity vary depending on its source. Cellulose is structured through hydrogen bonds which gives the chain rigidity and makes it difficult to dissolve in common solvent. Industrial processing of cellulose requires either cellulose chemical modification before dissolution and precipitation (Viscose process), or direct dissolving in a few selected solvent; the most used in industry is NMMO monohydrate (Lyocell process). Other solvents are able to dissolve cellulose at the lab scale, for purposes of forming coagulated cellulose objects or chemical modifications. Among those solvents, water-NaOH and ionic liquids are the most promising. In particular, ionic liquids allow dissolving cellulose up to 25%wt concentrations and forming various cellulose materials (fibres, films); however, these solvents are still rather expensive.

Pectin is a polysaccharide made of linear chains of partially esterified galacturonic acid. Pectin is a constituent of plant cell walls and is mainly extracted from waste from the food industry, such as apple pomace or citrus peel. Pectins are characterized by their galacturonic acid content, degree of esterification, and degree of methylation (DM). This polysaccharide is a well-known gelling agent used in the food industry; two gelling mechanisms can be distinguished: for high methoxy pectins, gelation occurs due to the formation of hydrogen bonds between chains, it is favored at low pH and in the presence of sugars. In the case of low methoxy pectins, gelation can be triggered by electrostatic bonding with divalent ions, such as calcium, at neutral to slightly alkaline pH. The gel strength and texture can be varied by changing the pH, temperature, or DM of the pectins.

Gels are porous solid networks whose pores are filled by a liquid. Aerogels are nanostructured gels in which the liquid phase has been replaced by air without prejudicial texture degradation. Drying gels in supercritical conditions, freeze drying, or evaporative drying in the case of some hydrophobic gels allows removing the solvent without damaging the pore structure. The most famous aerogels are silica aerogels. They can be made from various precursors: sodium silicate or silica alcoxydes. Chemical modification of silica gels allows adding various properties to silica aerogels, like hydrophobicity or flexibility. Silica aerogels have remarkable thermal properties: due to their small pore sizes in the range of mesoporosity they are able to confine air inside their pores, which reduces their thermal conductivity far below that of free air (0.025 $W.m^{-1}.K^{-1}$) in ambient conditions and make them superinsulating materials. Although silica aerogels remain too expensive, several commercial applications targeted at the superinsulation for the building industry have been elaborated in the past 10 years.

A brand new class of aerogels is aerogels made from natural polymers. We reviewed two kinds of these bio-aerogels: Aerocellulose and Aeropectin. Both are obtained from polysaccharide solutions let to gel or directly coagulated. After solvent exchange and supercritical drying with

$CO_2$, porous materials are easily obtained. They show quite low densities ($< 0.2$ g.cm$^{-3}$) and rather high specific surface areas in the 200-400 m².g$^{-1}$ range. Aeropectins are entirely bio-based superinsulating materials with thermal conductivities reported between 0.016 and 0.022 W.m$^{-1}$.K$^{-1}$.

Most works on cellulose hybrid/composite materials reported in the literature focus on the coating of cellulose fibers with silica, for functionalization or heat protection purposes. However, a few recent reports exist on nanostructured cellulose/silica composite aerogels. Impregnation of cellulose with a silica precursor, followed with the gelation of the silica phase has been attempted with TEOS derivatives as well as sodium silicate. Cellulose matrices were obtained from coagulated cellulose solutions, nanofiber dispersions or bacterial cellulose. Cellulose-silica composite aerogels with various degrees of flexibility and nanostructuration were obtained. The reported composite materials showed an increase in specific surface area, but up to date no significant improvement in their thermal conductivities.

# References

Aaltonen, O., & Jauhiainen, O. (2009). The preparation of lignocellulosic aerogels from ionic liquid solutions. *Carbohydrate Polymers*, 75, 125–129.

Achard P., Bisson A., Bonnardel P., De Candido M., Florent P., Pouleyrn G., Rigacci A., Procédé d'élaboration de xérogels de silice hydrophobes, Brevet FR 2 873 677 (17/08/2007)

Aeregeter, M.A et al. (eds), Aerogels Handbook, Springer Science, 2011, 215-234.

Anderson, A. M., & Carroll, M. K. (2011). Hydrophobic silica aerogels: Review of synthesis, properties and applications. In *Aerogels Handbook* (pp. 47-77). Springer New York.

Aravind, P. R., Niemeyer, P., & Ratke, L. (2013). Novel flexible aerogels derived from methyltrimethoxysilane/3-(2, 3-epoxypropoxy) propyltrimethoxysilane co-precursor. *Microporous and Mesoporous Materials*, *181*, 111-115.

Atalla, R. H., Vanderhart, D. L. (1984). Native Cellulose: A Composite of Two Distinct Crystalline Forms; *Science*, 223(4633), 283–285.

Baetens, R., Jelle, B. P., & Gustavsen, A. (2011). Aerogel insulation for building applications: a state-of-the-art review. *Energy and Buildings*, *43*(4), 761-769.

Bai, Y. X., & Li, Y. F. (2006). Preparation and characterization of crosslinked porous cellulose beads. *Carbohydrate polymers*, *64*(3), 402-407.

Bangi, U. K., Rao, A. V., & Rao, A. P. (2008). A new route for preparation of sodium-silicate-based hydrophobic silica aerogels via ambient-pressure drying. *Science and Technology of Advanced Materials*, *9*(3), 035006.

Barud, H.S., R. M. N. Assuncao, M. A. U. Martines, J. Dexpert-Ghys, R. F. C. Marques, Y. Messaddeq, S. J. L. Ribeiro ; *Bacterial cellulose–silica organic–inorganic hybrids* ; J Sol-Gel Sci Technol (2008) 46:363–367

Bhagat, S.D. (2007); Rapid synthesis of water-glass based aerogels by in situ surface modification of the hydrogels ; *Applied Surface Science* , 253, 3231–3236.

Bhagat, S. D., & Rao, A. V. (2006). Surface chemical modification of TEOS based silica aerogels synthesized by two step (acid–base) sol–gel process. *Applied surface science*, *252*(12), 4289-4297.

Bhagat, S. D., Oh, C. S., Kim, Y. H., Ahn, Y. S., & Yeo, J. G. (2007). Methyltrimethoxysilane based monolithic silica aerogels via ambient pressure drying. *Microporous and mesoporous Materials*, *100*(1), 350-355.

Biganska, O., & Navard, P. (2009). Morphology of cellulose objects regenerated from cellulose–N-methylmorpholine N-oxide–water solutions. *Cellulose*, 16,179–188.

Biesmans, G., Randall, D., Francais, E., & Perrut, M. (1998). Polyurethane-based organic aerogels' thermal performance. *Journal of Non-Crystalline Solids*, *225*, 36-40.

Bisson, A., Rigacci, A., Lecomte, D., Rodier, E., Achard, P. (2003). Drying of silica gels to obtain aerogels: phenomenology and basic techniques. *Drying technology*, *21*(4), 593-628.

Bisson, A. (2004). *Syntèse et étude de matériaux nanostructurés à base de silice pour la superisolation thermique* (PhD thesis, Paris, ENMP).

Boonstra, A. H., & Bernards, T. N. M. (1988). The dependence of the gelation time on the hydrolysis time in a two-step $SiO_2$ sol-gel process. *Journal of non-crystalline solids*, *105*(3), 207-213.

Braccini, I., and Pérez, S. (2001). Molecular basis of Ca2+-induced gelation in alginates and pectins: the egg-box model revisited. *Biomacromolecules*, *2*(4), 1089-1096.

Brinker, C. J., & Scherer, G. W. (2013). *Sol-gel science: the physics and chemistry of sol-gel processing*. Academic press.

Cai J, Liu J, Feng J, Kimura S, Wada M, Kuga S, Zhang L; (2012) Cellulose–silica nanocomposite aerogels by in situ formation of silica in cellulose gel. *Angewandte Chemie* 51:2076–2079

Cai J, Zhang LN, Zhou JP, Li H, Chen H, Jin HM (2004) Novel fibers prepared from cellulose in NaOH/urea aqueous solution. *Macromol Rapid Comm* 25:1558–1562

Cai, J., Kimura, S., Wada, M., Kuga, S., & Zhang, L. (2008). Cellulose aerogels from aqueous alkali hydroxide–urea solution. *ChemSusChem*, *1*(1-2), 149-154.

Cao, Y., Li, H., Zhang, Y., Zhang, J., & He, J. (2010). Structure and properties of novel regenerated cellulose films prepared from cornhusk cellulose in room temperature ionic liquids. *Journal of Applied Polymer Science*, *116*(1), 547–554.

Capel, F., Nicolai, T., Durand, D., Boulenguer, P., & Langendorff, V. (2006). Calcium and acid induced gelation of (amidated) low methoxyl pectin. *Food Hydrocolloids*, *20*(6), 901-907.

Chanzy, H., Nawrot, S., Peguy, A., Smith, P., & Chevalier, J. (1982). Phase behavior of the quasiternary system N-methylmorpholine-N-oxide, water, and cellulose. *Journal of Polymer Science: Polymer Physics*, *20*(10), 1909–1924.

Chanzy, H., Paillet, M., & Hagege, R. (1990). Spinning of cellulose from N-methyl morpholine N-oxide in the presence of additives. *Polymer*, *31*(3), 400-405.

Chen, H.-B., Chiou, B.-S., Wang, Y.-Z., & Schiraldi, D. a. (2013). Biodegradable pectin/clay aerogels. *ACS applied materials & interfaces*, *5*(5), 1715–21.

Colby M.W., Osaka, A., Mackenzie , J.D. (1986); Effects of temperature on formation of silica gel, J. *Non-Cryst. Solids,* 82, 37-41.

Cuissinat, C., & Navard, P. (2006). Swelling and Dissolution of Cellulose Part 1: Free Floating Cotton and Wood Fibres in N-Methylmorpholine-N-oxide–Water Mixtures. In *Macromolecular symposia* (Vol. 244, No. 1, pp. 1-18). WILEY-VCH Verlag.

Cunha, A.G. , Freire, C.S.R., Silvestre, A., Neto, C.P., Gandini,A., *(*2010); Preparation and characterization of novel highly omniphobic cellulose fibers organic–inorganic hybrid materials ; *Carbohydrate Polymers* 80, 1048–1056.

Davidson, G.F.; The dissolution of chemically modified cotton cellulose in alkaline solutions. part ii.—a comparison of the solvent action of solutions of lithium, sodium, potassium, and tetramethylammonium hydroxides; *Journal of the Textile Institute Transactions*, Volume 27, Issue 4, 1936

Dawsey, T. R., & McCormick, C. L. (1990). The lithium chloride/dimethylacetamide solvent for cellulose: a literature review. *Journal of Macromolecular Science—Reviews in Macromolecular Chemistry and Physics*, *30*(3-4), 405-440.

Deng, M., Zhou, Q., Du, A., van Kasteren, J., & Wang, Y. (2009). Preparation of nanoporous cellulose foams from cellulose-ionic liquid solutions. *Materials Letters*, *63*(21), 1851-1854.

Diascorn, N. (2014), PhD thesis, MinesParisTech

Ebert, H.P.; Thermal properties of aerogels.,In: M.A. Aeregeter et al. (eds), *Aerogels Handbook*, Springer Science, 2011., 537-564.

Ebner, G., Schiehser, S., Potthast, A., & Rosenau, T. (2008). Side reaction of cellulose with common 1-alkyl-3-methylimidazolium-based ionic liquids. *Tetrahedron Letters*, *49*(51), 7322–7324.

Egal, M., Budtova, T., & Navard, P. (2007). Structure of aqueous solutions of microcrystalline cellulose/sodium hydroxide below 0 C and the limit of cellulose dissolution. *Biomacromolecules*, *8*(7), 2282-2287.

El Seoud, O. A., Koschella, A., Fidale, L. C., Dorn, S., & Heinze, T. (2007). Applications of ionic liquids in carbohydrate chemistry: a window of opportunities. *Biomacromolecules*, *8*(9), 2629-2647.

Feng, L., & Chen, Z. L. (2008). Research progress on dissolution and functional modification of cellulose in ionic liquids. *Journal of Molecular Liquids*, *142*(1), 1-5.

Fink, H. P., Weigel, P., Purz, H. J., & Ganster, J. (2001). Structure formation of regenerated cellulose materials from NMMO-solutions. *Progress in Polymer Science*, *26*(9), 1473-1524.

Fraeye, I., Duvetter, T., Doungla, E., Van Loey, A., & Hendrickx, M. (2010). Fine-tuning the properties of pectin–calcium gels by control of pectin fine structure, gel composition and environmental conditions. *Trends in food science & technology*, *21*(5), 219-228.

Froix, M.F, Nelson, R. (1975); The Interaction of Water with Cellulose from Nuclear Magnetic Resonance Relaxation Times ; *Macromolecules*, 8 (1975) , 726–730.

García-González, C. A., Carenza, E., Zeng, M., Smirnova, I., & Roig, A. (2012). Design of biocompatible magnetic pectin aerogel monoliths and microspheres. *RSC Advances*, *2*(26), 9816.

Gardiner, E. S. and Sarko, A. (1985) Packing analysis of carbohydrates and polysaccharides. 16. The crystal structures of celluloses $IV_I$ and $IV_{II}$. *Can. J. Chemistry* 63, 173±180.

Garnier, C., Axelos, M. A., & Thibault, J. F. (1993). Phase diagrams of pectin-calcium systems: influence of pH, ionic strength, and temperature on the gelation of pectins with different degrees of methylation. *Carbohydrate Research*, *240*, 219-232.

Gavillon, R., & Budtova, T. (2007). Aerocellulose: new highly porous cellulose prepared from cellulose− naoh aqueous solutions. *Biomacromolecules*, *9*(1), 269-277.

Gericke, M., Fardim, P., & Heinze, T. (2012). Ionic liquids--promising but challenging solvents for homogeneous derivatization of cellulose. *Molecules* (Basel, Switzerland), *17*(6), 7458–502.

Gericke, M., Schlufter, K., Liebert, T., Heinze, T., & Budtova, T. (2009). Rheological properties of cellulose/ionic liquid solutions: from dilute to concentrated states. *Biomacromolecules*, *10*(5), 1188–94.

Gibson, L. J., & Ashby, M. F. (1999). *Cellular solids: structure and properties*. Cambridge university press.

Graenacher, C., & Sallmann, R. (1939). Cellulose solutions and process of making same. US patent 2,179,181.

Grant, G. T., Morris, E. R., Rees, D. A., Smith, P. J., & Thom, D. (1973). Biological interactions between polysaccharides and divalent cations: the egg-box model. *FEBS letters*, *32*(1), 195-198.

Guo, H., Nguyen, B. N., McCorkle, L. S., Shonkwiler, B., & Meador, M. A. B. (2009). Elastic low density aerogels derived from bis [3-(triethoxysilyl) propyl] disulfide, tetramethylorthosilicate and vinyltrimethoxysilane via a two-step process. *Journal of Materials Chemistry*, *19*(47), 9054-9062.

Huang, H., Orler, B., Wilkes, G.L. (1985); Ceramers: Hybrid materials incorporating polymeric/oligomeric species with inorganic glasses by a sol-gel process; *Polymer Bulletin*, 14, 557-564.

Harmon, K. M., Akin, A. C., Keefer, P. K., & Snider, B. L. (1992). Hydrogen bonding Part 45. Thermodynamic and IR study of the hydrates of N-methylmorpholine oxide and quinuclidine oxide. Effect of hydrate stoichiometry on strength of H-O-H…O-N hydrogen bonds; implications for the dissolution of cellulose in amine oxide . *Journal of Molecular Structure*, *269*(1–2), 109–121

Hayase, G., Kanamori, K., & Nakanishi, K. (2011). New flexible aerogels and xerogels derived from methyltrimethoxysilane/dimethyldimethoxysilane co-precursors. *J. Mater. Chem.*, *21*(43), 17077-17079.

Hayase, G., Kanamori, K., Abe, K, Yano, H., Maeno, H., Kaji, Nakanishi, H.K., (2014) Polymethylsilsesquioxane−Cellulose Nanofiber Biocomposite Aerogels with High Thermal Insulation, Bendability, and Superhydrophobicity, *ACS Appl. Mater. Interfaces*, 6, 9466−9471

Hegde, N. D., & Rao, A. V. (2007). Physical properties of methyltrimethoxysilane based elastic silica aerogels prepared by the two-stage sol–gel process. *Journal of materials science*, *42*(16), 6965-6971.

Heinze, T., Dorn, S., Schöbitz, M., Liebert, T., Köhler, S., & Meister, F. (2008, January). Interactions of ionic liquids with polysaccharides–2: Cellulose. In *Macromolecular symposia* (Vol. 262, No. 1, pp. 8-22). WILEY-VCH Verlag.

Hestrin, S.,Schramm, M. (1954); Synthesis of cellulose by Acetobacter xylinum, *Biochem. J.*, 58, 345.

Hoepfner, S., Ratke, L., & Milow, B. (2008). Synthesis and characterisation of nanofibrillar cellulose aerogels. *Cellulose*, 15(1), 121-129.

Hwang, S.H., et al. (2007); Effective preparation of crack-free silica aerogels via ambient drying; *J Sol-Gel Sci Techn*. 41, 139–146.

Innerlohinger, J., Weber, H. K., & Kraft, G. (2006, December). Aerocellulose: Aerogels and Aerogel-like Materials made from Cellulose. In *Macromolecular Symposia* (Vol. 244, No. 1, pp. 126-135). WILEY-VCH Verlag.

Isogai, A. and Atalla, R.H. (1998)*; Dissolution of cellulose in aqueous NaOH solutions; Cellulose*, 5, 309-319

Jeong, A. Y., Koo, S. M., & Kim, D. P. (2000). Characterization of hydrophobic SiO2 powders prepared by surface modification on wet gel. *Journal of Sol-Gel Science and Technology*, *19*(1-3), 483-487.

Jin, H., Nishiyama, Y., Wada, M., & Kuga, S. (2004). Nanofibrillar cellulose aerogels. *Colloids and surfaces A: Physicochemical and engineering aspects*, *240*(1), 63-67.

Kamide K., Saito, M., Kowsaka, K. (1987); Temperature Dependence of Limiting Viscosity Number and Radius of Gyration for Cellulose Dissolved in Aqueous 8% Sodium Hydroxide Solution*; Polymer Journal* , **19,** 1173-1181.

Kamide, K. and Okajima, K. (1987) U.S. Patent 4,634,470

Kamide, K., Okajima, K. and Kowsaka, K. (1992); Dissolution of Natural Cellulose into Aqueous Alkali Solution: Role of Super-Molecular Structure of Cellulose; *Polymer Journal*, 24, 71-86

Karatzos, S. K., Edye, L. A., & Wellard, R. M. (2011). The undesirable acetylation of cellulose by the acetate ion of 1-ethyl-3-methylimidazolium acetate. *Cellulose*, *19*(1), 307–312.

Keil, P., Kick, M., & König, A. (2012). Long-Term Stability, Regeneration and Recycling of Imidazolium-based Ionic Liquids. *Chemie Ingenieur Technik*, *84*(6), 859–866.

Kettunen, M., Silvennoinen, R. J., Houbenov, N., Nykänen, A., Ruokolainen, J., Sainio, J., & Ikkala, O. (2011). Photoswitchable superabsorbency based on nanocellulose aerogels. *Advanced Functional Materials*, *21*(3), 510-517.

Kistler,S.S. (1932); Coherent expanded aerogels, *J. Phys. Chem*. 36, 52-64.

Klemm, D. et al. (1998); Comprehensive cellulose chemistry; vol. 1 Fundamentals and analytical methods; Wiley.

Klemm, D., Heublein,B., Fink, H-P., Bohn, A. (2005); Cellulose: Fascinating Biopolymer and Sustainable Raw Material*; Angew. Chem. Int. Ed.*, 44, 3358 – 339.

Kobayashi, Y., Saito, T., & Isogai, A. (2014). Aerogels with 3D Ordered Nanofiber Skeletons of Liquid-Crystalline Nanocellulose Derivatives as Tough and Transparent Insulators. *Angewandte Chemie*, *126*(39), 10562-10565.

Kocon, L., Despetis, F., and Phalippou, J. (1998). Ultralow density silica aerogels by alcohol supercritical drying. *Journal of non-crystalline solids*, *225*, 96-100.

Koebel, M., Rigacci, A., & Achard, P. (2012). Aerogel-based thermal superinsulation: an overview. *Journal of sol-gel science and technology*, *63*(3), 315-339.

Köhler, S., Liebert, T., & Heinze, T. (2008). Interactions of ionic liquids with polysaccharides. VI. Pure cellulose nanoparticles from trimethylsilyl cellulose synthesized in ionic liquids. *Journal of Polymer Science Part A: Polymer Chemistry*, *46*(12), 4070–4080.

Kosan, B., Michels, C., & Meister, F. (2008). Dissolution and forming of cellulose with ionic Krässig, H.A. (1993); Cellulose: structure, accessibility, and reactivity. Gordon and Breach Science.

Kuang, Q.-L., Zhao, J.-C., Niu, Y.-H., Zhang, J., & Wang, Z.-G. (2008). Celluloses in an ionic liquid: the rheological properties of the solutions spanning the dilute and semidilute regimes. *The Journal of Physical Chemistry. B*, *112*(33), 10234–40.

Kuhn, J., Gleissner, T., Arduini-Schuster, M. C., Korder, S., & Fricke, J. (1995). Integration of mineral powders into SiO< sub> 2</sub> aerogels. *Journal of non-crystalline solids*, *186*, 291-295.

Kulpinski, P. (2005)*; Cellulose Fibers Modified by Silicon Dioxide Nanoparticles; Journal of Applied Polymer Science,* 98 ,1793–1798

Langan,P., Nishiyama,Y., and Chanzy, H. (1999);  A Revised Structure and Hydrogen-Bonding System in Cellulose II from a Neutron Fiber Diffraction Analysis*, J. Am. Chem. Soc*., 121, 9940-9946

Le, K. A., Rudaz, C., & Budtova, T. (2014). Phase diagram, solubility limit and hydrodynamic properties of cellulose in binary solvents with ionic liquid. *Carbohydrate polymers*, *105*, 237-243.

Le, K. A., Sescousse, R., & Budtova, T. (2011). Influence of water on cellulose-EMIMAc solution properties: a viscometric study. *Cellulose*, *19*(1), 45–54.

Lee, C. J., Kim, G. S., & Hyun, S. H. (2002). Synthesis of silica aerogels from waterglass via new modified ambient drying. *Journal of Materials Science*, *37*(11), 2237-2241.

Lee, D., Stevens, P. C., Zeng, S. Q., & Hunt, A. J. (1995). Thermal characterization of carbon-opacified silica aerogels. *Journal of non-crystalline solids*, *186*, 285-290.

Lee, K. H., Kim, S. Y., & Yoo, K. P. (1995). Low-density, hydrophobic aerogels. *Journal of non-crystalline solids*, *186*, 18-22.

Lenz, J., Schurz, J., & Wrentschur, E. (1992). Comparative characterization of solvent spun cellulose and high wet modulus viscose fibres by their long periods. *Acta polymerica*, *43*(6), 307-312.

Lerouxel, O., Cavalier, D.M., Liepman, A.H and K. Keegstra (2006); Biosynthesis of plant cell wall polysaccharides — a complex process, *Current Opinion in Plant Biology*, 9 : 621–630

Liebner, F. et al. (2011); Silica modified cellulosic aerogels ; *Cellulose* 18, 143–149.

Liebner, F., Haimer, E., Wendland, M., Neouze, M. A., Schlufter, K., Miethe, P., & Rosenau, T. (2010).; Aerogels from Unaltered Bacterial Cellulose: Application of scCO2 Drying for the Preparation of Shaped, Ultra-Lightweight Cellulosic Aerogels. *Macromolecular bioscience*, *10*(4), 349-352.

Liebner, F., Potthast, A., Rosenau, T., Haimer, E., & Wendland, M. (2008). Cellulose aerogels: highly porous, ultra-lightweight materials. *Holzforschung*, *62*(2), 129-135.

Liu W., Budtova T., Navard P. (2011); Influence of ZnO on the properties of dilute and semi-dilute cellulose–NaOH–water solutions. *Cellulose* (2011) 8:911–920

Liu, J. et al. ; (2011) Preparation of durable superhydrophobic surface by sol–gel method with water glass and citric acid; *J. Sol-Gel Sci. Technol*. 58 ,18–23.

Liu, S., Yu,T., Hu, N., Liu,R., Liu,X; (2013) High strength cellulose aerogels prepared by spatially confined synthesis of silica in bioscaffolds, *Colloids and Surfaces A: Physicochem. Eng. Aspects,* 439, 159– 166.

Lu A, Liu Y, Zhang L, Potthast A (2011); Investigation on metastable solution of cellulose dissolved in NaOH/urea aqueous system at low temperature. *J Phys Chem* B ,115:12801–12808

Lu, X., Nilsson, O., Fricke, J., & Pekala, R. W. (1993). Thermal and electrical conductivity of monolithic carbon aerogels. *Journal of Applied Physics*, *73*(2), 581-584.

Ma, H. S., Roberts, A. P., Prévost, J. H., Jullien, R., & Scherer, G. W. (2000). Mechanical structure–property relationship of aerogels. *Journal of non-crystalline solids*, *277*(2), 127-141.

Mackenzie, J.D., (1994); Structures and properties of Ormosils; *Journal of Sol-Gel Science and Technology*, 2, 81-86.

Maeda,H., Nakajima,T., Hagiwara, T., Sawaguchi, T., Yano, S.; (2006) Bacterial cellulose/silica hybrid fabricated by mimicking biocomposites ; *J Mater Sci* 41 5646–5656

Mao Y, Zhou JP, Cai J, Zhang LN (2006); Effects of coagulants on porous structure of membranes prepared from cellulose in NaOH/urea aqueous solution. *J Membrane Sci*, 279:246–255

Maleki, H., Durães, L., & Portugal, A. (2014). An overview on silica aerogels synthesis and different mechanical reinforcing strategies. *Journal of Non-Crystalline Solids*, *385*, 55-74.

May, C. D. (1990). Industrial pectins: sources, production and applications. *Carbohydrate Polymers*, *12*(1), 79-99.

Miner, M. R., Hosticka, B., & Norris, P. M. (2004). The effects of ambient humidity on the mechanical properties and surface chemistry of hygroscopic silica aerogel. *Journal of non-crystalline solids*, *350*, 285-289.

Mulik, S., Sotiriou-Leventis,C. ; Resorcinol-formaldehyde aerogels; In: M.A Aeregeter et al. (eds), Aerogels Handbook, Springer Science, 2011, 215-234.

Nishiyama, Y., Langan, P., Chanzy, H. (2002); Crystal Structure and Hydrogen-Bonding System in Cellulose Iβ from Synchrotron X-ray and Neutron Fiber Diffraction; *Journal of the American Chemical Society* 124, 9074–9082.

O'Sullivan A.C. (1997); Cellulose: the structure slowly unravels, *Cellulose* 4, 173-207

Oakenfull, D., and Scott, A. (1984). Hydrophobic interaction in the gelation of high methoxyl pectins. *Journal of Food Science*, *49*(4), 1093-1098.

Pajonk, G. M. (1989). Drying methods preserving the textural properties of gels. *Le Journal de Physique Colloques*, *50*(C4), C4-13.

Pajonk, G. M., Repellin-Lacroix, M., Abouarnadasse, S., Chaouki, J., & Klavana, D. (1990); From sol-gel to aerogels and cryogels. *Journal of Non-Crystalline Solids*, 121(1), 66-67.

Parmenter, K. E., & Milstein, F. (1998). Mechanical properties of silica aerogels. *Journal of non-crystalline solids*, *223*(3), 179-189.

Pekala, R.W. ,Alviso, C.T., LeMay, J.D.(1990); Organic aerogels: microstructural dependence of mechanical properties in compression, *Journal of Non-Crystalline Solids* 125 67-75

Perrut, M. (1999); Extraction supercritique ; Techniques de l'Ingénieur [j2770].

Phalippou J., Kocon L.; Aérogels: Aspects fondamentaux, Techniques de l'Ingénieur [AF 3 609].

Pierre, A.C.; Pajonk, G.M. (2002); Chemistry of aerogels and their applications. *Chem. Rev*, *102*, 4243–4266.

Pinto,R.J.B, Marques,P., Barros-Timmons,A.M., Trindade,T., Neto, C.P. (2008); Novel SiO$_2$/cellulose nanocomposites obtained by in situ synthesis and via polyelectrolytes assembly ; *Composites Science and Technology* 68, 1088–1093.

Pirard, R., Blacher, S., Brouers, F., & Pirard, J. P. (1995). Interpretation of mercury porosimetry applied to aerogels. *Journal of materials research*, *10*(08), 2114-2119.

Powell D.A., Morris, E.R., Giddley, M.J. and Rees, D.A. (1982); Conformations and interactions of pectins – II. Influence of residues sequence on chain association in calcium pectate gels. *J. Mol. Biol.*, 155, p. 517-531.

Quignard, F., Valentin, R., & Di Renzo, F. (2008). Aerogel materials from marine polysaccharides. *New Journal of Chemistry*, *32*(8), 1300.

Rao, A. P., Pajonk, G. M., & Rao, A. V. (2005); Effect of preparation conditions on the physical and hydrophobic properties of two step processed ambient pressure dried silica aerogels. *Journal of materials science*, *40*(13), 3481-3489.

Rao, A. V., Kulkarni, M. M., Amalnerkar, D. P., & Seth, T. (2003). Surface chemical modification of silica aerogels using various alkyl-alkoxy/chloro silanes. *Applied surface science*, *206*(1), 262-270.

Rao, A.V.; Kalesh, R.R. (2003); Comparative studies of the physical and hydrophobic properties of TEOS based silica aerogels using different co-precursors. *Sci. Technol. Adv. Mater.*, *4*, 509–515.

Rao, P., Rao, A.V., Bangi, U.K.H (2008); Low thermalconductive, transparent and hydrophobic ambient pressure dried silica aerogels with various preparation conditions using sodium silicate solutions; *J Sol-Gel Sci Technol* 47, 85–94.

Reichenauer, G., & Scherer, G. W. (2001). Nitrogen sorption in aerogels. *Journal of non-crystalline solids*, *285*(1), 167-174.

Rigacci, A., Marechal, J. C., Repoux, M., Moreno, M., & Achard, P. (2004). Preparation of polyurethane-based aerogels and xerogels for thermal superinsulation. *Journal of non-crystalline solids*, *350*, 372-378.

Rigacci, A.; Pierre, A.C. ; $SiO_2$ aerogels ; In: M.A Aeregeter et al. (eds), Aerogels Handbook, Springer Science, 2011, 21-45.

Rosenau, T., Potthast, A., Sixta, H., & Kosma, P. (2001). The chemistry of side reactions and byproduct formation in the system NMMO/cellulose (Lyocell process). *Progress in Polymer Science*, *26*(9), 1763-1837.

Roy, C., Budtova, T., Navard, P., & Bedue, O. (2001). Structure of cellulose-soda solutions at low temperatures; *Biomacromolecules*, *2*(3), 687-693.

Roy,C., Budtova, T., and Navard, P. (2003); Rheological Properties and Gelation of Aqueous Cellulose-NaOH Solutions; *Biomacromolecules* , 4, 259-264.

Rudaz, C. PhD thesis, MINES ParisTech 2013.

Rudaz, C., Courson, R., Bonnet, L., Calas-Etienne, S., Salee, H., & Budtova, T. (2014). Aeropectin: fully biomass-based mechanically strong and thermal super-insulating aerogel. *Biomacromolecules,* 15, 2188−2195.

Sai, H., Xing, L., Xiang, J., Cui, L., Jiao, J., Zhao, C., Li, Z., Lia,F., (2013); Flexible aerogels based on an interpenetrating network of bacterial cellulose and silica by a non-supercritical drying process, *J. Mater. Chem.* A, 1, 7963

Sai, H., Xing,L., Xiang, J, Cui, L., Jiao, J., Zhao,C., Li, Z., Lia, F., Zhanga, T.; (2014) Flexible aerogels with interpenetrating network structure of bacterial cellulose–silica composite from sodium silicate precursor via freeze drying process*; RSC Advances*, 2014,4, 30453-30461

Sarko A., R. Muggli (1974); Packing analysis of carbohydrates and polysaccharides. III. Valonia Cellulose and cellulose II; *Macromolecules*, 7, 486–494

Sarko, A., Southwick, J., Hayashi,J., (1976); Packing Analysis of Carbohydrates and Polysaccharides. 7. Crystal Structure of Cellulose IIII and Its Relationship to Other Cellulose Polymorphs*; Macromolecules*, 1976, 9 (5), pp 857–863

Scherer, G. W. (1993). Freezing gels. *Journal of Non-Crystalline Solids*, *155*(1), 1-25.

Scheuerpflug, P., Morper, H. J., & Neubert, G. (1991). Low-temperature thermal transport in silica aerogels. *Journal of Physics D: Applied Physics*, *24*(8), 1395.

Schmidt, M., Schwertfeger, F.(1998); Applications for silica aerogel products; *Journal of Non-Crystalline Solids*, 225 (1998) 364–368

Schwertfeger, F., Frank, D., & Schmidt, M. (1998). Hydrophobic waterglass based aerogels without solvent exchange or supercritical drying. *Journal of non-crystalline solids*, *225*, 24-29.

Schwertfeger, F., Glaubitt, W., & Schubert, U. (1992). Hydrophobic aerogels from Si (OMe)$_4$ / MeSi (OMe)$_3$ mixtures. *Journal of non-crystalline solids*, *145*, 85-89.

Seddon, K.R.; Stark, A.; Torres, M.-J. (2000); Influence of chloride, water, and organic solvents on the physical properties of ionic liquids. *Pure Appl. Chem.*, *72*, 2275–2287.

Sequeira, S., Evtuguin,D.V, Portugal, I. (2009); Preparation and properties of cellulose/silica hybrid composites; *Polymer Composites*, 30, 1275–1282.

Sequeira, S., Evtuguin,D.V, Portugal, I., Esculcas, A.P (2007); Synthesis and characterisation of cellulose/silica hybrids obtained by heteropoly acid catalysed sol–gel process; *Materials Science and Engineering* C 27, 172–179

Sescousse, R., Gavillon, R., & Budtova, T. (2011). Aerocellulose from cellulose–ionic liquid solutions: preparation, properties and comparison with cellulose–NaOH and cellulose–NMMO routes. *Carbohydrate Polymers*, *83*(4), 1766-1774.

Sescousse, R., Smacchia, A., Budtova, T.(2010); Influence of lignin on cellulose-NaOH-water mixtures properties and on Aerocellulose morphology; *Cellulose*, 17:1137–1146.

Shewale, P. M., Rao, A. V., Gurav, J. L., & Rao, A. P. (2009). Synthesis and characterization of low density and hydrophobic silica aerogels dried at ambient pressure using sodium silicate precursor. *Journal of Porous Materials*, *16*(1), 101-108.

Shewale, P.M., Venkateswara Rao, A., Parvathy Rao,A. (2008); Effect of different trimethyl silylating agents on the hydrophobic and physical properties of silica aerogel, *Applied Surface Science* 254 (2008) 6902-6907

Shi, F., Wang, L., & Liu, J. (2006). Synthesis and characterization of silica aerogels by a novel fast ambient pressure drying process. *Materials letters*, *60*(29), 3718-3722.

Sila, D. N., Van Buggenhout, S., Duvetter, T., Fraeye, I., De Roeck, A., Van Loey, A., & Hendrickx, M. (2009). Pectins in Processed Fruits and Vegetables: Part II-Structure- Function Relationships. *Comprehensive Reviews in Food Science and Food Safety*, *8*(2), 86–104.

Sinkó, K. (2010). Influence of chemical conditions on the nanoporous structure of silicate aerogels. *Materials*, *3*(1), 704-740.

Smirnova, I. (2011). Pharmaceutical Applications of Aerogels. In M. A. Aegerter, N. Leventis, & M. M. Koebel (Eds.), *Aerogels Handbook SE - 31* (pp. 695–717). Springer New York.

Sobue,H., Kiessig,H., Hess,H. (1939); The cellulose-sodium hydroxide-water system as a function of the temperature; *Z. Physik. Chem*. B

Stamm, A.J (1956); Thermal Degradation of Wood and Cellulose, *Industrial & Engineering Chemistry,* 48 (3), 413-417

Sugiyama, J., Vuong, R., Chanzy, H. (1991); Electron diffraction study on the two crystalline phases occurring in native cellulose from an algal cell wall, *Biomacromolecules*, 24, 4168-4175.

Swatloski, R. P., Spear, S. K., Holbrey, J. D., & Rogers, R. D. (2002). Dissolution of cellose with ionic liquids. *Journal of the American Chemical Society*, *124*(18), 4974-4975.

Tan, C., Fung, B. M., Newman, J. K., & Vu, C. (2001). Organic aerogels with very high impact strength. *Advanced materials*, *13*(9), 644-646.

Tingaut, P. (2006). *Modification de la structure chimique du bois par des alcoxysilanes diversement substitués* (Doctoral dissertation, Bordeaux 1).

Tibbits, C. W., MacDougall, A. J., & Ring, S. G. (1998). Calcium binding and swelling behaviour of a high methoxyl pectin gel. *Carbohydrate Research*, *310*(1), 101-107.

Tilgner , I.C., Fischer, P., Bohnen, F., Rehage, H., Maier, W.F. (1995); Effect of acidic, basic and fluoride catalyzed sol-gel transitions on the preparation of sub-nanostructured silica *Microporous Materials*, 5 77-90.

Tilly, G. (2010). Pectines. Techniques de l'ingénieur (ref. article : f5000), 0–12.

Tsioptsias, C., Stefopoulos, A., Kokkinomalis, I., Papadopoulou, L., & Panayiotou, C. (2008). Development of micro- and nano-porous composite materials by processing cellulose with ionic liquids and supercritical $CO_2$. *Green Chemistry*, *10*(9), 965

Tsioptsias, C., Stefopoulos, A., Kokkinomalis, I., Papadopoulou, L., & Panayiotou, C. (2008). Development of micro-and nano-porous composite materials by processing cellulose with ionic liquids and supercritical $CO_2$. *Green Chemistry*, *10*(9), 965-971.

Venkataswara Rao, A., & Kalesh, R. R. (2004). Organic surface modification of TEOS based silica aerogels synthesized by co-precursor and derivatization methods. *Journal of sol-gel science and technology*, *30*(3), 141-147.

Venkateswara Rao, A., & Pajonk, G. M. (2001). Effect of methyltrimethoxysilane as a co-precursor on the optical properties of silica aerogels. *Journal of Non-Crystalline Solids*, *285*(1), 202-209.

Venkateswara Rao, A., Bhagat, S. D., Hirashima, H., & Pajonk, G. M. (2006). Synthesis of flexible silica aerogels using methyltrimethoxysilane (MTMS) precursor. *Journal of colloid and interface science*, *300*(1), 279-285.

Venkateswara Rao, A., Kulkarni, M. M., Amalnerkar, D. P., & Seth, T. (2003). Superhydrophobic silica aerogels based on methyltrimethoxysilane precursor. *Journal of Non-Crystalline Solids*, *330*(1), 187-195.

Venkateswara Rao, A., Pajonk, G. M., & Haranath, D. (2001). Synthesis of hydrophobic aerogels for transparent window insulation applications. *Materials science and technology*, *17*(3), 343-348.

Venkateswara Rao, A., Parvathy, N.N. (1993); Effect of gel parameters on monolithicity and density of silica aerogels. *J. Mater. Sci.*, *28*, 3021–3026.

Ventkateswara Rao , A.et al.; Sodium silicate based aerogels via ambient pressure drying,In: M.A. Aeregeter et al. (eds), *Aerogels Handbook*, Springer Science, 2011., 103-123.

Wagh, P.B.; Begag, R.; Pajonk, G.M.; Rao, A.V.; Haranath, D. (1999); Comparison of some physical properties of silica aerogel monoliths synthesized by different precursors. *Mater. Chem. Phys.*, *57*, 214–218.

Walkinshaw, M.D., and Arnott, S. (1981).;  Models for junction zones in pectinic acid and calcium pectate gels. J. Mol. Biol., 153, p. 1075-1085

Wei, T. Y., Chang, T. F., Lu, S. Y., & Chang, Y. C. (2007). Preparation of monolithic silica aerogel of low thermal conductivity by ambient pressure drying. *Journal of the American Ceramic Society*, *90*(7), 2003-2007.

White, R. J., Budarin, V. L., & Clark, J. H. (2010). Pectin-Derived Porous Materials. *Chemistry-A European Journal*, *16*(4), 1326-1335.

White, R. J., Budarin, V., Luque, R., Clark, J. H., & Macquarrie, D. J. (2009). Tuneable porous carbonaceous materials from renewable resources. *Chemical Society reviews*, *38*(12), 3401–18.

Xie, K., Zhang, Y.,Yu, Y. (2009); Preparation and characterization of cellulose hybrids grafted with the polyhedral oligomeric silsesquioxanes (POSS); *Carbohydrate Polymers* 77, 858–862.

Xie, K.,Yu,Y. , Shi Y.; (2009); Synthesis and characterization of cellulose/silica hybrid materials with chemical crosslinking; *Carbohydrate Polymers* 78 (2009) 799–805.

Yamashiki, T., Kamide, K., Okajima, K., Kowsaka, K., Matsui, T., & Fukase, H. (1988). Some characteristic features of dilute aqueous alkali solutions of specific alkali concentration (2.5 mol L−1) which possess maximum solubility power against cellulose; *Polymer journal*, 20(6), 447-457.

Yamashiki, T., Matsui, T., Saitoh, M., Okajima, K., Kamide, K., & Sawada, T. (1990); Characterisation of cellulose treated by the steam explosion method. Part 1: Influence of cellulose resources on changes in morphology, degree of polymerisation, solubility and solid structure. *British Polymer Journal*, 22(1), 73-83.

Yang Q, Qi H, Lue A, Hu K, Cheng G, Zhang LN (2011) Role of sodium zincate on cellulose dissolution in NaOH/urea aqueous solution at low temperature. *Carbohyd Polym* , 83:1185–119.

Yang, X., Sun, Y., Shi, D., & Liu, J. (2011). Experimental investigation on mechanical properties of a fiber-reinforced silica aerogel composite. *Materials Science and Engineering: A*, *528*(13), 4830-4836.

Yano, S., Maeda, H., Nakajima, M., Hagiwara,T., Sawaguchi, T.; (2008) Preparation and mechanical properties of bacterial cellulose nanocomposites loaded with silica nanoparticles; *Cellulose*, 15, 111–120

Zhang LN, Ruan D, Gao SJ (2002) Dissolution and regeneration of cellulose in NaOH/thiourea aqueous solution; *J Polym Sci Part B Polym Phys ,* 40:1521–1529

Zhang, H., Wu, J., Zhang, J., & He, J. (2005). 1-Allyl-3-methylimidazolium chloride room

temperature ionic liquid: a new and powerful nonderivatizing solvent for cellulose. *Macromolecules*, *38*(20), 8272-8277.

Zhang, J., Zhang, H., Wu, J., Zhang, J., He, J., & Xiang, J. (2010). NMR spectroscopic studies of cellobiose solvation in EmimAc aimed to understand the dissolution mechanism of cellulose in ionic liquids. *Physical Chemistry Chemical Physics*, *12*(8), 1941-1947.

Zhou, B., Shen, J., Wu, Y., Wu, G., & Ni, X. (2007). Hydrophobic silica aerogels derived from polyethoxydisiloxane and perfluoroalkylsilane. *Materials Science and Engineering: C*, *27*(5), 1291-1294.

Zugenmaier, P. (2001); Conformation and packing of various crystalline cellulose fibers, *Progress in Polymer Science* 26, 1341-1417.

# Chapter II:

# Materials and methods

# Introduction

In this second chapter we present materials used in this study and the preparation and characterization methods for bio-aerogels from cellulose and pectin, and their hybrids with silica.

First, the main materials used in this work are presented: cellulose, pectin, and silica precursors sodium silicate and polyethoxydisiloxane, as well as the solvents and chemicals used for the dissolution of starting materials and the preparation of gels.

The procedure used to obtain hydrophobic cellulose aerogel by chemical modification of cellulose is also described.

The different steps of the preparation of polysaccharide gels, aerogels and composites are given in details: polysaccharide dissolution, gelation (if any) and coagulation, mixing or impregnation with silica precursor, washing and supercritical drying.

The gelation of cellulose solutions mixed with sodium silicate was studied with dynamic rheological measurements.

The dry aerogels were characterized in terms of bulk density, specific surface area and porosity (specific porous volume and pore size distribution). The morphology of all samples was thoroughly checked by Scanning Electron Microscopy (SEM). The silica contents of cellulose-silica composites were evaluated by elemental analysis and Energy diffractive X-ray spectroscopy coupled with SEM.

Hydrophobicity of chemically modified samples was assessed by water contact angle measurements. The humidity uptake of the treated aerogels over time was also recorded and compared to non-hydrophobized materials.

The mechanical properties were examined by uniaxial compression measurements. Young modulus, yield stress and strain plus stress at break were characterized. Some Young moduli were also determined by ultrasonic velocity measurements.

Finally, the thermal conductivity of samples was measured by two techniques: hot-wire method and heat-flowmetry.

## Introduction

Ce chapitre présente les méthodes d'élaboration et de caractérisation des bio-aérogels à base de cellulose et de pectine ainsi que leurs hybrides avec la silice.

Premièrement, nous présentons les matériaux utilisés: cellulose, pectine et précurseurs de silice (silicate de sodium et polyéthoxydisiloxane), ainsi que les solvants et les produits chimiques servant à leur dissolution et à la préparation des gels.

La procédure pour obtenir des aérogels hydrophobes par modification chimique de la cellulose est également décrite.

Les différentes étapes de préparation des gels à base de polysaccharides et de leurs composites avec la silice sont décrites en détails : dissolution des polysaccharides, gélification et/ou coagulation, mélange ou imprégnation de la matrice par la solution de précurseur de silice, lavage et séchage supercritique.

La gélification des mélanges cellulose-silicate de sodium a été étudiée par des mesures en rhéologie dynamique.

Les aérogels, une fois séchés, ont été caractérisés en termes de densité apparente, surface spécifique et porosité (distribution de tailles de pores et volume poreux spécifique). La morphologie de tous nos échantillons a été étudiée en détails au microscope électronique à balayage (MEB). La teneur en silice des aérogels composites a été évaluée par analyse élémentaire et spectroscopie dispersive en énergie des rayons X couplée au MEB.

L'hydrophobicité des échantillons de cellulose modifiée a été contrôlée par mesure d'angle de contact avec l'eau. La reprise hydrique des aérogels hydrophobisés a été également mesurée et comparée à celle d'échantillons de référence natifs i.e. hydrophiles.

Les propriétés mécaniques ont été analysées par mesures des modules d'Young, contrainte et déformations seuil, et contrainte à la rupture via des tests de compression uniaxiale. Les modules d'Young pour certains composites ont également été déterminés par mesure de la vitesse des ultrasons à travers un échantillon.

Enfin, la conductivité thermique des échantillons a été mesurée par la méthode du fil chaud et par thermo-fluxmétrie.

# 1. Preparation of polysaccharide and polysaccharide-silica composite aerogels

## 1.1. Materials

### 1.1.1. Cellulose

In this work two sources of cellulose were used:

Avicel PH101 was purchased from Sigma-Aldrich. It is microcrystalline cellulose (MCC) with a degree of polymerisation of 180, as given by the manufacturer. Avicel is a white microcrystalline powder with a mean size of particles around 50 μm. This cellulose was used as the basis of aerogels from cellulose-NaOH solutions (chapter III). It was also the starting material for cellulose chemical modifications to obtain hydrophobic materials (chapter V).

Cellulose of higher molecular weight was kindly provided by Thuringian Institute of Textile and Plastics Research (TITK), Rudolstadt, Germany; the degree of polymerization is 600, as provided by TITK. This material was used to elaborate the aerogels from cellulose-ionic liquids solutions (chapter IV).

### 1.1.2. Pectin

The pectin studied was citrus pectin, purchased from Sigma Aldrich. The proportion of galacturonic acid in this pectin is above 74% with at least 6.7% of methoxy groups as given by the manufacturer. The degree of etherification can be determined by IR spectroscopy (Synytsya, 2003; Rudaz, 2013): a strong band at 1740 cm$^{-1}$ is attributed to the C=O stretching of -COOCH$_3$ groups, while –COO$^-$ ions generate an absorption band at 1640 cm$^{-1}$. By using the peak height of the bands at 1740 and 1610 cm$^{-1}$, DE can be calculated with the following equation (eq.II.1), with $A_{COOCH3}$ being the area of the band corresponding to esterified carboxyl groups, and $A_{COO^-}$ the area of the band corresponding to free carboxyl groups:

$$DE = \frac{A_{COOCH3}}{A_{COOCH3} + A_{COO-}}$$
(II.1)

With (Eq.1), the degree of esterification of citrus peel pectin DE$_{citrus}$ = 52%.

### 1.1.3. Silica precursors

To elaborate one-pot composites (chapter III), sodium silicate solution (Na$_2$SiO$_3$, general purpose grade) was purchased from Fisher Scientific and used as received.

For the impregnation of coagulated polysaccharides (chapters IV, V and VI), the silica precursor used was a polyethoxydisiloxane (PEDS). PEDS, is the prepolymerized form of tetraethoxysilane (TEOS), prehydrolyzed under H$_2$SO$_4$ catalysis, with SiO$_2$ concentration of 20 wt% in ethanol. Analysis by dynamic light scattering (DLS) and sterical exclusion chromatography performed at Institut Charles Sadron, Strasbourg, France, showed that the mean length of PEDS oligomers was about 7 monomer units; the mean particle size was around 1nm, with a small quantity of bigger agglomerates (< 1μm) dispersed in the solution. It was kindly provided by ENERSENS, Bourgoin-Jallieu, Isère, France.

### 1.1.4. Solvents and other chemicals

Ionic liquid 1-ethyl-3-methylimidazolium acetate (EmimAc) was purchased from BASF. Dimethylsulfoxyde (DMSO, purity > 99%), N,N,dimethylformamide (DMF, purity >98%), methanol (98% purity), and ethanol (purity 98%) were purchased from Fischer Scientific. All solvents were used as received.

Hydrochloric acid (HCl aqueous solution, 32%wt) and citric acid ($C_6H_8O_7$, purity > 97%) was purchased from Fisher Scientific. The catalyst used for the gelation of the PEDS precursor was $NH_4OH$ (35 wt% aqueous solution), purchased from Sigma-Aldrich.

Reagents for the synthesis of tritylcellulose, lithium chloride (99% purity), triphenylmethyl chloride (the triphenylmethyl group will be referred as "trityl" in the following) (98% purity), N,N-dimethylformamide (DMF), N,N Dimethyl acetamide (DMAc, 99% purity), NaOH, and pyridine (purity > 95%) were purchased from Fisher Scientific.

## 1.2. Cellulose solutions and gels

### 1.2.1. General principle of making polysaccharide-based aerogels

The preparation of polysaccharide-based aerogels (or bio-aerogels) can be summed up in three essential steps (figure II.1): dissolution of polysaccharide in an appropriate solvent, gelation (if any) and coagulation, solvent exchange and drying with supercritical $CO_2$.
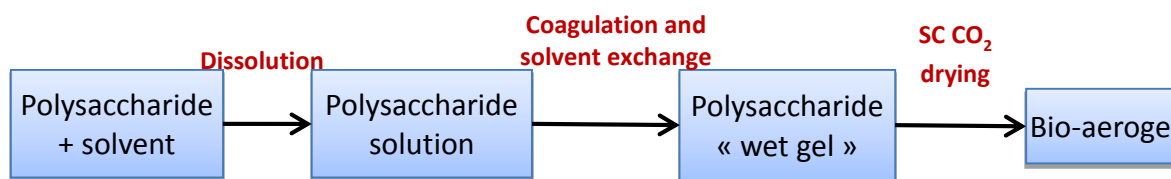


**Figure II.1 : Preparation of bio-aerogels**

### 1.2.2. Preparation of aerogels from 8%water-NaOH solutions : cellulose and cellulose-silica composites

The one-pot process followed for the synthesis of composite aerogels is presented on figure II.2. Cellulose was dried for 2 hours in a vacuum oven (50 °C, 50 mbar) before dissolution. So-dried cellulose was impregnated with water for 1h at 5 °C. 15.2%wt NaOH aqueous solution was prepared under magnetic stirring (250 rpm) and ZnO was added immediately after NaOH dissolution. After total dissolution of ZnO, this aqueous mixture was cooled to - 6 °C. ZnO was added to ensure better cellulose dissolution and to slow down cellulose gelation (see part 3.1). Then wet cellulose and aqueous NaOH-ZnO solution were mixed at - 6°C under mechanical stirring (500 rpm) for 2 h; final solutions were of 5 wt% cellulose dissolved in aqueous 8 wt%NaOH-1wt%ZnO, solution pH was 14.

40wt% sodium silicate solution was prepared by dissolving solid $Na_2SiO_3$ at 75 °C in distilled water under mechanical stirring (350 rpm) for about 2 h, until a clear solution was obtained. The pH of the resulting sodium silicate solution was 14.

The solution of sodium silicate was cooled to - 6°C (no precipitation was observed by eye) and mixed with cellulose-8%NaOH-1%ZnO solution at - 6°C in various proportions. The obtained mixtures were poured into cylindrical plastic moulds and sealed. The mixtures spontaneously

solidified in a few minutes at ambient temperature. Typical sample shape was a disk of 4 cm diameter and 1 cm height. The samples were then immersed in 100 ml of either 0.3M HCl or 0.2M citric acid solution to neutralize NaOH, coagulate cellulose and induce the formation of silica particles from $Na_2SiO_3$ inside the pores of coagulated cellulose, according to reaction (1). The volume of 0.3M HCl or 0.2M citric acid bath was such that the amount of acid was equal to one molar equivalent of NaOH (for neutralization) plus 2 molar equivalents of sodium silicate (necessary for silica condensation, reaction (1)). As a reference, some solidified samples were simply coagulated in water.

$$Na_2SiO_3 + 2HCl \rightarrow SiO_2 + 2\ NaCl + H_2O$$
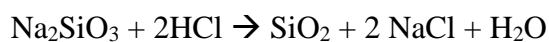
(a)
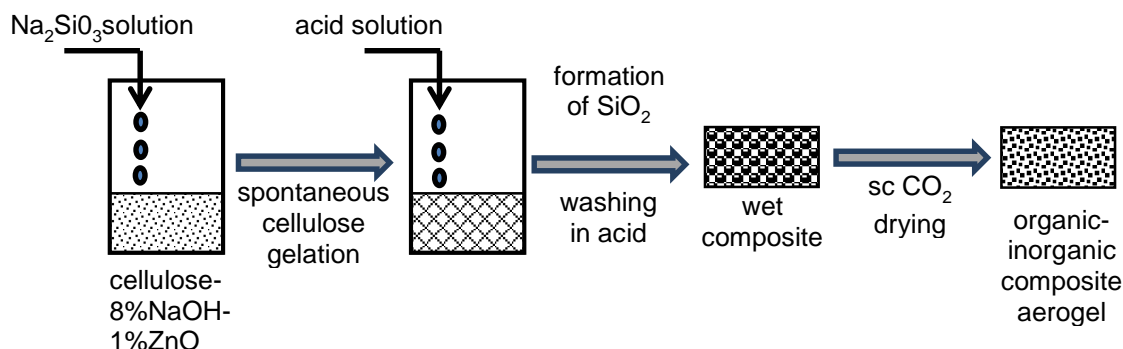


**Figure III.2 : Scheme of "one-pot" synthesis of organic-inorganic composite aerogels from mixed aqueous solutions of cellulose-8%NaOH-1%ZnO and sodium silicate (Demilecamps et al., 2014).**

This method allows an efficient mixing of cellulose and silica precursor, while controlling the gelation for each phase. NaOH-cellulose solution gels spontaneously depending on parameters such as temperature, cellulose concentration, or presence of other solutes. Sodium silicate only gels when the pH of the system is lowered, as is the case when it is put into an acid bath.

### 1.2.3.  Cellulose solutions from cellulose-EMIMAc solutions

First, cellulose powder was dried for 2 hours in a vacuum oven (50 °C, 50 mbar) before dissolution. Cellulose was dissolved in EMIMAc:DMSO = 80:20 for 16 h at 70 °C to form a 3 wt% cellulose solution. DMSO was used to facilitate cellulose dissolution due to solvent viscosity decrease; at this concentration of DMSO cellulose is completely dissolved according to the phase diagram obtained for EMIMAc:DMSO mixture (Le, Rudaz and Budtova, 2014). Cellulose solution was poured into plastic moulds and coagulated in ethanol. Then several washings with ethanol (the volume of ethanol being 3-5 times that of the gel) were performed, with solvent exchange every 24h, to fully remove the traces of cellulose solvents.

## 1.3.  **Synthesis of chemically hydrophobized cellulose: tritylcellulose**

### 1.3.1.  Synthesis procedure

The synthesis of tritylcellulose was performed using the procedure described in (Camacho Gomez et al., 1996; Pour et al., 2015). The grafting of triphenylmethyl groups on the carbon 6 of cellulose was done using an etherification reaction of MCC and tritylchloride, in the presence of pyridin. The cellulose solvent was DMAC/LiCl.
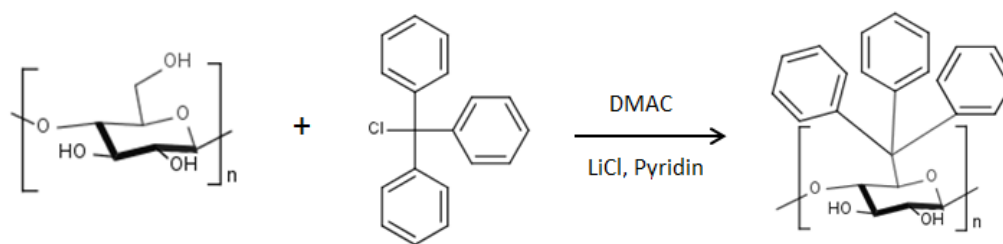
**Figure II.3: Reaction of tritylchloride and cellulose**

The molar proportions of each reactant, for a batch of 500 mL, is shown on table II.1. Cellulose was swollen in DMAc for 16 h at ambient temperature, under mechanical stirring (500 rpm), and then the system was heated for 2 hours at 130 °C. After cooling to 100 °C, lithium chloride was added and the mixture was let to cool until reaching ambient temperature. Tritylchloride (3 molar equivalent per anhydroglucose unit) was dissolved in DMAc in the presence of pyridine for 1~2 hours, and added to cellulose solution. The reaction was then carried out under mechanical stirring (500rpm) for 48 h at 70 °C.

**Table II.1 : Proportions of reagents necessary for the synthesis of a 500 mL batch of tritylcellulose with a DS of 0.62.**

|  | Cellulose | TritylCl | LiCl | DMAc (swelling) | DMAc (grafting) | Pyridin |
|---|---|---|---|---|---|---|
| **Molar Eq** | 1 | 3 | 5,7 | 35 | 17,5 | 9,38 |
| **M (g/mol)** | 162,14 | 278,78 | 42,39 | 87,12 | 87,12 | 79,09 |
| **m (g)** | 12,97 | 66,91 | 19,33 | 243,94 | 121,97 | 59,35 |
| **n (mol)** | 0,080 | 0,240 | 0,456 | 2,80 | 1,40 | 0,750 |
| **V (ml)** |  |  |  | 260,3 | 130,2 | 60,6 |

Tritylcellulose was then precipitated with a methanol/ethanol mixture (1:3 v/v) and filtered. The filtrate was re-dissolved in DMF, precipitated again with methanol/ethanol 1:3 and washed for a few hours in methanol at room temperature. The so-obtained wet white powder was dried for about 16 h at 40 °C in a vacuum oven under primary vacuum (50 mbar).

### 1.3.2. Preparation of tritylcellulose aerogels

Tritylcellulose was dissolved in DMF, polymer concentrations were 5, 7.5 and 10 wt%. Dissolution was performed at ambient temperature under nitrogen atmosphere. The solution was poured into the appropriate molds. Tritylcellulose was coagulated by delicately pouring methanol over the surface to avoid damaging the fragile coagulated gel. This step was repeated every 24 h until complete coagulation. Solvent exchange with ethanol was then performed every 24 h for at least 5 days to ensure there was no remaining methanol; resulting "alcogels" were ready either for drying to obtain tritylcellulose aerogels or for the impregnation with silica sol.

## 1.4. Preparation of pectin gels

### 1.4.1. Gelation in acid media

Pectin and 1M HCl solutions (with various pectin concentrations) were mixed and stirred vigorously at room temperature for 4 h. A viscous solution was obtained. Solutions were centrifuged at 6000 rpm for 20 min to eliminate residual undissolved materials. They were poured into moulds and let gelling for 24 h to 48h (depending on pectin concentrations).

### 1.4.2. Reticulation with calcium ions

Citrus pectin was dissolved at different concentrations in water for 4h at room temperature. The pH was adjusted with a KOH 0.5M solution, to obtain a basic solution (pH was varied between 7.5 and 13). The resulting solution was centrifuged for 20 min at 6000 rpm, then poured into the appropriate molds.

Calcium chloride, from a calcium chloride 1M solution was added to give an overall calcium concentration in the mixture of 10 to 50 mM, depending on sample. The system was left to gel at room temperature for a few hours.

### 1.4.3. Washing of pectin gels in ethanol

Gels were immersed in a 50/50 vol/vol water/ethanol bath to coagulate pectin. The ratio of ethanol in the coagulation bath was then increased progressively to 100% (by 20% increment). Ethanol baths were then changed every day for 3 to 5 days.

## 1.5. Impregnation of gels with the silica phase

### 1.5.1. Diffusion-controlled impregnation

Coagulated-in-ethanol polysaccharides (cellulose or pectin gels) were immersed for 24h in a 16%wt PEDS solution in ethanol. The targeted concentration of silica was of 8%wt in the sample; thus we had $m_{gel} = m_{PEDS}$. Once the impregnation was complete, the sample was removed from the flask and immersed into the catalyst solution (1.3%wt $NH_4OH$ in ethanol-water 95:5 solution) for 24h at room temperature. The samples were then washed with ethanol, and stored in ethanol until drying.

### 1.5.2. Forced-flow impregnation

To increase the speed of cellulose impregnation, we used a pressure gradient to force the PEDS solution to pass through the porosity of the coagulated-in-ethanol polysaccharide matrix (chapter IV). Using 3-D printer, a homemade "filter" system was designed for the impregnation of wet disc-shaped samples with 4 cm diameter (figure II.4).



Filter

Primary vacuum

Tank

Gasket

Filter grid

Funnel
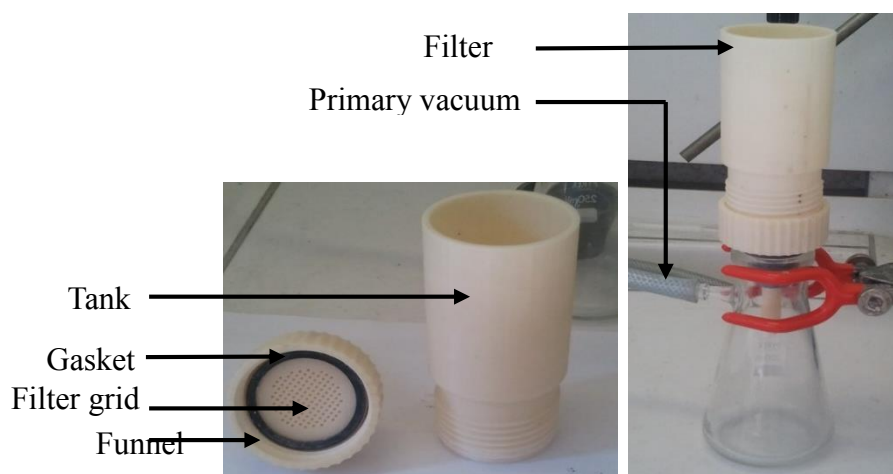
**Figure II.4: Homemade filter apparatus for forced-flow impregnation of polysaccharide gels.**

The filter system was fixed above a Büchner flask linked to a water-connected vacuum pump. The upper tank of the filter apparatus was filled with 16%wt PEDS solution so that $m_{PEDS} =$

2m$_{gel}$. The vacuum pump was run for 20-60 minutes, depending on sample thickness. The filtrate was recovered at different impregnation times; the impregnation was considered complete when the dry mass of the filtrate equaled the dry mass of the initial PEDS solution. Once the impregnation was complete, the gelation of the silica phase was performed immersed into the catalyst solution (1.3%wt NH$_4$OH in ethanol-water 95:5 solution) for 24h at room temperature.

## 1.6. Drying methods

### 1.6.1. Supercritical drying

A functional scheme of the supercritical (sc) CO$_2$ drying facility used at MINES ParisTech, Centre PERSEE, is shown on figure II.5.
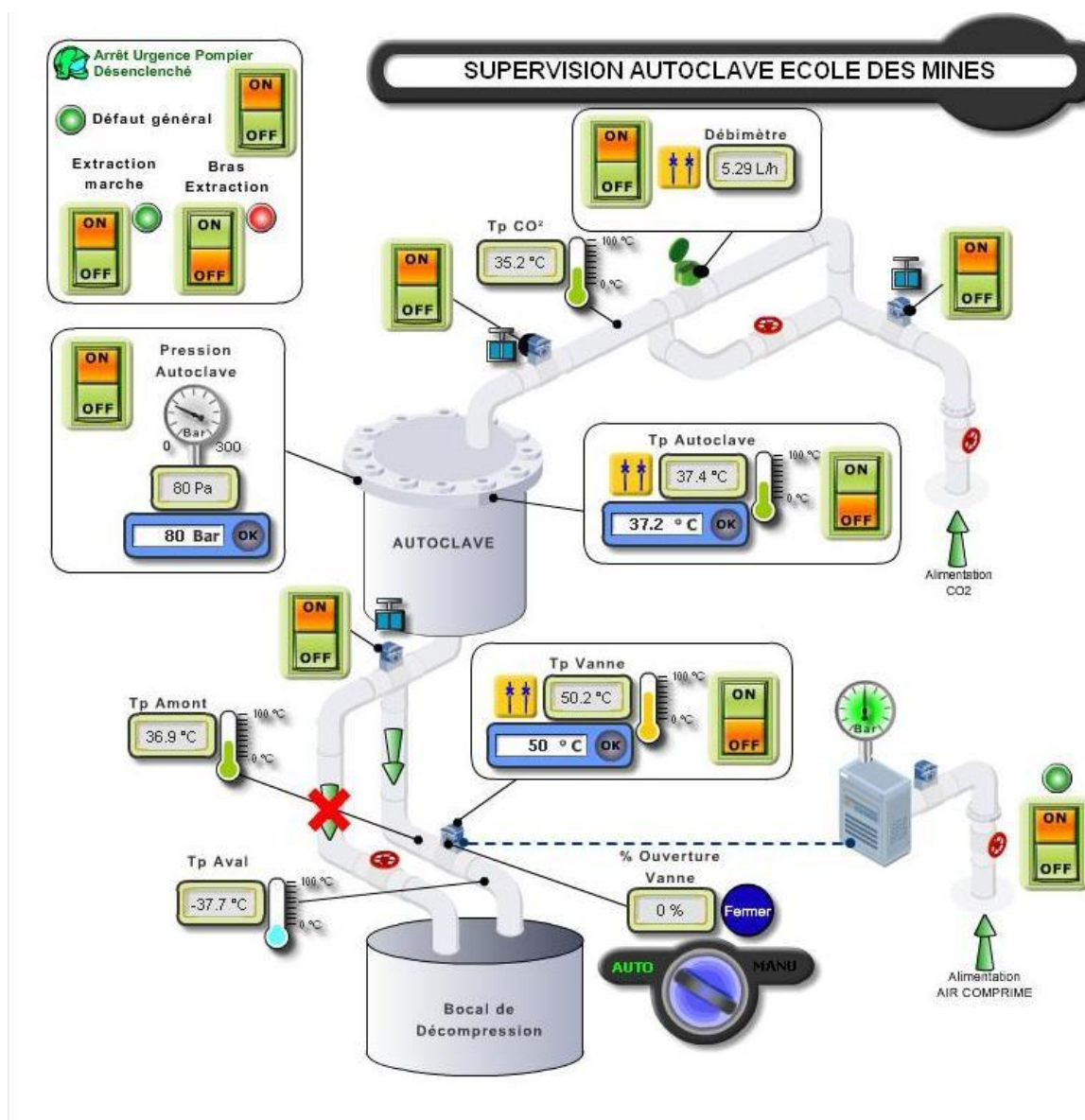


**Figure II.5: Functionnal scheme of the supercritical CO$_2$ facility at Centre PERSEE, MINES ParisTech..**

Gels were placed in a 1 litre autoclave filled with ethanol in order to avoid evaporation before the beginning of sc drying. The system was closed, pressurized to 50 bars with gaseous CO$_2$, and heated to 37 °C. The excess of ethanol was purged, maintaining the pressure and the temperature constant with gaseous CO$_2$. The system was then pressurized until the operating

conditions were reached: 80 bars and 37 °C. When the thermodynamic equilibrium was reached, the liquid phase in the pores of the precursor was exchanged with sc $CO_2$ through a dynamic washing step (80 bars, 37 °C, 5 kg of $CO_2$ per hour) over approximately 7 hours. The system was then slowly and isothermally depressurized (4 bars per hour at 37 °C) to avoid condensation of liquid $CO_2$ and cracking because of very low permeability of the matrices. Once the atmospheric pressure was reached, the system was cooled down to ambient temperature and the autoclave was opened (Masmoudi et al., 2006).

### 1.6.2. Freeze-drying

When a freeze-drying procedure was used in this work (chapter III), cellulose and cellulose-silica composite samples was coagulated directly in water and no washing in ethanol was performed. These swollen-in-water samples were placed first in a glass beaker. A close contact with glass walls is preferable since it will optimize heat transfer during freezing. Beakers were immersed in either in a liquid nitrogen (-196°C) bath for 3 minutes or in an ethanol bath placed in a freezer for about an hour. Frozen samples were then placed in a freeze-dryer Cryotec Cosmos 80. Vacuum was slowly made inside the chamber so that cracks were avoided. Samples were let drying for 48 hours. Water vapour was condensed in the refrigerated unit (Figure II. 6)
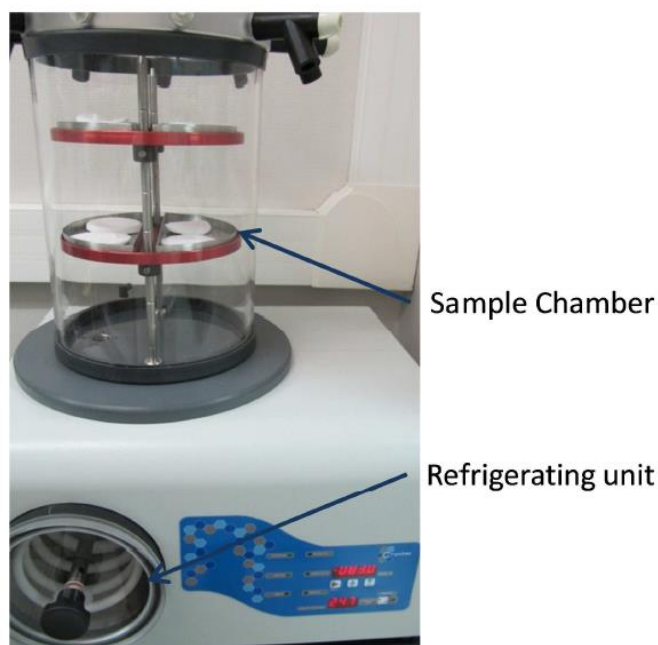


**Figure II.6: Freeze drying apparatus.**

### 1.6.3. Ambient pressure drying

Ambient pressure drying was performed at 60 °C overnight in a hermetic lab oven, or at ambient temperature for 7 days. In order to increase ambient humidity around the gels and minimize convection effects during drying (Cervin et al., 2013) the gels were placed in a petri dish and covered with a perforated aluminium cap.

# 2. Characterization of the materials

## 2.1. Rheological study of cellulose and cellulose-sodium silicate solutions and mixtures

### 2.1.1. Determination of the gel point of cellulose-sodium silicate solutions

The determination of gel point was performed following the procedure established by (Winter and Chambon, 1986) on polymethildisiloxane gelling systems. The method follows the evolution of elastic modulus, G', and viscous modulus G'' over time at constant frequency. At first the gelling system behaves like a viscous fluid: the viscous modulus is higher than the elastic modulus. As gelation goes on, both moduli increase over time, until the system behaves as an elastic solid when G' becomes higher than G''. The gel point $t_{gel}$ is taken at the time where G'=G''(figure II.7).
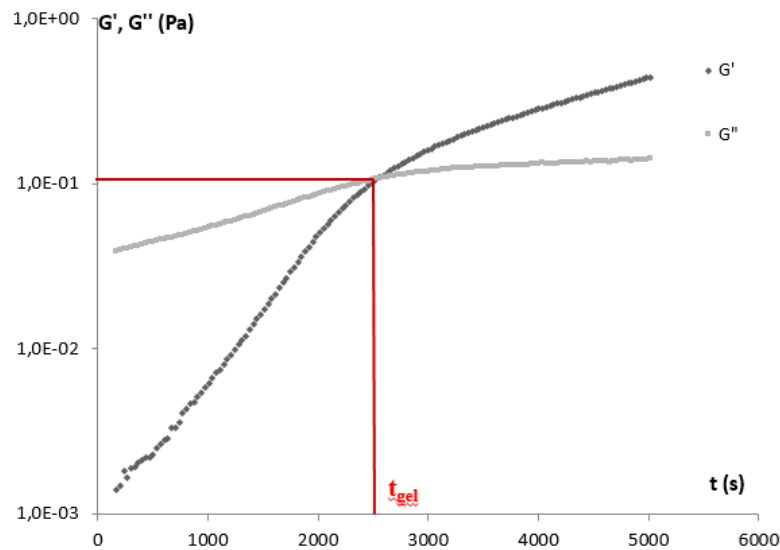


**Figure II.7: Example of the determination of gel point for a cellulose-sodium silicate solution at 25 °C.**

Measurements of dynamic rheology of cellulose-sodium silicate solutions were performed on a Bohlin Gemini rheometer equipped with cone-plate geometry (4°–40 mm) and Peltier temperature control system. The measurements were done at a frequency of 0.1 Hz and the stress was 0.1 Pa to ensure being in the linear regime, and temperatures between 0 °C and 40 °C were studied.

## 2.2. Chemical composition of polysaccharides and polysaccharide-silica composites

### 2.2.1. Elemental analysis

To evaluate the silica to cellulose ratio in the composite materials, elemental analysis was done in CNRS Service Central d'Analyse (Villeurbanne, France), with a microanalyzer CHN. Wt% of silicium ($wt\%_{Si}$) was measured allowing the calculation of wt% of silica ( $wt\%_{SiO_2}$) (eq.2) and silica mass yield in the dry aerogel ( $Yield_{SiO_2}$) (eq.II.2):

$$wt\%_{SiO_2} = \frac{M_{SiO_2}}{M_{Si}} wt\%_{Si}$$

(II.2)

where $M_{Si} = 29$ g/mol and $M_{SiO_2} = 61$ g/mol are the molar mass of silicon and silica, respectively.

$$Yield_{SiO_2} = \frac{wt\%_{SiO_2}}{wt\%_{SiO_2}(th)}$$ (II.3)

The theoretical yield in $SiO_2$ is expressed as follows (eq II.4):

$$wt\%_{SiO_2}(th) = \frac{wt\%_{SiO_2,max}}{wt\%_{cellulose} + wt\%_{SiO_2,max}}$$ (II.4)

where $wt\%_{SiO_2,max}$ is the silica concentration in the dry material (for a given initial proportion between cellulose and silica) in case of total silica conservation in the sample during processing (coagulation, washing and drying steps).

### 2.2.2. FTIR spectroscopy

Fourier-transform infrared (FTIR) spectroscopy was performed using a Bruker Tensor 27 TGA-IR (figure II.8) with OPUS 5.6 software. Samples were analyzed in attenuated total reflectance mode (ATR) using a Pike MIRacle accessory equipped with a Ge crystal (Pike Technology). The spectrum has been collected 16 times and corrections for $CO_2$ and water were applied to eliminate background noise.



**Figure II.10: Infrared spectrometer Brüker Tensor 27 with ATR equipment.**

## 2.3. Electron microscopy

### 2.3.1. Scanning Electron microscopy

Scanning electron microscopy (SEM) gives information on the morphology of a sample at the micrometer scale. A focused beam of electrons is scanning the sample in a high vacuum environment; the interaction of the electron beam with the sample produces the emission of various particles (electrons, photons) that are analysed through a detector. The electrons from the beam interact with the surface within a pear-shaped volume called the *interaction volume* (figure II.9.a). Depending on the depth of interaction and the energy of the electrons re-emitted by the sample, several types of detected particles can be distinguished (figure II.9.b):
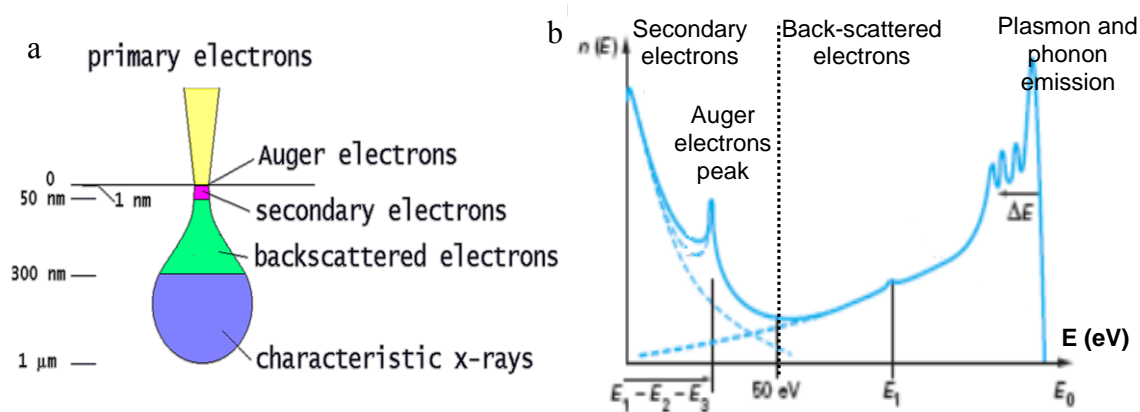
**Figure II.11: (a) Interaction volume of electrons on a sample surface and (b) Energy diagram of the electrons re-emitted by the scanned sample. $E_1$ corresponds to the ionisation energy.**

Secondary electrons originate from inelastic interactions with the electron cloud of atoms near the surface of the sample. They have low energy ($< 50$ keV). The detection of these electrons give information about the topography of the sample, up to a depth of a few tens of nm. Secondary electron detectors allow higher resolution images than back-scattered detectors.

Back-scattered electrons are the result of elastic or quasi-elastic interaction with the atom cores of the sample. Their energy is higher than that of secondary electrons, and is close to the energy of the incident beam. They come from deeper inside the sample. Back-scattered electrons give information on the sample atomic composition, as the number of re-emitted electrons increase with the atomic number.

Finally the Auger electrons are emitted from extreme surface atoms which had an electron from an inner layer ejected by the action of the incident beam. An electron of higher energy may fill the vacant space left, resulting in a release of energy; this energy can be transferred to another atomic electron, which is ejected in turn from the atom; this phenomenon is called Auger emission.

In order to get sufficient signal from secondary electrons, and to avoid accumulation of electrostatic charge at the surface, the samples must be electrically conductive. Insulating samples, such as the aerogels studied in this work, must be metallized by a thin (few nm) coating of gold or platinum, and are glued to a metallic support by a conductive adhesive, like carbon tape or silver glue. Metallization is performed by putting the samples in a small vacuum chamber. Then, argon gas is ionized by the action of an electric field; the positively charged argon ions interact with a negatively charged gold or platinum foil. The argon ions knock gold/platinum atoms from the surface of the foil. These gold atoms then settle onto the surface of the sample producing a thin metallic coating.
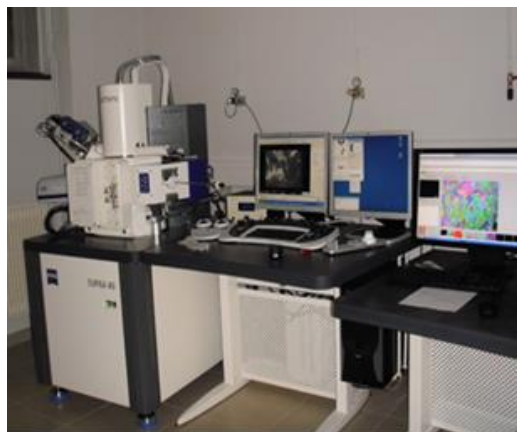
**Figure II.12: High-resolution scanning electron microscope Zeiss Supra 40**

The morphology of our aerogel samples was studied using high resolution scanning electron microscope SEM-FEG Zeiss Supra 40 (figure II.10). Acceleration voltage was set up at 3 keV and a diaphragm of 20µm. Samples were coated with a 7 nm platinum layer on a QUORUM Q150T rotating metallizer before observations.

### 2.3.2. Energy diffractive spectroscopy

Energy diffractive spectroscopy (EDS) analyses the elemental composition of a sample, by detecting X-rays emitted by the sample surface during the interaction with an electron beam from a SEM. The beam excites atoms in the sample, and they release energy in the form of X-rays. The energy of emitted X-rays is characteristic from the atoms that produced them. Thus a spectrum can be obtained, where the different elements in the sample are identified by peaks at characteristic energy values. The electron beam can be precisely controlled, to analyze selected areas of the material.

In the case of EDS analysis, metallized samples could not be used because the signal from the surface metal coating partly masks the signal from the sample. Non-metallized, electrically insulating samples had to be studied with an environmental electron microscope. This type of SEM allows to study samples in back-scattered electrons at low vacuum (0.1 to 1.3 mbar), which does not requires the samples to be metallized.
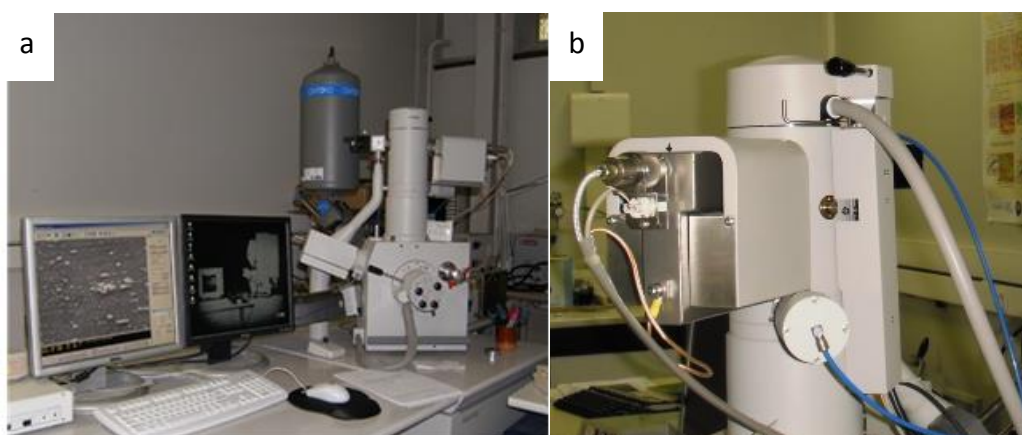


**Figure II.13: (a) XL30 environmental scanning electron microscope and (b) Column and EDS X-ray detector**

Philips XL30 environmental scanning electron microscope (figure II.11.a) coupled with an X-ray detector (figure II.1.b) was used to study silicon distribution inside the composite aerogels by Energy Diffractive Spectroscopy (EDS). An acceleration voltage of 12 keV was used and the vacuum pressure in the chamber was 0.5mbar.

## 2.4. Density and porosity measurements

### 2.4.1. Density measurements

The bulk (or apparent) density of a sample is defined as the ratio between its mass and the volume of ist enveloppe (eq II.5).

$$\rho_{bulk} = \frac{m}{V} \tag{II.15}$$

If a sample shape is not regular, it is difficult to precisely evaluate its volume by simple geometric measurements. The volume of samples was thus evaluated via powder pycnometry.

The measurements were done using a powder pycnometer Geopyc 1360 from Micromeritics (figure II.12). A glass chamber is filled with a powder of small, rigid spheres of ceramics and graphite with a heterogeneous granulometry (40 to 230 μm). The powder has a high degree of flowability, and is called under the commercial name DryFlo®. For all experiments we assumed that the powder could not penetrate pores smaller than 15 μm.



**Figure II.12: Powder pycnometry densimeter Geopyc 1360**

The powder is compressed inside a glass tube by a piston applying a determined force. First, the displacement $l_0$ of the piston with the powder alone is registered for the predefined force. Then the sample is weighted and introduced into the tube with the powder. The sample must be fully enveloped by the powder to ensure reliable measurements. Then the displacement of the piston l at the same compression force is recorded; the sample volume can be calculated from the tube diameter D and the displacement values (eq. 6).

$$V = \left(\frac{D}{2}\right)^2 \times (l - l_0) \times \pi \tag{II.6}$$

A 19.1 mm sample chamber and a force of 25 N were used within this study, particularly optimized for fragile porous materials based on our internal expertise.

### 2.4.2. Determination of apparent porosity

Porous materials such as aerogels and foams are materials containing cavities or channels, filled with air, called pores, and a solid backbone. The porosity of a material is defined as the ratio between the volume of void space and the total volume (solid + voids). Apparent porosity (*i.e.* open porosity) can thus be determined from the bulk and skeletal density (equation 7). The bulk density is generally determined by mercury porosimetry or powder pycnometry. The skeletal density $\rho_{skeletal}$ of a sample is the density of the material calculated when excluding all open pores and open spaces, it is generally calculated from helium pycnometry.

$$\varepsilon = \frac{V_{pores}}{V_{total}} = 1 - \frac{\rho_{bulk}}{\rho_{skeletal}} \tag{II.7}$$

To be as precise as possible, we can make a distinction between open and closed pores. The former are easily characterized by gas adsorption techniques as well as pycnometry (mercury or powder), while the latter cannot be accessed by these molecules. The total pore volume is the sum of the volume of open and closed pores.

### 2.4.3. Principle of gas adsorption

Nitrogen adsorption at 77 K was used to determine the specific surface area and pore size distribution in the materials. Gas adsorption is the accumulation of gas molecules over the surface of a material, at the gas-solid interface. We can distinguish between chemisorption, where the gas molecules form chemical covalent bonds with the adsorbent, and physisorption, where the gas is connected to the adsorbent by weaker physical links such as Van der Waals interactions.

Physisorption experiments are conducted at the boiling point of liquid nitrogen (77 K) at atmospheric pressure. The adsorption isotherm plots the adsorbed quantity of gas per gram of adsorbate as a function of equilibrium relative pressure $p/p^0$, where p is the equilibrium pressure of adsorbate gas and $p^0$ the vapour pressure of nitrogen. Adsorption is reversible and the opposite phenomenon is called desorption. The adsorption/desorption isotherms are a way to evaluate the porosity of materials. According to IUPAC there are six different types of adsorption isotherms (Sing et al., 1985) (figure II.13).
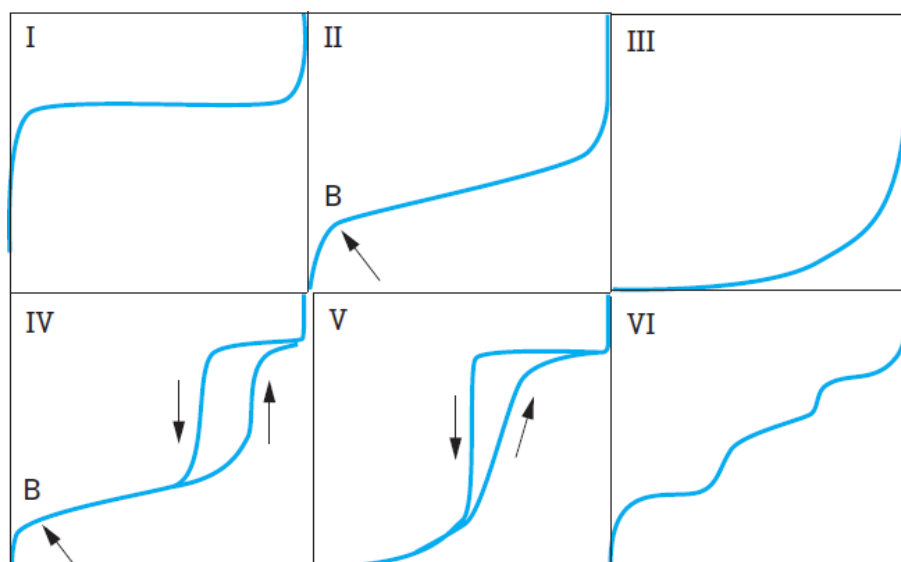
**Figure II.13: The six types of adsorption/desorption isotherms according to IUPAC classification (adapted from Luciani, Denoyel and Rouquerol, 2003).**

Type I isotherm has a horizontal plateau due to the saturation of the absorbent event with increasing pressure. It is typical for microporous solids with small external surfaces.

Type II isotherm has a gradual increase of adsorbed quantity with pressure and is obtained for macroporous or non-porous solids. The adsorbed layer is thickening gradually and is typical of multilayer adsorption.

Type IV isotherm is similar to type II for low relative pressure. At higher relative pressure, a saturation plateau is observed with variable length. It is typical for mesoporous adsorbent. A hysteresis loop is observed during desorption, due to capillary condensation, which is unique to each adsorbate/adsorbent system.

Type III and V isotherms are not common and have a convex plot due to very weak interactions between adsorbate and adsorbent. They are more typical for water vapour adsorption on hydrophobic surface.

Type VI isotherm was observed for adsorption by energetically homogeneous surfaces on which gas layers are successively adsorbed.

The properties of porous materials strongly depend on the pores shape and diameter. Three categories of pores are defined by IUPAC depending on size (Sing et al., 1985):

- Macropores have a diameter above 50 nm.
- Mesopores have diameters between 50 and 2 nm.
- Micropores have a diameter below 2 nm

### 2.4.4. Specific surface area by BET method

Specific surface area is the total open pore surface surface per gram of matter. The specific surface area is strongly related to particle diameters and size distribution as well as their surface rugosity; as a consequence materials with many small pores gives higher specific surface area. Thus it is an important characteristic for porous materials. The Brunauer, Emmett and Teller method was defined in 1938 to determine the specific surface areas of porous solids. The BET

model is based on a multilayer adsorption model, assuming an absence of interaction between adsorption layers, the number of adsorption layers on a solid is infinite, and thus the Langmuir theory can be applied to each layer. In a relative pressure range between 0.05 and 0.3, the adsorption isotherm is quasi-linear and follows the following equation (eq II.8):

$$\frac{{}^p/_{p^0}}{q_{ads}(1 - {}^p/_{p^0})} = \frac{(C - 1){}^p/_{p^0}}{q_m C} + \frac{1}{q_m C} \tag{II.8}$$

where $q_{ads}$ the amount of gas adsorbed at the relative pressure $p/p^0$, $q_m$ the monolayer capacity (corresponding to the quantity of adsorbate necessary to fill an adsorption monolayer), and C the BET constant.

When the available pore surface is completely covered by adsorbed molecules, specific surface area can be determined by (eq. II.9):

$$S_{BET} = \left(\frac{q_{ads}}{m_s}\right) N_A \sigma_m \tag{II.9}$$

with $N_A$ the Avogadro number ($N_A = 6.022.10^{23}$), $\sigma_m$ the cross section covered by each nitrogen molecule ($\sigma_m = 0.162$ mm²) and $m_s$ the mass of adsorbent.

As the apparatus measures the volume of adsorbed gas $v_{ads}$, the quantity adsorbed is obtained by (eq.10):

$$q_{ads} = \frac{v_{ads}}{v_l} \tag{II.10}$$

with $v_l$ the molar volume of perfect gas defined by $v_l = 22\ 414$ cm³.mol⁻¹.

Thus the BET equation becomes (eq.II.11):

$$S_{BET} = \left(\frac{v_m}{m_s}\right) \frac{N_A \sigma_m}{v_l} \tag{II.11}$$

Experimentally, $S_{BET}$ was obtained by plotting $\frac{{}^p/_{p^0}}{v_{ads}(1-{}^p/_{p^0})}$ as a function of ${}^p/_{p^0}$ between 0.05 and 0.3. The slope and y-intercept of the linear curve give the constant C and the value of $q_{ads}$, allowing the direct calculation of $S_{BET}$.

### 2.4.5. Pore size distribution by BJH method

The pore size distribution of mesopores can be obtained by the Barett, Joyner and Halenda (BJH) method. It is based on capillary condensation of nitrogen inside mesopores. The Kelvin law can be applied (eq.II.12):

$$\ln\left({}^p/_{p^0}\right) = \frac{-2\gamma V_l}{r_K RT} \tag{II.12}$$

with $\gamma$ the surface tension, $V_l$ the molar volume of the adsorbed liquid at temperature T, and $r_K$ the radius of the liquid meniscus inside the pore.

In the case of nitrogen at 77K, the Kelvin law is:

$$r_K = -0.415(^p/_{p^0})$$

<div align="right">(II.13)</div>

The pore size distribution can be reconstructed from equation 12 for each relative pressure. The calculations are generally performed on the desorption curve, and gives information on pores with a radius lower than 80 nm.

### 2.4.6. Experimental setup for BET and BJH measurements

Specific surface area and BJH pore size distribution was determined using treatment of $N_2$ adsorption isotherms at 77 K on ASAP 2020 apparatus from Micromeritics (figure II.14). All samples were degassed for 300 minutes at 70 °C before analysis. To ensure consistent BET values without increasing too much the equilibration time, the mass of samples taken for measurements were comprised between 100 and 300 mg.
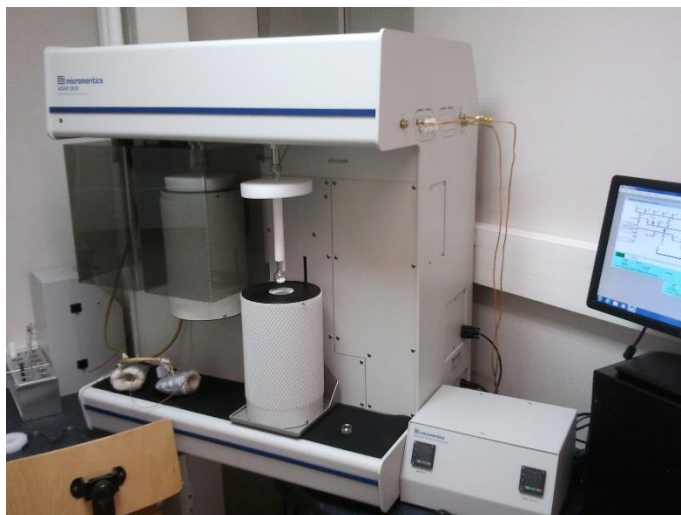


**Figure II.14: Gas adsorption apparatus Micromeritics ASAP 2020 for the analysis of specific surface area and pore size distribution.**

## 2.5. Study of hydrophobic properties

### 2.5.1. Water contact angle analysis

The simplest way to assess the hydrophobicity of a material is the measurement of the contact angle of the material with water. When a drop of water is deposed at the surface of a material, a thermodynamical equilibrium between the solid, liquid and gas phases is reached (figure II.15).
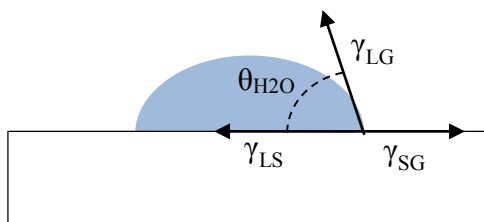


**Figure II.15: Contact angle and interfacial tensions at a sample surface.**

The surface tensions between the different phases are noted $\gamma_{SG}$ for the solid-gas interface, $\gamma_{LG}$ for the liquid-gas interface and $\gamma_{LS}$ for the liquid-solid interface; the contact angle $\theta_{H2O}$ can be theoretically determined from Young-Dupré equation (eq. 14):

$$\gamma_{SG} - \gamma_{LG} - \gamma_{LS}cos\theta_{H2O} = 0 \qquad \text{(II.14)}$$

Samples showing contact angles with water superior to 90° are considered hydrophobic. Generally the contact angle is measured directly at the surface of the sample. For all aerogels studied in this work, water contact angle measurements were performed with a Krüss Drop Analyzer DSA 100 goniometer in controlled atmosphere (20°C, 50%RH). 50mm$^3$ droplets were deposited on a sample flat and horizontal surface. The contact angle was measured from pictures of the droplets using Drop Shape Analysis software.

### 2.5.2. Aging studies in an humid environment

For water vapor uptake measurements, the sample was placed in controlled climate chamber Binder MKF 230 (figure II.16) at 20 °C and 20% relative humidity (%RH) for 24 hours and the mass $m_0$ and volume $V_0$ of the sample at this "dry point" was recorded. The sample was then submitted to 30 °C and 80% RH during 30 hours, and sample mass and volume, $m_t$ and $V_t$, respectively, were recorded as a function of time.



**Figure II.16: Controlled climate chamber Binder MKF 230.**

Mass and volume ratio at equilibrium, $H_m$ and $H_v$, respectively, were calculated as follows: (eq II.15 and II.16):

$$H_m(\%) = \frac{m_t - m_0}{m_0} * 100 \qquad \text{(II.15)}$$

$$H_V(\%) = \frac{V_t - V_0}{V_0} * 100 \qquad \text{(II.16)}$$

Long term aging tests over 45 days were performed by Markku Leivo and Tuomo Ojanen, at the Technical Research Centre of Finland (VTT, Helsinki) within the frame of the FP7 AEROCOINS project. The tests were carried out using closed containers including salt solutions producing known relative humidity conditions under constant temperature. The vessels were equipped with fans that circulate the air in order to ensure equal humidity distribution in the closed air space.

The aerogel samples were set in lightweight aluminum vessels, each set of material placed in its own vessel. First the test samples were dried out initially under 0 % RH. Then they were set in the containers having known relative humidity. The weight of the vessels containing the test materials were monitored until there were no significant changes. The final weights were used to solve the equilibrium moisture contents. The weight change under different relative humidity conditions were compared to the dry weight levels to acquire the moisture content of the material using eq. II.15.

Three different relative humidity levels were used in the experiments to find out the equilibrium moisture content levels. The samples were stabilized under different humidity conditions starting from 75 % RH and increasing the humidity to next level (85%RH and 95%RH) after the equilibrium was reached. The experiments were stopped if the samples showed signs of deterioration. All tests were performed at a constant temperature of 20°C.

## 2.6. Mechanical characterization

### 2.6.1. Sound velocity measurements

The mechanical properties of cellulose-silica composite aerogels from direct mixing of cellulose-NaOH and sodium silicate solutions (chapter III) were determined by sound velocity measurements performed by Gudrun Reichenauer (Bavarian Center for Applied Energy Research, Am Galgenberg 87, 97074 Wurzburg, Germany). It was established by (Gross, Reichnauer and Fricke, 1988) that the sound velocity in aerogel samples depended on sample bulk density with a scaling law.

Disc-shaped samples with 4 cm diameter and 1 cm thickness were placed between two piezoelectric sensors, one being the emitter, the second one the captor. An ultrasonic pulse was run through the sample; measuring the sound circulation time allows calculating sound velocity V.

Young's modulus $E$ of the samples can then be calculated from the density $\rho_{bulk}$ and the longitudinal sound velocity of the samples determined by ultrasonic run time (eq.II.17) (Gross, 1992):

$$E = \rho_{bulk} V^2 \frac{1 - \mu - 2\mu^2}{1 - \mu} = C_{11} \frac{1 - \mu - 2\mu^2}{1 - \mu} \qquad (\text{II}.17)$$

with $C_{11}$ being the elastic constant and $\mu$ the Poisson´s ratio which is equal to zero for Aerocellulose (Sescousse et al, 2011); thus we assumed $E = C_{11}$ for cellulose aerogels.

### 2.6.2. Uniaxial compression measurements

The mechanical properties of aerogels from cellulose, tritylcellulose, and pectin, as well as their composites with silica (chapters IV, V and VI) were characterized by uniaxial compression measurements. The experiments were carried out on Zwick mechanical testing machine. The samples were placed between two parallel plates. Before measurements, samples were polished to make upper and lower surfaces planar and parallel which was verified with a micrometric sensor. Two different loads were applied, as suggested in (Rudaz et al., 2014).

-100 N for precise measurements of Young modulus (E) in the linear visco-elastic regime.

-2000 N for complete stress-strain curve.

The samples were cylindrical in shape, with a diameter/length ratio of 2/3.

The tests were performed at room temperature (20-22 °C), atmospheric pressure and around 40%RH. The displacement rate was 1 mm/min and experiments were performed until 75-80% deformation or until sample break. These experimental conditions were chosen to be the same as in the works done previously in CEMEF on Aerocellulose samples (Gavillon, 2007). At least three samples per formulation were tested to ensure reproducibility and mean values for Young modulus and fracture stress were calculated. The experimental errors were determined, for each formulation, from standard deviation.

The compression for cellulose and pectin aerogels is uniform and the cross-section area of the cylindrical samples does not change during the tests (Sescousse et al., 2011; Rudaz et al., 2014). The stress $\sigma(t)$ is directly related to the ratio between the applied force $F(t)$ and the initial cross-section $A_0$ (eq.II.18):

$$\sigma(t) = \frac{F(t)}{A_0} = \frac{4F(t)}{\pi d^2} \tag{II.18}$$

The strain is defined by equation II.19:

$$\varepsilon = \frac{l(t) - l_0}{l_0} \tag{II.19}$$

with $l(t)$ the length of the sample at a given strain and $l_0$ its initial length.

The ratio between axial and transversal strains of a sample is the Poisson ratio, noted $\nu$ (eq. II.20).

$$\nu = \frac{\frac{L(t) - L_0}{L_0}}{\frac{l(t) - l_0}{l_0}} \tag{II.20}$$

with $L(t)$ the width of the sample at a given strain and $L_0$ the initial width.

An example of stress-strain curve for Aerocellulose is shown on figure II.17.
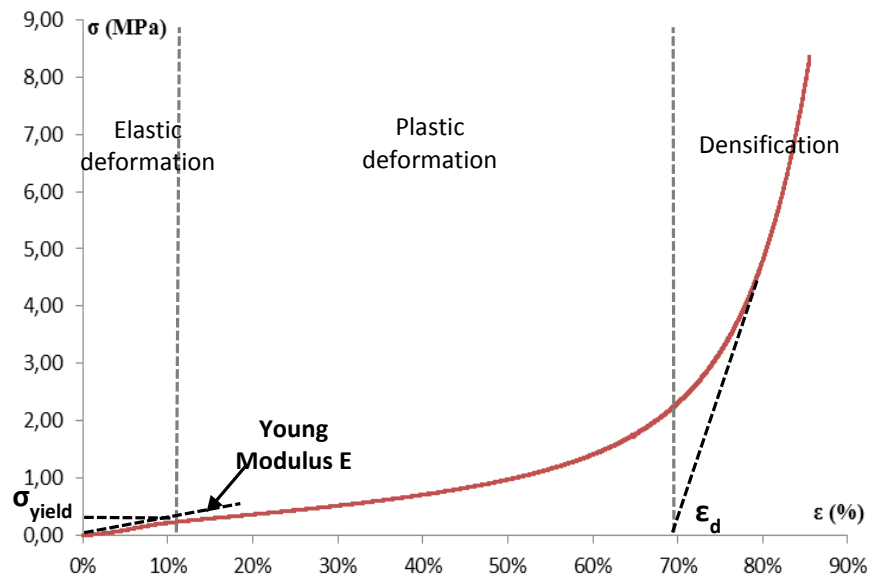
**Figure II.17: Example of stress-strain curve for an aerocelllose from 3%wt cellulose in EMIMAc/DMSO solution.**

On the stress-strain curve three domains can be distinguished:

The elastic domain corresponds to elastic, reversible deformation of the material. The cell walls are deformed under the stress but recover when the stress is released. In this domain stress is directly proportional to strain, and the proportionality coefficient is the Young modulus E. Thus the Young modulus can be determined by the slope of the curve $\sigma = f(\varepsilon)$.

Then the plasticity domain is reached: cell walls start to collapse irreversibly by buckling under the increasing stress. The observed plateau on the stress-strain curve is called the plasticity plateau. The onset of plasticity is defined by the yield stress $\sigma_{yield}$ and yield strain $\varepsilon_{yield}$. During this step the material is absorbing energy.

The third domain of the stress-strain curve is the densification domain. Cell walls start to touch each other, leading to pore collapse and the stress steeply increases as a result. The start of densification is given by the densification strain $\varepsilon_d$.
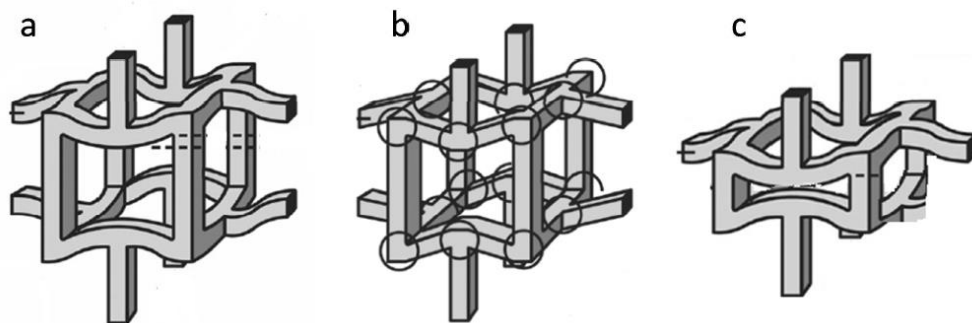


**Figure II.18: Schematic of the deformation of cell walls according to the open-foam model by (Gibson and Ashby, 1999), with a) elastic deformation; b) plastic deformation and c) pore collapse and densification.**

The total absorbed energy during the elastic + plastic domains is noted W. It is defined as the area under the stress-strain curve from 0 to the start of densification set at the densification strain $\varepsilon_d$. It can be calculated with (eq.II.21):

$$W = \int_0^{\varepsilon_d} \sigma(t)dt \qquad \text{(II.21)}$$

The mechanical properties of bio-based and silica aerogels can be compared with those of other cellular materials. A model for open-cell foams was described by (Gibson and Ashby, 1999). The model predicts a power-law dependence of Young modulus and yield stress with material bulk density (eq. II.22 and II.23).

$$E \sim \rho^m \qquad \text{(II.22)}$$

$$\sigma \sim \rho^n \qquad \text{(II.23)}$$

The model predicts a scaling exponent around 2 for foams. The power-law dependency of mechanical properties with bulk density was verified in the case of aerogels from silica (Alaoui et al., 2008), resorcinol-formaldehyde (Pekala et al.,1990), or cellulose (Gavillon, 2007; Sescousse, 2010; Sescousse et al., 2011). The scaling exponents calculated for aerogels were in all cases close to 3. This may be explained by inhomogeneities formed during gelation, such as side branches or dangling end chains, which do not contribute to the elastic properties of the main solid backbone (Ma et al., 2000).

## 2.7.  Thermal properties

The thermal conductivity of porous materials is the sum of three components: the solid backbone conduction, the conduction of the gas confined in the pores, and the radiative heat transfer contribution (eq. II.24).

$$\lambda = \lambda_{skeletal} + \lambda_{gas} + \lambda_{radiative} \qquad \text{(II.24)}$$

Two methods used in this study to measure the thermal conductivity are described below: hot wire dynamic measurements and hot plate steady state measurements.

### 2.7.1.  Hot wire measurements

Within the frame of AEROCOINS project thermal conductivities of cellulose and cellulose-silica composites (chapters III and V) were measured by the hot-wire method by Gudrun Reichnauer in Bavarian Center for Applied Energy Research (ZAE), Wurzburg, Germany, following the procedure described by (Nilsson et al., 1989). The experimental setup is pictured on figure II.19.
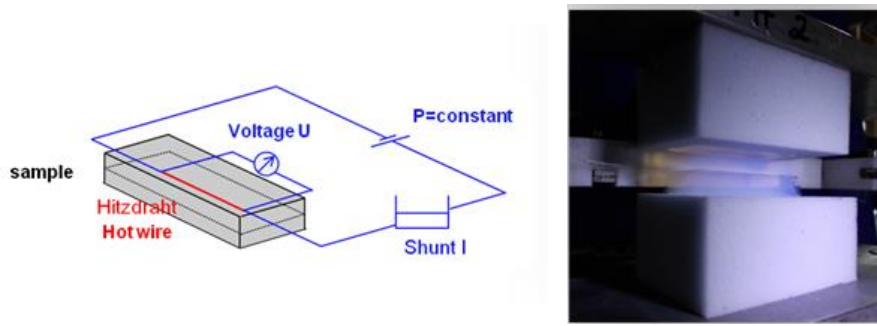
**Figure II.19: Functional scheme and picture of the hot wire apparatus used in ZAE. Courtesy of G. Reichnauer.**

The principle is as follows: a heating wire and a temperature sensor are placed between two identical samples with flat and parallel surfaces, a "thermal shock" is applied to the sample and the temperature increase is monitored over time. If the sensor is far enough from the extremity of the wire, the heating wire can be assimilated to an ideal, infinite, linear heat source. The sample thickness must be sufficient so that its external surface is considered isotherm, fitting the hypothesis of a semi-infinite media. Therefore the heat transfer can be considered one-dimensional and the heat transfer equation becomes, in long times (eq. II.25):

$$\Delta T = \frac{Q}{4\pi\lambda} ln \left(\frac{4.a.t}{r^2.C}\right) \tag{II.25}$$

with $Q$ the heat production of the thermal shock per unit time and unit length of the heating wire (W.m$^{-1}$),

- $\lambda$ the thermal conductivity (W.m$^{-1}$.K$^{-1}$),

- $a$ the thermal diffusivity (m².s$^{-1}$) with $a = \dfrac{\lambda}{\rho C_p}$ with $\rho$ the bulk density (kg.m$^{-3}$) of the sample and $C_p$ the heat capacity (J.kg$^{-1}$.K$^{-1}$).

- $r$ the distance between the wire and the thermocouple (m)

- $C$ a constant (C~1.781),

- $t$ is time.

The thermal conductivity of the sample can thus be determined by measuring the evolution of temperature of the sensor with time (eq. 26).

$$\lambda = \frac{Q}{4\pi} \frac{ln t_2 - ln t_1}{T_2 - T_1} \tag{II.26}$$

The heating wire and temperature sensor used in our experiments were a Pt-wire, 50 μm in diameter. It was placed in between two discs of 4 cm diameter and 1 cm thickness. The Pt-wire serves as the heating element and temperature sensor at the same time. At t = 0 the temperature of the wire was raised by an application of a constant electric power. Subsequently, the temperature was measured as a function of time for typically 20 s.

The temperature profile recorded depends on the thermal conductivity of the surrounding media i.e. the aerogel sample here. It was evaluated by fitting the experimental data with an analytical

solution that takes into account the contact resistance between the wire and the sample, as well as thermal losses along the wire (Ebert et al., 1993). To ensure good contact with the wire the sample surfaces facing the Pt-wire were carefully polished with sand paper. The samples were measured at ambient conditions (P, T and %RH). To provide better statistics each pair of identical samples was measured 10 times in a row. The resulting curves were averaged and used to calculate the mean thermal conductivity (eq. II.26).

### 2.7.2. Heat flow meter

Steady state hot-plate measurements were also performed to measure the thermal conductivity of bio-aerogels and their silica-based composites. A disc-shaped sample with flat and parallel surfaces was placed between two plates. The upper plate (or "hot plate") is heated at a temperature $T_h$ and the lower plate (or "cold plate)" is put at a lower temperature, noted $T_c$ (figure II.20). Once the temperature of each plate is constant, the heat flow passing through the sample from the hot to the cold plate is measured with a heat flux sensor; the thermal conductivity is given by equation II.27:

$$\lambda = \frac{Q.d}{A.(T_h - T_c)} \tag{II.27}$$

with $Q$ the quantity of heat through the sample (W), $A$ the sample area in m² and $d$ the thickness of the sample.
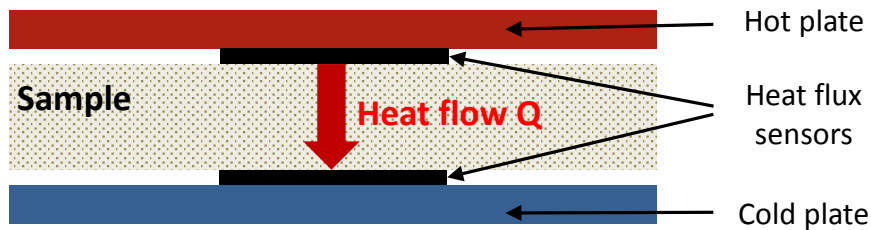


**Figure II.20: Principle of heat flowmetry.**

Two different heat flow meters were used for the measurements within this study:

- Laser Comp Fox 150 in PERSEE MINES ParisTech (chapter IV). This setting required samples of a minimal surface of 5 cm × 5 cm. The apparatus is pictured on figure II.21.



**Figure II.2: Fox 150 heat-flow meter in PERSEE MINES ParisTech.**

The temperature difference ΔT betwen hot and cold plates was fixed at 20 °C for all measurements. The thermal conductivity values were determined directly by the equipped flowmeter software *WinTerm32*.

- Micro-flowmeter Laser Comp Fox 200 in CSTB, Grenoble (chapter VI). Measurements were kindly performed by Hébert Salée. This setting was particularly adapted to the analysis of smaller samples, i.e. discs of 2-4 cm diameter. The setup and process is shown on figure II.22.
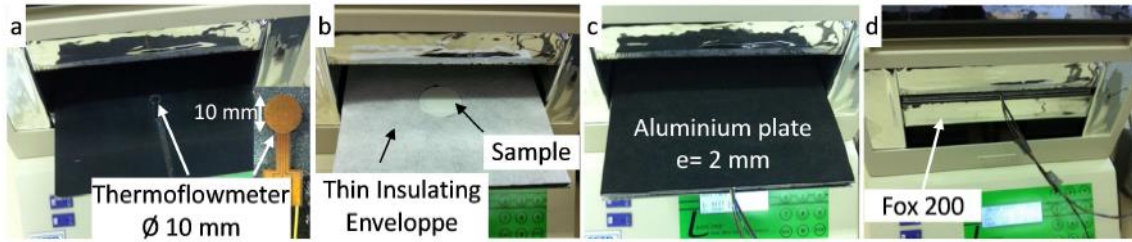


**Figure 14 Micro-heat-flowmeter from CSTB, Grenoble. (a) micro-flowmeters with 10 mm diameter; (b) sample embedded in a thin insulating envelope; (c) sample + microflowmeters and insulating envelope are placed between two aluminium plates (d) measurement of sample thermal conductivity in the heat flowmeter.**

The micro-flowmeter experiments were calibrated with reference commercial samples of known thermal conductivity: a glass wool IRMM-440 A with a thermal conductivity $\lambda = 0,0317 \pm 0,0002$ W.m$^{-1}$.K$^{-1}$, and a thin blanket Spaceloft® from the company ASPEN ($\lambda = 0,0160 \pm 0,0003$ W.m$^{-1}$.K$^{-1}$).

## Conclusions

In this chapter we have shown the materials used for preparing polysaccharide and silica based aerogels, as well as polysaccharide-silica composite aerogels.

The aerogel preparation is based on the dissolution of polysaccharides, cellulose or pectin, in an appropriate solvent, followed by gelation (case of pectin) and coagulation, solvent exchange with ethanol, and supercritical $CO_2$ drying. To make polysaccharide-silica composites, two methods are presented:

- "one-pot" or direct mixing of sodium silicate and cellulose solutions. The particular gelation of these mixtures was characterized by dynamic rheological measurements.
- Impregnation of a coagulated-in-ethanol polysaccharide by polyethoxydisiloxane solution.

Moreover, some hydrophobic aerogels can be prepared from chemically modified cellulose with tritylchloride.

The properties of the final aerogels were characterized in details.

Bulk density measurements were performed with powder pycnometry, and specific surface area analysis by nitrogen adsorption method. The morphology was characterized by SEM observations.

To assess the fraction of silica in the polysaccharide-silica composite, we evaluated the silica content by elemental analysis of silicium; the silica distribution inside the composites was evaluated by EDS spectroscopy coupled with SEM.

Some of the aerogels elaborated in this work are hydrophobic. To quantify their hydrophobic properties, we conducted water contact angle measurements, and water uptake of hydrophobized samples and non-hydrophobized ones was determined by putting the sample in controlled humidity and temperature environments for determined durations.

The mechanical properties of polysaccharide and composite aerogels were examined. Young modulus, yield stress and strain, and stress at break were determined from stress-strain curves from uniaxial compression measurements. In some cases, Young modulus was measured by measuring the run time of an ultrasonic pulse through a sample.

For the evaluation of thermal insulation properties of the various aerogels studied, two methods were used to determine the overall thermal conductivity of the materials in transitory and steady-date conditions: the hot wire and hot-plate methods respectively.

# References

Alaoui, A. H., Woignier, T., Scherer, G. W., & Phalippou, J. (2008). Comparison between flexural and uniaxial compression tests to measure the elastic modulus of silica aerogel. *Journal of Non-Crystalline Solids*, *354*(40-41), 4556–4561.

Camacho Gomez J.A., Erler U.W., Klemm D.O. (1996); 4-methoxy substituted trityl groups in 6-O protection of cellulose: homogeneous synthesis, characterization, detritylation, *Macromol. Chem. Phys.*, 197, 953-964.

Cervin N.T., Andersson L., Sing Ng J.B., Olin P., Bergström L., Wagberg L. (2013); Lighweight and strong cellulose materials made from aqueous foams stabilized by nanofibrillated cellulose, *Biomacromolecules,* 14, 503-511.

Ebert, H.P., Bock, V., Nilsson, O., Fricke,J. (1993); The hot-wire method applied to porous materials of low thermal conductivity, *High Temperatures-High Pressures,* 25, 391-402.

Gavillon, R. (2007). Préparation et caractérisation de matériaux cellulosiques ultra poreux. *PhD thesis*, Ecole des Mines de Paris.

Gross J, Fricke J, (1992) Ultrasonic Velocity-Measurements in Silica, Carbon and Organic Aerogels. Journal of Non-Crystalline Solids 145, 217-222.

Gross, J., Reichenauer, G., & Fricke, J. (1988). Mechanical properties of SiO2 aerogels. *Journal of Physics D: Applied Physics*, *21*(9), 1447.

Le, K.A, Rudaz, C., Budtova, T. (2014); Phase diagram, solubility limit and hydrodynamic properties of cellulose in binary solvents with ionic liquid, in press, *Carbohydrate Polymers*, 105 237–243.

Liu,W., Budtova,T., Navard, P. (2011); Influence of ZnO on the properties of dilute and semi-dilute cellulose-NaOH-water solutions ; Cellulose, 18, 911–920.

Luciani, L., Denoyel, R., & Rouquerol, J. (2003). Texture des matériaux pulvérulents ou poreux, *Techniques de l'Ingénieur*, 1-24.

Ma, H. S., Roberts, A. P., Prévost, J. H., Jullien, R., & Scherer, G. W. (2000). Mechanical structure–property relationship of aerogels. *Journal of non-crystalline solids*, *277*(2), 127-141

Masmoudi Y., Rigacci A., Ilbizian P., Achard P. (2006) ; Diffusion during the supercritical drying of silica gels. *Drying Technology*, 24, p. 1121-1125.

Nilsson, O., Rüschenpöhler, G., Groß, J., Fricke,J. (1989); Correlation between thermal conductivity and elastomechanical properties of compressed porous media, *High Temperatures - High Pressures* 21 267 – 274.

Pekala, R. W., Alviso, C. T., & LeMay, J. D. (1990). Organic aerogels: microstructural dependence of mechanical properties in compression. *Journal of Non-Crystalline Solids*, *125*(1–2), 67–75.

Rudaz, C. PhD thesis, MINES ParisTech 2013.

Rudaz,C., Courson,R., Bonnet,L., Calas-etienne,S., Sallee, H., and Budtova,T. (2014); Aeropectin: fully biomass-based mechanically strong and thermal super-insulating aerogel", *Biomacromolecules*, 15, 2188−2195.

Sescousse, R. (2010). Nouveaux matériaux cellulosiques ultra-poreux et leurs carbones à partir de solvants verts. *PhD thesis*, Mines ParisTech.

Sescousse, R., Gavillon, R., & Budtova, T. (2011). Aerocellulose from cellulose–ionic liquid solutions: Preparation, properties and comparison with cellulose–NaOH and cellulose–NMMO routes. *Carbohydrate Polymers*, *83*(4), 1766–1774.

Sing, K. S. W., Everett, D. H., Haul, R. A. W., Moscou, L., Pierotti, R., Rouquerol, J., & Siemieniewska, T. (1985). Reporting physisorption data for gas/solid systems with special reference to the determination of surface area and porosity. *Pure Appl Chem*, 57(4), 603–619.

Synytsya, A. (2003); Fourier transform Raman and infrared spectroscopy of pectins, *Carbohydrate Polymers*, *54*(1), 97–106.

Winter, H., & Chambon, F. (1986). Analysis of linear viscoelasticity of a crosslinking polymer at the gel point. *Journal of Rheology*, *30*(2), 367–382.

# Chapter III:

# Preparation of cellulose-silica composite aerogels through "one-pot" synthesis.

## Introduction

In this third chapter we describe the preparation of cellulose-silica composite aerogels, through a "one-pot" synthesis process. The properties of the composite aerogels were investigated in details. The goal was to elaborate composite combining the good mechanical properties of cellulose aerogels with the thermal superinsulating properties of silica aerogels. We aim to generate a cellulose-silica interpenetrated aerogel structure: thus we chose to sart by directly mixing in solution cellulose and silica precursor, followed by cellulose coagulation and in situ generation of silica structure inside the aerocellulose porosity.

First we determined a suitable solvent system for direct mixing of cellulose and silica to obtain interpenetrated composite aerogels. As cellulose is only soluble in a limited array of solvents, it is difficult to find a suitable solvent allowing the direct mixing of cellulose with a silica precursor solution without an incontrollable phase separation. An aqueous alkaline media is chosen, as water-8%wtNaOH-cellulose solution could readily be mixed with an alkaline sodium silicate solution, which can form silica matrix by a sol-gel process upon acidification.

The gelation of both pure sodium silicate and cellulose-sodium silicate mixtures was investigated by oscillatory rheological measurements at constant frequency. First, the influence of temperature and nature of catalyst on the gelation time of alkaline sodium silicate was investigated. It is known that cellulose-8%NaOH-water solutions are gelling with time and temperature increase. Thus the next step was to study the effect of temperature and amount of sodium silicate on cellulose gelation, and the gelation kinetics were compared to that of pure cellulose-NaOH solutions.

The composite aerogels were obtained after cellulose coagulation from the cellulose-sodium silicate mixtures and silica formation in an acid bath, followed by supercritical drying with $CO_2$. The effects of various preparation parameters, such as the presence of additives, the composition of the coagulation bath, and the silica content on composite bulk density were studied. The morphology of the composite was investigated by scanning electron microscopy (SEM), and was related to the specific surface area, mechanical properties and thermal conductivities of the composites.

## Introduction

L'objet de ce troisième chapitre est l'élaboration d'aérogels composites combinant les bonnes propriétés mécaniques des Aérocelluloses aux propriétés super-isolantes des aérogels de silice. Le but ciblé est l'obtention d'aérogels cellulose-silice nanostructurés, présentant une structure de réseaux organiques-inorganiques interpénétrés. Un procédé « one-pot », c'est-à-dire à partir un mélange direct en solution de la cellulose avec un précurseur de silice a été choisi en premier lieu. Les propriétés de ces composites ont été caractérisées en détails.

Premièrement nous avons déterminé un solvant adapté au mélange de la cellulose avec un précurseur de silice. En effet la cellulose n'est soluble que dans un nombre très limité de solvants, et il est difficile de trouver un système adapté au mélange de la cellulose avec un précurseur de silice sans provoquer une séparation de phase. Une solution de cellulose dans 8%wt NaOH a pu être mélangée avec une solution aqueuse de silicate de sodium, qui donne naissance à la phase silicique via une réaction sol-gel après acidification.

La gélification des solutions de silicate de sodium, ainsi que des mélanges cellulose-silicate de sodium a été caractérisée par des mesures rhéologiques, en mode oscillatoire, à fréquence constante. D'abord, l'influence de la température et de la nature du catalyseur sur le temps de gélification du silicate de sodium ont été étudiées. Les solutions de cellulose-8%NaOH-eau sont connues pour gélifier avec le temps et l'augmentation de la température. L'étape suivante a donc été l'étude des effets de la température et de la quantité de silicate sur le temps de gélification dans le cas des mélanges cellulose-silicate de sodium. La cinétique de gélification des mélanges cellulose-silicate a été comparée à celle obtenue pour les solutions de cellulose pure. Les effets de l'addition du silicate de sodium sur la gélification ont été étudiés.

Les aérogels composites ont été obtenus à partir des mélanges cellulose-silicate après coagulation de la cellulose, formation de silice dans un bain acide, et séchage au $CO_2$ supercritique. Les effets de plusieurs paramètres sur la densité des aérogels, tels que la présence d'additifs, la composition du bain de coagulation et la quantité de silice ont été examinés. La morphologie des composites a été caractérisée par microscopie électronique à balayage, et a été corrélée avec la surface spécifique, ainsi que les propriétés mécaniques et thermiques des composites.

# 1. Experimental approach for the preparation of cellulose-silica composites

## 1.1. Choice of a silica precursor for "one-pot" process

The preparation of cellulose-silica composites requires the mixing of cellulose with a silica precursor. Indeed in this chapter we aim to elaborate cellulose-silica composite aerogels by a one-pot process. The impregnation of cellulose alcogels will be discussed in details in chapter IV. The preparation processes of aerogels from cellulose and silica have many similarities: in both cases a precursor is dissolved or dispersed in a solvent (sol), and forms a gel either by chemical reticulation (silica gel) or by physical interactions (cellulose). The gelation is followed by washing and solvent exchange steps, to eliminate reaction by-products. Supercritical $CO_2$ drying is used to dry the porous material without significantly damaging its internal porosity.

These similarities should allow a direct mixing of both precursors in a common solvent, followed by controlled gelation of both precursors and a supercritical drying. The main problem is finding a common solvent and precursors soluble in said solvents, to avoid direct phase separation or uncontrolled gelation upon mixing. Cellulose solutions could not be directly mixed with the most common silica aerogel precursors, polyethoxydisiloxanes or other TEOS derivatives, as far as solvents of silica are non-solvents of cellulose. Furthermore cellulose solvent 8wt%NaOH-water, is extremely basic, inducing a rapid and uncontrolled gelation of the silica phase. The resulting materials were dramatically heterogeneous. Thus we needed a silica precursor soluble in basic aqueous solutions. Sodium silicate ($Na_2SiO_3$) was chosen for this purpose as it is water-soluble and strongly basic (pH of a saturated solution being 13-14) which is similar to 8%NaOH-water (pH 14). The details of the preparation process of one-pot composites was shown in Chapter II.

## 1.2. Rheological study: gelation of sodium silicate solution

### 1.2.1. Nature of catalyst

The conditions of silica gel formation inside the cellulose matrix were selected to match the conditions for sodium silicate gelation. In this section we study the gelation of sodium silicate solutions induced by two different catalysts: 0.3M hydrochloric acid and 0.2M citric acid. The acid was added to an 8%wt sodium silicate solution and the evolution of elastic modulus G' and viscous modulus G" was monitored with time (see example in Figure III.1). The measurements were done at a frequency of 0.1 Hz and the stress was 0.1 Pa, at a temperature of 20 °C. The initial pH of the sodium silicate solution was ~ 13.5; addition of both acids lowered the pH around 2. As already explained, the gelation time $t_{gel}$ was measured as the moment where G' = G".
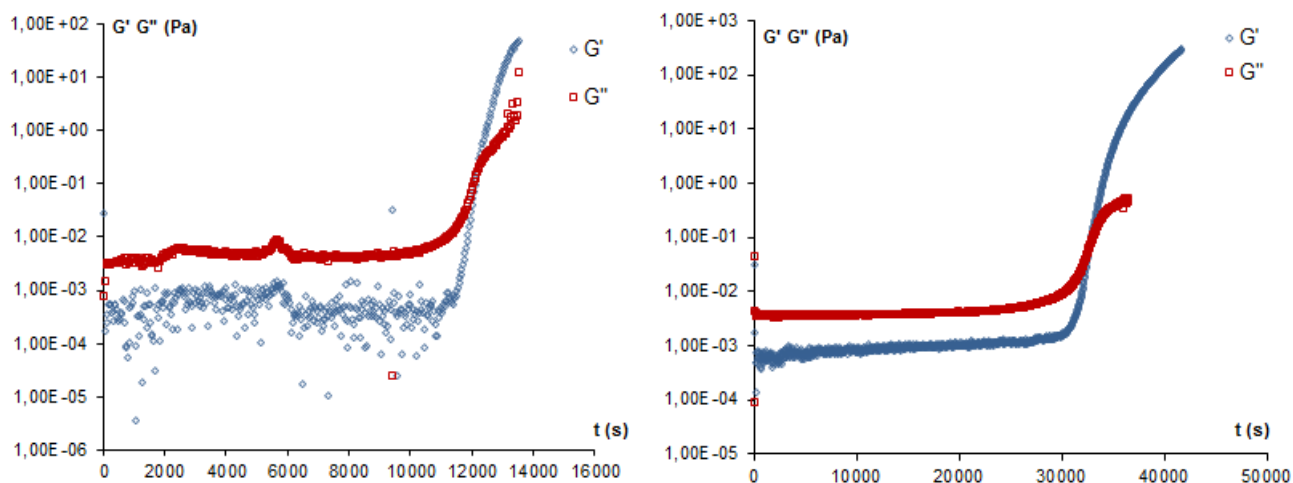
**Figure III.1 : Evolution with time of the viscous (G') and elastic (G'') moduli during gelation of 8%wt sodium silicate solution catalyzed by (a) 0.3 M HCl and (b) 0.2 M citric acid, both at 20 °C.**

The observed rheological behavior matches with what is expected of a gelling system. Before sol-gel transition the system behaves essentially as a viscous liquid, and the viscous modulus is superior to the elastic modulus. With time, silica agglomerates formed inside the system by reaction with the acid reach a limiting concentration, or percolation threshold, at which the condensation of silicic acid into $SiO_2$ leads to a continuous network. Viscosity increases drastically, up to the point where the system behaves as an elastic solid: the elastic modulus becomes higher than the viscous modulus. Past the gel point, the gels were rather fragile and easily cracked even under the low stress values imposed by the experiment.

8%wt sodium silicate solution had an initial viscous modulus around $3.10^{-3}$ Pa. For both catalysts the modulus of the system when crossing gel point was near 0.1 Pa. In similar conditions, HCl gives a faster gelation than citric acid: $t_{gel}$ for HCl was 12060 s (3 h 21min) against 32880 s (9 h 08 min) for citric acid at 20°C. It was expected that HCl, being a strong acid, would have a stronger reaction and induce faster gelation. In our case we aim for a rapid formation of a silica gel inside the pores of cellulose, to avoid loss of unreacted sodium silicate during the washing steps; the positive effect of using HCl on yield in $SiO_2$ will be investigated in section 4.2.

### 1.2.2. Effect of temperature on sodium silicate gelation

The influence of temperature on sodium silicate gelation catalyzed by HCl was studied. A molar ratio HCl: $Na_2SiO_3$ of 1:3 was fixed, and sodium silicate concentration was fixed at 8%wt. The gel point was measured at the crossing of G' and G'' curves for different temperatures between 0 and 40 °C. Increasing the temperature speeds up sodium silicate gelation. Kinetic parameters were extracted from the experimental data by plotting the dependence of the logarithm of gelation time as a function of the inverse temperature. The data were fitting an Arrhenius-type law (eq.III.1):

$$\ln t_{gel} = \ln C + \frac{E_a}{R.T} \tag{III.1}$$

113

where $t_{gel}$ is the gelation time (s), $E_a$ the apparent activation energy (in $J.mol^{-1}$), R the ideal gas constant (R = 8.314 $J.mol^{-1}.K^{-1}$) and T the temperature (K).
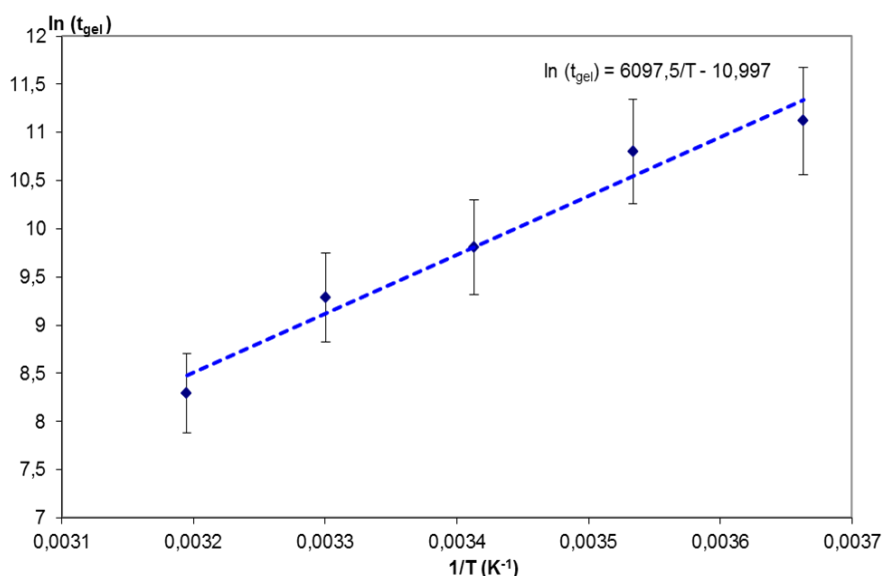


**Figure III.2: Logarithmic dependence of the gelation time of sodium silicate aqueous solutions with temperature. The Na$_2$SiO$_3$:HCl molar ratio was 1:3.**

The experimental curve gives *lnC* as the y-intercept coordinate, and the plot of the curve is $\frac{Ea}{R}$. Thus we have:

$$E_a = 50.7 \text{ kJ.mol}^{-1}$$

$$lnC = -10.997$$

The activation energy value obtained for the gelation of sodium silicate solutions is in the same order of magnitude as what was observed from gelation of alcoxysilanes, tetramethoxysilane (TMOS) or tetraethyl orthosilicate (TEOS) (Colby et al., 1986; Ponton et al., 2002). We compared the apparent activation energies for different silica forming systems in table III.1.

Table III.1: Comparison of apparent activation energies calculated for different silica sol-gel systems

| Precursor | Catalyst | E$_a$ (kJ.mol$^{-1}$) | Reference |
|---|---|---|---|
| **TEOS** | HF | 61.1 | Colby et al, 1986 |
| | HCl | 55.2 | *ibid* |
| **TMOS** | HF | 39.8 | *ibid* |
| | HCl | 49.4 | *ibid* |
| | Base (DMAP) | 37.5 | Ponton et al., 2002 |
| **Sodium silicate** | HCl | 50.7 | this work |

The activation energy for the gelation of sodium silicate in HCl is around 50 kJ.mol$^{-1}$, closer to those of alcoxysilanes sol-gel forming systems with HCl catalysis than with base or HF catalysis. It is known that when HCl is used to catalyze the sol-gel reactions of alcoxydes, polycondensation is the kinetically determinant step as hydrolysis is faster at low pH. The activation energy values suggest a similar trend for the sodium silicate system, with first a rapid protonation of silicate into silicic acid, followed by slower condensation of silicic acid

molecules on one another. Colby et al. attributed the higher activation energies observed for TEOS gelation to steric hindrance of the ethoxy groups, larger than "simple" metoxy- groups or oxygen atoms.

## 2. Study of the gelation of cellulose-NaOH-sodium silicate mixtures

### 2.1. Preliminary studies

#### 2.1.1. Effect of additives on the cellulose-sodium silicate system

Direct mixing of sodium silicate with the cellulose-NaOH solution at room temperature induces spontaneous "solidification" of the cellulose matrix. At this pH silicate ions cannot form a gel because of strong electrostatic repulsion. As it will be explained later, most probably cellulose is gelling and partially coagulating at the same time, but for simplicity we shall call this "gelation". This so-called gelation step results in very inhomogeneous gels. To improve the mixing of cellulose-NaOH solution and sodium silicate solution, we needed to slow down cellulose gelation. A first step was to mix the sodium silicate with the cellulose-NaOH solution at - 6°C, the temperature used for cellulose dissolution. In this case the mixing was easier but gelation still occurred too fast to correctly mold the gels.

Several additives are known to delay cellulose gelation time in water-NaOH solutions. Two of these additives were investigated previously: zinc oxide (ZnO) and urea (Egal, 2006; Liu et al., 2011). Those additives can be easily eliminated during the solvent exchange steps before drying the gels. The formulations of the different cellulose-additive systems are summed up in table III.2. The cellulose was first fully dissolved in water/NaOH at - 6°C in the presence of additives, and then the sodium silicate solution was added. The mass ratio between cellulose and silicate was kept at R = 1 for all the mixtures. Gel time was only evaluated qualitatively from the moment the solution was poured into the molds.

**Table III.2: Formulations of composite gels from cellulose/NaOH + ZnO or Urea + Na₂SiO₃.  (For all samples R$_{cellulose/silica}$ = 1)**

| Additive | % weight cellulose in the mixture | % weight additive | t $_{gel}$ cellulose (at 25°C) |
|---|---|---|---|
| **ZnO** | 3.33% | 1% | **5 min** |
| | 5.33% | 1% | **3 min** |
| | 5.33% | 1.5% | **3 min** |
| **Urea** | 5.33% | 4% | **2 min** |
| | 5.33% | 6% | **instantaneous** |

When ZnO was used as an additive, a relatively fluid cellulosic solution was obtained, which eased mixing with the sodium silicate solution. After mixing, all solutions gelled in a few minutes. In one sample, cellulose concentration was 3.33%: for this sample the gelation time was slower as far as gelation time of cellulose solutions decreases when increasing cellulose concentration. However, the wet composite gel made from this cellulose concentration was quite fragile, and cracked during the subsequent solvent exchange and supercritical drying steps.

Increasing the quantity of ZnO from 1 to 1.5%wt had no visible gelation slowing effect. Samples containing 4%wt urea were gelling in around 2 minutes. The solutions were more viscous. Increasing the quantity of urea induced a very fast gelation of the system.

We can conclude that ZnO appears a suitable additive for delaying cellulose gelation, even in the presence of sodium silicate. We used a ZnO concentration of 1%wt in all samples used in the following of the study.

### 2.1.2. Choice of experimental parameters.

As we observed rapid spontaneous solidification or gelation when cellulose and sodium silicate solutions were mixed, we had to select experimental parameters for which gelation time was in the detection frame of the rheological set up. In order to investigate the influence of sodium silicate on cellulose solution behavior, solutions of lower concentrations as compared with the ones used for preparing cellulose-silica composite aerogels were made to reach measurable gelation times. 5wt% cellulose-8%NaOH-1%ZnO solutions were mixed with sodium silicate solutions in various proportions; the resulting mixtures were of 4wt%cellulose and 2 to 5wt% of sodium silicate.

Mass ratio between cellulose and sodium silicate $R_1$ in the mixture was calculated as (eq.III.2):

$$R_1 = \frac{m_{Na_2SiO_3}}{m_{cellulose}} \tag{III.2}$$

where $m_{Na_2SiO_3}$ and $m_{cellulose}$ are sodium silicate and cellulose dry mass in the mixture, respectively.

## 2.2. Influence of sodium silicate concentration on cellulose gelation

An example of elastic G' and viscous G" moduli evolution with time of aqueous cellulose/sodium silicate mixtures at 15 °C is presented in Figure III.5. Mixtures of two compositions, 4%cellulose-2% $Na_2SiO_3$ ($R_1 = 0.5$) and 4%cellulose-4% $Na_2SiO_3$ ($R_1 = 1$) are shown. Similar data were obtained for other compositions with $R_1$ varying from 0.50 to 1.25, keeping cellulose concentration in the mixture constant and equal to 4wt%. Classically, the gelation time $t_{gel}$ was determined as the time at which G' = G".
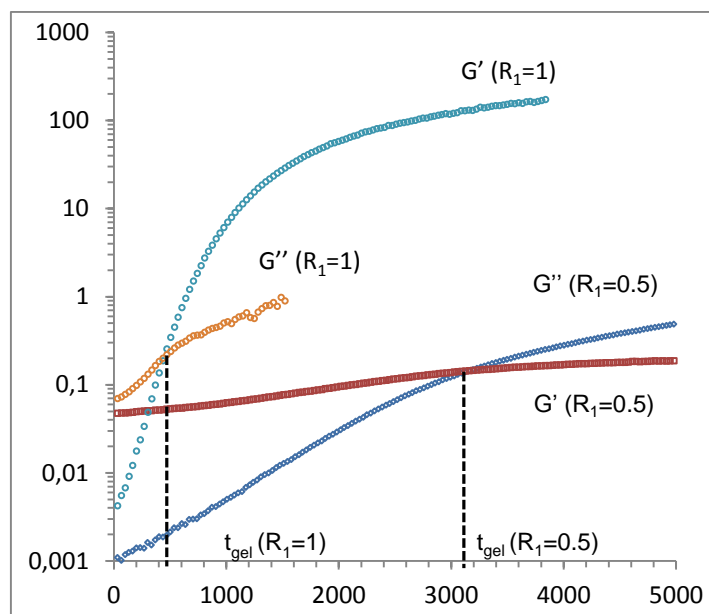
**Figure III.3: Time evolution of elastic (*G'*) and viscous (*G''*) moduli at 15 °C for two mixtures with mass ratio cellulose/sodium silicate *$R_1$* = 0.5 (triangles) and *$R_1$* = 1 (circles) (Demilecamps et al., 2014)**

Figure III.3 shows that higher sodium silicate concentrations in the mixture (i.e. higher values of $R_1$) result in a shorter gelation time. It should be noted that 4%cellulose-8%NaOH solution is gelling at 15 °C in about 3 days and 4%cellulose-8%NaOH-1%ZnO does not form a gel within the measurable times (Liu et al. 2011). There is a clear evidence of a dramatic acceleration of cellulose gelation in the presence of sodium silicate solution. Gelation time varies with the concentration of sodium silicate following a power-law (Figure III.4). The calculated power law exponent was 2.5.

$$t_{gel} \sim R_1^{2.5}$$ (III.3)

A similar phenomenon was recorded when aqueous cellulose-8%NaOH was mixed with organosolv lignin dissolved in the same solvent (Sescousse et al. 2010). When another solute is mixed with cellulose-NaOH solution, it interacts with the solvent and disrupts the H-bonds between cellulose and NaOH hydrates; as a result cellulose chains tend to aggregate and phase separation occurs.
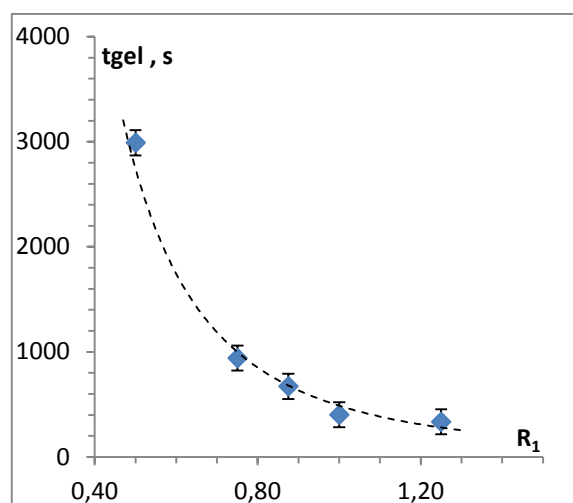
**Figure III.4 : Gelation time (s) of cellulose-sodium silicate mixtures (cellulose concentration in all mixtures is 4wt%) at 15 °C as a function of $R_1$. Dashed line is power law approximation with $t_{gel} \sim R_1^{-2.5}$ (Demilecamps et al., 2014)**

## 2.3. Effect of temperature on the gelation of cellulose-sodium silicate systems

The influence of temperature on gelation time of cellulose/sodium silicate mixture of a given composition, 4%cellulose-2%$Na_2SiO_3$ ($R_1$=0.5), is presented in Figure III.5, and compared with gelation times for aqueous 4%cellulose-8%NaOH solution and for 4%cellulose-8%NaOH-0.7%ZnO (data taken from Liu et al. 2011). As demonstrated by Liu et al., the exponents characterising the order of gelation kinetics, $t_{gel} \sim exp(aT)$ where $a$ is a constant, are similar for cellulose dissolved in 8%NaOH-water and in 8%NaOH-ZnO-water, for ZnO concentrations varying from 0 to 1.5wt%. The reason is that cellulose gelation mechanism is the same with or without ZnO; gelation is simply delayed due to the presence of ZnO. It was also shown in the same work that ZnO does not change the properties of cellulose on the molecular level and does not improve the thermodynamic quality of solvent, 8%NaOH-water, towards cellulose. The exponent $a$ describing cellulose gelation in the presence of sodium silicate is lower by a factor of two as compared to that in NaOH-ZnO solvent.
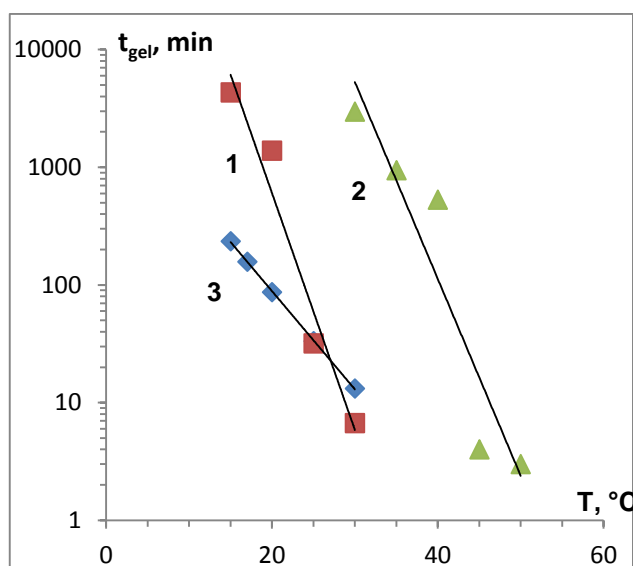
**Figure III.5 : Temperature dependence of gelation time (min) for different 4%cellulose aqueous solutions: in 8%NaOH (1), in 8%NaOH-0.7%ZnO (2), both sets of data are taken from (Liu et al. 2011) and in 8%NaOH-1%ZnO mixed with 2% sodium silicate, $R_1 = 0.50$ (3). Lines correspond to exponential approximations. (Demilecamps et al., 2014)**

When cellulose solution is mixed with sodium silicate at - 6 °C, the mixture becomes turbid which is an indication of the formation of micrometer-size entities that are scattering light. As it will be shown in part 4, when coagulated, a phase separation between cellulose and silica occurs: cellulose forms a network and silica is condensing forming beads inside cellulose matrix; obviously there are no attractive interactions between two phases.

Another possible reason for the rapid gelation of the system could be the lowering of the pH due to sodium silicate addition: as cellulose is not soluble in non-alkaline solutions, a change in pH will induce cellulose phase separation. However, both solutions are of the same initial high pH, around 13.5 - 14, resulting in the mixture with pH = 13.5 - 14 as measured. The high concentration of sodium silicate was chosen specifically to reduce the added volume of sodium silicate so that the dilution effects are negligible; NaOH and cellulose concentrations after mixing are still in the "solubility zone" of the cellulose-NaOH-water phase diagram at - 6°C.

The viscosity of sodium silicate aqueous solutions is below 5 mPa.s. This means that in no way sodium silicate can "thicken" cellulose-8%NaOH-1%ZnO solution even if the total concentration of dissolved matter is slightly increasing with the increase of $R_1$ from 2 to 5 %wt of sodium silicate.

Finally, at this pH sodium silicate is a stable solution (not gelling, not precipitating): the gelation of sodium silicate cannot happen until the pH is lowered below 9. Thus the most probably phenomenon that occurs is cellulose coagulation after the addition of sodium silicate. We obtain a continuous network of coagulated cellulose impregnated by an aqueous solution where NaOH and sodium silicate are fully dissolved.

Consequently, attractive interactions between silicate and cellulose leading to coagulation, lowering of the pH of the solution, significant viscosity increase due to a thickening effect of the added sodium silicate solution, or simultaneous formation of both gels just after mixing are not likely reasons for the quick gelation of the system.

Cellulose "gelation" as a function of temperature is strongly accelerated since other mechanisms are involved in the presence of sodium silicate. While ZnO interacts mostly with free water and thus slows down the phase separation between cellulose and solvent, sodium silicate enters in direct competition with cellulose for solvatation. The presence of sodium silicate further diminishes the solvent thermodynamical quality, and thus considerably speeds up cellulose gelation. When increasing temperature, molecular movement is increased: this means more contacts between cellulose chains and faster aggregation, but also more contacts between silicate ions and water-NaOH complexes, thus more disrupting of the H-bonds stabilizing the cellulose solution.

It is known that in 7-9%NaOH-water cellulose does not form a molecular solution (Lu et al. 2011). With time and temperature and above the overlap concentration cellulose solution is gelling and gelation is accompanied by micro-phase separation (Roy et al. 2003, Gavillon and Budtova 2008): solutions are transparent and gels are opaque. In overall, cellulose dissolved in 7-9%NaOH-water is not stable, cellulose chains are self-associating with time leading to gelation. The addition of sodium silicate perturbs the equilibrium and leads to the formation of cellulose-rich and cellulose-poor domains; "gelation" is thus accelerated. Cellulose is most probably close to coagulation point after being mixed with sodium silicate; we will analyse the morphology of composite aerogels in the next section to confirm this hypothesis.

## 3. Properties of « one-pot » composite aerogels from cellulose/sodium silicate mixtures

### 3.1. Effect of gelling conditions on aerogels bulk density

To prepare composite materials, cellulose-8%NaOH-1%ZnO-water and aqueous sodium silicate solutions were mixed in different proportions. Several constraints have to be taken into account if willing to prepare homogeneous materials. First, it is not possible to make composite samples containing less than 3wt% of cellulose as far as cellulose is hardly making a 3D-network upon coagulation at lower concentrations (the overlap concentration of microcrystalline cellulose in 8%NaOH-water is $1 - 1.5$ wt% (Roy et al, 2003). Second, it was not possible to prepare cellulose-8%NaOH solutions of cellulose concentration higher than 7wt% because of the limit of cellulose dissolution in this solvent (Egal, 2007) and very quick gelation above this concentration. Finally, as it was demonstrated in the previous section, mixing cellulose and sodium silicate solutions with high content of silica induces very quick mixture "solidification" which prevents making homogeneous materials.

Taking into account the constraints mentioned above, mixtures with cellulose concentrations varying from 3 to 5wt% and $SiO_2$/cellulose weight ratios from 0.5 to 1.5 were prepared. After homogenization of the mixture and rapid spontaneous solidification, samples were coagulated in different baths: water, 0.3M HCl and 0.2M $C_6H_7O_8$. Water was used as a reference. Hydrochloric acid is a standard catalyst for sodium silicate gelation (Kistler, 1932), and citric acid was already used to make cellulose fibres coated with silica (Liu et al., 2011). After renewing coagulation bath by fresh acid solutions several times, the samples were washed in water to eliminate NaCl formed during the reaction of acid with sodium silicate, water was exchanged by ethanol and the resulting alcogels were dried with supercritical $CO_2$. Monolithic,

mechanically stable and cohesive white samples were obtained, from the very first glance similar to pure Aerocellulose (Figure III.6).
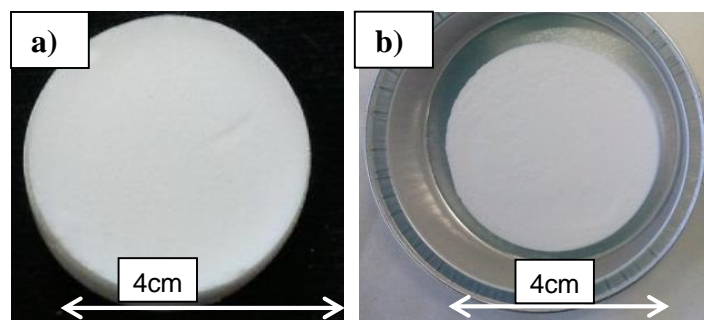


**Figure III.6 : Photos of a) pure Aerocellulose from 5%cellulose-8%NaOH-1%ZnO and b) cellulose-silica composite aerogel from 5%cellulose-8%NaOH-1%ZnO-5%SiO2 ($R_{2,th}$ =1) coagulated in 0.3M HCl (Demilecamps et al., 2014)**

When placed in an acid medium, sodium silicate is converted into silica and sodium chloride (NaCl) is removed during the washing steps. Thus in the following, when characterizing cellulose-silica composite properties we shall reason in $SiO_2$ and not $Na_2SiO_3$ concentrations. The theoretical and experimental values of the ratio between $SiO_2$ and cellulose mass are noted $R_2$:

$$R_{2,th} = \frac{m_{SiO_2}}{m_{cellulose}}$$ (III.4)

$$R_{2,exp} = \frac{m_{SiO_2}}{m_{cellulose}} \times Yield_{SiO_2}$$ (III.5)

Samples' characteristics from various formulations prepared in different coagulation baths are given in Table III.4. The total concentration of cellulose given take into account the dilution involved by the addition of sodium silicate solution. Dried cellulose-silica composite aerogels have rather low bulk densities, in overall lower than 0.2 g.cm$^{-3}$. Total shrinkage upon drying is rather important, volume loss in the 40-60% range for most composites is observed. Gelling and coagulation of some samples at higher 50 °C was attempted, in order to fasten the gelation of the silica phase and increase the yield in silica. However, samples gelled at higher temperature all had high shrinkage and their bulk densities were superior to 0.25 g.cm$^{-3}$, which is rather high for aerogels particularly when dealing with thermal insulation application: coagulation and washing at ambient temperature was preferred in the following in order to obtain aerogel with lower densities. Overall, total volume shrinkage after sc drying was less pronounced for cellulose concentration near 5%wt than when the cellulose concentration was in the 3-4%wt range. However, there is no clear correlation between global shrinkage and total matter concentration in the samples.

**Table III.4: Apparent densities and total volume shrinkage after sc drying of cellulose-silica composite aerogels of various compositions coagulated in different acid baths.**

| Coagulation bath | Coagulation temperature | $C_{cell}$ wt% | $R_{2,th}$ | Volume shrinkage | $\rho$ (g/cm$^3$) |
|---|---|---|---|---|---|
| H$_2$O | 25 °C | 3.33% | 1.07 | 46% | 0.115 |
| | | 3.08% | 1.40 | 61% | 0.185 |
| | | 5.33% | 0.67 | 15% | 0.154 |

| | | 3.81% | 0.67 | 50% | 0.130 |
|---|---|---|---|---|---|
| HCl | 25 °C | 3.33% | 1.07 | 60% | 0.168 |
| | | 3.08% | 1.40 | 42% | 0.136 |
| | | 5.33% | 0.67 | 49% | 0.204 |
| | 50 °C | 3,33% | 0.67 | 63% | 0.272 |
| Citric acid | 25 °C | 3.81% | 0.67 | 70% | 0.217 |
| | | 3.33% | 1.07 | 48% | 0.273 |
| | | 3.08% | 1.40 | 60% | 0.174 |
| | | 5.33% | 0.67 | 29% | 0.134 |
| | 50 °C | 3,33% | 0.67 | 69% | 0.379 |

The apparent densities of the composites of various formulations prepared via coagulation in 0.3M HCl as a function of total matter concentration in solution are presented in Figure III.7. Total matter concentration is the sum of cellulose and silica concentrations in the precursor (before supercritical drying) with a 40% yield of silica (as calculated from elemental analysis, see details in next section) taken into account. In overall, the higher the matter concentration in the sample, the higher is apparent density, as expected. In the view of small interval of cellulose and silica concentrations used, it is not possible to analyze the input of each component to the final composite apparent density.
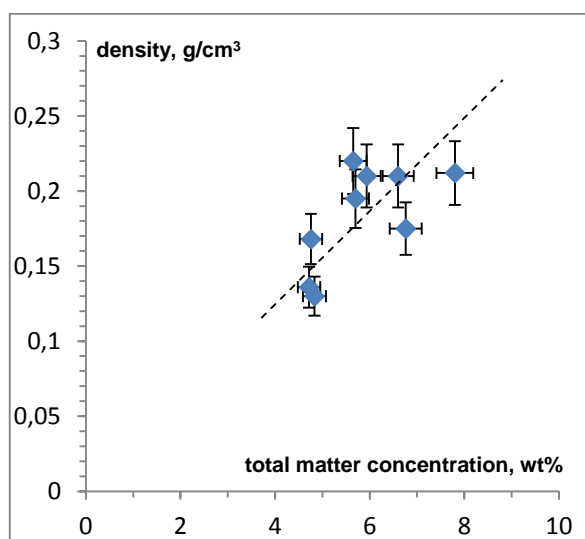


**Figure III.7 : Apparent density of supercritically dried cellulose-silica composites (coagulation in 0.3 M HCl) as a function of total matter concentration in the precursor. Dashed line is linear approximation (Demilecamps et al., 2014).**

## 3.2. Evaluation of the amount of silica in the aerogel composites

The acid bath volume used was taken to correspond to one molar equivalent of NaOH, necessary for neutralization, plus a stoichiometric quantity for reaction with sodium silicate. The evolution of the pH of the coagulation bath, just after immersion of the cellulose hydrogel and after 48h, is shown in table III.5. When the sample is washed in pure water, the only phenomenon is the diffusion of the solutes, NaOH and $Na_2SiO_3$, outside the porous cellulosic

network into the solution until an equilibrium concentration is reached between the porous system and the outside solution: as a result the pH of the bath increases up to ~13. When a strong acid bath (HCl) is used, the pH of the bath remains low (~1) after neutralization and reaction with sodium silicate. Citric acid is a weaker acid, and is not fully dissociated in solution; neutralization and reaction with sodium silicate do occur, but the final pH of the bath is higher. Ideal conditions for the gelation of sodium silicate are considered at pH between 5 and 9; however, our composite materials are a particular case, as silicate ions are not free in solution but are "included" in the pores of the cellulosic solid network. The reaction of the silicate is thus limited by its diffusion inside and outside the porous network.

**Table III.5 : Evolution of the pH of acid coagulation baths after coagulation, neutralization and condensation of sodium silicate into $SiO_2$.**

| Coagulation bath | pH bath (t = 0) | pH bath (t= 48h) |
|---|---|---|
| $H_2O$ | 6,5 | 13 |
| HCl | 0,5 | 1 |
| Citric acid | 1,5 | 6,5 |

The composition of dry cellulose-silica composites was examined using EDS. The examples of spectra from the cross-sections of two samples prepared from the same mixture with $R_{2,th} = 1.07$ but in different coagulation baths (0.3 M HCl and 0.2 M citric acid) are presented in Figure III.8. EDS spectra show a Si $K_\alpha$ peak at 1.73 keV. Sodium ($K_\alpha$ at 1.04 keV) and chloride ($K_\alpha$ at 2.62 keV) peaks come from residual salts formed during the reaction of sodium silicate with the acid that were not removed by washing. A rather low intensity of the sodium peaks for the case when hydrochloric acid is used confirms that most of the salts are washed out from the composite before drying. No Zn ($L_\alpha$ at 1.01 keV and $K_\alpha$ at 8.63 keV) peak appears indicating that ZnO has been dissolved completely in acid baths and washed away during the processing route.
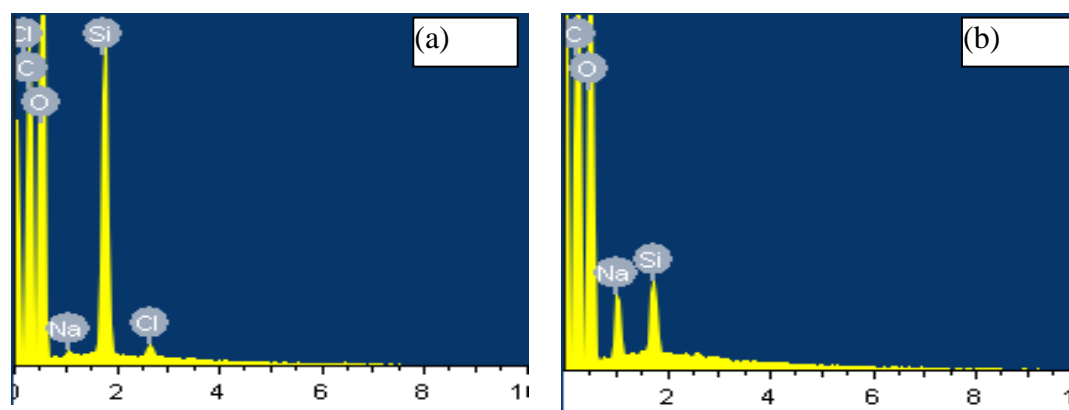


**Figure III.8: EDS spectra from a cross-section of samples obtained with R2,th = 1.07 coagulated in (a) 0.3M HCl and in (b) 0.2 M citric acid.**

Peak intensity is proportional to matter content in the observed zone. The intensity of the peak corresponding to Si in the composite coagulated in 0.3M HCl (Figure II.8.a) is much higher than that in the composite coagulated in 0.2 M $C_6H_7O_8$ (Figure II.8.b). The qualitatively obtained higher concentration of silica in samples coagulated in hydrochloric acid, as compared

to citric acid, was confirmed by elemental analysis. Table III.5 shows that when coagulated in water, practically all silica is washed out: the yield is 3wt%. The yield of silica in the dry composite is about 20wt% after coagulation in 0.2 M citric acid and is twice higher after coagulation in 0.3 M hydrochloric acid (~ 40wt% $\pm$ 4).

**Table III.5: Mass yields in SiO₂ in composite aerogels of various R, obtained in different coagulation baths, as calculated from elemental analysis.**

| Coagulation bath | $C_{cell}$ (wt%) | $R_{2,th}$ | $Yield_{SiO_2}$, % |
|---|---|---|---|
| H₂0 | 5.00 | 0.00 | **0** |
| | 3.33 | 1.07 | **3.3** |
| HCl | 5.33 | 0.67 | **36** |
| | 3.33 | 1.07 | **44** |
| | 5.00 | 1.40 | **42** |
| Citric acid | 3.33 | 1.07 | **20** |

When "solidified" cellulose/sodium silicate is placed in an acid bath, sodium silicate enters in contact with the acid and condensates as SiO₂ particles. It is a diffusion driven process, accompanied by the formation of NaCl and the release of NaOH into the bath. With a weaker acid, non-reacted sodium silicate diffuses out from cellulose network. Hydrochloric acid, being stronger and more reactive, appears a better gelation agent of sodium silicate in our conditions for having higher yield of silica as compared with citric acid. As we have observed in part 2.1, the gelation of sodium silicate in the presence of citric acid is slower. A slower gelation will favor the diffusion of silicate outside of the cellulose pores. This silicate is thus "lost" for the composite, hence a significant lower silica yield when using citric acid. Further increase of acid concentration was attempted to decrease the silica formation time, but this leads to the formation of large amounts of NaCl crystals inside the cellulose pores, which are difficult to wash out.

## 3.3. Morphology of the cellulose-silica composite aerogels

### 3.3.1. Structure of the composite aerogels

The morphology of cellulose-silica composites is shown in Figure III.9. Pure Aerocellulose from 5%cellulose-8%NaOH-water solution has a fibrous network-like structure (Figure III.9,a), as already reported in the literature (Gavillon and Budtova, 2008) with pore size ranging from a few tens of nanometers to few microns. Silica aerogel reference sample obtained from the aqueous 8wt%sodium silicate gelled after the addition of 0.3M HCl appears as assembly of small roughly spherical silica particles of a size between 10-100 nm (Figure III.9,b). In composites, when silica is formed inside the cellulose porosity (Figure III.9, c, d), silica condensates as larger monodisperse spherical particles, except few agglomerates probably

formed due to coalescence. Their size distribution is shown in Figure III.10. Two cases can be distinguished: $R_{2,th} > 1$ giving beads with most of diameters located around 500-600 nm, and $R_{2,th} < 1$ with slightly higher diameter around 800 nm. Figure III.9 c, d shows that beads are homogeneously distributed in cellulose network and that silica and cellulose are forming separate phases in the organic-inorganic composite. Detailed titration studies are needed to better understand the processes occuring in this complex system.
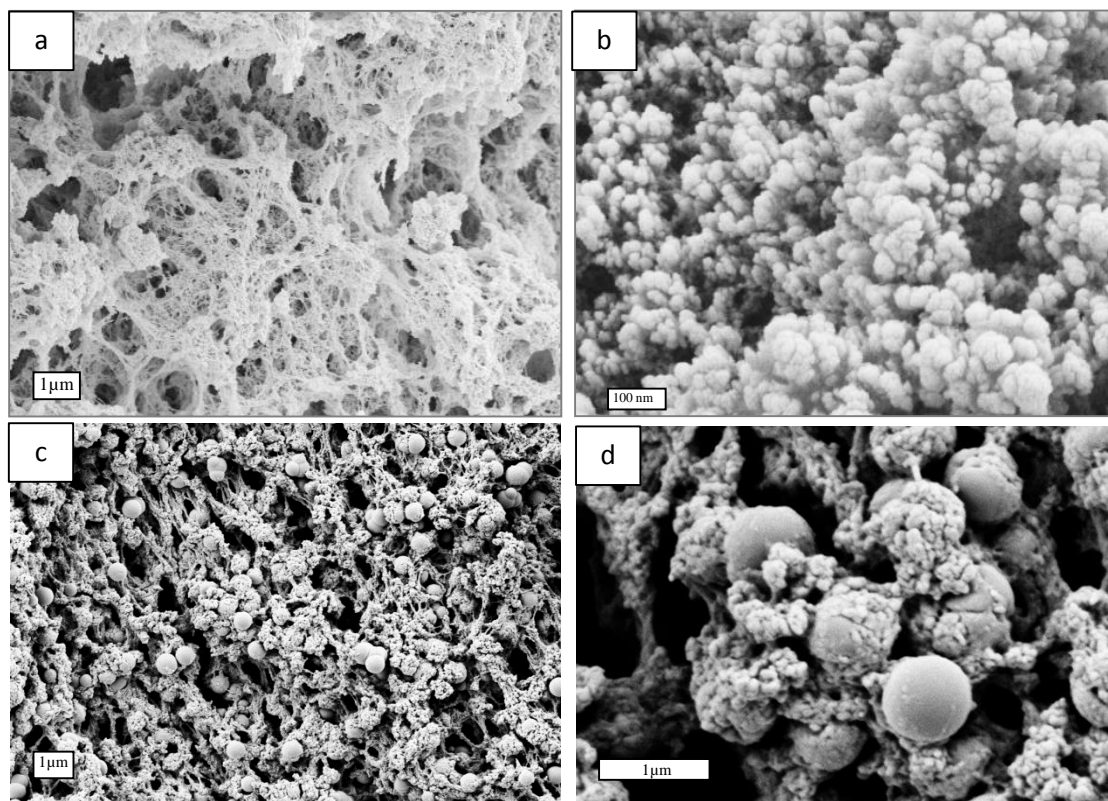


**Figure III.9 : SEM images of (a) pure Aerocellulose from5%cellulose-8%NaOH solution coagulated in water; (b) silica aerogel from 8%wt sodium silicate coagulated with 0.3M HCl and (c, d) cellulose-silica composite from 5%cellulose solution with $R_{2,th}$= 0.67 coagulated in 0.3M HCl (Demilecamps et al., 2014).**
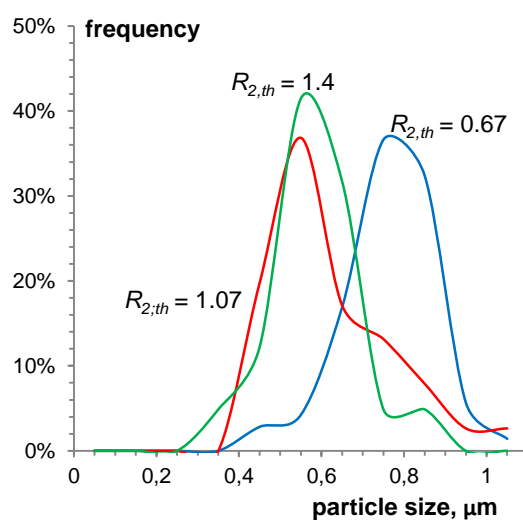


**Figure III.10: Silica particle size distribution in cellulose-silica composite aerogels (coagulation in 0.3M HCl) of different $R_{2,th}$. (Demilecamps et al., 2014)**

The morphology of cellulose in the composite is different from the one in pure Aerocellulose. In the latter case cellulose makes a network of homogeneous cellulose "strands" of diameter of some tens of nanometers. In the composite, the "strands" are composed of small beads assembled together. A similar morphology was found in Aerocelluloses when cellulose was directly coagulated from a solution, either in ionic liquid or in hot N-methylmorpholine-N oxide monohydrate, contrary to the case of NaOH-water solvent in which cellulose solution is gelling. As suggested by (Sescousse et al, 2011), when directly coagulated from solution, cellulose is undergoing a phase separation via spinodal decomposition mechanism which leads to a formation of small regular spheres. When coagulated from a gelled solution, cellulose already underwent microphase separation during gelation in NaOH-water. Cellulose morphology in composites with silica suggests that cellulose was coagulating in the presence of sodium silicate. Formation of coagulated cellulose network (and not of a "gel" in the proper sense of the term) is thus the reason of the significant acceleration of cellulose-sodium silicate mixture "solidification".

### 3.3.2. Specific surface area

As already underlined, the specific surface area $S_{BET}$ was measured by G. Reichenauer from Bavarian Center for Applied Energy Research, Wurzburg, Germany. $S_{BET}$ was obtained from sorption isotherms at $0.05 < p/p_0 < 0.3$ A typical $N_2$ adsorption-desorption curve for a so-prepared composite aerogel with $R_{2,th} = 0.67$ and a density of $0.220$ g.cm$^{-3}$ is presented on III.11. The hysteresis appears close to a relative pressure $p/p_0$ of 1, which is indicative of presence of large macropores. The variations in total adsorbed volume and shape of the adsorption-desorption curves did not appear clearly related to the total matter concentration in the samples.
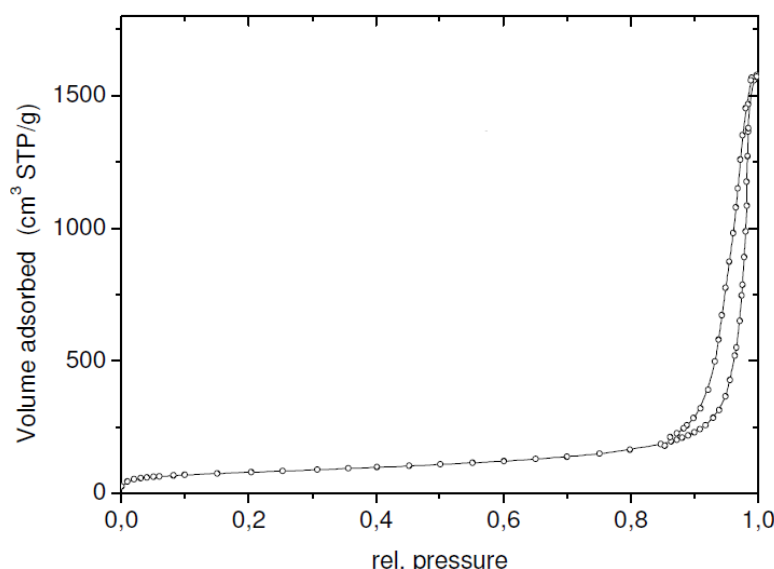


**Figure III.11 : N₂ adsorption isotherm for cellulose-silica composite aerogel with cellulose concentration of 5%wt and R₂,th of 0.67**

The specific surface areas of Aerocellulose-silica composites of various formulations coagulated in 0.3 M HCl is presented in Figure III.12 as a function of $R_{2,exp}$. Three cases with 3, 4 and 5wt% cellulose in the initial mixture are shown. $S_{BET}$ is systematically decreasing with the increase of silica fraction in the composite. One of the reasons for this trend is likely the fact that the silica particles are neither porous nor have a surface with roughness on the nanoscale (see Figure III.12,d). Assuming that the silica particles do not contain accessible

porosity within the particles, the particles themselves are too large to provide any significant contribution to total specific surface area of the composite. Therefore the silica phase can be assumed to essentially only increase the mass (or density) rather than the surface area of the composite, yielding the following relationship:

$$S_{BET,composite} = S_{BET,cellulose} \cdot \frac{1}{1+R_{2,exp}} \tag{III.6}$$

where $S_{BET,composite}$ and $S_{BET,cellulose}$ are specific surfaces of Aerocellulose-silica composite and the pure Aerocellulose, respectively.
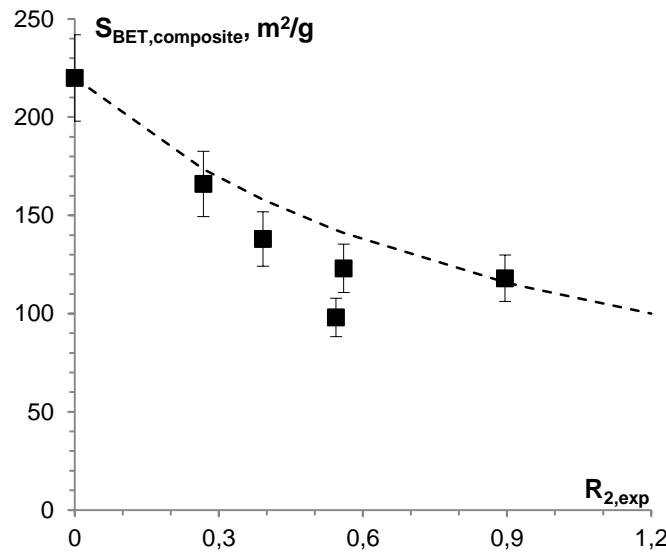


**Figure III.12 : Specific surface area of Aerocellulose-silica composites as a function of silica-to-cellulose ratio $R_{2exp}$. Dashed line corresponds to eq.6 which suggests the absence of porosity in silica particles.**

The specific surface area of the composite calculated via eq. (6) is shown by the dashed line in Figure III.12 with $S_{BET,cellulose} = 220$ m$^2$/g. A good agreement between experimental data and calculated $S_{BET,composite}$ confirms the assumption that silica phase represents a "dead" mass that is not contributing to the specific surface of the final composite.

## 3.4. Mechanical and thermal properties of composite aerogels

### 3.4.1. Mechanical strength

Young's modulus $E$ of the samples was measured by G. Reichenauer from Bavarian Center for Applied Energy Research, Wurzburg, Germany. It was calculated from the bulk density $\rho$ and the longitudinal sound velocity $V$ of the samples determined by ultrasonic run time (Gross, 1992):

$$E = C_{11} \frac{1-\mu-2\mu^2}{1-\mu} \tag{III.7}$$

with $C_{11} = \rho V^2$ being the elastic constant and $\mu$ the Poisson's ratio which is equal to zero for Aerocellulose (Sescousse et al, 2011); thus $E = C_{11}$.

Young's modulus $E$ was determined from sound velocity measurement, as described in Methods section. For Aerocellulose-silica composite the Young's modulus varied from 30 to 40 MPa, while for pure Aerocellulose with a bulk density of 0.117 the modulus is about 20 MPa. Although the composites always showed an increase in modulus compared to the one of pure Aerocellulose, the values were not systematically related to either synthesis parameters or the bulk density of the composite. The modulus of the composite is also higher than that of silica aerogels of a similar density (0.20-0.25 g.cm$^{-3}$) synthesized either from tetramethoxysilane (TMOS) and measured with the same method at Montpellier, 10-25 MPa (Alaoui et al 2008; Gross et al, 1988) or from polyethoxydisiloxane (PEDS) measured at EMPA by uniaxial compression 10–20 MPa (Wong et al, 2014). Measurements performed in centre PERSEE on PEDS-based aerogels with bulk densities around 0.1 g.cm$^{-3}$ shown Young moduli in the 1-2MPa range; however for aerogels the Young modulus is linked to bulk density with a power law; (Diascorn, 2014) found a power-law exponent of 3.8 and a prefactor of 6765 for PEDS based aerogels; thus for silica aerogels with densities around 0.200 g.cm$^{-3}$, Young moduli near 15 MPa shall be expected.

Table III.6: Young modulus and densities for cellulose-silica composites with different values of $R_{2,th}$

| Cellulose concentration | $R_{2th}$ | $\rho$ (g.cm$^{-3}$) | Young modulus (MPa) |
|---|---|---|---|
| 5% | 0 | 0.117 | 20 |
| 5% | 0,67 | 0,210 | 40 |
| 5% | 1,07 | 0,203 | 24 |
| 5% | 1,40 | 0,212 | 30 |

### 3.4.2. Thermal conductivity

The thermal properties of cellulose-silica composite aerogels have been evaluated by hot-wire measurements by G. Reichenauer from Bavarian Center for Applied Energy Research, Wurzburg, Germany. The thermal conductivity of pure Aerocellulose in ambient conditions is in the range of 0.035-0.040 W.m$^{-1}$.K$^{-1}$ depending on cellulose concentration. The composites show higher conductivities at ambient pressure, in the 0.045-0.050 W.m$^{-1}$.K$^{-1}$ range (table III.7).

Table III.7: Thermal conductivities measured by hot wire method in room conditions for cellulose-silica composites with different values of $R_{2,th}$. Cellulose concentration was 5%wt.

| $R_{2th}$ | $\rho$ (cm$^3$.g$^{-1}$) | $\lambda_{,amb}$ (mW.m$^{-1}$.K$^{-1}$) |
|---|---|---|
| 0 | 0.117 | [35 ; 40] |
| 0,67 | 0,210 | 50 |
| 1,07 | 0,203 | 45 |
| 1,40 | 0,212 | 46 |

The high values for the composites conductivities had to be expected as we demonstrated that the silica particles formed into the cellulose network have a smooth surface and are not contributing to the porosity of the network. Although the silica particles do fill some of the larger Aerocellulose pores, they do not form a continuous mesoporous network. In this case we can assume that the added silica particles only contribute to increase the total material conductivity, by affecting the solid heat transfer along the composite backbone. A conductivity of 0.050 $W.m^{-1}.K^{-1}$ is obtained for the samples where $R_{2,th}= 0.67$ against 45-46 $mW.m^{-1}.K^{-1}$ for higher values of $R_{2,th}$ , despite the fact that the later have higher contents of silica. The contribution of silica particles to the solid conductivity of the samples can be illustrated by measuring the variation of the thermal conductivity of a sample with decreasing pressure. A comparison between Aerocellulose and a cellulose-silica composite aerogel can be visualized on figure III.13.
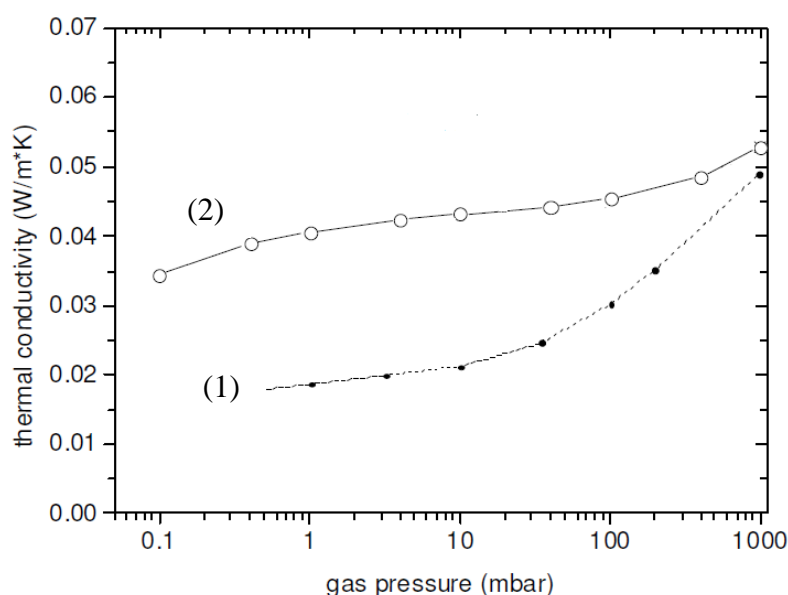


**Figure III.13 : Thermal conductivity as a function of pressure for (1) pure Aerocellulose ($\rho_{Aerocellulose}$ = 0.117 g.cm$^{-3}$) and (2) cellulose-silica composite with R$_{2,th}$= 0.67 ($\rho_{Composite}$ = 0.210 g.cm$^{-3}$)**

When the pressure is decreased, the gas contribution to the thermal conductivity is lowered and can disappear when sufficient level of vacuum is reached; in that case, the conductivity under vacuum only includes the radiative and solid thermal contributions. At a pressure of 0.1 mbar, the thermal conductivity of the composite has dropped from 0.050 to ~ 0.035 $W.m^{-1}.K^{-1}$, while for Aerocellulose it dropped from 0.044 to ~ 0.017 $W.m^{-1}.K^{-1}$. Even if the lowest conductivity level with vacuum is not reached nor for Aerocellulose, neither for composites, the shape of the conductivity curves as a function of pressure tends to indicate a higher solid (and possibly radiative) contribution in the case of the cellulose-silica composite aerogel as compared to pure Aerocellulose, confirming that the non-porous silica particules mostly contribute to the composite total conductivity by increasing notably the solid backbone conductivity.

## 4. Freeze-drying of cellulose-silica composites

Another way to obtain porous, light materials from wet gels is freeze drying. Unlike drying in supercritical $CO_2$, freeze-drying can be performed without water to ethanol solvent exchange, as the solvent is directly eliminated by sublimation. The freeze-drying procedure was performed

as described in materials and methods section. Briefly, hydrogel composite samples were immersed in liquid nitrogen to freeze the solvent, followed by drying at 25 °C under high vacuum. The same formulations as given in Table III.8 were freeze-dried to compare with the morphology and properties of cellulose-silica composite aerogels. Freeze-dried samples appeared white and homogeneous; however surface cracks appeared on most samples during drying (figure III.14).
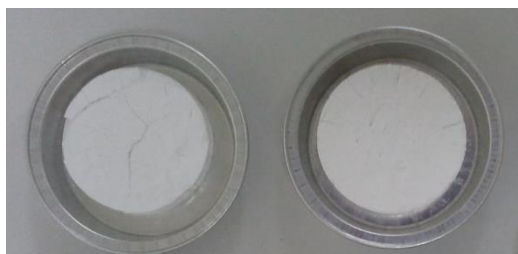


**Figure III.14: Visual aspect of freeze-dried cellulose-silica composites with $R_{2,th}=1.07$**

Figure III.15 compares apparent densities of freeze-dried composites of varying $R_{2,th}$ with those of composite aerogels with similar formulations. The apparent densities for freeze-dried samples are in the 0.10-0.15 $cm^3.g^{-1}$ range, slightly lower than for the corresponding sc $CO_2$-dried materials, thanks to lower volume contraction of freeze-dried samples upon drying, as well as the formation of macropores during the freezing step. Obviously, bulk densities slightly increase when increasing silica content. Specific surface area for freeze-dried samples is consequently significantly lower than for supercritically dried samples: the specific surface area for cryogels from 5%wt cellulose is only 37 $m^2.g^{-1}$ against 220 $m^2.g^{-1}$ for supercritically dried Aerocellulose.
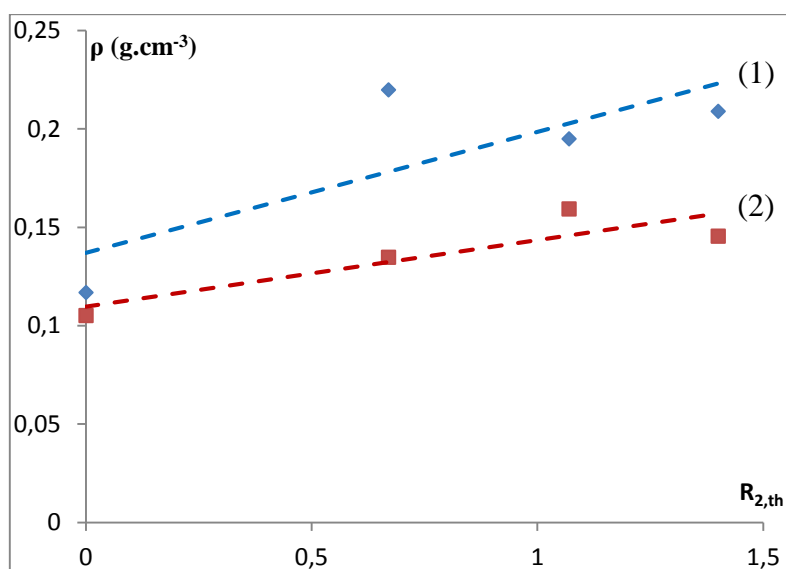


**Figure III.15: Comparison of apparent densities for cellulose-silica composites (1) dried with sc $CO_2$ and (2) freeze-dried.**

The morphology of the freeze-dried samples was examined by SEM (figure III.15). The microstructure of freeze-dried cellulose is a porous network; however the pores appear larger overall than for supercritically dried cellulose: most pores are in the 1-10µm range. Mesopores present on Aerocellulose were mostly interstices between cellulose strands of a few nanometers in diameter. In the case of freeze-dried samples, the cellulose backbone appears non-fibrous,

and the cellulose walls are flattened, sheet-like structures. This is attributed the growth of ice crystals during the water freezing step, which compresses the pore wall structure, leading to the contraction of the smaller pores.

Silica particles can be observed on all composite samples. As silica particles are formed during the coagulation step, as described in part 4.3.1. They present similar characteristics as the ones observed in sc $CO_2$ dried samples: roughly spherical geometry and diameter in the 0.5-0.8 µm range (fig III.16.d).
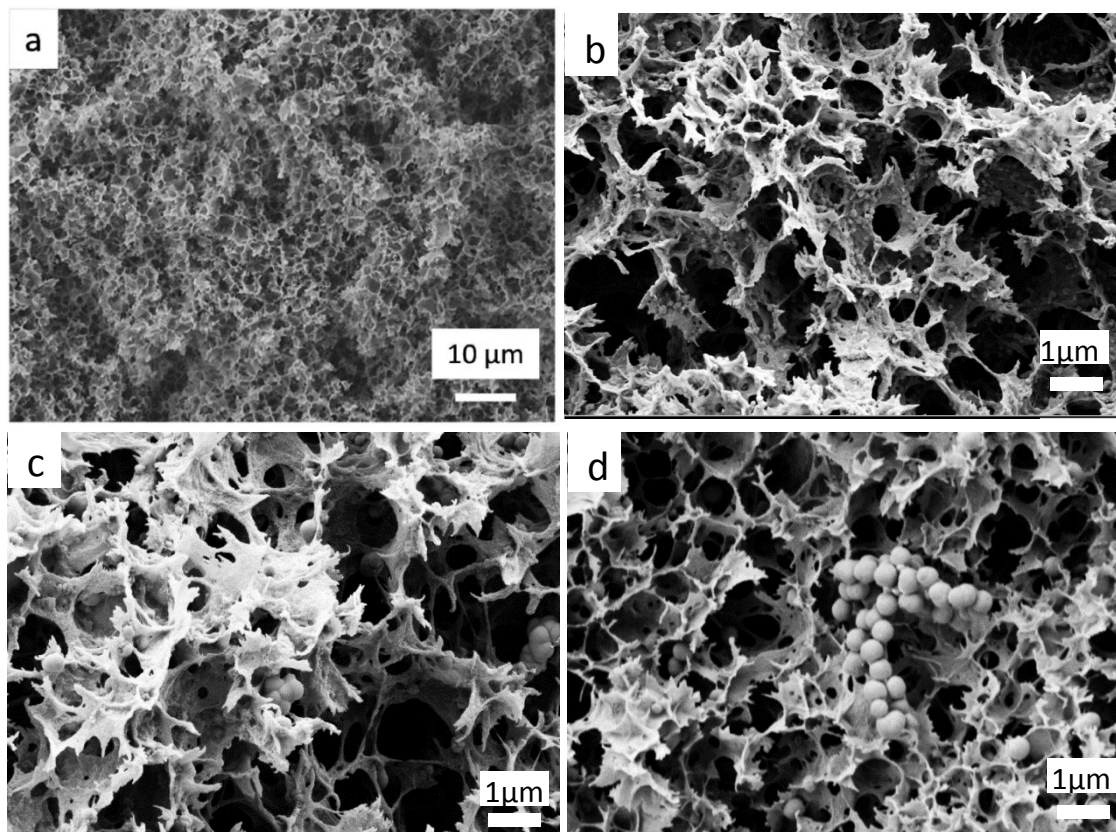


**Figure III.16 : SEM images of freeze-dried cellulose-silica composites obtained from 5%wt cellulose solutions, with varying silica contents (a) $R_{2,th}=0$ ; (b) $R_{2,th} = 0.67$ ; (c) $R_{2,th} = 1.07$ and (d) $R_{2,th} =1.40$.**

The thermal conductivities of freeze-dried cellulose-silica composites were measured with heat flow meter apparatus in PERSEE/MINES ParisTech, as described in materials and methods section. Table III.8 compares the conductivities of freeze dried and sc $CO_2$ samples.

**Table III.8: comparison of thermal conductivities of freeze-dried cellulose-silica composites with those of samples dried in supercritical $CO_2$**

| $R_{2,th}$ | $\lambda_{sc\ CO2}$ ($mW.m^{-1}.K^{-1}$) | $\lambda_{freeze-dried}$ ($mW.m^{-1}.K^{-1}$) |
|---|---|---|
| **0,67** | 51 | 47 |
| **1,07** | 45 | - |
| **1,4** | 46 | 45 |

As could be deduced from SEM pictures, the macroporosity of freeze-dried samples result in high conductivity values around 45 $mW.m^{-1}.K^{-1}$. The thermal conductivity values for freeze-dried samples are similar to those of composite aerogels, due to the conductive nature of the

silica particles. The slightly lower thermal conductivity value for freeze-dried samples as compared to supercritically dried ones can be attributed to their lower density.

## Conclusions

The preparation of cellulose-silica composite aerogels through one-pot process was reported.

Water-8%wt NaOH is a well-known "green" solvent for cellulose; however it is not possible to mix a cellulose-NaOH solution with most of silica precursors because of the reactivity of the alkaline media towards silica on one hand, and silica solvent incompatibility with cellulose inducing cellulose phase separation on the other hand. To ensure a better mixing of cellulose and silica and thus making homogeneous composite, sodium silicate was chosen as silica precursor: its alkaline nature makes it suitable for mixing with cellulose-NaOH solutions. The mixtures were prepared at - 6°C and in the presence of ZnO, a gelation-delaying additive so that cellulose gelation was delayed and the final material was more homogeneous.

Sodium silicate forms a gel in acidic conditions. Using dynamic rheology we demonstrated that the gelation time of sodium silicate solution in the presence of strong acid, HCl, is decreased as compared to citric acid, a weak acid. The temperature dependence of the gelation time of sodium silicate follows Arrhenius-type law, and the activation energy of 50 kJ.mol$^{-1}$ was determined when HCl was used as the catalyst. This value is comparable to other silica-based sol-gel systems reported in the literature. The behaviour ("solidification") of the cellulose-sodium silicate system was studied for different cellulose/silicate proportions and as a function of temperature. Cellulose gelation time strongly decreased when increasing sodium silicate concentration, following a power law. The gelation time dependence on temperature follows the exponential law, with characteristic exponents being twice lower than those obtained for gelation of pure cellulose-NaOH solutions. The addition of sodium silicate on the cellulose-NaOH system had a strong destabilizing effect, inducing rapid association of cellulose which in turn leads to a microphase separation because of the competition for the solvent between silicate and cellulose.

The composite aerogels were obtained by supercritical drying of the coagulated mixtures. Cellulose concentrations were varied between 3-5wt% and silica/cellulose mass ratio was varied from 0 to 1.4. The bulk densities of the composites were around 0.2 g.cm$^{-3}$. The higher yield in silica (40% ±4) was obtained when coagulating the composite in an HCl bath, favoring a rapid reaction of sodium silicate and limiting its loss by diffusion outside of cellulose porous network. The morphology of the composite aerogels was rather different from that of aerogels based on neat materials: cellulose appeared as a network formed of small beads, characteristic of a coagulated system, while silica formed large particles with diameters in the 600-800 nm.

The presence of such large silica particles filling the pores of Aerocellulose lowered significantly the specific surface area, proving that those silica particles are non-porous. Thermal conductivity was increased from 0.035-0.040 W.m$^{-1}$.K$^{-1}$ for pure Aerocellulose to 0.045-0.050 W.m$^{-1}$.K$^{-1}$ for the composites, due to the dense silica particles increasing the solid contribution of the aerogels backbone to the total conductivity. Finally, the Young modulus of the composite was increased as compared to pure Aerocellulose, showing that the silica particles acted as a reinforcing additive for the cellulose matrix. However, this "one-pot" method proved ineffective for the preparation of nanostructured cellulose-silica composites (particularly for thermal insulation application), as the two starting materials can only be mixed in a very limited range of concentrations, in which condition the formation of a silica aerogel structure cannot be obtained.

# References

Alaoui AH, Woignier T, Scherer GW, Phalippou J.  (2008) Comparison between flexural and uniaxial compression tests to measure the elastic modulus of silica aerogel; *Journal of Non-Crystalline Solids*, 354, 4556–4561

Colby, M.W, Osaka,A., Mackenzie,J.D. (1986) ; Effects of temperature on formation of silica gel, *J. Non-Cryst. Solids* 82, (1986) 37-41.

Demilecamps, A., Reichenauer,G., Rigacci,A., Budtova,T. (2014); Cellulose-silica composite aerogels from "one-pot" synthesis, *Cellulose*, 2, 2625–2636

Diascorn, N. (2014), PhD thesis, MinesParisTech

Egal, M. Structure and properties of cellulose/NaOH aqueous solutions, gels, and regenerated objects; Thèse Doc., Sciences et génie des Matériaux, Sophia-Antipolis : CEMEF, 2006.

Gavilon R, Budtova T (2008) Aerocellulose: New Highly Porous Cellulose Prepared from Cellulose−NaOH Aqueous Solutions. *Biomacromolecules*, 9, 269-277

Gross J, Fricke J, (1992) Ultrasonic Velocity-Measurements in Silica, Carbon and Organic Aerogels. *Journal of Non-Crystalline Solids* 145, 217-222.

Liu,W.,  Budtova,T., Navard, P. (2011); Influence of ZnO on the properties of dilute and semi-dilute cellulose-NaOH-water solutions ; *Cellulose*, 18, 911–920.

Ponton, A., Warlus, S.*,* Griesmar, P. (2002); Rheological Study of the Sol–Gel Transition in Silica Alkoxides; *Journal of Colloid and Interface Science* 249, 209–216.

Roy,C., Budtova,T., Navard, P. (2003);  Rheological Properties and Gelation of Aqueous Cellulose-NaOH Solutions; *Biomacromolecules*, 4, 259-264

Sescousse R et al. (2011) Aerocellulose from cellulose–ionic liquid solutions: Preparation, properties and comparison with cellulose–NaOH and cellulose–NMMO routes. *Carbohydrate Polymers* 83, 1766–1774.

Wong JCH, Kaymak H, Brunner S, Koebel MM. (2014) Mechanical properties of monolithic silica aerogels made from polyethoxydisiloxanes. *Microporous and Mesoporous Materials* 183, 23–29.

# Chapter IV:
# Cellulose-silica composite aerogels from impregnation of cellulose porous matrices with polyethoxydisiloxane sols

## Introduction

This fourth chapter focuses on the preparation of cellulose-silica composite aerogels from the impregnation of a cellulose matrix with a polyethoxydisiloxane (PEDS) sol. The cellulosic matrix was obtained from cellulose coagulated from 3%wt cellulose-EMIMAc-DMSO solution. In situ formation of silica gel was then performed by immersion of the impregnated material in a basic catalyst solution. Drying with supercritical $CO_2$ resulted in cellulose-silica composite aerogels.

First we studied the impregnation process and followed the impregnations kinetics. Two impregnation methods were investigated. The first one was diffusion-controlled impregnation, where a coagulated-in-ethanol cellulose porous matrix was immersed in a PEDS solution. In this case the PEDS slowly penetrated into the cellulose matrix following a mechanism of molecular diffusion. Studying the mass increase of the sample for different impregnation times allowed evaluating the impregnation kinetics. As diffusion-controlled impregnation is a slow process particularly when working with mesoporous networks to be intruded, a forced-flow setup was thus designed to decrease the impregnation time. In this setup the PEDS solution is forced to penetrate the cellulose matrix by generating a pressure gradient from on surface to another. The dry mass of the filtrate was studied to confirm the very large improvement in impregnation time from more than 7 hours (diffusion) to about 30 minutes (forced-flow). Energy diffractive spectroscopy (EDS) was used to compare the silica distribution between diffusion and forced-flow impregnated samples obtained after sc drying.

The aerogel composites obtained with supercritical $CO_2$ drying of the impregnated samples were then characterized. Bulk densities, morphology, specific surface areas, mechanical properties under the uniaxial compression experiments and thermal conductivities of the composites were compared between forced-flow and diffusion impregnated samples, as well as to those of pure silica and cellulose aerogels.

# Introduction

Dans ce chapitre nous avons étudié l'élaboration d'aérogels composites cellulose-silice, à partir de l'imprégnation d'une matrice poreuse nanostructurée de cellulose par un sol de polyethoxydisiloxane (PEDS). La matrice de cellulose a été obtenue par la coagulation d'une solution de cellulose 3%wt dans l'EMIMAc dans l'éthanol. La formation de l'aérogel de silice a été réalisée *in situ* par immersion d'échantillons imprégnés dans une solution de catalyseur basique.

Premièrement, nous avons étudié le procèdé d'imprégnation et suivi sa cinétique. Deux méthodes d'imprégnation ont été étudiées. La première était l'imprégnation par diffusion, consistant à immerger une matrice poreuse de cellulose coagulée dans une solution de PEDS. Dans ce cas le PEDS pénètre lentement à l'intérieur de la matrice cellulosique via un mécanisme de diffusion moléculaire. L'étude de l'augmentation massique d'échantillon pour différents temps d'imprégnation nous a permis d'évaluer la cinétique du procédé. L'imprégnation par seule diffusion moléculaire étant un procédé long tout particulièrement dans le cas de substrat mésoporeux, un système d'imprégnation par flux forcé a été mis au point. Il consiste à forcer la pénétration du PEDS dans la matrice de cellulose en générant un gradient de pression entre les surfaces de la matrice cellulosique. La masse sèche du filtrat a été étudié pour confirmer la très importante diminution du temps d'imprégnation obtenu via cette méthode par rapport à l'imprégnation par diffusion moléculaire, de plus de 7 heures à environ une demi-heure.

Les aérogels composites obtenus après séchage au $CO_2$ supercritique ont été caractérisés. Les densités apparentes, morphologies, surfaces spécifiques ainsi que les propriétés mécaniques en compression uniaxiale et la conductivité thermique des composites ont été comparées, d'une part entre les échantillons élaborés via diffusion moléculaire et flux forcé, d'autre part par rapport à des aérogels de cellulose et de silice de référence.

# 1. Preparation of the cellulose-silica composites by impregnation

## 1.1. Strategy for cellulose impregnation

The goal of this chapter is to prepare monolithic composite aerogels made of interpenetrated networks of nanostructured and (partly) mesoporous cellulose and silica. The idea is "filling" the pores of cellulose matrix with superinsulating silica phase in order to decrease the thermal conductivity of Aerocellulose while reinforcing the silica aerogel thanks to the more mechanically resistant cellulose matrix. As nanostructured silica could not be obtained through one-pot synthesis as previously demonstrated, we opted for a two-step impregnation process. Cellulose can be coagulated from solutions in ionic liquids in a non-solvent, generally ethanol. After several washings with the non-solvent to remove the traces of ionic liquids, a cellulose continuous network, "alcogel", impregnated with ethanol is obtained. Given the open pore nature of coagulated cellulose, "mixing" cellulose with a silica precursor solution can be obtained by filling the cellulose porosity by an ethanol solution containing the dissolved silica precursor. TEOS or TMOS derivatives are the most common silica aerogel precursors, and are soluble in ethanol. Silica can be formed directly inside cellulose porosity by subsequent immersion of the impregnated wet material in an acid or basic catalyst bath. Drying the composite gels in supercritical $CO_2$ then yields a composite cellulose-silica aerogel.

For this study we used a polyethoxydisiloxane (PEDS) as the silica precursor. The formulation used to form silica was based on that used by (Achard et al., 2007, Bisson et al., 2004): the objective is to obtain a concentration of 8%wt PEDS inside the impregnated matrix.

We considered two ways for impregnating cellulose: first, the direct immersion of the alcogel in an alcoholic PEDS sol would lead to PEDS diffusion inside the cellulose pores until an equilibrium concentration is reached between the inside of the alcogel structure and the outside. This diffusion-driven process will be investigated in details in part 1.2.2. Secondly, in order to decrease the impregnation time, the forced impregnation of the PEDS sol inside the alcogel pores was obtained by applying a pressure gradient, until a target concentration of precursor inside the alcogel was reached. The forced-flow impregnation process will be investigated in part 1.2.3.

## 1.2. Preparation of composite celulose-silica aerogels

### 1.2.1 Preparation of the cellulose matrix.

The cellulose matrix was prepared from a cellulose solution in an ionic liquid solvent. The cellulose concentration was fixed at 3%wt to ensure faster penetration of silica precursor in the cellulose matrix thanks to the low cellulose concentration, while keeping good mechanical properties. The ionic liquid used was 1-ethyl-2-methylimidazolium acetate (EMIMAc). DMSO was used as a co-solvent to lower the viscosity of the system, the proportion EMIMAc:DMSO was 20:80 in weight. The solution was coagulated by pouring ethanol over the sample surface, followed by several consecutive steps of washing with ethanol. The detailed procedure was described in Materials and method section (Chapter II).

### 1.2.1. Diffusion process

Cellulose alcogel was immersed in 16 %wt silica solution in ethanol ($m_{alcogel} = m_{silica\ solution}$) for 24 h at room temperature, then extracted and placed in alcolohic catalyst solution in the proportion $m_{catalyst\ solution} = m_{gel}$ for the next 24 h (Figure IV.1) resulting in in situ silica gelation.
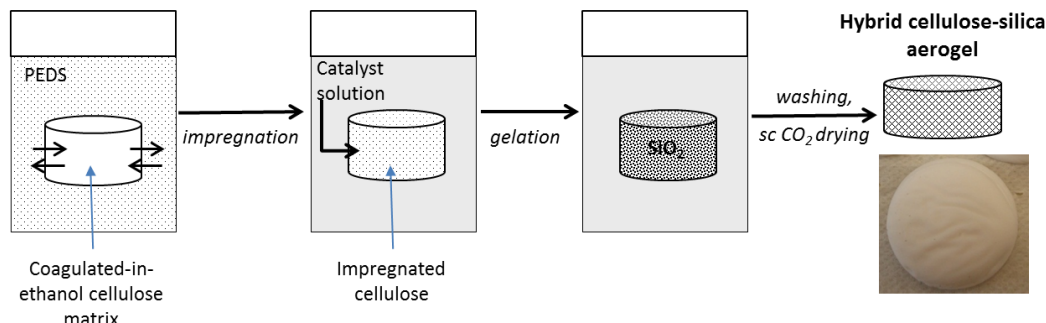


**Figure IV.1 : A schematic presentation of the preparation route of cellulose-silica composite aerogels via the diffusion process.**

The impregnation of the cellulose matrix in this case is controlled by molecular diffusion. In a first approximation, the diffusion coefficient of molecules in a fluid can be estimated thanks to the Stokes-Einstein formula (eq. IV.1):

$$D = \frac{k_B T}{6\pi\eta R} \tag{IV.1}$$

where $k_B$ is Boltzmann constant ($k_B = 1.38 \times 10^{-23}$ m$^2$.kg.s$^{-2}$.K$^{-1}$), T is temperature in K, $\eta$ the viscosity of the medium (Pa.s), R the radius of the diffusion entity (m).

The distance L made by a particle over a given time $t$ can be calculated from equation IV.2:

$$L = \sqrt{Dt} \tag{IV.2}$$

In the case of the PEDS used in this study, the mean particle diameter was measured by dynamic light scattering (DLS) experiments by the Institut Charles Sadron (Strasbourg, France). The size for 95% of the particles is around 1 nm, with a minor quantity ($< 5\%$) of larger agglomerates around 1000-1500 nm, which can easily be eliminated by filtering the solution. Thus we used R = 1 nm. In our samples the PEDS concentration is around 8%wt, and it can be considered as a dilute solution. Considering the viscosity of ethanol is $1.2.10^{-3}$ Pa.s, we obtain, for T = 25°C, $D_{PEDS} = 1.8.10^{-10}$ m².s$^{-1}$. In table IV.1, we estimate the distance a PEDS particle can travel during a given time.

**Table IV.1: Theoretical distance made by a PEDS particle with R = 1 nm at different times in the case of PEDS dilute solution.**

| t (h) | $L_{PEDS}$ (mm) |
|---|---|
| 1 | 0,81 |
| 3 | 1,40 |
| 8 | 2,29 |
| 24 | 3,96 |
| 48 | 5,61 |

To follow experimentally the impregnation kinetics of cellulose alcogels by PEDS via molecular diffusion (before immersion in the catalyst solution), wet disks of 5 mm diameter were extracted from silica solution at various impregnation times and dried in a vacuum oven at 80 °C and 150 mbar up to constant weight. The evolution of the mass of the disks as a function of impregnation time was recorded. The relative mass of silica in the dried gel was measured as follows (eq. IV.3):

$$w_{rel,1}(t) = \frac{w_1(t)}{w_{max,1}} \tag{IV.3}$$

where $w_1(t)$ is the dry weight of the impregnated cellulose at time $t$ and $w_{max,1}$ is the theoretical maximal dry weight of impregnated cellulose matrix calculated assuming silica fully penetrating cellulose porosity and thus a PEDS concentration inside the impregnated material equal to 8%wt.

To estimate the theoretical impregnation time, we have to consider that the theoretical $L_{PEDS}$ has to be doubled in the case of a disc-shaped sample where impregnation occurs through both free faces. We assumed that the diffusion front is regular throughout the sample and perpendicular to its lateral surface. Thus we can deduce the volume of sample impregnated by the silica sol, and theoretical relative silica weight by using equation (IV.4):

$$w_{rel,th}(t) = \frac{(1 - wt\%_{cell}).V_{impregne}(t).\rho_{PEDS}}{V_{total}.\rho_{gel}} \tag{IV.4}$$

As the fraction of each constituent in the gel is low as compared to the quantity of solvent(3%wt for cellulose and maximum 8%wt for silica), we considered that $\rho_{PEDS} \approx \rho_{gel}$. The theoretical filling of the silica gel was plotted along the experimental points on figure IV.2.
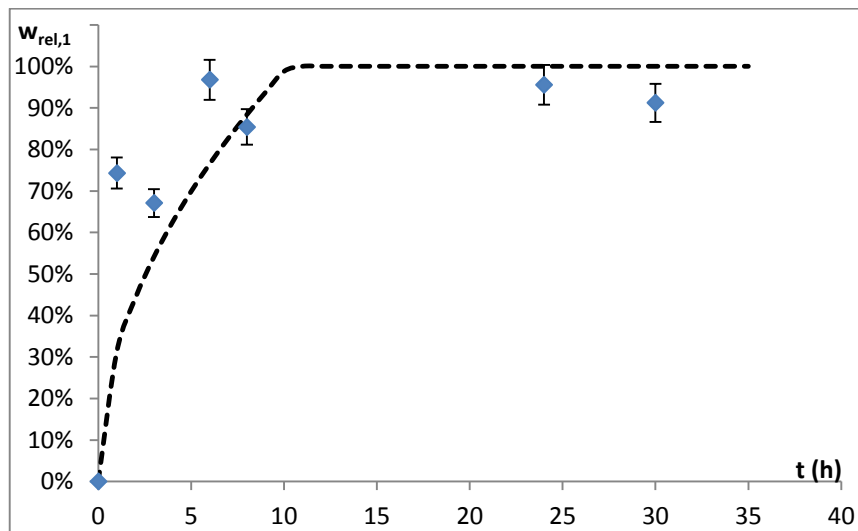


**Figure IV.2 : Silica relative weight as a function of impregnation time during diffusion impregnation of cellulose alcogel made from a 3%wt cellulose-EMIMAc-DMSO solution. Dotted line correspond to theoretical value calculated according to equation (IV.4) Sample thickness is 5 mm.**

The impregnation by diffusion occurs in two steps: first quick silica penetration into cellulose alcogel ($w_{rel,1}$ increases by about 70% within the first 3 hours) and then slow approach to equilibrium. Diffusion is slowed down because of silica "filling" the pores of cellulose matrix close to sample surface and creating silica concentration gradient reducing permeability of the

media. In overall, the impregnation process by molecular diffusion is very slow. The theoretical calculation based on the estimated diffusion coefficient of PEDS gives an estimated time for 100% impregnation of 10h in the case of a 5 mm thick cellulose alcogel disk. At equilibrium, it seems that silica weight inside cellulose matrix is reaching 90% of the theoretical maximal value $w_{max,1}$ within 10% experimental error.

Although the theoretical calculation is a rough approximation, the experimental points fit rather well the theoretical values of silica relative weight over time. Probably due to the low cellulose concentration, PEDS diffusion does not appeared slowed down by the presence of the cellulose network, as the best fitting for the experimental points was obtained using the diffusion coefficient estimated for "free" PEDS. However, diffusion should be slowed down considerably when the solute is moving inside a porous polymer matrix. Based on results obtained on the diffusion of NaOH molecules in coagulating cellulose (Gavillon and Budtova, 2007, Sescousse et al., 2011), the diffusion coefficient of NaOH in dilute solution is $D_{NaOH} = 1.5.10^{-9}$ m².s$^{-1}$, and it is lowered by a factor of 3-10 in the presence of a cellulose porous matrix, depending on cellulose concentration. The impregnation time will obviously increase strrongly if increasing sample thickness and/or cellulose concentration.

### 1.2.2. Forced-flow process

In order to accelerate silica impregnation, we developed a set-up to perform so-called "forced flow impregnation". Cellulose alcogel disc of the same thickness as for molecular diffusion impregnation was placed in a home-made plastic funnel fixed on a grid, the whole setup placed above a Büchner flask connected to a primary vacuum pump (Figure IV.3). 16wt% PEDS solution was poured over the gel ($m_{sol} = 2 \times m_{alcogel}$). A pressure gradient was generated using the vacuum pump to force the transport of silica sol through cellulose disk porosity. The impregnated gel was then immersed in the catalyst solution in the same way as described above for simple molecular diffusion impregnation.
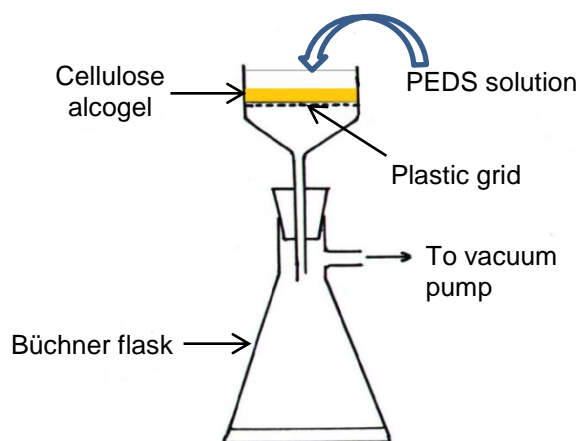


**Figure IV.3 : Scheme of the forced-flow impregnation set-up.**

The impregnation kinetics was followed by the increase of the relative silica weight in the filtrate, $w_{rel,2}$ (t):

$$w_{rel,2}(t) = \frac{w_2(t)}{w_{max,2}} \times 100\% \qquad (IV.5)$$

where $w_2(t)$ is the silica weight in the filtrate at time $t$ and $w_{max,2}$ is the theoretical maximal silica weight in the filtrate calculated assuming the initial silica concentration in the sol is decreased by 2/3 as far as $m_{sol} = 2 \times m_{alcogel}$, resulting in 10.6%wt PEDS in the porosity of the cellulosic wet gel.
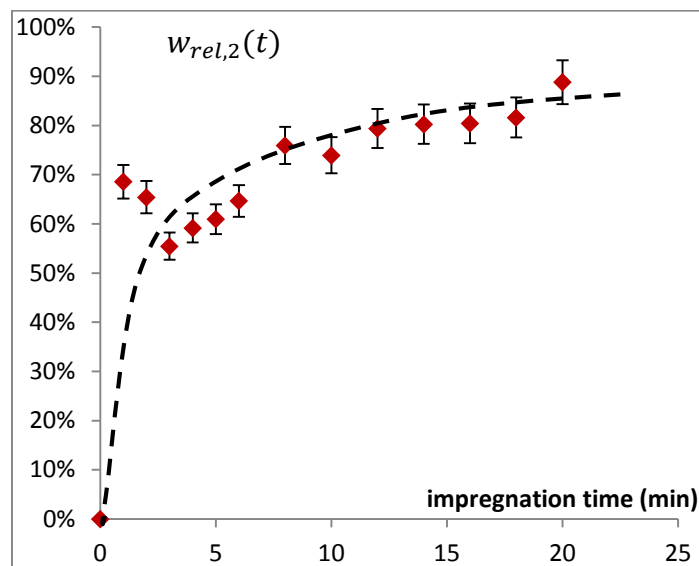


**Figure IV.3 : Silica relative weight in the filtrate as a function of time for forced flow impregnation of cellulose alcogel from a cellulose-EMIMAc coagulated sample. Sample thickness is 5 mm.**

The rate of impregnation via forced flow set-up is much faster as compared to molecular diffusion process: the time needed to reach 80-90% of the theoretical maximal impregnation of cellulose matrix of 5 mm thickness is drastically reduced from 7 hours for diffusion to ~ 15-20 minutes for forced flow. It should also be noted that for diffusion-controlled impregnation the effective impregnation distance is equal to the half-thickness of the sample while for the forced-flow it is the whole thickness of the disk. "Filling" a 2.5 mm thick disk via forced-flow impregnation would be thus at least four times quicker than what is shown in figure IV.3 as far as time is roughly proportional to the distance in power two.

To prepare the aerogels composites, silica gel was formed in the cellulose porosity by immersion in $NH_4OH$ catalyst solution as shown in figure IV.1. The wet composites from forced flow and diffusion controlled impregnation were dried with supercritical $CO_2$ as described in materials and methods section.

## 2. Properties of composite aerogels

### 2.1. Distribution of silica in the composite aerogels.

Because we target the decrease of Aerocellulose thermal conductivity by "filling" its pores with silica aerogel (a materials far less conducting than entrapped air), it is important to understand if silica is homogeneously distributed in the cellulose matrix. This was done using EDS spectroscopy. The spectra were taken on a transversal cut of samples prepared via molecular diffusion as well as forced flow impregnation (figure IV.4). One spectrum was taken every 100 μm over a straight line along the sample cross-section. The weight per cent of Si, wt%$_{Si}$, was

determined from the intensity of the silicon Kα peak at 1.71 keV and the concentration of $SiO_2$ was calculated as follows (eq. IV.6):

$$wt\%_{SiO_2} = \frac{M_{SiO_2}}{M_{Si}} wt\%_{Si}$$

(IV.6)

where $M_{Si}$ = 29 g/mol and $M_{SiO_2}$ = 61 g/mol are the molar mass of silicon and silica, respectively.
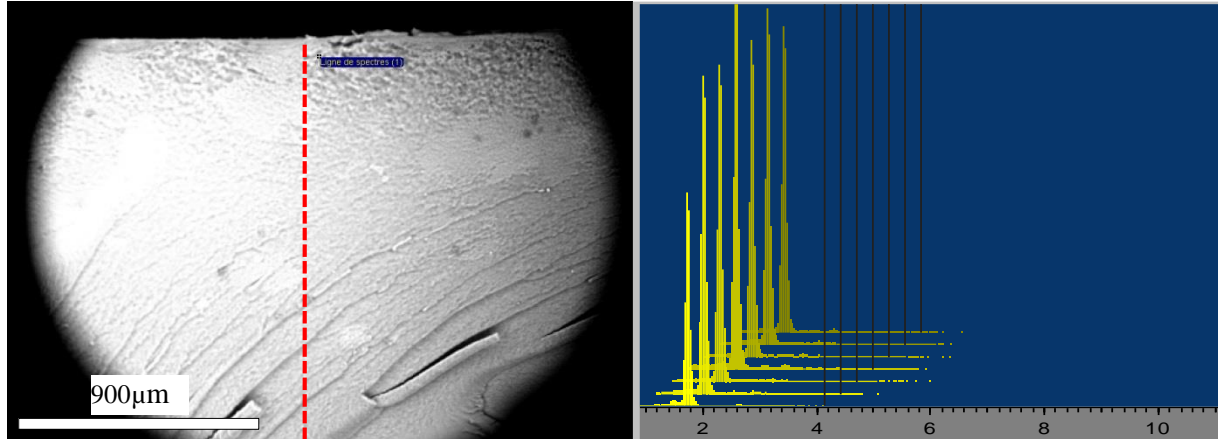


**Figure IV.4: Example of a cross-section of a cellulose-silica composite aerogel from 3%wt cellulose, as seen by SEM. The EDS spectra shown on the right were taken along the red line. The peak shown on the spectra corresponds to the Si Kα at 1.71 keV.**

Figure IV.5 shows the distribution of $SiO_2$ along the cross-section of composite aerogel, as a function of the distance $l$ from the sample surface, for both diffusion and forced flow impregnation. For diffusion-controlled impregnation, both sides of the sample are equivalent in terms of silica impregnation, while for the forced flow impregnation $l = 0$ corresponds to the upper sample surface in contact with PEDS solution.
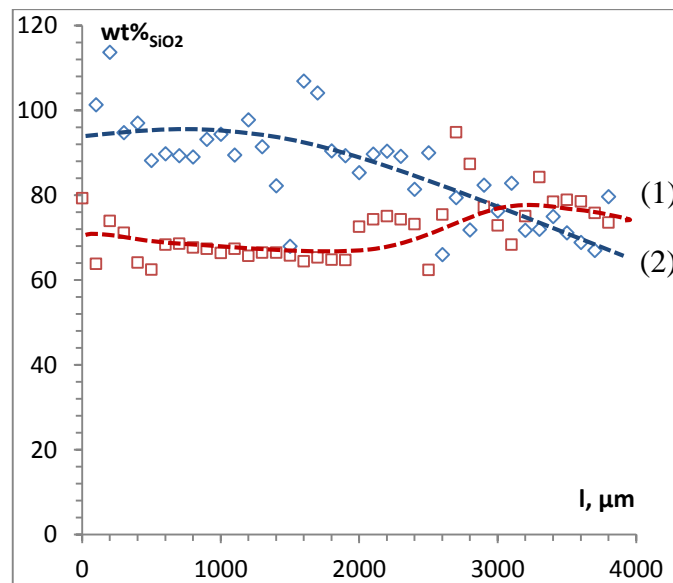


**Figure IV.5: %wt of silica along the transversal cut of composite aerogels impregnated by (1) molecular diffusion for 24 h and (2) forced-flow process (after 1h) as a function of distance from the upper surface of the sample (with thickness equal to 5 mm). Dashed lines are given to guide the eye.**

EDS shows local elemental composition on the surface of the sample cross-section and does not analyse the bulk of the sample. The obtained high values of silica concentration indicate that most of the signals come from Si element. This means that cellulose is well coated by silica resulting in overestimated values of silica concentration as compared to the maximal bulk theoretical value of 72 wt%. Despite the fact that EDS is not reflecting average bulk silica concentration, it gives valuable information on silica penetration and distribution inside the sample. The sample impregnated with forced flow process shows slightly higher silica concentration as compared to diffusion process, especially near sample upper surface. Diffusion-controlled impregnation is showing a more homogeneous silica distribution in the cellulose matrix as compared to forced-flow impregnated composites: in the latter case, silica concentration gradient appears with the distance from the upper sample surface. In overall, forced flow impregnation appears to be an efficient way to reduce impregnation times while keeping a good filling of the cellulose matrix with silica.

In order to estimate silica average concentration in composite aerogel, elemental analysis was done in CNRS Service Central d'Analyse laboratory (Villeurbanne, France) using atomic absorption spectroscopy. Weight concentration of silicon ($wt\%_{Si}$) was measured allowing evaluation of wt% of silica ($wt\%_{SiO_2}$) using equation 6 and silica mass yield in the dry aerogel ($Yield_{SiO_2}$) was determined as follows:

$$Yield_{SiO_2} = \frac{wt\%_{SiO_2}}{wt\%_{SiO_2}(th)} \tag{IV.7}$$

where $wt\%_{SiO_2}(th) = \frac{wt\%_{SiO_2,max}}{wt\%_{cellulose} + wt\%_{SiO_2,max}}$ with $wt\%_{SiO_2,max}$ being theoretical silica concentration in the wet material in case of total silica conservation in the sample during coagulation and washing steps. We thus obtain, for the initial proportion between cellulose and silica used, $wt\%_{SiO_2,max} = 8\%$ and $wt\%_{SiO_2}(th) = 72\%$.

Silica yield for both impregnations was calculated according to eq. 6: it is around 70 and 77% for diffusion and forced flow processes, respectively (table IV.3). The amount of silica wt% in the dry samples obtained with each method is very similar (51 wt % for diffusion against 56 wt % for forced flow impregnation), confirming the observations by EDS spectroscopy that cellulose impregnation using both methods results in a similar filling of cellulose porosity by silica. The silica mass ratio was also consistent with the dry mass measured by drying the samples just after impregnation. It is likely that a loss of silica occurs during the catalysis step, when the impregnated sample is immersed in the NH₄OH solution. The gelation of silica takes about 10 minutes in these conditions (Achard et al., 2007) and partial diffusion of silica sol from cellulose matrix into the catalyst solution can occur even in this short time. Some silica transparent gel was observed around the impregnated cellulose after the catalysis step, confirming a partial loss of the silica due to diffusion from the matrix prior to gelation.

**Table IV.3: Experimental (via elemental analysis) and theoretical silica content in hybrid aerogels and the corresponding impregnation yields for diffusion and forced flow impregnation.**

| Method of impregnation | $wt\%_{SiO_2}$ (exp) | $wt\%_{SiO_2}(th)$ | Yield, % |
|:---:|:---:|:---:|:---:|
| **Diffusion** | 51% | 72% | 70% |
| **Forced flow** | 56% | 72% | 77% |

In ambient temperature and in the mild basic conditions required to form silica aerogel, there is no apparent reason for the formation of covalent bonds between cellulose and silica. To confirm the absence of chemical bonds between cellulose and silica, an FTIR spectrum of an impregnated composite gel was compared to that of pure Aerocellulose and a reference silica aerogel (figure IV.6).
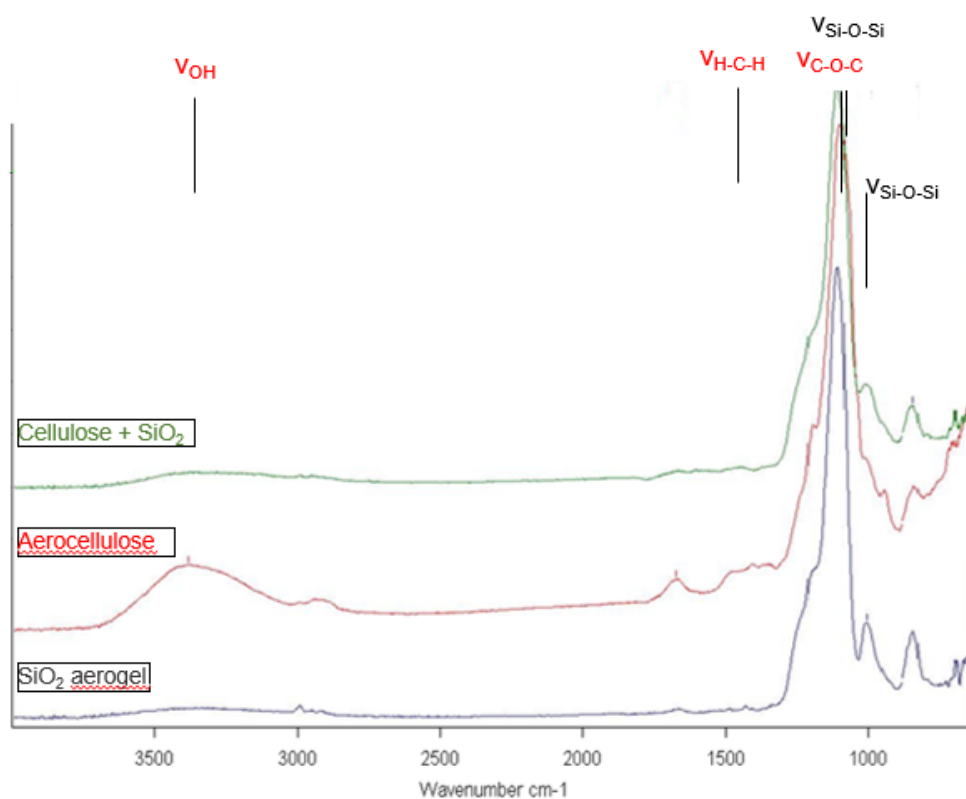


**Figure IV.6: FTIR spectra of reference Aerocellulose and silica aerogels, compared to that of a cellulose-silica composite aerogel.**

Cellulose ether and silica (Si-0-Si) bonds are both vibrating in 1100 cm$^{-1}$ wavenlenght domains which makes difficult to detect the difference between the composite and raw silica. The apparent decrease the –OH absorption band in the [3700-3000] cm$^{-1}$ region as well as that of the band at 900 cm$^{-1}$ observed on the Aerocellulose spectrum in composite aerogel is due to a scaling effect because of the high intensity of the 1100 cm$^{-1}$ band in the composite. We cannot see any disappearance or appearance of any absorption band in the composite spectrum compared to those of the reference components which could account for a chemical bonding.

## 2.2.  General properties of the composite aerogels

### 2.2.1  Morphology

The visual aspect of reference Aerocellulose from 3%wt solution in EMIMAc, a silica aerogel from 8%wt PEDS and a composite aerogel are shown in figure IV.7. Supercritically dried cellulose reference and composite aerogels were white, rigid and monolithic, without visible cracks. On pure cellulose and silica-impregnated composite samples, the upper surface of the samples is slightly deformed during the coagulation step, when ethanol was poured over the cellulose-EMIMAc solution. However, the samples appeared homogeneous and the smooth surfaces necessary for thermal characterization were obtained easily by polishing the surface of the dry sample with abrasive paper.
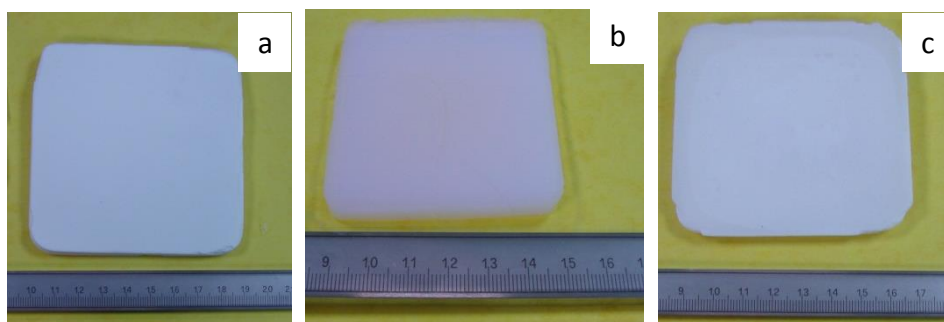


**Figure IV.7: Visual aspect of the aerogels from (a) pure cellulose (b) reference silica aerogel from 8%wt PEDS and (c) cellulose-silica composite aerogel.Drying was done at SEPAREX SA, Nancy, France, in the frame of the AEROCOINs project.**

The morphology of composite aerogels obtained with both impregnation methods, as well as the reference samples (Aerocellulose and silica aerogel) was analysed by SEM (figure IV.8). Aerocellulose (Figure IV.8.a) has a hierarchical structure with "hairy" beads assembled together, as demonstrated previously for Aerocellulose from cellulose-ionic liquid solutions (Sescousse et al., 2011). The beads are supposed to be formed via spinodal decomposition during cellulose coagulation from solution (Sescousse et al., 2011). The inside morphology of a bead is a "network" of fine cellulose strands. Characteristic pores size varies from several tens of nanometers to several microns, as seen by SEM and also studied by non-intrusive mercury porosimetry (Rudaz, 2013). Silica aerogel morphology (figure 5b) is typical of base-catalysed silica aerogels. It looks like a colloidal network formed of "nanometric" silica beads with pore diameter being few tens of nanometer, with no macropores observable by SEM (Pierre and Rigacci, 2011).
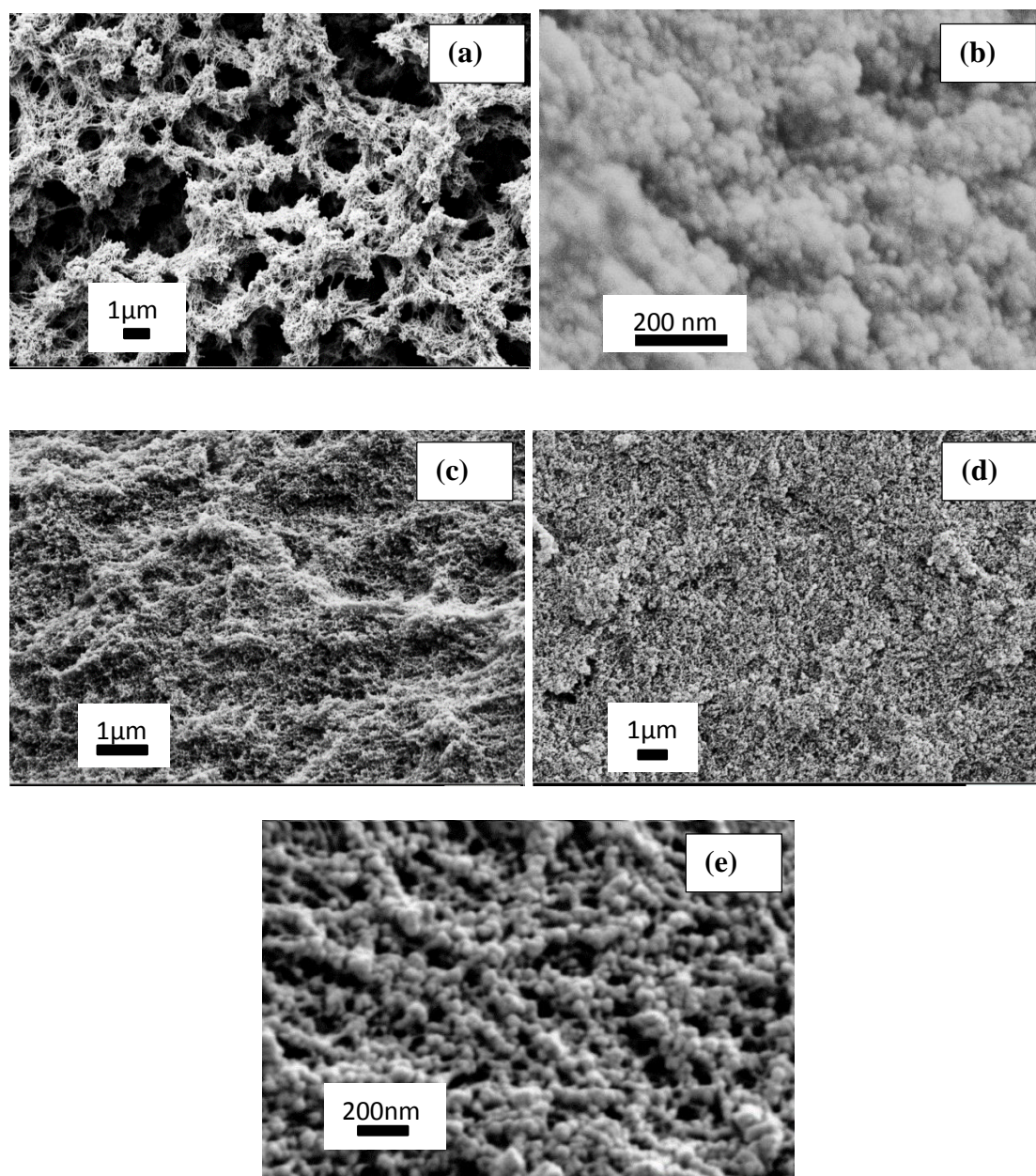
**Figure IV.8: SEM images of Aerocellulose from 3% cellulose-EmimAc-DMSO solution (a); reference silica aerogel (b) and hybrid aerogels obtained with molecular diffusion (c) and forced flow (d, e) impregnation.**

SEM images of composite aerogels are shown in Figure IV.8.c for molecular diffusion-controlled and Figure IV.8.d, e for forced-flow impregnation. In both cases, silica phase appears homogeneously distributed all over cellulose network confirming the formation of organic and mineral interpenetrated networks. The cellulose strands are difficult to see on the images as the cellulose backbone is mostly covered by silica; however the fiber-like shapes seen on figure IV.8.c can be interpreted as cellulose strands. Silica is filling the macroporosity present in Aerocellulose matrix and is "coating" cellulose backbone itself. The latter explains high values of silica concentration obtained by EDS. Figure IV.8.e shows the zoom of the morphology of composite sample obtained with forced flow impregnation: the silica phase is made of agglomerated "nanoparticles". The pore size in the silica phase seems to be in the range of some tens of nanometers.

### 2.2.2 Density and evaluation of porosity

The porosity $\varepsilon(\%)$ was estimated as a ratio between the specific volume of voids $V_{pores}$ and the total specific volume (solid + voids) $V_{total}$ which can also be expressed as a function of bulk and skeletal $\rho_{skeletal}$ densities:

$$\varepsilon(\%) = \frac{V_{pores}}{V_{total}} = 1 - \frac{\rho_{bulk}}{\rho_{skeletal}} \qquad \text{(IV.8)}$$

A theoretical specific pore volume $V_{th}$ was calculated according to equation IV.9:

$$V_{th} = \frac{1}{\rho_{bulk}} - \frac{1}{\rho_{skeletal}} \qquad \text{(IV.9)}$$

Bulk density $\rho_{bulk}$ of composite aerogels and of cellulose and silica reference samples was measured as described in Experimental section and porosity $\varepsilon\%$ was calculated according to eq.1; the values are given in table IV.4. Porosity was calculated supposing cellulose and silica skeleton density being roughly 1.5 (Rudaz, 2013) and 2.0 (Ayral, Phalippou and Woignier, 1992) g.cm$^{-3}$, respectively. The average skeletal density of composite aerogels was calculated taking into account the amount of silica for each impregnation case as obtained with elemental analysis, 51 wt% for diffusion and 56 wt% for forced flow. The density of composite materials appears higher, as expected, and porosity slightly lower than that of each of the reference samples. In overall, the porosity of composite aerogels is around 90%.

**TableIV.4: Bulk density, porosity ε %, theoretical specific pore volumeV$_{theor}$ , specific surface area S$_{BET}$, for cellulose and silica reference samples and composite aerogels.**

| Formulation | $\rho_{bulk}$, g/cm$^3$ | ε, % | $V_{th}$, cm$^3$/g | S$_{BET}$, m$^2$/g |
|---|---|---|---|---|
| Aerocellulose | 0.123 | 0.92 | 8.8 | 290 |
| SiO$_2$ aerogel | 0.130 | 0.94 | 8.2 | 975 |
| Diffusion | 0.225 | 0.87 | 5.0 | 810 |
| Forced-flow | 0.156 | 0.91 | 7.0 | 750 |

Assuming silica aerogel fills the entirety of the porosity of Aerocellulose, and that the bulk density of the aerogel formed inside the cellulose porosity is the same as the pure SiO$_2$ aerogel synthesized in similar conditions, the theoretical apparent density for maximal filling of the composites by SiO$_2$ can be expressed as follows:

$$\rho_{max} = (1 - \varepsilon_{cellulose}) \cdot \rho_{bulk,cellulose} + \varepsilon_{cellulose} \cdot \rho_{SiO2}$$

$$\rho_{max} = 1.5 \times 0.08 + 0.92 \times 0.130$$

$$\rho_{max} = 0.240 \text{ g. cm}^{-3}$$

The comparison of the measured apparent density of the composites with $\rho_{max}$ suggests that in the case of diffusion impregnated samples, 93% of the cellulose pores are filled with silica aerogel, while in the case of forced-flow impregnation only 65% of the cellulose porosity is filled by silica. This result seems to be inconsistent with the silica mass percentages calculated from elemental analysis, which were very close to fully impregnated samples obtained through diffusion or forced-flow methods. However, in the case of the composites silica gel has been synthesized inside the cellulose pores, i.e in a confined environment where the catalyst had to diffuse to reach the PEDS. These conditions may induce a certain difference in the silica synthesis conditions. Thus we can speculate that the density of the silica synthesized within the cellulose porosity may be someway different than that of silica synthesized in the absence of cellulose. This point could be studied more in details in future works.

As compared to Aerocellulose, the specific surface area of both composites increased significantly, reaching values that are comparable with the ones characteristic to silica aerogels. This result is a direct confirmation of the formation of finely nanostructured silica aerogel in the pores of cellulose matrix. The complete adsorption-desorption $N_2$ isotherms for both composite samples and for reference aerogels (figure IV.9) correspond to type IV according to IUPAC classification.
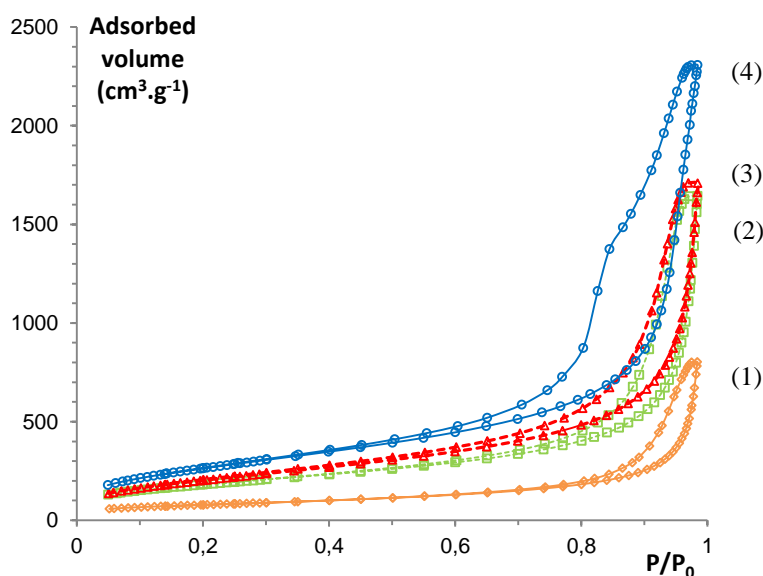


**Figure IV.9 : $N_2$ sorption-desorption isotherms for Aerocellulose from 3wt%cellulose-EmimAc solution (1), diffusion-controlled (2) and forced flow (3) impregnated composites and reference silica aerogel (4)**

The total volume of adsorbed nitrogen in composite aerogels is the same for both impregnation techniques and more than twice higher than that for reference Aerocellulose, attesting a larger total pore surface area due to nano-structured silica.

There is a significant difference between the theoretical pore volume calculated from density measurements and the pore volume measured by BJH method from $N_2$ isotherms: 50 to 80% of the total pore volume is ignored by BJH measurements. It is known for cellulose (Rudaz et al., 2014) as well as for silica aerogels (Reichnauer and Scherrer, 2001) that BJH approach does not provide the information on pores of a diameter larger than few hundred nanometers which does not cover the whole range of pore sizes in Aerocellulose (see SEM pictures in part 2.1.2).

Thus we shall not rely on BJH method to quantify the porosity in the case of cellulose-silica composites. From the results of the elemental analysis of silica content as well as the analysis of composite density, we can assume that silica do not fill entirely the cellulose porosity: it is likely that some large open pores remain in the composite.

## 2.3.   Mechanical properties and thermal conductivity

### 2.2.3   Mechanical properties

Uniaxial compression of reference and composite aerogels is presented in Figure IV.10 as stress-strain plots; the values of Young modulus E and fracture stress $\sigma^*$ and strain $\varepsilon^*$ are reported in table IV.5. Each compression experiment was performed to the moment when the sample was starting to break. Because of the restricted sample geometry for forced-flow impregnation set-up, only diffusion-impregnated composite were studied.
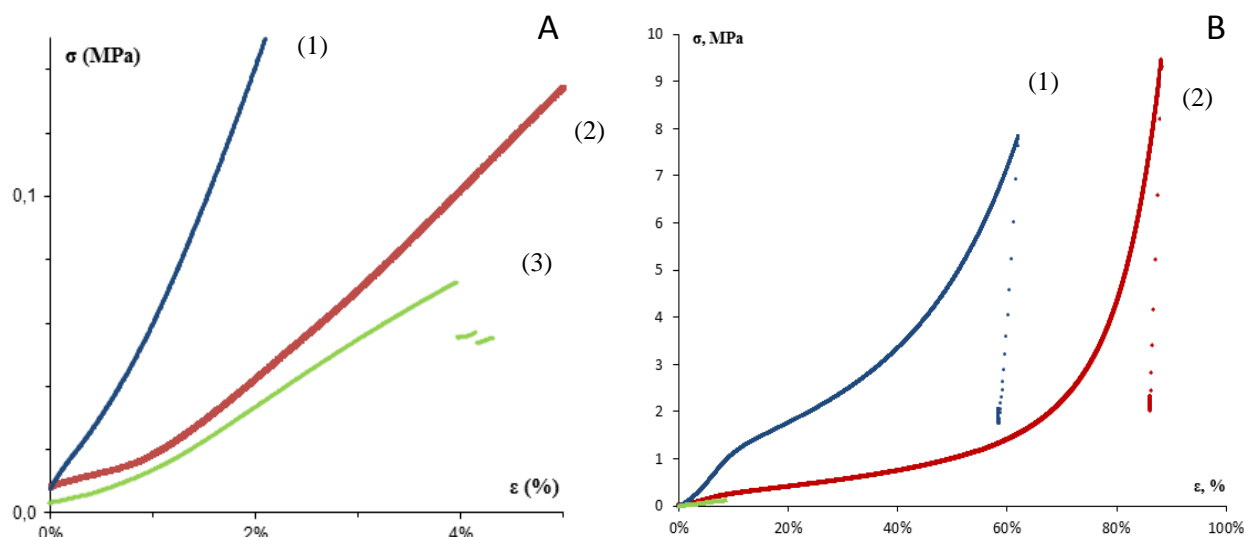


**Figure IV.10: Stress-strain uniaxial compression curves for cellulose-silica composite aerogels obtained via molecular diffusion impregnation (1), reference Aerocellulose (2) and silica (3) aerogels. Graph A is a zoom at low stresses and strains, while graph B shows the complete stress-strain curves until break.**

**Table IV.5: Young modulus (E), strain ($\varepsilon^*$) and stress ($\sigma^*$) at break for 3%wt aerocellulose from cellulose-EMIMAc solution, reference silica aerogel, and cellulose-silica composite aerogels.**

| Formulation | E, MPa | $\sigma^*$, MPa | $\varepsilon^*$, % |
|---|---|---|---|
| Aerocellulose | $2.8 \pm 0.47$ | $9.20 \pm 0.12$ | 80 |
| $SiO_2$ aerogel | $1.9 \pm 0.10$ | $0.07 \pm 0.007$ | 4 |
| Composite aerogel (via diffusion impregnation) | $11.5 \pm 1.11$ | $6.30 \pm 1.55$ | 60 |

Stress-strain curve for the reference Aerocellulose (figure IV.10, curve 1) is typical for bio-aerogels such as Aerocelluloses prepared from cellulose dissolved in aqueous 8%NaOH or in ionic liquid (Sescousse et al., 2007) or Aeropectins from pectin dissolved in acid medium (Rudaz et al., 2014). Three regions can be distinguished: linear regime at low strains, long plastic deformation region with pore walls bending and finally densification due to pore walls collapse.

Aerocellulose shows very high deformability, up to 70-80% strain, but does not recover its shape after being highly compressed. The reference silica aerogel is brittle, breaking at low strains of a few per cent, and with lower (as compared to Aerocellulose) values of fracture stress and Young modulus (table IV.5). According to a recent study of the mechanical properties of hydrophobic (silylated) silica aerogels from the same PEDS precursor (Wong et al. 2014), silica aerogels with densities between 0.1 and 0.2 g.cm$^{-3}$ show an elastic-like behavior deforming till 40% strain and partially "springing back" to their original shape when the stress is released. Their Young moduli were from $\approx$ 1 to 10 MPa and fracture stress from $\approx$ 0.02 to 2.5 MPa in this bulk density interval. Aerogel with densities above 0.2 g.cm$^{-3}$ were shown to exhibit a brittle behavior, while those with the densities lower than 0.1 g.cm$^{-3}$ were highly compressible. In our case, silica aerogels with bulk densities around 0.13 g.cm$^{-3}$ have Young modulus of around 2 MPa and fracture stress of 0.07 MPa, but broke at low strains and showed no measurable elastic recovery probably because no hydrophobisation was performed consistent with other observation done on similar formulations (Diascorn, 2014).

Cellulose-silica composite aerogel shows significantly improved Young modulus as compared to its reference counterparts, both Aerocellulose and silica aerogel (Figure 6, curve 1 and Table 1). With a mean value of Young modulus around E=11.5 MPa the composite is three-four times stiffer than each of reference materials with E = 2.8 and 1.8 MPa for Aerocellulose and silica aerogel, respectively. The composite aerogel can also withstand deformation up to 60% before break, which is similar to Aerocellulose and is ten times higher than what is obtained for the reference silica aerogel. One of the reasons of high Young modulus is composite higher density, 0.156 vs 0.123 and 0.130 g.cm$^{-3}$ as compared to each of reference aerogels, Aerocellulose and silica, respectively. However, even if considering that Young modulus is proportional to aerogel density in power ~ 3 (Ma et al., 2000), the increase in modulus is higher than what could be theoretically expected from density increase. Cellulose is clearly playing an important reinforcing role but more data (such as mechanical properties of individual cellulose strands) are needed to quantify this phenomenon. The synergy of cellulose-silica interpenetrated network provides stiff and ductile aerogel materials, despite at this stage there is no evidence of chemical interaction between the two components, as suggested by FTIR spectra (see part 2.1.1)

### 2.2.4 Thermal conductivity

Silica aerogels are known to be amazing thermal superinsulating materials in room conditions, as also obtained in this work, see Table 1: $\lambda_{20°C}$ = 0.015 W.m$^{-1}$.K$^{-1}$. The main reason for a low-density porous material to fall into superinsulation region is air confinement in the pores of size below the free mean path of air molecule (Knudsen effect); at atmospheric conditions it is around 70 nm. Mesoporous and light-weight silica aerogels satisfy these conditions. Here the conductivities of reference silica aerogels are compared to those of pure Aerocellulose and cellulose-silica composites made from impregnation and forced-flow processes. All tested

samples were obtained from 3%wt cellulose in EMIMAc-DMSO. The thermal conductivities were measured with heat flow meter apparatus in PERSEE/MINES ParisTech, as described in materials and methods section.

**Table IV.6 : Bulk densities and thermal conductivities in ambient conditions of reference Aerocellulose, reference silica aerogel, and diffusion and forced flow cellulose-silica composites obtained from cellulose 3%wt in EMIMAc**

| Formulation | $\rho_{bulk}$, g/cm$^3$ | $\lambda_{25°C}$ (W.m$^{-1}$.K$^{-1}$) |
|---|---|---|
| Aerocellulose | 0.123 | 0.033 |
| SiO$_2$ aerogel | 0.130 | 0.015 |
| Composite aerogels via diffusion impregnation | 0.225 | 0.026 |
| Composite aerogel via forced-flow impregnation | 0.156 | 0.028 |

Aerocellulose also has low bulk density, but the presence of numerous large macropores, as seen on figure IV.8.a, results in relatively high thermal conductivity values, 0.033 W.m$^{-1}$.K$^{-1}$ in room conditions. In composite cellulose-silica aerogels, superinsulating silica aerogel is filling Aerocellulose pores in general and macropores in particular: thermal conductivity is thus decreased to $0.027 \pm 0.001$ W.m$^{-1}$.K$^{-1}$ but remains rather high because notable increase in density. This result demonstrates the feasibility of decreasing thermal conductivity by "incorporating" a superinsulating silica aerogel into cellulose matrix. The thermal superinsulation level, i.e. a thermal conductivity below that of air (0.025 W.m$^{-1}$.K$^{-1}$) is not achieved yet for the present composites. Possible complementary reasons are the presence of some remaining macropores not filled with silica aerogel phase; however these macropores could not be detected precisely through BJH analysis because this method detects pores under 200 nm diameter. The conditions in which the silica aerogel phase was formed, within the pores of the coagulated cellulose, can possibly also affect the thermal properties of the silica phase. Slight modifications in the formulation of silica, such as varying water-to-PEDS or catalyst-to-PEDS molar ratios, could be investigated in future in order to optimize the thermal conductivity of the silica phase. The presence of -OH groups on the surface of cellulose strands should also be taken into consideration as a potential source of "perturbation" of silica gelation.

## Conclusion

This part dealt with the preparation of cellulose-silica composite aerogel by "impregnation" technique. A 3%wt cellulose was dissolved in EMIMAc-DMSO, coagulated in ethanol and used as the cellulose matrix. A solution of polyethoxysiloxane (PEDS) in ethanol was used as the silica precursor. Strong, light (bulk density around 0.2 $g.cm^{-3}$) and monolithic crack-free cellulose-silica composite aerogels have been prepared by impregnation of wet coagulated cellulose with PEDS solution, followed by immersion of the impregnated sample in a water/ethanol $NH_4OH$ catalyst solution, silica gelation, solvent exchange, and supercritical $CO_2$ drying.

Two impregnation routes were performed: either by molecular diffusion or by a forced flow process where the silica sol was forced to penetrate inside the cellulose matrix due to a pressure difference. Energy diffractive spectroscopy and SEM analysis were performed to compare silica spatial distribution in both series of samples. Forced flow impregnation method significantly reduced processing times as compared to impregnation driven by simple molecular diffusion: impregnation times were reduced from ~ 7 hours to less than 30 minutes for a sample with the same geometry. The morphology of diffusion impregnated and forced-flow impregnated samples was similar: cellulose matrix was filled with nanostructured silica.

BET analysis confirmed the formation of nanostructured silica inside cellulose matrix: specific surface area increased from $\approx$ 300 $m^2.g^{-1}$ for Aerocellulose to 750-800 $m^2.g^{-1}$ for silica-impregnated composites. The thermal conductivity in room conditions was reduced from 0.033 $W.m^{-1}.K^{-1}$ for aerocellulose to 0.027 $W.m^{-1}.K^{-1}$ $\pm$ 0.001 for composite aerogels due to the superinsulating properties of silica aerogel itself, demonstrating that the concept of impregnation for decreasing the total thermal conductivity of a porous matrix with large macropores works. Finally, composite aerogels were strongly reinforced as compared with the reference aerogels still keeping high ductility characteristic to Aerocellulose: Young modulus of composite aerogel increased in 3-4 times as compared to pure silica aerogel, and fracture strain remained very high, about 60% for the composite against 4-10% for reference silica aerogels showing that the concept of using cellulosic matrix to reinforce silica aerogels works as well.

# References

Achard P., Bisson A., Bonnardel P., De Candido M., Florent P., Pouleyrn G., Rigacci A., Procédé d'élaboration de xérogels de silice hydrophobes, Brevet FR 2 873 677 (17/08/2007)

Ayral, A., Phalippou J., Woignier,T. (1992); Skeletal density of silica aerogels determined by helium pycnometry, *Journal of Materials Science*, 27, 1166-1170.

Bisson, A; Rigacci, A; Lecomte, D; et al. (2004), Effective thermal conductivity of divided silica xerogel beds, *J. of Non-Cryst Solids*, 350, 379-384

Diascorn, N., PhD thesis, MinesParisTech, 2014.

Gavillon R., Budtova T. (2007); Kinetics of Cellulose Regeneration from Cellulose-NaOH-Water Gels and Comparison with Cellulose-N-Methylmorpholine-N-Oxide-Water Solutions; *Biomacromolecules*, 8, 424-432.

Ma, H. S., Roberts, A. P., Prévost, J. H., Jullien, R., & Scherer, G. W. (2000). Mechanical structure–property relationship of aerogels. *Journal of non-crystalline solids*, *277*(2), 127-141.

Pierre A.C, Rigacci A., "Silica aerogels" in Aerogels Handbook, M.A. Aegerter, N. Leventis, M. Koebel (Eds), Springer (2011).

Reichenauer, G., & Scherer, G. W. (2001). Nitrogen sorption in aerogels. *Journal of non-crystalline solids*, *285*(1), 167-174.

Sescousse, R., Gavillon, R., Budtova,T. (2011); Aerocellulose from cellulose–ionic liquid solutions: Preparation, properties and comparison with cellulose–NaOH and cellulose–NMMO routes. *Carbohydrate Polymers*, 83 1766–1774.

Wong, J. C., Kaymak, H., Brunner, S., & Koebel, M. M. (2014). Mechanical properties of monolithic silica aerogels made from polyethoxydisiloxanes. *Microporous and Mesoporous Materials*, *183*, 23-29

# Chapter V:
# Hydrophobic cellulose-silica composite aerogels and xerogels.

## Introduction

In the previous chapter we showed that the approach of introducing superinsulating silica phase in the pores of cellulose matrix allows and a significant improve of the mechanical properties and decreasing thermal conductivity as compared to pure cellulose as compared to silica aerogels. However, Cellulose-silica composites described in the previous chapter are highly hydrophilic, as cellulose and silica phase bear hydroxyl and silanol groups, respectively, which are responsible for the high water sensitivity of the materials. Water adsorption in aerogels may lead to pores collapse, apparition of cracks, densification and loss of thermal and mechanical properties. An application of aerogels for superinsulation in the building industry requires aerogels to be resistant to ambient humidity so that they keep their thermal properties over long periods of time.

To decrease cellulose hydrophilicity it has to be chemically modified. This was done by functionalizing cellulose with triphenylmethylchloride, allowing to graft very hydrophobic triphenyl (abbreviated trityl) groups on cellulose chains. We called the modified cellulose "tritylcellulose". After the chemical modification of cellulose, dissolution of the tritylcellulose in dimethylformamide (DMF), followed by coagulation in a non-solvent and supercritical drying allows to obtain tritylcellulose aerogels.

As seen on chapter IV, impregnation of a cellulose matrix with PEDS allows to make cellulose-silica composites with decreased thermal conductivity. The same approach was taken with tritylcellulose gels to make tritylcellulose-silica composites: coagulated tritylcellulose was impregnated with polyethoxisiloxane, and silica gel was formed with basic catalysis inside the pores of the tritylcellulose matrix. Hexamethyldisilazane (HMDZ) treatment was performed to hydrophobize the silica phase. Supercritical $CO_2$ drying gives composite tritylcellulose-silica aerogels.

Another improvement that can be performed is the process of aerogels preparation. The supercritical $CO_2$ drying process is time and energy consuming. For silica-based aerogels a successful alternative route was developed: pores surface of a wet gel is chemically modified by silylation. In this case subcritical drying in conditions close to ambient does not lead to dramatic pore collapse responsible for high densification. Such an ambient-pressure drying results in materials historically called "xerogels" and currently named "ambient-dried aerogels" as far as their structure and properties are very similar to their aerogel counterparts. The route of silica hydrophobisation for making xerogels was taken as an example for making cellulose xerogels from tritylcellulose.

The morphology and bulk density, of tritylcellulose and tritylcellulose-silica composite aerogels and xerogels will be studied in details. A viscosimetric study will be performed on tritylcellulose-DMF solutions to compare its properties with common cellulose solutions.

We will study the mechanical properties of hydrophobized aerogels and composite aerogels by uniaxial compression measurements. The thermal properties of the aerogels will be studied by hot wire method.

The hydrophobic nature of the composites, as compared to untreated hydrophilic reference materials, will be studied through water contact angle measurements, an accelerated aging test

for two days at 30°C and 80% relative humidity, and long-term aging tests in an humid environment over 45 days.

Finally, we will examine the morphology, bulk density, apparent porosity and hydrophobic properties of tritylcellulose xerogels and tritylcellulose-silica composite xerogels; the possibility of elaborating fully hydrophobic xerogels of low density from cellulose-silica composites will be discussed.

## Introduction

Dans le chapitre précèdent, nous avons montré que la génération d'une phase de silice superisolante au sein d'une matrice cellulosique poreuse permet une diminution sensible de la conductivité thermique du composite par rapport à la conductivité de l'Aérocellulose pure. Le composite ainsi élaboré présente également une amélioration significative des propriétés mécaniques par rapport aux aérogels de silice de référence. Cependant, ces composites cellulose-silice sont très hydrophiles, les phases cellulose et silice portant respectivement des groupements hydroxyl et silanols en grandes quantités. Ces groupements sont responsables de la forte sensibilité à l'eau de ces matériaux. L'adsorption d'eau par les aérogels peut conduire après condensation à un effondrement des pores, à l'apparition de fissures, et à une perte des propriétés mécaniques et thermiques. L'application des aérogels à l'industrie de la superisolation pour le bâtiment comme nombre d'autres applications nécessite des matériaux résistants à l'humidité et pouvant ainsi conserver leurs propriétés thermo-mécaniques avec le temps.

Pour diminuer l'hydrophilie de la cellulose, il est nécessaire de la modifier chimiquement. Dans ce chapitre nous avons fonctionnalisé la cellulose avec le triphenylmethylchloride, par une réaction d'étherification permettant de greffer aux chaînes de cellulose des groupements triphenyl (abrégé *trityl*) très hydrophobes. La cellulose ainsi modifiée est appelée « tritylcellulose ». Après cette modification chimique de la cellulose, la tritylcellulose peut être dissoute dans le dimethylformamide (DMF), coagulée dans un non solvant puis séché en conditions supercritiques, ce qui permet d'obtenir des aérogels de tritylcellulose.

Comme nous l'avons vu au chapitre IV, l'imprégnation d'une matrice cellulosique avec un polyethoxydisiloxane permet d'élaborer des composites à la conductivité thermique réduite. La même approche a été envisagée avec les gels de tritylcellulose pour élaborer des composites tritylcellulose-silice : une matrice de tritylcellulose coagulée a été imprégnée par le PEDS de cette étude, et le gel de silice a été formé en catalyse basique dans les pores de la matrice de tritylcellulose lors d'une seconde étape. Un traitement à l'hexaméthyldisilazane (HMDZ) a été réalisé afin d'hydrophobiser la phase silice. Le séchage au $CO_2$ supercritique de ces gels permet d'obtenir des aérogels composites tritylcellulose-silice.

Une autre amélioration rendue possible par l'hydrophobisation des gels se trouve au niveau du procédé d'élaboration. Le séchage au $CO_2$ supercritique est connu pour être long et consommateur en énergie. Pour les aérogels de silice, la sylilation de la surface des pores permet un séchage à pression atmosphérique sans effondrement de la structure poreuse ou densification. Les matériaux ainsi obtenus sont appelés « xérogels » ou « aérogels séchés à pression ambiante » ; ils possèdent des propriétés proches de celles des aérogels séchés en conditions supercritiques. L'élaboration de xérogels de cellulose à partir de tritylcellulose et de composites tritylcellulose-silice sera ainsi réalisée.

La morphologie et la densité des aerogels de tritylcellulose et leurs composites avec la silice sera étudiée en détails. Une étude viscosimétrique des solutions de tritylcellulose dans le DMF a été réalisée afin de comparer les propriétés de cette solution à celles de la cellulose pure.

Ensuite nous étudierons les propriétés mécaniques des aérogels et aérogels composites hydrophobisés par des mesures en compression uniaxiale. Leurs conductivités thermiques seront également étudiées par la méthode du fil chaud.

L'hydrophobicité des composites, par comparaison à des matériaux non traités et hydrophiles sera étudiée par mesure de l'angle de contact avec l'eau, test de vieillissement accéléré durant deux jours à 80% d'humidité relative et 30°C, et test de vieillissement « long », *i.e.* durant 45 jours en environnement humide contrôlé.

Enfin, nous examinerons la morphologie, la densité, la porosité et les propriétés hydrophobes des xérogels à base de tritylcellulose et de composites tritylcellulose-silice ; la possibilité d'élaborer des xérogels composites à base de cellulose et de silice, entièrement hydrophobés et de basse densité sera discutée.

# 1. Principle of synthesizing hydrophobic organic-inorganic composite aerogels

## 1.1. Hydrophobisation of cellulose and silica phases

### 1.1.1. Principle of grafting tritylchloride on cellulose

Cellulose sensitivity to humidity is detrimental to the properties of the cellulose and cellulose-silica composite aerogels described in chapter IV. For example, after two month storage in ambient temperature and humidity, specific surface area of untreated cellulose-silica composite made from 3%wt cellulose solution in EMIMAc-DMSO impregnated with silica decreased from 650-700 $m^2.g^{-1}$ to 470 $m^2.g^{-1}$. The aged composites strongly contracted over the same two month period, resulting in a density increase of 80%. The thermal conductivity of cellulose-silica composites exposed to ambient humidity also increased with time. These strong aging effects are due to cellulose hydrophilicity. Water from air humidity gets adsorbed at the surface of cellulose fibers. In porous cellulosic materials as well as aerogels in general, this can create capillary stresses among the pore walls if condensation occurs, leading to pores collapse and ultimately sample contraction. To prevent such detrimental humidity adsorption by cellulose and subsequent degradation of cellulose aerogels properties with time, hydrophobization of cellulose must be performed. Moreover, hydrophobization of cellulose may allow to avoid an energy-consuming supercritical drying, and to obtain monolithic and ultraporous xerogels via ambient pressure drying.

To obtain hydrophobic cellulose, a homogeneous etherification reaction with triphenylmethylchloride (abridged *tritylchloride* in the following) (figure V.1) described in the literature was chosen (Camacho Gomez et al., 1996). The preparation of the modified cellulose was performed as described in details in Materials and methods section (Pour et al., 2015). The resulting material was called tritylcellulose.
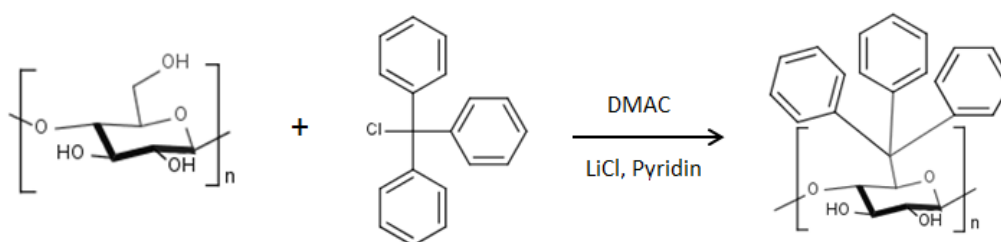


**Figure V.1: Reaction scheme of the modification of cellulose with tritylchloride**

The tritylcellulose powder was then dissolved in DMF, and coagulated in methanol. Wet coagulated tritylcellulose was obtained after several washings in ethanol. Supercritical $CO_2$ drying leads to tritylcellulose aerogels.

### 1.1.2. Degree of substitution of tritylcellulose

The degree of substitution (noted DS in the following) is the mean number of trityl groups per anhydroglucose unit. As each AGU contains three –OH groups available for etherification, the maximum DS value correspond to the substitution of every hydroxyl on the cellulose backbone, i.e. $DS_{max} = 3$. However, triphenylmethyl is a large functional group: because of sterical hindrance, the substitution of the –OH group on $C_6$ is favored, as this is the most easily available hydroxyl group on AGU (Camacho Gomez et al., 1996). DS values for tritylcellulose were

determined through elemental analysis of carbon. The mass percentage of carbon, *C%,* measured in the sample is given by equation (V.1), M being the molar mass of the repeating unit and $N_C$ the total number of carbon atoms in the sample:

$$C\% = \frac{12 \times N_C}{M_{tritylcellulose}} \tag{V.1}$$

An AGU unit contains 6 carbon atoms and its molecular weight is $M_{AGU} = 162$ g.mol$^{-1}$. The trityl group contains 19 carbon atoms, for a molar mass of $M_{Trityl} = 242$ g/mol. We have :

$$N_c = 6 + DS \times 19 \tag{V.2}$$

$$M_{tritylcellulose} = M_{AGU} + DS \times M_{trityl} = 162 + DS * 242 \tag{V.3}$$

Then:

$$C\% = \frac{12 \times (6 + DS \times 19)}{162 + DS \times 242} \tag{V.4}$$

$$C\% = \frac{72 + 228DS}{162 + 242DS} \tag{V.5}$$

$$DS = \frac{72 - 162 * C\%}{242 * C\% - 228} \tag{V.6}$$

Elemental analysis was performed over 4 batches prepared in the same proportions of 3 molar equivalent of tritylchloride per glucose unit. This formulation was used as the basis of all materials used in the present chapter. An average degree of substitution DS = 0.62 was obtained.

### 1.1.3. Preparation of tritylcellulose matrix

Tritylcellulose dissolution-coagulation procedure is described in details in materials and methods section. Before coagulation, the solution was poured into the appropriate molds, usually discs of 4 cm diameter and 1 cm thickness. For mechanical characterization, the shape was cylinders with a length/diameter ratio of 3/2. The preparation processes of aero- and xerogel from tritylcellulose (and composites with silica) is schematized in figure V.2.
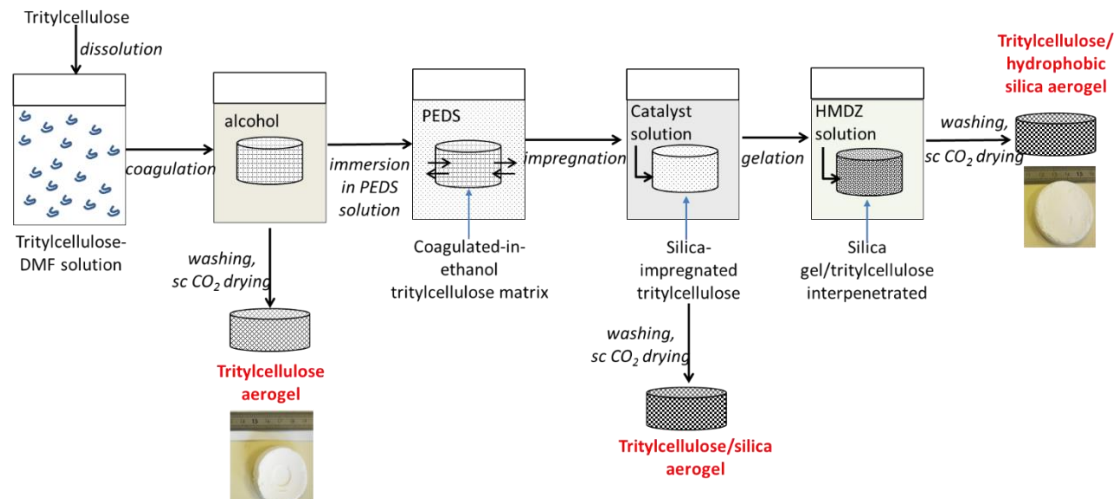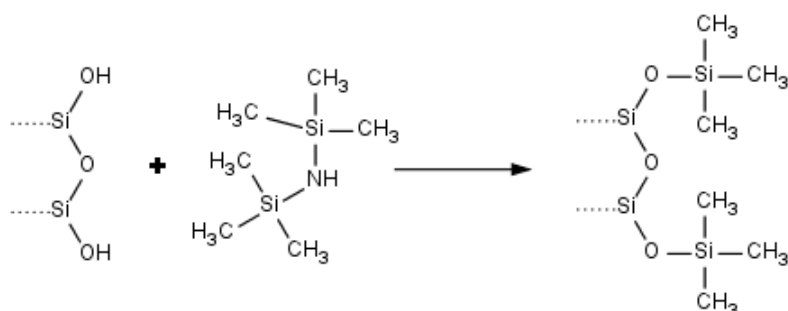


**Figure V.2: Schematic presentation of synthesis of tritylcellulose and tritylcellulose-silica aerogels.**

To obtain composite aerogels the impregnation was performed as follows: cellulosic alcogels were immersed first in 16 wt% PEDS ($m_{PEDS\ solution} = m_{alcogel}$) for 24h and then in $NH_4OH$ catalyst solution (1.3 wt% in ethanol-water 95/5 wt/wt) for another 24 h to form *in situ* silica gel inside the pores of coagulated tritylcellulose. These samples were either dried with supercritical $CO_2$, and named "tritylcellylose-silica composite aerogel", or silica phase was hydrophobised before drying with HMDZ (as described below for the reference silica aerogels) and named "tritylcellulose-hydrophobic silica aerogel composite" (Figure V.2). All samples were washed in ethanol before drying to remove non-reacted chemicals.

### 1.1.4. Hydrophobization of the silica phase

Silica aerogels contains many –OH surface groups that are responsible for humidity adsorption and degradation of insulating and mechanical properties. In the objective of making fully hydrophobic cellulose-silica composites, the silica phase must be hydrophobized as well as the cellulose phase. In chapter I we described several examples of synthesis methods aiming to turn the hydrophilic Si-OH groups on silica aerogels surface into hydrophobic $Si(CH_3)_3$ groups. In our tritylcellulose-silica composite route, silica is formed directly inside cellulose porosity. Thus hydrophobization of the silica phase was performed in situ after silica gel formation. Hexamethyldisilazane (HMDZ) is a compound that is now often used for surface modification of silica gels (Rao et al., 2004; Shewale et al, 2008), to prepare hydrophobic aerogels or xerogels. The reaction of HMDZ on silica is schematized on (figure V.3).



**Figure V.3: Schematic presentation of silica hydrophobisation with HMDZ**

The gels were immersed in HMDZ solution for 16h at 60°C, washed in ethanol and stored in this solvent until drying. The quantity of HMDZ was calculated to be 35%wt relative to the theoretical maximal weight of silica. HMDZ-treated gels were dried in supercritical $CO_2$ to obtain composite aerogels, or overnight at 60 °C in a laboratory oven to obtain composite xerogels.

## 1.2. Determination of intrinsic viscosity of tritylcellulose in DMF

Intrinsic viscosity is an important property of dissolved polymer, directly related to the molecule gyration radius and is thus an indicator of the solvent thermodynamic quality. Capillary viscosimetric studies were performed on tritylcellulose-DMF solutions. The usual method for the determination of intrinsic viscosity was applied as follows: the flow time through a capillary viscosimeter was measured. At low values of polymer concentration, the solvent viscosity $\eta_0$ and solution viscosity $\eta$ are directly related to the flow time t by a constant directly depending on the capillary diameter. The intrinsic viscosity is defined by equation 7:

$$[\eta] = \lim_{C \to 0} \frac{\eta_{spe}}{C} = \lim_{C \to 0} \eta_{reduced} \qquad (V.7)$$

where C is polymer concentration, and $\eta_{spe}$ the specific viscosity defined by (eq. 8):

$$\eta_{spe} = \frac{\eta}{\eta_0} - 1 \qquad (V.8)$$

The intrinsic viscosity was determined at different temperatures at the y-intercept coordinate of the $\eta_{reduced}= f(C)$ curve (Figure V.4).
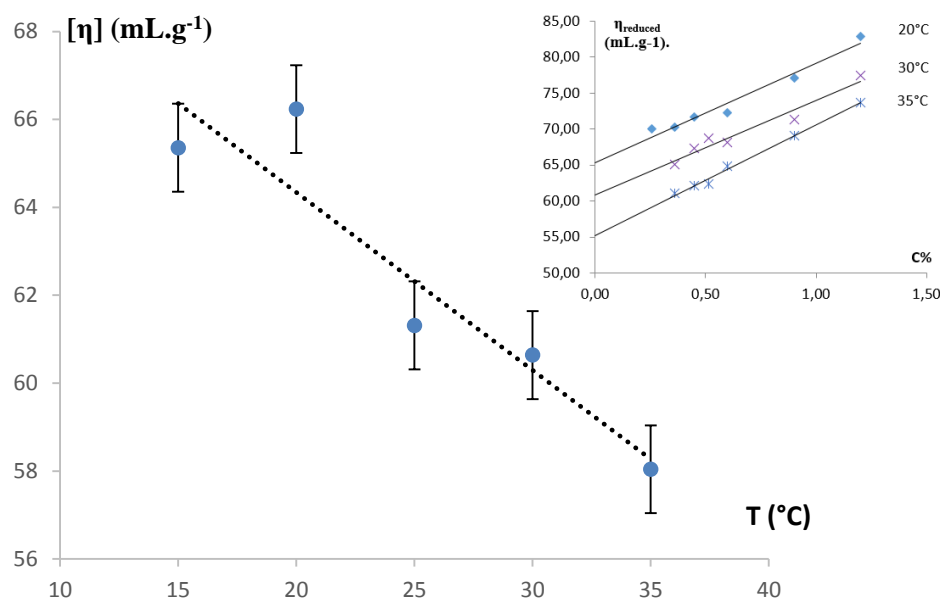


**Figure V.4 : Intrinsic viscosity of tritylcellulose in DMF as a function of temperature. Inset : determination of intrinsic viscosity at three different temperatures**

The intrinsic viscosity of tritylcellulose dissolved in DMF decreases when temperature increases. This is indicative of a lowering of the thermodynamic quality of the solvent with temperature. A similar phenomenon was observed for cellulose dissolved in NaOH solutions (Roy, 2003) and in ionic liquid solutions (Sescousse, 2010). In the case of cellulose-NaOH systems at higher concentrations the lowering of the solvent quality is accompanied by a micro-phase separation leading to gelation. Tritylcellulose-DMF solution does not gel with increasing temperature or over time.

# 2. Properties of tritylcellulose and tritylcellulose-silica composite aerogels

## 2.1. Structure and density of aerogels

### 2.1.1. Chemical composition of tritylcellulose-silica composites

FTIR spectra for tritylcellulose-silica composites, treated or not with HMDZ, are compared with spectra for non-modified Aerocellulose and pure tritylcellulose on figure V.6. The spectra for tritylcellulose, (figure V.6.a and V.6.b) show a flattened –OH peak at 3342 cm$^{-1}$ as compared to pure aerocellulose from microcrystalline cellulose Avicel. This is due to the substitution of –OH groups of cellulose by tritylchloride. Peaks at 3062cm$^{-1}$ and 1490 cm$^{-1}$ on tritylcellulose

spectra (fig V.5 b, c, d and table V.1) are attributed to aromatic double bonds. Si-O-Si peaks around 1000 cm$^{-1}$, and 800 cm$^{-1}$ are observed for silica-impregnated tritylcellulose (fig V.5 c and 1d). The 1000 cm$^{-1}$ peak is particularly intense, and is overlapping with the ether peaks for cellulose in the same region. Two additional peaks on the FTIR spectrum for HMDZ-treated sample (fig. V.5 d) are visible: one at 2980 cm$^{-1}$, corresponding to -CH$_3$ ; and 849 cm$^{-1}$, corresponds to Si-C bonds from HMDZ (Shewale and Rao, 2008). The detailed identification of the main FTIR peaks is presented in table V.1.
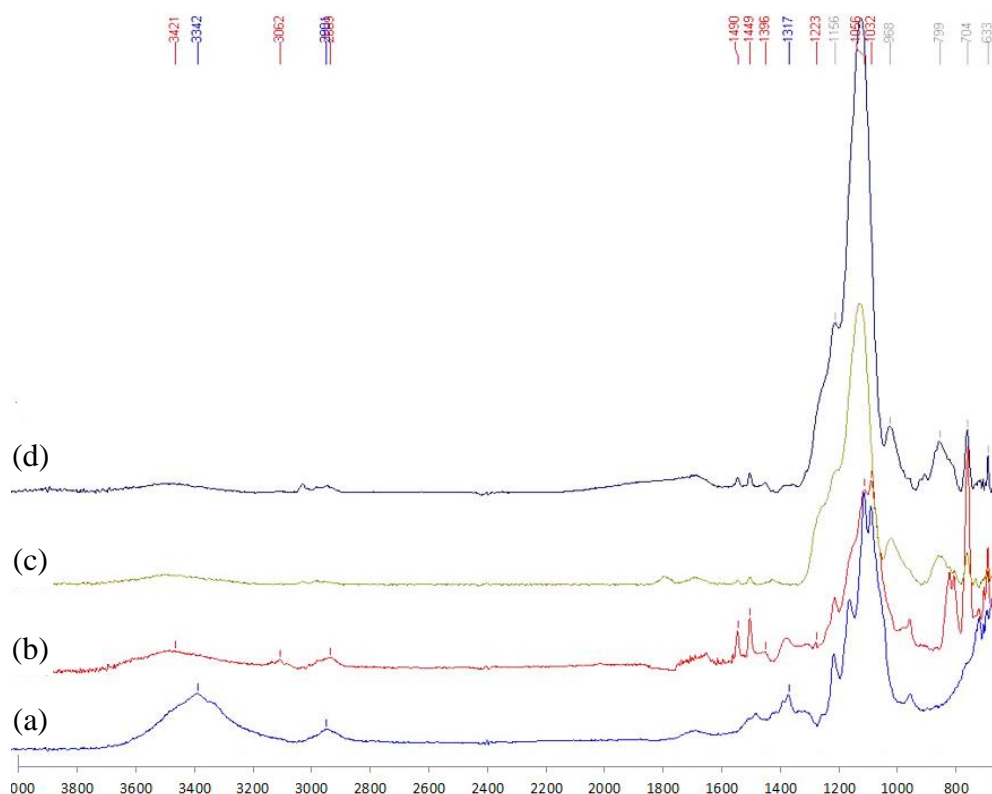


**Figure V.5 : FTIR spectra of (a) aerocellulose from avicel 5%wt in NaOH (b) aero-tritylcellulose from 5%wt solution in DMF (c) Silica-impregnated aero-tritylcellulose and (d) Silica-impregnated aero-tritylcellulose with HMDZ treatment.**

**Table V.1: FTIR peak attributions for reference Aerocellulose, aero-tritylcellulose, and tritylcellulose-silica composites aerogel.**

| Peak attribution | Aerocellulose (cm$^{-1}$) | Aero tritylcellulose (cm$^{-1}$) | Aerotritylcellulose +SiO$_2$ (cm$^{-1}$) | Aerotritylcellulose +SiO$_2$ + HMDZ (cm$^{-1}$) |
|---|---|---|---|---|
| ν OH | 3342 | 3428 | 3433 | 3431 |
| ν C=CH (aromatic) | - | 3062 | - | - |
| ν CH2 | - | 2930 | 2933 | 2930 |
| ν CH3 (HMDZ) | - | - | - | 2980 |
| ν CH2 | 2901 | 2889 | 2895 | 2897 |
| ν C-C=C (aromatic) | | 1490 | 1491 | 1491 |
| ν H-C-H | 1429 | 1449 | 1449 | 1449 |
| ν CO (ether) | 1107 | 1158 | 1152 | 1156 |
| ν Si-O-Si | - | - | ~1000 | ~1000 |
| ν Si-C | - | - | - | 849 |
| ν Si-O-Si | - | - | 802 | 799 |

The distribution of silica in the bulk of composite aerogels was evaluated by means of EDS spectroscopy on 4-5 mm thickness samples. The composition along sample internal cross-section was recorded every 100 µm. Figure V.6 shows a typical silicon repartition in tritylcellulose-silica (non hydrophobised) composite aerogel as a function of $l$, the distance from the sample surface. Mass percentage of silicon was calculated from the intensity of the silicon Kα peak at 1.71 keV and compared to mass percentage of silicon corresponding to a theoretical maximal value in the case of homogeneous impregnation (here for the case of composite aerogel prepared from 5wt% tritylcellulose solution impregnated by 8wt% PEDS solution).
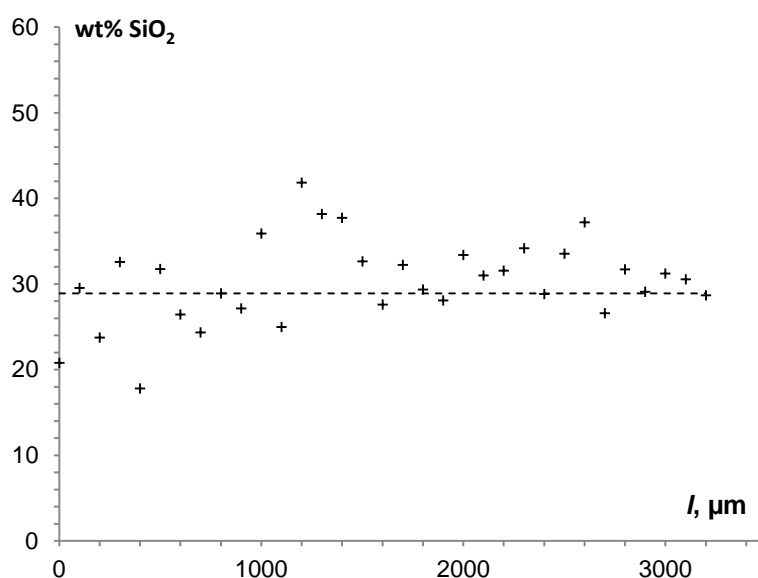


**Figure V.6 : EDS analysis of the silicon distribution along the internal cross-section of tritylcellulose-silica composite aerogel (non-hydrophobised) prepared from 5wt% tritylcellulose solution. Dashed line is theoretical maximal silicon mass percentage in the sample**

Silicon and thus silica is well distributed in the composite sample. A number of points on figure V.6 display silicon percentages above the expected theoretical maximal value for tritylcellulose-silica composites. The measured values of silicon concentration are overestimated, as EDS gives only a "local" composition on the studied surface. As far as the cellulosic network is covered by silica, the presence of cellulose is not detected by EDS, thus the spectra only accounts for the silica.

### 2.1.2. Morphology

Tritylcellulose aerogels are white, cohesive, monolithic solids (figure V.7). Surface irregularities can be observed on some samples, due to surface perturbation during coagulation or to the intrinsic form of the moulds. Tritylcellulose-silica composites have a similar external aspect as pure tritylcellulose aerogels. The composites seem to be more rigid than the pure tritylcellulose samples, for all concentrations.
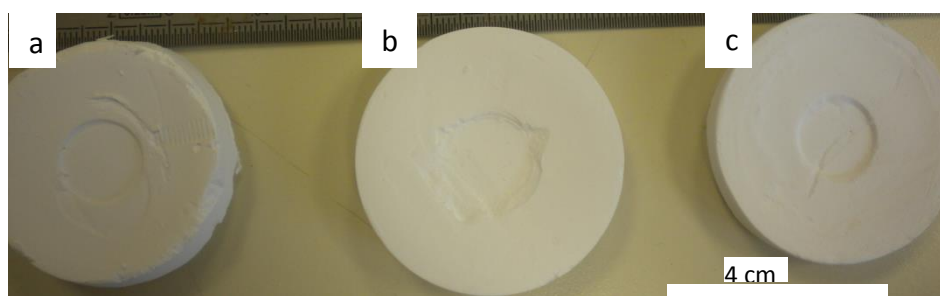
**Figure V.7 : Aerogels from (a) 5%wt tritylcellulose ; (b) 5%wt tritylcellulose-silica composite aerogel (c) tritylcellulose-silica composite treated with HMDZ.**

Figure V.9 (a-c) shows the representative morphologies of aerogels prepared from tritylcellulose, silica and tritylcellulose-silica (non-hydrophobised) composite, respectively, as seen by SEM. Tritylcellulose-silica composites hydrophobized with HMDZ present a similar aspect as non-hydrophobised samples.
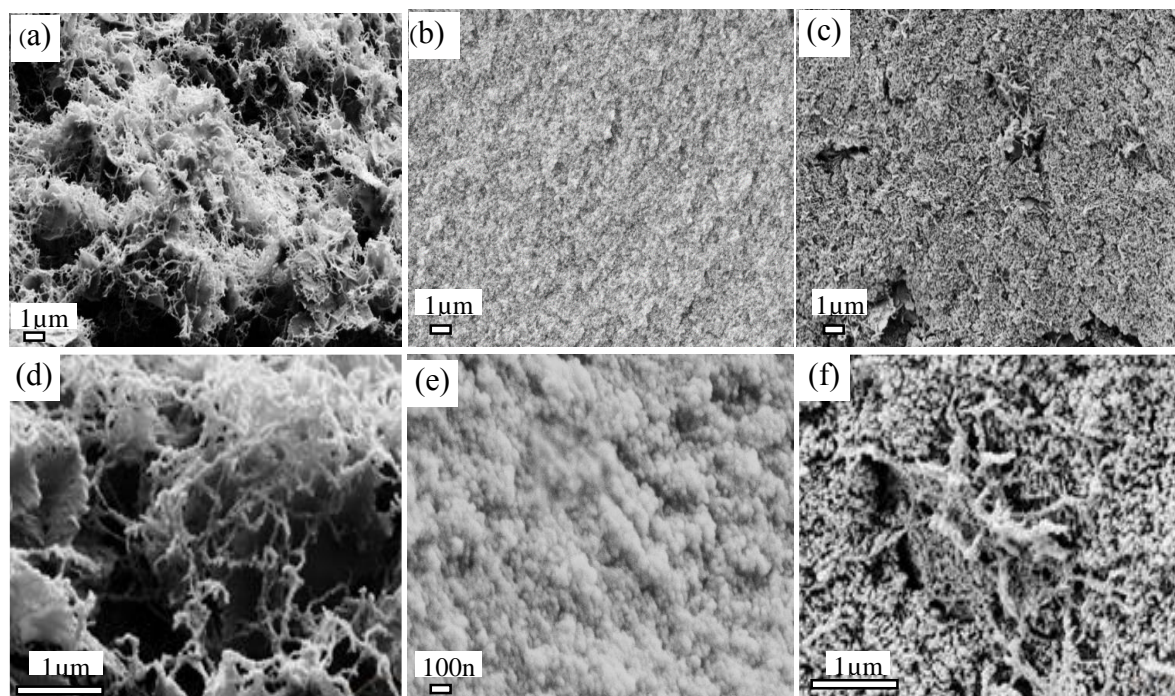


**Figure V.8: SEM micrographs of aerogels based on tritylcellulose (a, d), silica (b, e) and tritylcellulose-silica composite aerogel (c, f). The concentration of tritylcellulose in solution in (a), (d) and (c), (f) was 5wt%.**

Tritylcellulose aerogels morphology is a network of intertwined fibrils (Figure V.8.a,d). The porous network leave us consider a potential wide pore size distribution, pore diameter ranging from several tens of nanometers to several microns. This morphology is similar to that of Aerocellulose, obtained from unmodified cellulose dissolved, coagulated and dried with sc $CO_2$ (Gavillon 2008). Silica aerogel morphology (figure V.8.b) is a colloidal network formed of silica beads with no macropores observable by SEM. A nanostructured network formed of nanoparticles in the tens of nm with pores of a few nm is a common morphology for base-catalysed silica aerogels (Brinker and Scherer, 1990); however SEM pictures only are not enough to precisely quantify the particle sizes for our aerogels. Figure V.8.c shows the morphology of tritylcellulose-silica composite aerogel. Cellulosic network is coated by the silica phase; some cellulosic fibrils can be seen emerging from the silica network (fig V.8.f).

### 2.1.3. Bulk density and porosity

The densities of the reference Aerocellulose, and aerogels based on tritylcellulose and tritylcellulose-silica composites are summarized in table V.2. Porosity was calculated according to (equation V.10), considering the skeleton density of tritylcellulose to be roughly equal to that of cellulose (1.5 g.cm$^{-3}$) and the silica skeleton density to be 2.0 g.cm$^{-3}$ (Ayral, Phalippou and Woignier, 1992).

$$\varepsilon(\%) = \frac{V_{pores}}{V_{total}} = 1 - \frac{\rho_{bulk}}{\rho_{skeletal}} \qquad (V.10)$$

Tritylcellulose aerogels are ultra-light: their bulk densities are around 0.08 g.cm$^{-3}$ which is lower than that of the reference Aerocellulose. The volume contraction of 5%wt tritylcellulose and tritylcellulose-silica composite aerogels from wet to dry state is very low, 8.8% and 4.3% respectively, while non-modified cellulose sample is shrinking by about 40-50% (Sescousse and Budtova, 2009). Most of the shrinkage occurs during drying; it is known to depend on the chemical affinity of the gels with supercritical CO$_2$. Grafting trityl groups onto cellulose chains increases the cellulosic gel chemical affinity with SC CO$_2$ and thus the gels contract less upon drying. Lower volume contraction during drying results in lower densities in the final aerogels. Tritylcellulose-silica aerogel composites, with silica phase hydrophobised and not, are of higher densities (0.23-0.24 g.cm$^{-3}$) as the silica phase is added to the tritylcellulose network without significant macroscopic volume variation.

**Table V.2: Densities, specific surface areas and estimated porosities of a reference 5%wt cellulose aerogel, tritylcellulose aerogels and tritylcellulose-silica composite aerogels.**

| Aerogel Sample | Hydrophobization of silica | Cellulose concentration (wt%) | ρ g/cm³ | S$_{BET}$ (m²/g) | ε % |
|---|---|---|---|---|---|
| **Aerocellulose** | n/a | 5% | 0.15 | 210 | 90% |
| **Tritylcellulose** | n/a | 5% | 0.079 | 330 | 95% |
| **Tritylcellulose** | n/a | 7.5% | 0.080 | 250 | 95% |
| **Tritylcellulose-silica composite** | Non-hydrophobized | 5% | 0.244 | 850 | 87% |
| **Tritylcellulose-silica composite** | Hydrophobized with HMDZ | 5% | 0.232 | 750 | 87% |
| **Tritylcellulose-silica composite** | Hydrophobized with HMDZ | 7.5% | 0.240 | 610 | 87% |

Specific surface area of tritylcellulose aerogels is 200-300 m².g⁻¹, in line with what has been observed for other non-modified cellulose based aerogels (Sescousse et al., 2011; Liebner et al., 2009; Demilecamps et al., 2014). For the composite aerogels, the specific surface area is increased enormously, up to 600-850 m²/g, depending on tricylcellulose initial concentration as well as silylation of the silica backbone. The increase of specific surface area for tritylcellulose-silica composites can be considered a direct proof of the in-situ formation of finely nanostructured silica aerogel phase in the pores of tritylcellulose matrix.

## 2.2. Mechanical and thermal properties

### 2.2.1. Mechanical characterization

The uniaxial compression of cylindrical samples was used to assess the mechanical properties of aerogels; stress-strain cures are shown in Figure V.9. Aerogels from tritylcellulose and it composites were prepared from tritylcellulose solutions of 5, 7.5 and 10wt%, a reference non hydrophobised silica aerogel is also shown in the inset.
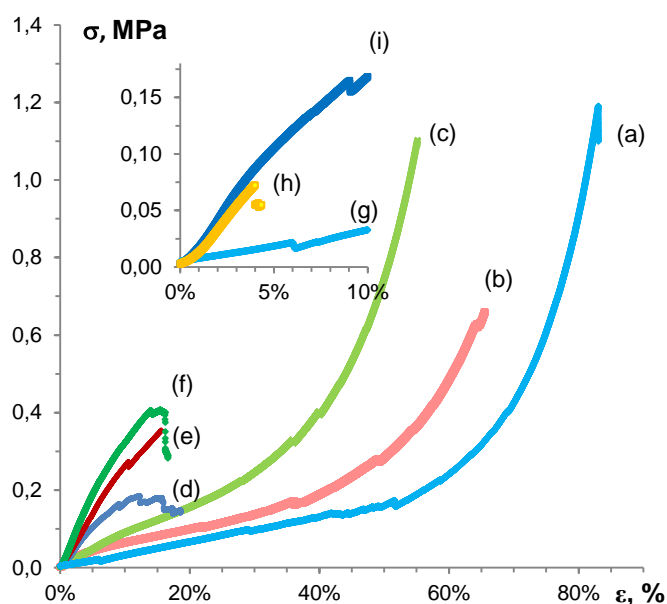


**Figure V.9: Stress-strain compression curves for aerogels from tritylcellulose solution of 5% (a), 7.5% (b) and 10% (c) and composite tritylcellulose-nonhydrophobised silica from the impregnated 5% (d), 7.5% (e) and 10% (f) tritylcellulose solution.**

**Inset: reference silica aerogel (g) and aerogels from 5% tritylcellulose solution (h) and its composite counterpart (i).**

No buckling and no diameter increase were observed during the whole compression experiment indicating that the Poisson ratio is close to zero. The same was reported for the Aerocellulose (Sescousse, 2011). Stress-strain curves of tritylcellulose aerogels are very similar to those of bio-aerogels, Aerocellulose (Sescousse, 2011) and Aeropectin (Rudaz, 2014) and can be divided in three regions: linear elastic region at low strains $\varepsilon < 10\%$ allowing determination of the Young modulus E; plastic deformation up to $\varepsilon \sim 40\text{-}60\%$ (depending on polymer concentration) and densification phase when the pore walls collapse under the pressure. At the end of plastic region small cracks appear on the surface of tritylcellulose aerogels leading to irregularities in the stress-strain curves. Young modulus increases with the increase of polymer concentration (Table V.3). Per analogy to reference polysaccharide aerogels, we can assume

that the variation of modulus with bulk density follows a power law (Gibson and Ashby, 1997); however, as the differences in bulk density between tritylcellulose of 5, 7.5 and 10% concentrations are small, there are not enough points to precisely determine the scaling exponent. Young modulus values for tritylcellulose aerogels are comparable with those of Aerocellulose of similar density (Sescousse, 2011).

**Table V.3: Young modulus E, maximal stress at break $\sigma_m$ and deformation at break $\varepsilon_m$ for the reference silica aerogel, tritylcellulose and tritycellulose-silica composite aerogels**

| Sample | Tritylcellulose concentration, wt% | $\rho$ g/cm$^3$ | E (MPa) | $\sigma_m$ (MPa) | $\varepsilon_m$ (%) |
|---|---|---|---|---|---|
| Reference silica aerogel | 0 | 0.130 | 1.9 | 0.07 | 4 |
| Tritylcellulose aerogel | 5 | 0,087 | 0.3 | 1.2 | 83 |
| | 7.5 | 0,100 | 1.0 | 0.7 | 64 |
| | 10 | 0,099 | 0.9 | 1.1 | 55 |
| Tritylcellulose-silica composite aerogel | 5 | 0,171 | 2.2 | 0.1 | 12 |
| | 7.5 | 0,182 | 2.7 | 0.2 | 11 |
| | 10 | 0,213 | 4.0 | 0.1 | 13 |

All tritylcellulose-silica composite aerogels have better mechanical characteristics as compared to the reference silica aerogel: composites are stiffer and have a larger plastic region with higher stress and deformation at break. As compared to tritylcellulose aerogels, composites are more than twice stiffer but more brittle: composite aerogels break at lower stresses and strains than tritylcellulose aerogels due to fragile silica phase. In overall, tritylcellulose fibrous network can act as a reinforcing "skeleton" for silica aerogels just as Aerocellulose studied in chapter IV.

## 2.3. Hydrophobicity of tritylcellulose and tritycellulose-silica composite aerogels

### 2.3.1. Water uptake and contact angle with water

The hydrophobic properties of Aerocellulose, tritylcellulose aerogels and tritylcellulose-silica composite aerogels were assessed by water contact angle measurements (table V.5). An aging study of the samples was also performed for 30 h at 30°C and 80% humidity rate, to study the kinetics of water vapour uptake by measuring the variation of sample mass and volume over time. The mass uptake $H_m$ and volume contraction $H_v$ were determined according to equations II.15 and II.16 respectively, described in materials and methods section. The mass uptake values at equilibrium are reported in Table V.4.

Due to the hydrophilicity of native cellulose, water contact angle values for Aerocellulose could not be measured, as the droplet was absorbed immediately when placed on the surface of Aerocellulose. The same happens for untreated silica aerogels and tritylcellulose-nonhydrophobised silica hybrid aerogel. Without hydrophobisation treatment, the native silica network is covered by silanols groups ($\sim$ 3-5 [OH]/nm²) (Iler, 1979) which are hydrophilic species. In the case of the composite, silica phase represents the majority of hybrid material filling the pores of tritylcellulose and covering cellulosic network. Tritylcellulose aerogels are highly hydrophobic, as shown by the contact angle with water around 125°. Even higher surface hydrophobicity is reached when silica phase is HMDZ-treated in composite aerogels: the contact angle is 133°.

**TableV.4: Contact angle with water $\theta_{H2O}$, mass uptake at equilibrium $H_m$ and corresponding volume loss $H_v$ when submitted for 24h to 30°C and 80% RH for the reference Aerocellulose, tritylcellulose and composite aerogels.**

| Aerogel Sample | Cellulose concentration (%wt) | HMDZ treatment | $\theta_{H2O}$ | $H_m$ % | $H_v$ % |
|---|---|---|---|---|---|
| Aerocellulose | 5% | no | drop absorbed immediately | 13.5 | > 70 |
| Silica reference | - | no | drop absorbed immediately | 22 | - |
| Silica reference | - | yes | 135° | 1 | < 1 |
| Tritylcellulose aerogel | 5% | no | 125° | 2.3 | 6.6 |
| Tritylcellulose aerogel | 7.5% | no | 125° | 1.6 | 3.5 |
| Composite aerogel | 5% | no | drop absorbed | 6.4 | 18.6 |
| Composite aerogel | 5% | yes | 133° | 3.5 | 1.9 |
| Composite aerogel | 7.5% | yes | 133° | 1.6 | 0.5 |

Figure V.10 shows the mass increase of the aerogels over time from the "dry" state (24 h at 20% RH) to "humid" state at 30°C and 80% relative humidity. The mass of hydrophilic samples (untreated Aerocellulose and tritylcellulose impregnated with untreated silica) increases as water is adsorbed inside the sample. Hydrophilic aerogels, Aerocellulose and its untreated

composite with silica, reach the equilibrium $H_m$ and $H_v$ in about 30 hours. The mass of hydrophobic samples (tritylcellulose and tritylcellulose impregnated with silica and treated with HMDZ) increases by 1 to 3% in 1 – 1.5 hours, after what they become stable in mass and volume.
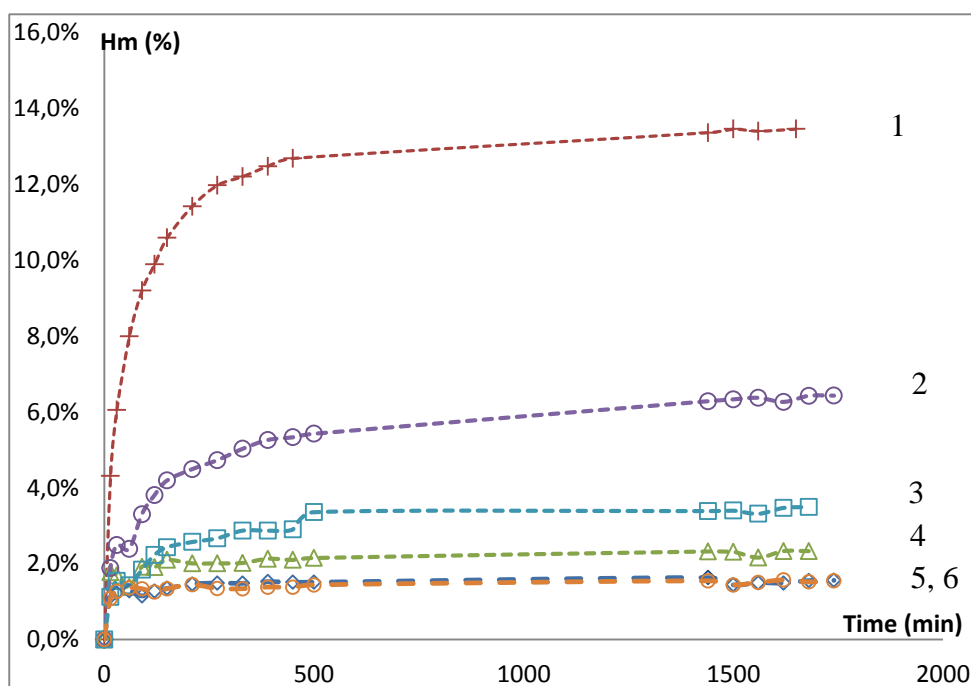


**Figure V.10 : Kinetics of water vapour uptake at 30°C and 80%RH, expressed in wt% for the following aerogels: (1) reference 5%wt Aerocellulose, (2) 5wt% tritylcellulose-silica composite with non hydrophobised silica; (3) 5wt% tritylcellulose-silica composite with HMDZ-treated silica, (4) 5wt% tritylcellulose , (5) 7.5%wt tritylcellulose; and (6) 7.5%wt tritylcellulose-silica composite treated with HMDZ (6).**

Reference Aerocellulose exhibits spectacular volume shrinkage, more than 70%, even though the mass uptake is only around 13%. In humid conditions pores are contracting. The aerogel prepared from 5%wt tritylcellulose solution adsorbs much less humidity: 2.33% in mass and "loses" only 6.6% of its initial volume; lower values were obtained for the aerogel from 7.5wt% tritylcellulose ($H_m$ = 1.6 % and $H_v$ = 3.5%). Hydrophobized silica aerogels adsorbs less than 1% in weight and barely shrink at all, while untreated silica can absorbs up to 20% of its own weight in water. Instead of shrinking, untreated silica gels tend to fracture into small irregular parts when submitted to such humidity levels. The very slightly higher sensitivity to water vapors of tritylcellulose aerogels as compared to fully hydrophobic silica can be explained by the presence of non-substituted groups on anhydroglucose unit. The volume stability of tritylcellulose-silica aerogels treated with HMDZ is the highest among the composites: $H_v$ = 1.9 and 0.5% for aerogels prepared from 5 and 7.5wt% impregnated tritylcellulose, respectively. Summarizing, contact angle and water vapor adsorption show that the tritylcellulose-silica composite aerogels not submitted to HMDZ treatment are hydrophilic despite the hydrophobicity of tritylcellulose, with $H_m$ and $H_v$ values three times higher than its HMDZ-treated counterpart. As shown in table V.5, the sililated tritylcellulose-silica composites had similar $H_m$ at equilibrium than sililated silica aerogels, showing that our approach of synthetizing fully hydrophobized composites is very efficient in improving the overall material resistance to humidity.

### 2.3.2.    Aging of the aerogels in humid environment

Moisture adsorption and aging tests over 45 days at varying humidity levels on reference Aerocellulose and silica aerogel, as well as tritylcellulose and tritylcellulose-hydrophobised silica composite aerogels, were performed by Markku Leivo and Tuomo Ojanen, at the Technical Research Centre of Finland (VTT), Helsinki within the frame of AEROCOINs project. The samples were submitted for 20 days to 75% relative humidity, then 15 days at 85% and finally 15 days at 95% at 25 °C.

The visual aspect of some of the tested samples after the humidity aging tests is presented in figure V.11). Only the non-hydrophobized silica reference samples had macroscopic damages that could be seen, cracking and eventually falling into small pieces; no other sample had visual signs of material deterioration. The pure aerocellulose samples changed their appearance during the 15 days exposure under 95 % RH. Clear shrinkage had taken place and the material pore structure has likely collapsed due to the moisture load. For the reference composites from non-modified cellulose and silica, as well as tritylcellulose-nonhydrophobised silica composites, only limited shrinkage was observed. The presence of the silica phase in the composite has a stabilizing effect towards humidity induced shrinkage; the higher stiffness of the composites (see part 2.2.1) may help prevent shrinking.
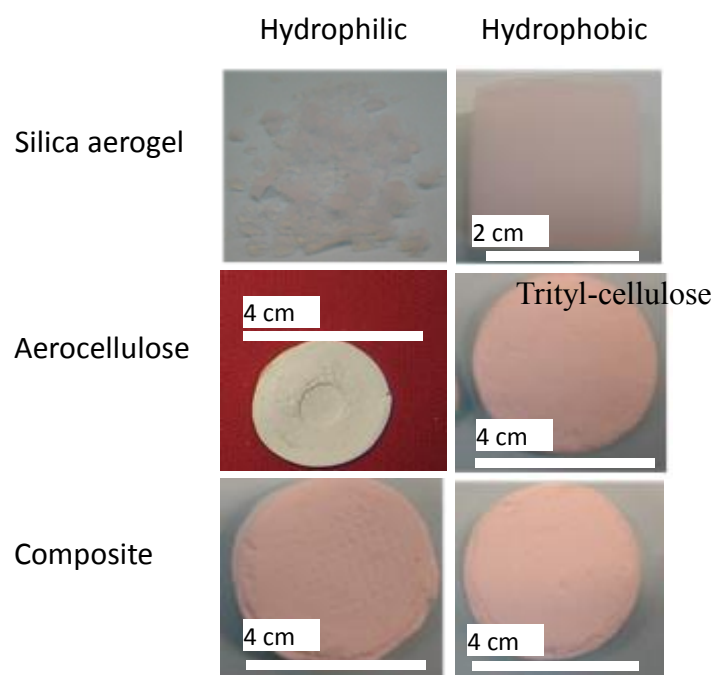


**FigureV.11 : Visual aspect of reference silica, cellulose, tritylcellulose and tritylcellulose-silica composites after being submitted to the aging tests up to 95% humidity rate. Cellulose, tritylcellulose and tritylcellulose-silica composites were all 4cm in dialeter before the tests.**

The analysis was first performed on reference, non-hydrophobized Aerocellulose and Aerocellulose-silica composites from chapter IV, followed by tests on reference silica aerogels, tritylcellulose aerogel, and tritylcellulose-silica aerogel composites. In the case of pure silica aerogels and tritylcellulose-silica composites, HMDZ-treated samples were compared to untreated ones.

Figure V.12.a presents the evolution of $H_m$ as a function of time at various humidity levels and Figure V.12b shows the values at equilibrium as a function of relative humidity.
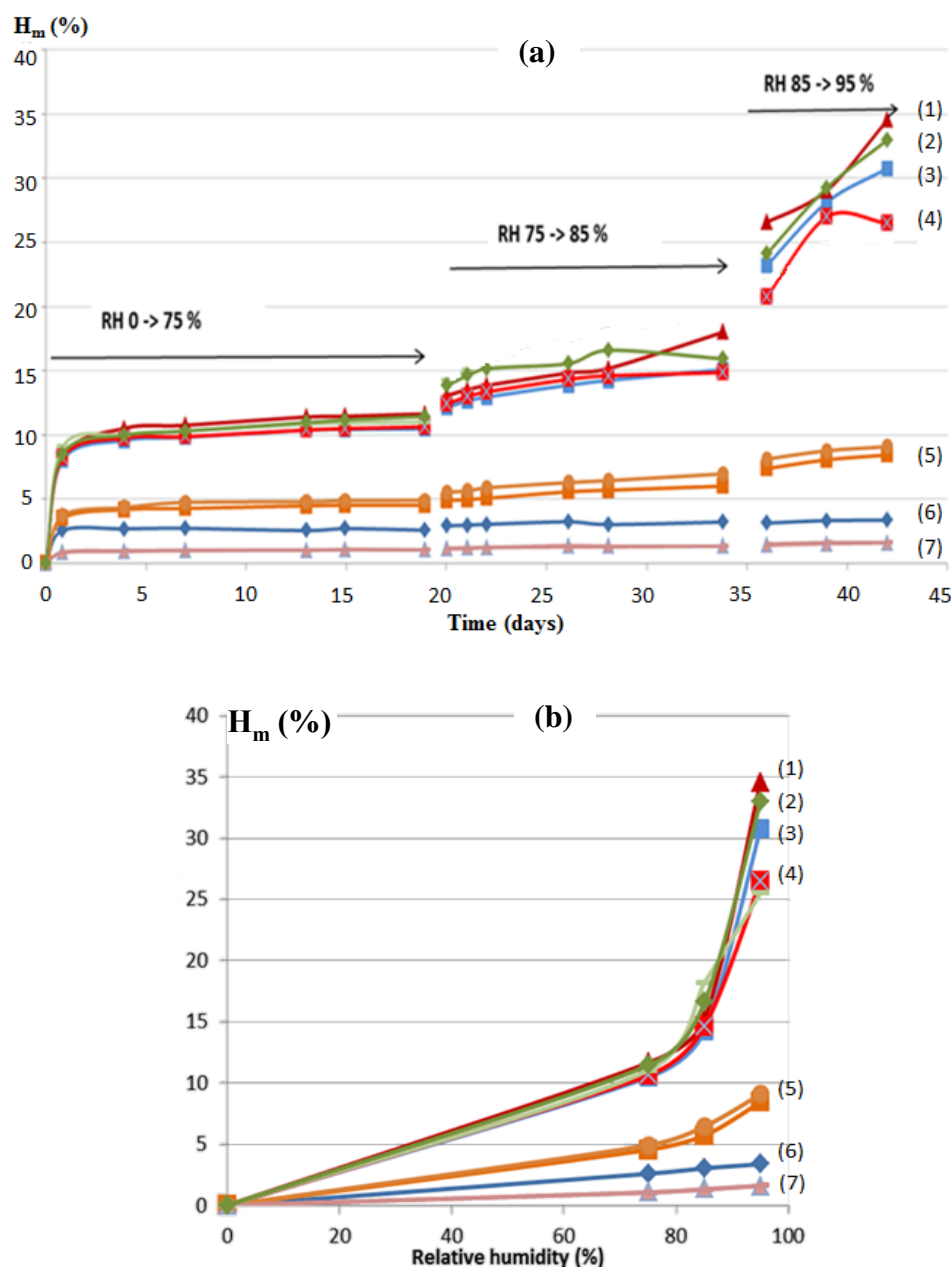
**Figure V.12 : (a) mass uptake over time during the aging tests at increasing humidity and (b) Sorption curves showing maximum water mass uptake depending on relative humidity. The following aerogel samples were analysed, with courtesy of Markku Leivo and Tuomo Ojanen, Technical Research Centre of Finland (VTT), Helsinki:**

(1) **3%wt cellulose-silica composite, non-hydrophobized.**

(2) **Silica aerogel, non-hydrophobized.**

(3) **3%wt aerocellulose reference.**

(4) **3%wt tritylcellulose-silica composite, non-hydrophobized.**

(5) **5%wt tritylcelluose-silica composite hydrophibized with HMDZ. (2 identical samples)**

(6) **5%wt Tritylcellulose.**

(7) **Silica aerogel, hydrophobized with HMDZ**

The sorption curves on figure V.14 highlight very well the difference between hydrophilic samples (refered as 1-4 on the graphs) and hydrophobic samples (5-7 on the graphs).

Hydrophilic samples have a relatively similar water adsorption behaviour. At 75% relative humidity, they show a rapid weight increase of 10-13%wt over 2-3 days after which they reach an equilibrium state. Then, when the humidity is increased, $H_m$ increases again: at 85% relative humidity $H_m$ goes up to 15-17%; the weight increase is spectacular at 95% relative humidity, reaching 34% for reference aerocellulose and 27% for cellulose-silica composite. Interestingly, the mass uptake curve of the tritylcellulose-silica composites that were not treated with HMDZ (curve number 4 on figure V.12) is extremely similar to that of the untreated silica, confirming that the untreated silica phase is responsible for the water sensitivity in the composite.

Hydrophobic samples, i.e silica aerogel treated with HMDZ, tritylcellulose aerogel, and tritylcellulose-silica composite treated with HMDZ present low humidity absorption. $H_m$ for hydrophobic samples is below 7 % by weight at equilibrium under 95 % RH. Untreated silica and untreated tritylcellulose-silica composites had higher moisture accumulation, exceeding 25 % by weight under 95 %RH. The starting of the water uptake curves at 75%RH is very similar to the tests performed in our laboratories at 30 °C and 80%RH: the equilibrium appears to be reached in less than 48h, after what the sample mass does not increase until the humidity rate is raised.

Overall, the long-term water vapour adsorption tests performed in VTT confirm the results of the accelerated aging and water contact angle tests: the hydrophobization of both cellulose and silica phases is necessary to obtain fully hydrophobic composites.

### 2.3.3. Thermal conductivity

The thermal properties of tritylcellulose and tritylcellulose-silica composite aerogels have been evaluated by hot-wire measurements by G. Reichenauer from Bavarian Center for Applied Energy Research, Wurzburg, Germany. The measured thermal conductivities are presented in table V.5.

**Table V.5: Thermal conductivities for tritylcellulose and tritylcellulose-silica composites.**

| Aerogel Sample | Hydrophobization of silica phase | Cellulose concentration (%wt) | $\lambda$ (W.m$^{-1}$.K$^{-1}$) |
|---|---|---|---|
| Aerocellulose | n/a | 5% | 0.035 |
| Silica aerogel | Hydrophobised (HMDZ) | - | 0.012 |
| Tritylcellulose | n/a | 5% | 0.027 |
| Tritylcellulose | n/a | 7.5% | 0.029 |
| Tritylcellulose-silica composite | n/a | 5% | - |
| Tritylcellulose-silica composite | Hydrophobised (HMDZ) | 5% | 0.021 |
| Tritylcellulose-silica composite | Hydrophobised (HMDZ) | 7.5% | 0.022 |

Tritylcellulose aerogels appear notably thermally less conductive than non-modified Aerocellulose, with conductivities of 0.027-0.029 W.m$^{-1}$.K$^{-1}$ as opposed to 0.035 W.m$^{-1}$.K$^{-1}$. Two potential reasons explaining this difference can be given:

a) Lower intrinsic conductivity of the tritylcellulose aerogel backbone as compared to the non-modified cellulose, due to loose packing of chains because of the steric hindrance induced by grafted trityl groups. This could be verified by measuring the thermal conductivity of tritylcellulose under vacuum and low temperature to eradicate radiative transfer.

b) Significantly higher hydrophobicity of tritylcellulose aerogels which reduces the presence of bound water.

The conductivity of composite aerogels based on tritylcellulose-hydrophobic silica is 0.021-0.022 W.m$^{-1}$.K$^{-1}$: these composites are thus a promising new thermal super-insulation material, if their conductivity can be lowered a bit further (below 0.020 W.m$^{-1}$.K$^{-1}$). The presence of the hydrophobic nanostructured silica phase filling the pores of tritylcellulose matrix allowed a significant reduction of air conduction, thus lowering the total conductivity of the materials, even if it is accompanied by a certain increase in bulk density.

# 3. Tritylcellulose and tritylcellulose-silica composite xerogels

## 3.1. Morphology and bulk density

### 3.1.1. Influence of drying conditions on tritylcellulose xerogel properties

Tritylcellulose and HMDZ-treated tritylcellulose-silica composites being highly hydrophobic, they may be suitable for the preparation of xerogels via ambient pressure drying. Tritylcellulose coagulated in ethanol from 5%wt solution were dried at ambient pressure at two different temperatures: 20 and 60 °C. The evaporative drying was continued until the mass of the xerogel was constant: the drying time was 2h for 60 °C and 24h for 20 °C. First of all, it is important to underline that the samples remain monolithic after evaporative drying at atmospheric pressure. The visual aspect of the xerogels, as compared to tritylcellulose aerogel of a similar concentration is shown on figure V.13. Tritylcellulose xerogels show a high volume contraction upon drying: around 85-88% against only 8.8% when tritylcellulose is dried in supercritical $CO_2$. On the xerogel that was slowly dried at 20 °C, the surface shows a concave deformation (a kind of bending) indicating the formation of a meniscus during solvent evaporation. The xerogels contraction indicates that pore collapse upon ambient pressure drying because of inherent capillary tensions also happens with tritylcellulose, resulting in strong volume shrinkage.



**Figure V.13: Visual aspect of (a) tritylcellulose xerogel dried at 20°C ; (b) tritylcellulose xerogel dried at 60°C and (c) aerotritylcellulose dried in SC CO₂**

The bulk density of tritylcellulose xerogels was compared to that of untreated cellulose xerogels in different drying conditions; a theoretical density, assuming no volume contraction during the drying, is shown as a reference for each particular case (figure V.14). The values are compared with aerogel and xerogel prepared from pure cellulose.
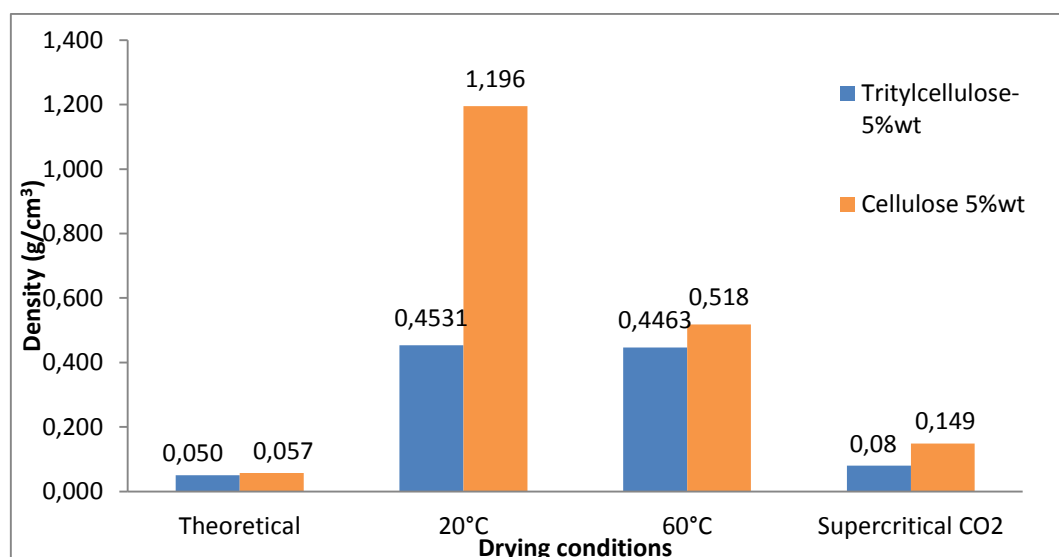
**Figure V.14: Bulk densities of tritylcellulose xerogels from 5%wt tritylcellulose-DMF solution, as compared to untreated cellulose of similar concentration, depending on drying conditions. The theoretical density corresponds to hypothetical samples showing no shrinkage upon drying and aging.**

Slow drying at 20 °C produces the higher bulk density xerogels, for both cellulose and tritylcellulose. A reference cellulose xerogel dried in these conditions has a density of 1.19 g.cm$^{-3}$, which becomes close to the bulk density of native cellulose (1.5 g.cm$^{-3}$). The bulk density of the tritylcelllulose xerogel dried in the same conditions is 2.6 times lower than that of the reference cellulose xerogel. When the drying is performed faster, i.e. at 60 °C, the bulk density of the native cellulose xerogel comes closer to that of the tritylcellulose one. Although xerogels with bulk densities comparable to those of supercritically dried material were not obtained for the given drying conditions, we have to note that the bulk densities of tritylcellulose xerogels show no dependence on the drying temperature, being around 0.45 g.cm$^{-3}$ at 20 °C and 60 °C, contrary to Aerocellulose.

The influence of subcritical drying conditions on the microstructure of the materials was examined by SEM for tritylcellulose and native cellulose xerogels. Figure V.15 compares the morphology of modified and unmodified cellulose xerogels dried at 20 and 60 °C.
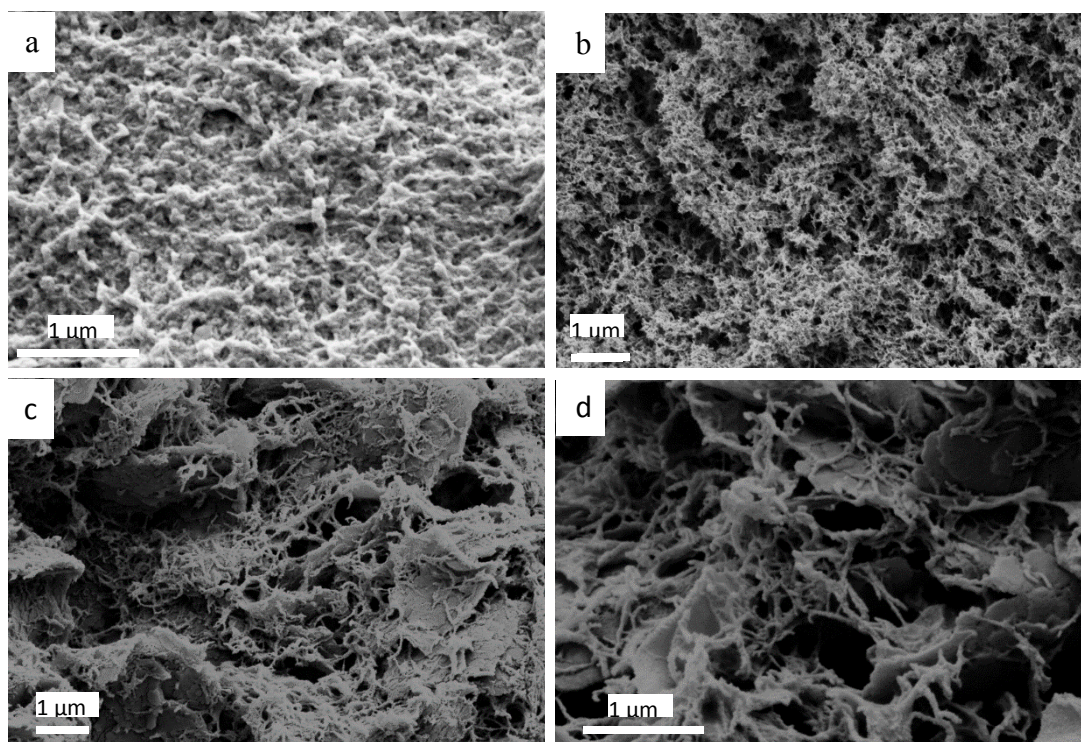
**Figure V.15: SEM images of the microstructure of (a) cellulose xerogel dried at 20 °C ; (b) cellulose xerogel dried at 60 °C ; (c) tritylcellulose xerogel dried at 20 °C ; (d) tritylcellulose xerogel dried at 60 °C.**

The structure of tritylcellulose xerogels is similar to that of the corresponding aerogels, with interwined fibers forming a porous network, with pore sizes expected to range from 100 nm to a few microns. However, the xerogel present some plate-like structures (figure V.17 c and d), with characteristic dimensions between 1 and 10 µm in length. Although those plate-like structures can sometimes be seen in supercritically dried tritylcellulose, they are much more abundant in the xerogels, and are particularly visible in samples slowly dried at 20 °C.

We can assume that the formation of these plate-like structures is due to the material shrinkage during drying, and seems to be favored by slow drying kinetics at ambient temperature. It should be noted that the "fiber network plus plates" structure of tritylcellulose is not observed on non-modified cellulose xerogels (figure V.15 a and b): when hydrophilic cellulose is dried at 20 °C the fibers are still visible but appear totally condensed with no visible porosity; the sample dried at 60 °C shows a fibrous and slightly porous structure, somehow similar to that of aerocellulose despite the significant increase in bulk density in the xerogel.

Besides drying conditions had a significant effect on specific surface area of cellulose and tritylcellulose xerogels. Tritylcellulose xerogels show a very low specific surface area of 39-42 $m^2.g^{-1}$. The plate-like structure observable of the SEM micrographs of the gels seem not to contain either meso- or micropores or to have microrugosity. Surprisingly, despite its density increase and volume shrinkage, hydrophilic cellulose xerogels dried at 60 °C have a specific surface area of 191 $m^2.g^{-1}$, against 220 $m^2.g^{-1}$ for supercritically dried samples coming from gels of similar concentrations. This later result, albeit surprising considering cellulose densification upon ambient pressure drying, is consistent with the microstructure observed in figure V.15.b.
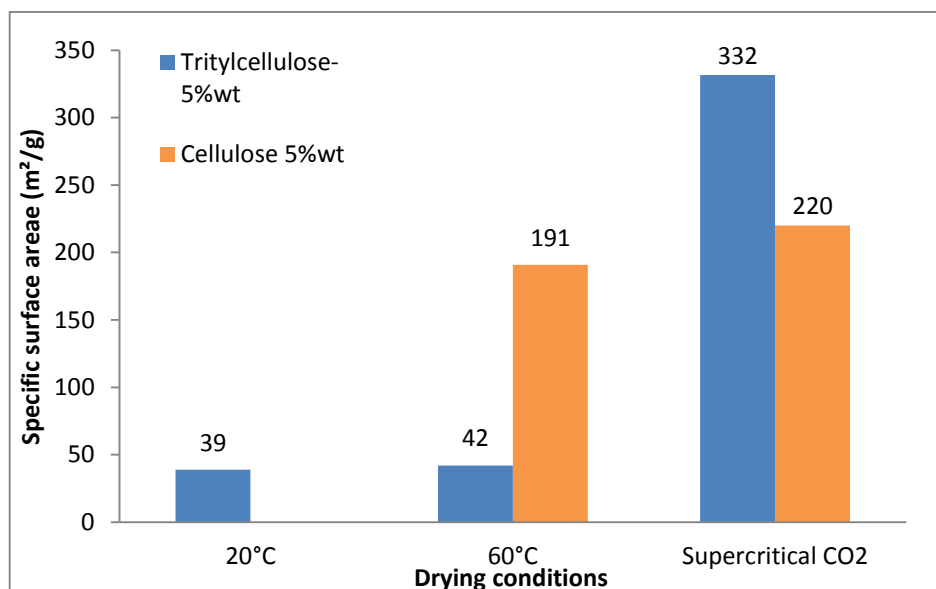
**Figure V.16: Specific surface areas of tritylcellulose xerogels from 5%wt tritylcellulose-DMF solutions depending on drying conditions.**

### 3.1.2. Evolution of xerogel density as a function of degree of substitution of tritylcellulose

It is known from previous studies (Pour et al., 2015) that the degree of substitution of tritylcellulose affects strongly the final properties of aero- and xerogels. Figure V.17 displays the experimentally measured densities for 5%wt tritylcellulose aerogels and xerogels, dried for 2h at 60°C, for different values of DS.
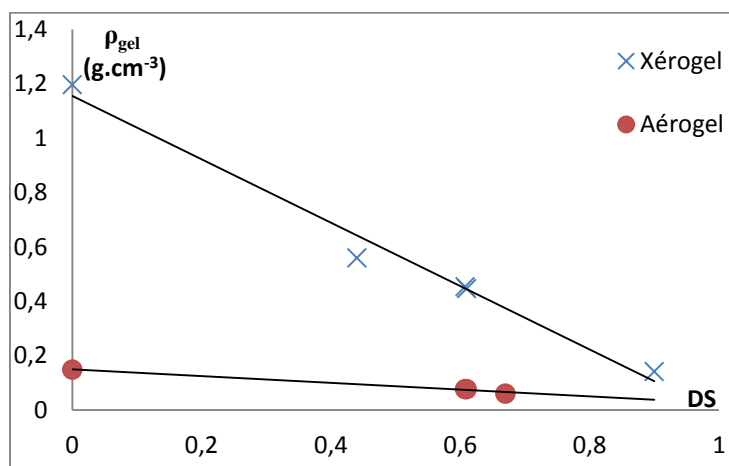


**Figure V.17: Densities of tritylcellulose aero- and xerogels in function of cellulose DS**

A higher degree of substitution leads to lower apparent densities in the xerogels, as expected. A DS of 1 or higher needs to be achieved to obtain bulk densities comparable to aerogels, i.e. lower than 0.15 $g.cm^{-3}$. In the case of supercritically dried materials, a slight decrease of the apparent density when increasing DS is observed. A high DS means a higher number of trityl groups grafted on cellulose chains, thus more important steric hindrance between chains. Plus, the interfacial tension between ethanol and pore walls is also suspected to change with the increase of DS. These two factors play a role in preventing sample contraction during supercritical drying.

### 3.1.3. Properties of tritylcellulose-silica composite xerogels

Tritylcellulose-silica composites from 5%wt tritylcellulose-DMF solutions impregnated with PEDS were dried at ambient pressure, for 2h at 60 °C. Samples treated with HMDZ were compared with untreated composites. Figure V.18 shows the visual aspect of the composite xerogels. The volume loss of the untreated and HMDZ-treated composites upon evaporative drying are rather equal, being 78% and 76% respectively.
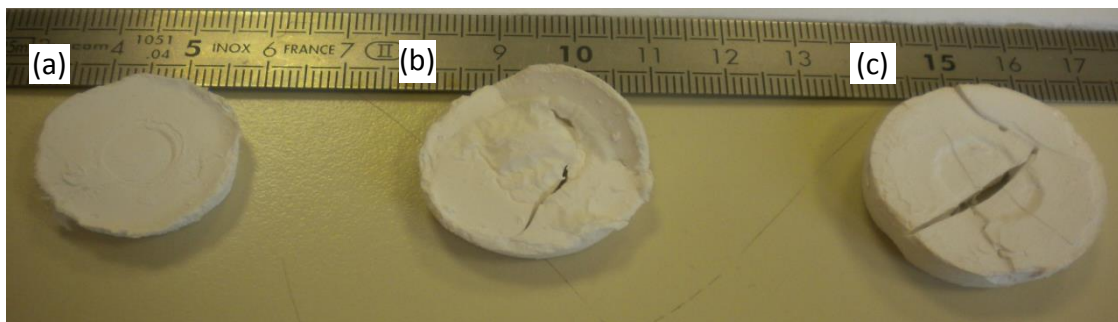


**Figure V.18: Visual aspect of tritylcellulose-based xerogels : (a) 5% tritylcelllulose; (b) 5%tritylcellulose-silica composite; and (c) 5% tritylcellulose-silica composite treated in HMDZ.**

The composite xerogels show visible cracks, although they do not fall apart during drying which is the case of HMDZ-treated silica xerogels. The cellulose matrix helps holding the composite together and prevents the silica phase from falling apart during ambient pressure drying.

The density, specific surface area and estimated theoretical porosity (calculated with eq. V.10) of the composite xerogels, as compared to the corresponding composite aerogels (see part 2.1.3) is shown on table V.6.

**TableV.6: Bulk densities, specific surface areas and estimation of porosity for tritylcellulose-silica composites xerogels and aerogels elaborated from 5%wt tritylcellulose solution impregnated with PEDS.**

| | Type of material | density (g.cm$^{-3}$) | S BET (m².g-1) | ε (%) |
|---|---|---|---|---|
| **Tritylcellulose-silica composites** | aerogel | 0,244 | 849 | 87% |
| | xerogel | 0,636 | 877 | 65% |
| **Tritylcellulose- HMDZ-treated silica composites** | aerogel | 0,232 | 746 | 87% |
| | xerogel | 0,628 | 847 | 66% |

The important volume contraction of tritylcellulose xerogels upon drying in ambient conditions resulted in densities that are three times higher than the corresponding aerogels. The subsequent hydrophobization of the silica phase does not appear to have an effect on the final composite density. The estimated porosity of the composite xerogels is logically lower than that of the aerogels, 65-66% against 86-87%. Specific surface area, however, do not change significantly in composite xerogels as compared to composite aerogels, still being in the 700-850 m².g$^{-1}$ range, confirming the formation of a nanostructured silica phase in the porosity of tritylcellulose. As tritylcellulose xerogels show low specific surface area, and considering that the macroporosity of tritylcellulose is largely filled with the nanostructured silica phase, the silica aerogel contained in the tritylcellulose porosity accounts for the major part of the materials specific surface area even without posterior hydrophobization.

Figure V.21 shows the typical microstructure of tritylcellulose-silica composite xerogels as seen by SEM.
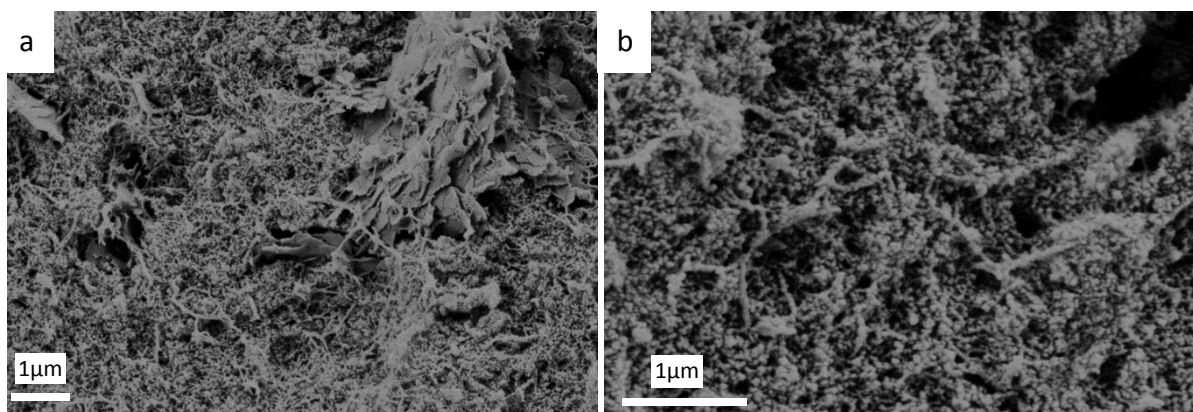


**Figure V.19: SEM pictures of (a), (b) 5%wt tritylcellulose-silica composite xerogel dried at 60 °C and ambient pressure at two different magnifications.**

SEM micrographs confirm the presence of the silica phase, forming an interpenetrated network with the tritylcellulose. The larger plate-like structures characteristic of tritylcellulose xerogels can be seen on figure V. 19.a.

Given their strong volume shrinkage and frequent cracking upon drying, it was not possible to reliably evaluate the thermal and mechanical properties of tritylcellulose and tritylcellulose-silica composite xerogels. However, given their high apparent density, it is unlikely that these xerogels will show good thermal and mechanical properties. Tritylcellulose with higher DS should be used in further development to obtain ambient-dried hydrophobic materials with lower bulk density and higher porosity, thus more suited to thermal superinsulation applications.

## 3.2.  **Hydrophobic properties of the xerogels**

The hydrophobic properties of tritylcellulose and tritylcellulose-silica composite xerogels were evaluated through water contact angle measurements and accelerated aging at 30 °C and 80% relative humidity. The contact angle values are displayed in table V.7 and the values of mass and volume uptake in the humidity tests is displayed on figure V.22. For the untreated tritylcellulose-silica composite xerogel, the water contact angle could not be measured as the water drop was absorbed when touching the sample surface.

**TableV.7: Water contact angle for tritylcellulose and tritylcellulose-silica composite xerogels depending on evaporative drying conditions. The composite dried at 20 °C could not be measured because of cracks inducing an irregular surface.**

| drying conditions | 20 °C | 60 °C |
|---|---|---|
| Tritylcellulose xerogel | 133° | 125° |
| Tritylcellulose-HMDZ-treated silica composite + xerogel | - | 148° |

The contact angle values indicate that the xerogels are strongly hydrophobic; the treated composite xerogels have a very high contact angle with water, 148°. Although the functionalization by tritylchloride did not allow the synthesis of low-density xerogels, the trityl groups still provide a good surface hydrophobization.

181
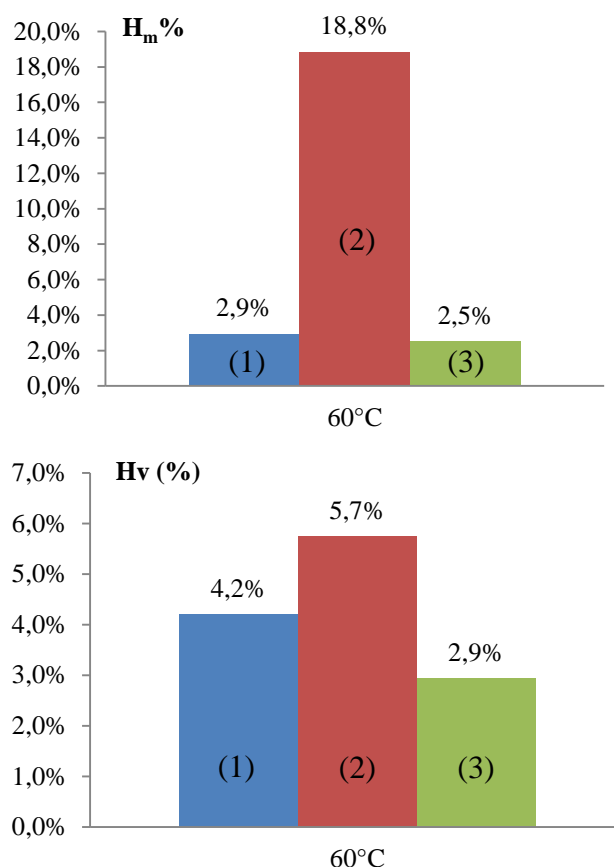
**Figure V.22 : values of mass uptake (H_m) and volume variation (Hv) of (1) pure tritylcellulose xerogel and (2) tritylcellulose-silica composite xerogels impregnated with untreated silica and (3) tritylcellulose-silica composite xerogels impregnated with HMDZ-treated silica, when submitted to 30 °C and 80% RH for 48h.**

The water uptake results on the xerogels are very similar to what was observed for the aerogels in part V.2.3.1. Fully hydrophobic composite xerogel (tritylcellulose and HMDZ-treated tritylcellulose-silica samples) show low mass uptake values of 2.9% and 2.5% respectively, while the xerogel impregnated with untreated silica is hydrophilic, absorbing 18.8% in mass. The volume contraction for all xerogel is lower than 6%, even for the untreated composite xerogels. However, it shall be noted that the xerogels already underwent strong volume shrinkage upon drying.

## Conclusions

The hydrophobization of cellulose and cellulose-silica composite was investigated. We hydrophobized cellulose by using a homogeneous chemical modification process, to graft triphenylmethyl functions on cellulose chains. The resulting material was called tritylcellulose and it was with the degree of substitution 0.62. Aerogels from tritylcellulose dissolved in DMF and coagulated in ethanol were obtained.

Composite aerogels were prepared by impregnation of wet tritylcellulose with PEDS. To obtain fully hydrophobic composites, wet tritylcellulose impregnated with PEDS was treated with hexamethyldisilazane (HMDZ).

The obtained organic-inorganic aerogels were finely nanostructured, with high specific surface areas between 600 and 800 $m^2.g^{-1}$ confirming the presence of a nanostructured network interpenetrated with the tritylcellulose. The morphology of the hydrophobized composites was similar to that of those based on non-hydrophobized materials. Composite aerogels were stiffer than pure tritylcellulose and pure silica aerogels, with Young moduli ranging around 2-4 MPa vs 0.3 to 1 MPa for tritylcellulose and 1.9 MPa for silica aerogels. The presence of silica phase in the pores of tritylcellulose in composite aerogels reinforces the material but makes it more brittle. It should be underlined that the mechanical properties of composite organic-inorganic aerogels are strongly improved as compared with pure silica aerogels. The maximal stress at break of tritylcellulose-silica composite aerogels is lower than the value for cellulose-silica composites (chapter IV). Improving the mechanical properties of tritylcellulose may require further chemical modification, such as chemical cross-linking between cellulose chains.

Tritylcellulose and tritylcellulose-HMDZ-treated composite aerogels were resistant towards humidity: contact angles with water were 125° and 133°, respectively and water mass uptake was reduced from 13% for the untreated material to 1-3% in rather severe conditions. The results of accelerated aging of the samples at 80% relative humidity (%RH) were confirmed by long term uptake measurements over 45 days in more severe conditions: while the mass of hydrophobic silica, tritylcellulose and hydrophobized tritylcellulose-silica composite aerogels increased only by 2-5%, composites impregnated with non hydrophobized silica gained up to 30% in mass at 95% RH.

The thermal conductivity of tritylcellulose aerogels were measured; it is lower than that of aerocellulose, 0.027 $W.m^{-1}.K^{-1}$ vs 0.035 $W.m^{-1}.K^{-1}$., most probably due tritylcellulose hydrophobicity and lower bulk density. Organic-inorganic fully hydrophobised composite aerogels appeared to be thermal superinsulating materials, showing a thermal conductivity in room conditions of 0.021-0.022 $W.m^{-1}.K^{-1}$. This result shows that the concept of interpenetrated organic-inorganic hydrophobic networks allows obtaining monolithic, nanostructured, mechanically strong, and thermally superinsulating materials.

Finally we studied the effect of ambient pressure drying on the hydrophobised cellulose (tritylcellulose) and tritylcellulose-silica composites. While the xerogels obtained showed very high hydrophobicity with contact angles of 120°-148° depending on evaporative drying conditions, they exhibited very strong volume shrinkage upon subcritical drying, resulting in high densification and loss of porosity. The microstructure of the tritylcellulose xerogels showed a mixture of condensed, plate-like structures and fibrous network. The composite

xerogels had high specific surface area due to the presence of the silica phase within the tritylcellulose network. Composite xerogels were almost monolithic contrary to silica xerogels which break under drying; this result shows that cellulose "holds" silica phase in a certain manner. While overall the hydrophobization process was successful, the synthesis of tritylcellulose with higher degree of substitution appears necessary to obtain lower density, highly porous xerogels potentially suitable for thermal superinsulation.

# References

Ayral, A., Phalippou J., Woignier,T. (1992); Skeletal density of silica aerogels determined by helium pycnometry, *Journal of Materials Science*, 27, 1166-1170

Brinker, C.J, Scherer, G.W (1990), Sol-Gel Science, the physics and chemistry of sol-gel processing, Academic Press.

Camacho Gomez J.A., Erler U.W., Klemm D.O. (1996); 4-methoxy substituted trityl groups in 6-O protection of cellulose: homogeneous synthesis, characterization, detritylation, *Macromol. Chem. Phys. 197*, 953-964

Demilecamps, A., Reichenauer, G., Rigacci, A., & Budtova, T. (2014); Cellulose–silica composite aerogels from "one-pot" synthesis, *Cellulose*, 2014, 21 (4), 2625-2636.

Gibson, L. J., & Ashby, M. F. (1997). Cellular solids. Structure and properties (2nd ed.). Cambridge University Press

Iler, R.K.; (1979), The Chemistry of Silica, Ed. John Wiley & sons (1979).

Liebner, F., Haimer, E., Potthast, A., Loidl, D., Tschegg, S., Neouze, M. A., Rosenau, T. (2009); Cellulosic aerogels as ultra-lightweight materials. Part 2: Synthesis and properties 2nd ICC 2007, Tokyo, Japan, October 25–29, 2007. *Holzforschung*, *63*(1), 3-11.

Pour,G., Beauger, C., Rigacci, A., Budtova, T. (2015); Xerocellulose: a New Class of Lightweight, Porous and Hydrophobic Cellulose Prepared via Ambient-Drying; *Journal of Materials Science*, submitted.

Rao, A. V., & Kalesh, R. R. (2004). Organic surface modification of TEOS based silica aerogels synthesized by co-precursor and derivatization methods, *Journal of sol-gel science and technology*, *30*(3), 141-147.

Roy, C., Budtova, T., & Navard, P. (2003). Rheological properties and gelation of aqueous cellulose-NaOH solutions. *Biomacromolecules*, *4*(2), 259-264.

Rudaz, C., Courson, R., Bonnet, L., Calas-Etienne, S., Salee, H., & Budtova, T. (2014) ; Aeropectin: fully biomass-based mechanically strong and thermal super-insulating aerogel, *Biomacromolecules* 15, 2188−2195.

Sescousse, R., Budtova, T. (2009); Influence of processing parameters on regeneration kinetics and morphology of porous cellulose from cellulose–NaOH–water solutions, *Cellulose*, *16*(3), 417-426.

Sescousse, R., Le, K. A., Ries, M. E., & Budtova, T. (2010). Viscosity of cellulose−imidazolium-based ionic liquid solutions. *The Journal of Physical Chemistry B*, *114*(21), 7222-7228.

Sescousse, R., Gavillon, R., & Budtova, T. (2011). Aerocellulose from cellulose–ionic liquid solutions: preparation, properties and comparison with cellulose–NaOH and cellulose–NMMO routes. *Carbohydrate Polymers*, *83*(4), 1766-1774.

Shewale, P.M, Venkateswara Rao, A., Parvathy Rao,A. (2008); Effect of different trimethyl silylating agents on the hydrophobic and physical properties of silica aerogel, *Applied Surface Science* 254, 6902-6907.

# Chapter VI:

# Aeropectin and aeropectin-silica composites.

# Introduction

This chapter focuses on the preparation and properties of brand new bio-based aerogels made with pectin and their composites synthesized with silica. In previous chapters we determined that cellulose-silica composites elaborated through impregnation of a wet cellulose matrix showed a reduced thermal conductivity (chapter IV), and superinsulating properties were obtained on hydrophobized cellulose-silica composites (chapter V).

The thermal conductivities of polysaccharide and polysaccharide-silica composites could be further improved by using another polysaccharide matrix allowing for a significantly lower thermal conductivity. In a very recent work (Rudaz et al., 2014), pectin-based aerogels called "Aeropectins" were elaborated from pectin aqueous solutions. They were shown to possess extremely interesting properties for thermal superinsulation, such as low bulk densities lower than $0.1$ g.cm$^{-3}$, very high porosity, and thermal conductivities in room conditions in the 0.018-0.025 mW.m$^{-1}$.K$^{-1}$ range. Pectin has also the advantage of being fully soluble in water, which contrary to cellulose allows to process it without the use of specific and expensive solvents such as ionic liquids.

In this last chapter we study an alternative method to elaborate aeropectins: reticulation of pectin chains by calcium ions. The morphology, density, porosity and specific surface areas of calcium-reticulated aeropectins will be compared to those of acid-gelled samples. The influence of different synthesis parameters such as pH, pectin concentration and calcium to carboxylate molar ratio on the morphology of calcium-reticulated aeropectins will be studied.

The mechanical properties of calcium reticulated aeropectins will be studied as a function of aeropectins bulk densities by uniaxial compression, and compared to those of acid gelled aeropectins, as well as aerocelluloses and reference silica aerogels.

To vary the morphology and properties of polysaccharide-based aerogels, aeropectin-silica composites were synthesized using the same methods as described for cellulose-silica composites in Chapter IV: forced-flow and diffusion controlled impregnation. The composites were characterized in terms of density, morphology and silica content. The thermal conductivities of calcium reticulated aeropectins will be measured by microflowmetry and compared to those of acid-gelled aeropectins and reference silica aerogels.

Finally, the hydrophobization of the composites will be considered through the surface treatment of the silica phase by three well-known hydrophobizing agents. Hydrophobicity of the treated composites will be checked by measurements of water uptake and water contact angle.

# Introduction

Ce chapitre étudie l'élaboration et les propriétés de nouveaux aérogels à base de pectine, ainsi que de leurs composites avec la silice. Au cours des chapitres précédents nous avons montré que l'imprégnation d'une matrice de cellulose par le PEDS permettait d'obtenir des aérogels composites cellulose-silice de conductivité thermique réduite comparée à l'Aérocellulose pure (Chapitre IV). Des propriétés superisolantes ont pu être obtenues pour des composites cellulose-silice hydrophobes (Chapitre V).

Les conductivités thermiques des aérogels basés sur les polysaccharides et de leurs composites élaborés avec la silice peuvent encore être améliorés en utilisant une autre matrice polysaccharide permettant d'atteindre une conductivité nettement moindre. Au cours de très récents travaux (Rudaz, 2014), des aérogels à base de pectine, appelés « aéropectines » ont été élaborés à partir de pectines en solution aqueuse. Ces aéropectines possèdent des propriétés extrêmement intéressantes pour la superisolation thermique, telles de basses densités ($< 0.1$ g.cm$^{-3}$), une porosité importante, et des conductivités thermiques comprises entre 0.018-0.025 mW.m$^{-1}$.K$^{-1}$. La pectine a également pour avantage notable d'être entièrement soluble dans l'eau, ce qui contrairement à la cellulose permet de la mettre en forme sans recourir à des solvants coûteux tels que les liquides ioniques.

Dans ce chapitre nous étudierons une nouvelle méthode visant à l'élaboration des aéropectines: la réticulation par les ions calcium. La morphologie, la densité apparente, la porosité et la surface spécifique d'aéropectines réticulées par les ions calcium seront comparées à celles d'aéropectines gélifiées en milieu acide. L'influence de différents paramètres de préparation tels le pH, la concentration de pectine et le rapport molaire entre ions calcium et groupements carboxylate sur la morphologie des aéropectines réticulées par les ions calcium sera étudiée.

Les propriétés mécaniques des aéropectines réticulées par les ions calcium seront étudiées en fonction de la densité des matériaux par mesures de compression uniaxiale. Ces données seront comparées aux valeurs obtenues pour des aéropectines gélifiées en milieu acide, à l'aérocellulose ainsi qu'aux aérogels de silice de référence.

Pour faire varier la morphologie et les propriétés des aéropectines, des composites « aéropectine-silice » seront élaborés en utilisant les méthodes décrites au Chapitre IV pour l'élaboration de composites « cellulose-silice » : imprégnation par diffusion moléculaire et par flux forcé. Les composites seront caractérisés en termes de densité, morphologie et teneur en silice. Les conductivités thermiques des composites seront mesurées par micro-fluxmétrie et comparées à celles des aéropectines pure et des aérogels de silice.

Enfin, nous considérerons l'hydrophobisation des composites via le traitement de surface de la phase silice par trois agents d'hydrophobisation bien connus. L'hydrophobicité des composites sera contrôlée par mesures d'angle de contact avec l'eau et de reprise hydrique en atmosphère humide.

# 1. Structural properties of calcium-reticulated aeropectin.

## 1.1. Comparison of acid-gelled and calcium-reticulated aeropectins

### 1.1.1. Preparation of aeropectins

Aeropectin can be prepared via a dissolution-gelation-coagulation process, quite similar to the preparation of Aerocellulose from cellulose solutions: after dissolution in water and gelation of the pectin solution, the pectin is washed in a non-solvent (ethanol) and dried in supercritical $CO_2$ to obtain aeropectin (figure VI.1). The detailed experimental procedure is described in materials and methods section.
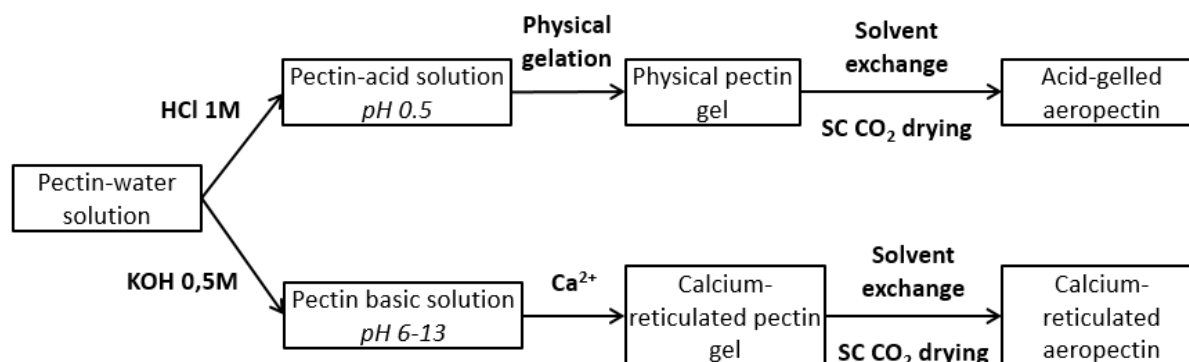


**Figure VI.1: General schematization of two methods used in the preparation of aeropectins**

Pectin solutions in water can form gels following two different mechanisms (Tilly, 2010):

- Physical gelation in acid media (figure VI.2.a): at pH lower than 3, the carboxylic acid groups on pectin chains are mostly in their protonated form. Hydrogen bonds can then be formed between polymer chains in a way similar to the gelation of cellulose-NaOH solutions. In the following aeropectins obtained from gelation of pectin in an acid media will be referred by "*acid-gelled aeropectins*". This method is more suited to pectins with high degree of esterification (DE).

- Reticulation through the formation of ionic bonds between pectin chains by a divalent cation (figure VI.2.b): cation-triggered pectin gelation occurs at neutral or basic pH values. The main component of the pectin chain, D-galacturonic acid, has a pKa of 3.51 (Kohn and Kovac, 1978); the pKa of pectin has been evaluated to be 2.90 (Ralet et al., 2001). Thus a ionic bridge between negatively charged deprotonated carboxylic groups on pectin chains can be formed at basic pH by binding with bivalent cations, such as calcium ions. The "egg-box" model has been suggested for describing the calcium induced gelation of alginates and pectins (Grant et al., 1973). In this model pectin chains form dimers when reticulated by calcium ions; the oxygen atoms on the hydroxyl groups on $C_2$ and $C_3$, as well as the ones from the ring and glycosidic bonds also participate in the binding of the calcium ions through complexation. In the following, aeropectins obtained with this method will be referred to as "*calcium-reticulated (CR) aeropectins.*"
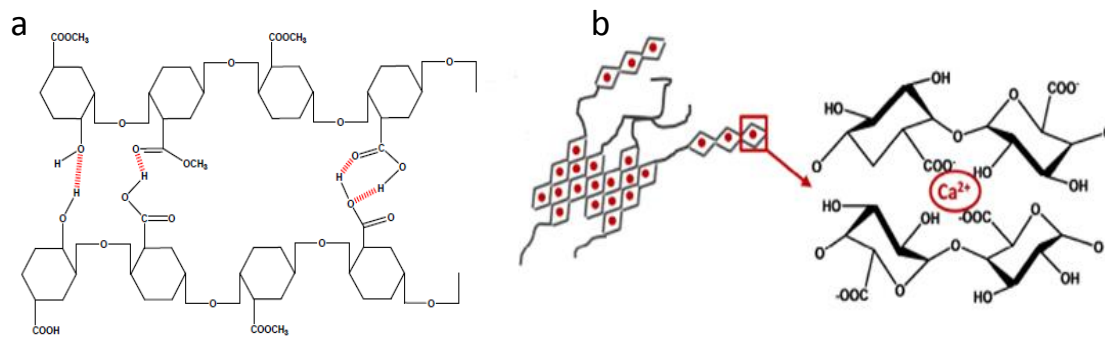
**Figure VI.2: Schematic view of the molecular structure of (a) physical pectin gels obtained in acidic conditions and (b) CR pectin gels (Tilly, 2010).**

In the present work we focused on making aeropectins from calcium reticulated pectin solutions in water. The pectin used for the study is a relatively highly methylated pectin extracted from citrus peel, with a DE about 56%, as confirmed by FTIR measurements (Synytsya et al., 2000; Rudaz, 2013). Pectins of a higher DE are less suited to reticulation with calcium ions because of their lower number of free carboxyl groups that can be bind by calcium ions; nevertheless the calcium-induced gelation of HM pectins is also possible and the properties of such gels have been reported by (Tibbits et al., 1998).

The source of calcium ions used in this work is calcium chloride (CaCl$_2$). The molar ratio between carboxylic moieties and calcium ions is an important factor in the understanding of calcium reticulated pectin properties. The calcium-to-carboxyl molar ratio is defined by equation VI.1:

$$R = \frac{n_{Ca^{2+}}}{n_{RCOO^-}} = \frac{[Ca^{2+}]}{[RCOO^-]} \tag{VI.1}$$

with [Ca$^{2+}$] the calcium molar concentration (mol.L$^{-1}$) and [RCOO$^-$] the molar concentration of deprotonated carboxyl groups in the solution. The proportion between galacturonic acid and its deprotonated form at a given pH can be calculated by equation VI.2 and VI.3.

$$pH = pKa + log\frac{[RCOO^-]}{[RCOOH]} \tag{VI.2}$$

$$\frac{[RCOO^-]}{[RCOOH]} = 10^{pH-PKa} \tag{VI.3}$$

As the pectin pKa is 2.90, for a pH superior to 6 the concentration of galacturonic acid becomes negligible as compared to its deprotonated form. In the following the overall concentration of free carboxyl groups can be assimilated to the concentration of deprotonated galacturonic acid [RCOO$^-$]. The concentration of carboxyl groups can be evaluated from the degree of esterification and molar mass of galacturonic acid, the repeating unit of pectin chains, as follows (eq. VI.4):

$$[RCOO^-] = \frac{n_{RCOO^-}}{V_{pectin\ solution}} = \frac{wt\%_{pectin}(1-DE)/M_{galacturonic\ acid}}{V_{pectin\ solution}} \tag{VI.4}$$

with $n_{RCOO^-}$ the amount of carboxylate group in pectin solution, $V_{pectin\ solution}$ the volume of the gelling pectin solution, $M_{galacturonic\ acid}$ = 192 g.mol$^{-1}$ and DE = 56%.

Calcium reticulated aeropectins will be compared with previously studied (Rudaz, 2013) acid-gelled aeropectins obtained from the same pectin starting material. In the following, we study the influence of different preparation parameters (pectin concentration, pH, calcium to carboxyl groups molar ratio) on the morphological properties of calcium reticulated aeropectins.

### 1.1.2. Effect of pectin concentration on morphology and bulk density of aeropectins

Calcium reticulated pectin gels were prepared at initial pectin concentration between 1 and 5 %wt. To reliably study the influence of concentration on pectin morphology, the calcium-to-carboxyl molar ratio was fixed at 0.20 for all samples. Below 1%wt, the pectin solution did not gel upon addition of calcium ions at any calcium-to-caboxyl molar ratio. From this observation we can assume that the minimal concentration of pectin to obtain a stable pectin fibrous network is around 1%wt. For pectin with high degree of esterification (around 70%) of molecular weight between $3.10^4$ and $10.10^4$, the intrinsic viscosity was shown to vary from 100 to 600 mL/g (Harding et al., 1991), which gives the overlap concentration (minimal concentration need to form a gel) around 0.2 – 1 wt%. The conformation of that pectin was reported to be a rigid rod. The pectin used in our study was with lower degree of esterification which should lead to more flexible conformation; we can thus assume that indeed the overlap concentration is roughly around 0.5 – 1wt%.

Gels with pectin concentration below 2%wt were quite fragile. The higher the concentration (and thus the higher the initial solution viscosity), the faster was gelation. At higher concentrations than 5%wt, pectin solution was too viscous and heterogeneous to be handled. In some cases, air bubbles remained trapped into the wet samples, generating visible surface irregularities after drying. Moreover, the surface of the samples becomes concave, forming a meniscus during the solvent exchange with ethanol. After supercritical $CO_2$ drying, monolithic, white samples were obtained (figure VI.3).



**FigureVI.3: Visual aspect of CR aeropectins from different pectin initial concentrations in wt%.**

Most of the overall contraction of aeropectins occurred during sc drying. Volume contraction of samples during supercritical $CO_2$ drying was quite high, reaching 30 to 50%. As seen in previous chapters, Aerocelluloses shrink by about 30% upon sc drying. Mechanical constraints are not likely to induce this shrinkage, as supercritical drying avoids capillary constrains between the pore walls. Supercritical $CO_2$ is an inorganic, apolar and aprotic solvent with which the polar polymers (here, polysaccharides) have less chemical affinity. During supercritical drying, the solvent (ethanol) filling the pores of coagulated polysaccharide is replaced with $CO_2$, then air, forcing the polymer chains to reach a new state of equilibrium by contracting. The extent of this phenomenon depends on polymer chains flexibility and chemical affinity of the polymer for the solvent. Shrinkage upon drying up to 85% has been observed previously for several aerogels based on organic polymers, such as cellulose acetate (Fischer et al., 2006) or polyurethane (Diascorn, 2014).

Similar observations were made by studying the effect of pectin concentration on the gelation and physical aspect of acid-gelled pectin (Rudaz, 2014). It has to be noted that gelation by calcium reticulation of pectin chains occurs much faster than physical gelation of pectin in acid media: few minutes to one hour are necessary for the former, while the latter may require a few hours to even several days at low pectin concentrations.
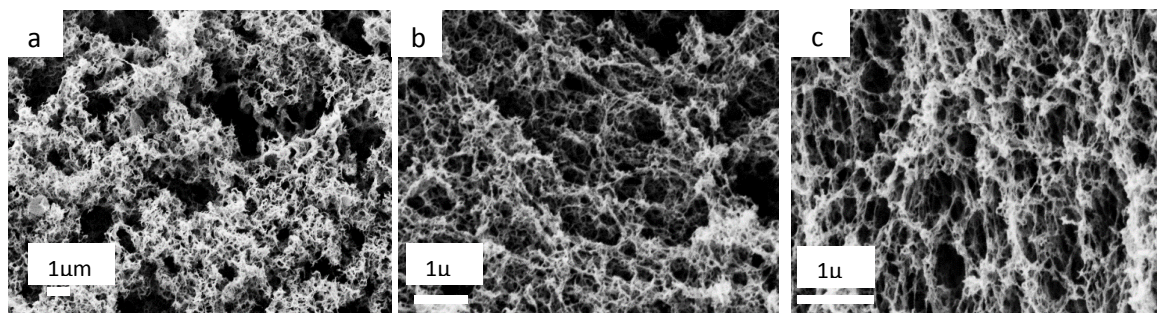
The densities of calcium-reticulated aeropectins obtained from pectin solutions of different initial concentrations are shown on figure VI.4, data for acid-gelled from (Rudaz, 2014) are added for comparison. Theoretical density, assuming no volume contraction upon the whole synthesis process, was calculated and is shown for reference on the figure as a solid line.
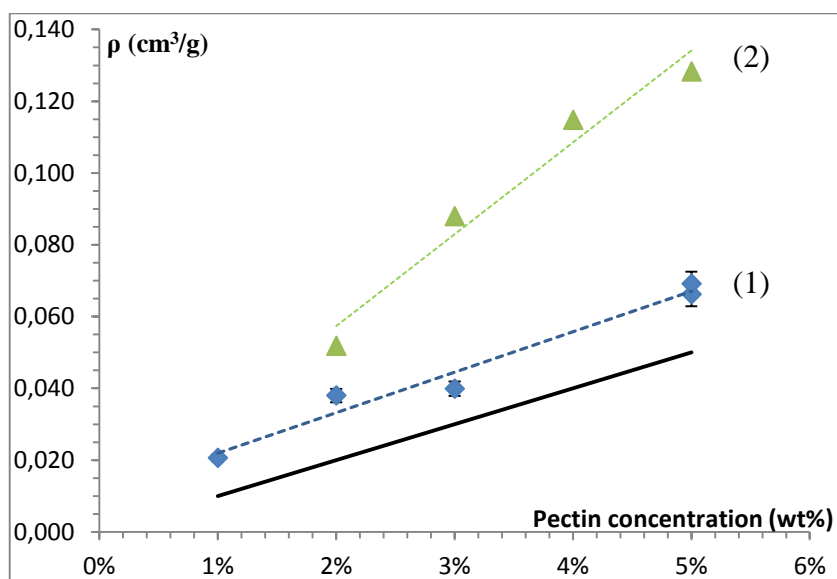


**Figure VI.4: Bulk density as a function of pectin initial concentration for (1) CR aeropectins and (2) aeropectin from pectin gelled in acid conditions (data taken from Rudaz et al., 2014). Solid line is theoretical bulk density of aeropectins assuming no volume contraction upon processing.**

All aeropectins show low bulk densities in 0.02-0.12 g.cm$^{-3}$ range. Volume change upon drying does not vary significantly when increasing pectin concentration; thus the densities linearly increase with concentration increase. The bulk densities of CR pectins are much lower than those of acid-gelled pectins and closer to the theoretical density values.

The microstructure of calcium reticulated aeropectins as seen by SEM is shown on figures VI.5 and VI.6. Aeropectins are formed of a porous network of entangled "nanofibers", as is the case for aerocellulose. However, in aeropectin case, the pore sizes are lower: while for aerocellulose typical pore sizes are spread out between 10 μm and a few tens of nm, for aeropectins very few pores have a diameter superior to 1 μm, and most of them are from few tens to few hundreds nanometer range. For aeropectins obtained from pectin concentrations lower than 2 %wt, the structure present more "open" spaces, and micrometric pores of 1-5 μm can be seen. Higher pectin concentrations, of 3 and 5 %wt, give denser aerogels with more uniform and smaller pore sizes around 10-500 nm.

**Figure VI.5: SEM images of CR aeropectins with initial pectin concentrations of (a) 1 %wt; (b) 2 %wt and (c) 3 %wt.**

Figure VI.6 shows the structure at the nanometer scale of calcium reticulated (CR) aeropectins, as seen by SEM. Image analysis allow to situate more precisely the diameter of nanofibers in the 10-30 nm range. The small pores were also measured from these high magnification pictures, confirming their diameters to be from a few tens to a few hundreds of nm. Acid-gelled and calcium reticulated aeropectins are very similar in terms of microstructure.
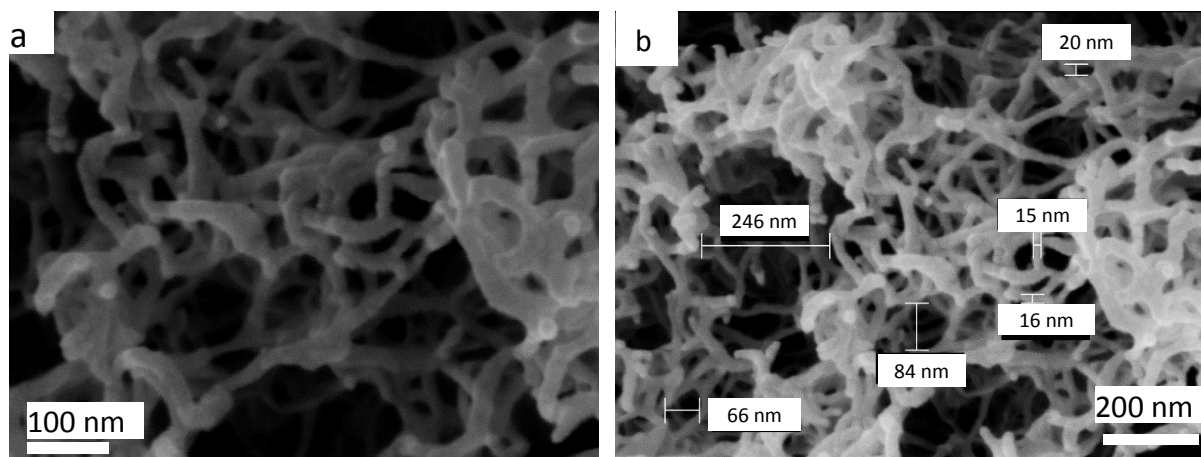


**Figure VI.6: SEM pictures showing the morphology of a CR aeropectin (R = 0.28) from 3 %wt solution at various scales with some examples of pore size and pore wall thickness.**

Theoretical porosities $\varepsilon$ and specific pore volume $V_{th}$ of calcium reticulated aeropectins at different concentrations were determined from sample apparent and skeletal densities with eq. VI.5 and VI.6. The skeletal density $\rho_{skeletal} = 1.57$ g.cm$^{-3}$ $\pm 0.03$ for citrus pectin was determined by helium pycnometry in the L2C laboratory of the university of Montpellier, France (Rudaz, 2013).

$$\varepsilon(\%) = \frac{V_{pores}}{V_{total}} = 1 - \frac{\rho_{bulk}}{\rho_{skeletal}} \qquad (VI.5)$$

$$V_{th} = \frac{1}{\rho_{bulk}} - \frac{1}{\rho_{skeletal}} \qquad (VI.6)$$

The porosities, theoretical specific pore volumes and specific surface area $S_{BET}$ of CR aeropectins obtained by nitrogen adsorption using the BET method are shown in table VI.1. Pore diameter can be estimated as follows, even though nitrogen adsorption only provides very limited information on the aerogels porosity:

$$D_{pore} = \frac{4V_{th}}{S_{BET}} \qquad (VI.7)$$

**Table VI.1: Densities, porosity, theoretical specific pore volume and diameter and specific surface areas of CR aeropectins at different pectin concentrations in solution.**

| Pectin concentration (wt%) | $\rho$ (g/cm³) | $\varepsilon_{th}$ (%) | $V_{th}$ (cm³.g⁻¹) | $D_{pore}$ (nm) | $S_{BET}$ (m².g⁻¹) |
|---|---|---|---|---|---|
| 1% | 0,021 | 99% | 47,0 | 712 | 264 |
| 2% | 0,038 | 98% | 25,7 | 351 | 293 |
| 3% | 0,044 | 97% | 22,1 | 294 | 301 |
| 5% | 0,066 | 96% | 14,5 | 289 | 201 |

The theoretical porosities of CR aeropectins are very high, between 96% and 99%, the direct consequence of their low bulk density. Pore volume $V_{th}$ decreases with the increase of polymer concentration in solution (and density), as expected.

Specific surface areas are close to those of aerocellulose and acid-gelled aeropectins, with $S_{BET}$ values of 200-300 m².g⁻¹. As was previously observed for aerocellulose and acid-gelled pectins, no obvious correlation can be determined between polymer concentration and specific surface area.

## 1.2. Effect of pH on CR aeropectin gelation and bulk density

To investigate the effect of pH on the bulk density of CR aeropectins, the pH of a 2%wt pectin solution was varied from 5 to 13 by addition of a 0.1M KOH solution. Calcium chloride was added (the R value being 0.20 for all samples) and the solution was left to gel at room temperature. The macroscopic appearance of CR aeropectin depending on pH is shown on figure VI.7.



**Figure VI.7: Visual aspect of calcium reticulated aeropectins gelled at different pH.**

Practically no gelation was observed at a pH lower than 7; gels formed at pH 6 and 7 were extremely fragile and the gelation was relatively slow (few hours) for pH < 8. For pH values of 11 and 13, syneresis was observed rapidly after gelation, and the gels contracted more than at lower pH; these high pH gels had a yellowish color, while the other where white. The difference of coloration observed for the wet gels is carried on during sc drying. Gels formed at a lower pH form a more pronounced meniscus during the solvent exchange process, as they are more flexible and easier to deform. Aerogels formed at a higher pH (especially those made at pH 11-13) are the more rigid and harder to break.

Figure VI.8 shows the evolution of bulk density of CR aeropectin samples as a function of solution pH.
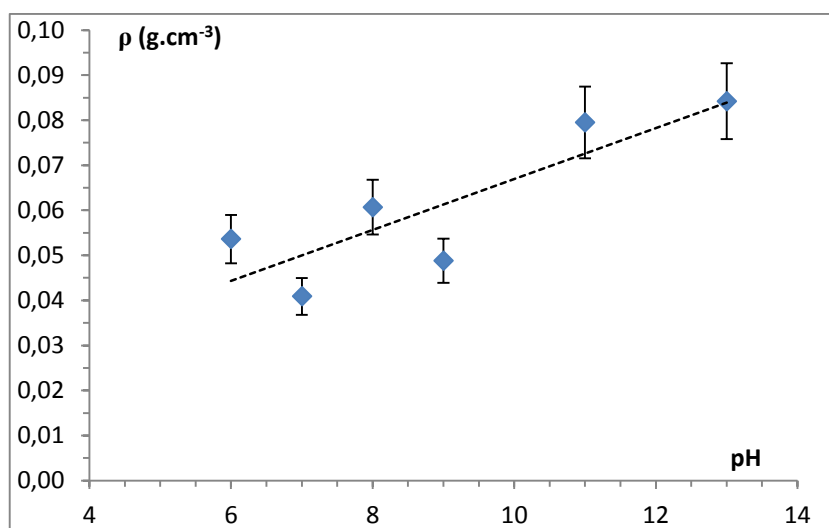
**Figure VI.8: Bulk density variation of CR aeropectins from 2%wt pectin solution as a function of solution pH.**

Aeropectins densities increase with the solution pH. As could be expected from the volume contraction observed on these aerogels, CR aeropectins gelled at pH 11 and 13 have noticeably higher densities at 0.08 g.cm$^{-3}$ because of higher contraction. As the pKa of pectin is 2.9, the vast majority of the carboxyl groups are in deprotonated form and thus able to bind with calcium ions in the pH range studied. However, in highly basic conditions, a saponification reaction can occur between ester functions and the OH$^{-}$ from the KOH solution used to adjust the pH. Partial de-esterification of pectin leads to the formation of new carboxylate ions able to bind with calcium, resulting in faster gelation and the formation of a more rigid gel.

Thus, to obtain low-density samples and cohesive gels, the ideal pH is between 8 and 10. All samples synthesized in the following were gelled at pH 8 to optimize their properties.

### 1.3. Influence of calcium concentration

To evaluate the effect of calcium concentration on aeropectins morphology, the calcium concentration in pectin gels was varied from 10 to 150 mM at pectin concentrations of 1%wt, 2%wt and 3%wt, corresponding to values of R between 0.05 and 0.45. Gels obtained with the highest calcium concentrations were stronger, which is consistent with what is reported in literature about pectin-calcium gels (Fraeye et al., 2006; Capel et al., 2010). The gelation time decreased when increasing the calcium concentration; however, all pectin gels visually had a similar aspect before and after supercritical drying. The evolution of bulk density with calcium to carboxyl group molar ratio R is displayed on figure VI.9.
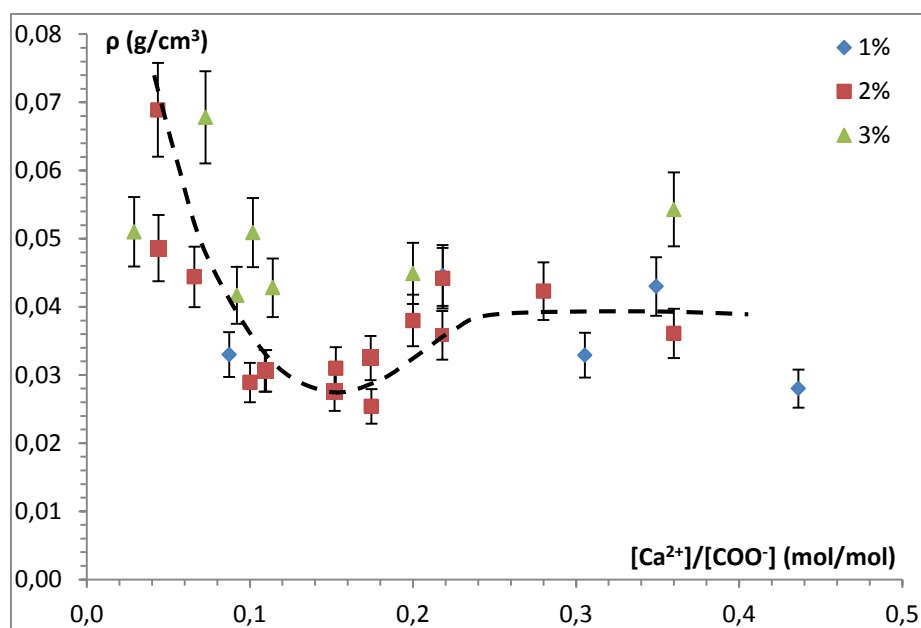
**Figure VI.9 : Bulk density of CR aeropectins of different pectin concentrations as a function of calcium to carboxylate molar ratio. Dotted line shows the general trend of density versus R.**

As expected, bulk density is globally higher for more concentrated samples. At very low R values (R < 0.1), the aeropectins are more dense, in the 0.04-0.07 g.cm$^{-3}$ range. For values of R between 0.1 and 0.2, a local minimal value for density is reached, with densities around 0.03 g.cm$^{-3}$ for 2 wt% aeropectins and 0.04 for 3 wt% aeropectins. Past this point the density slightly increases but the variation with R is less noticeable. It must be kept in mind that given the extremely low densities of calcium reticulated aeropectins, experimental errors are important as illustrated directly on the graph: bulk density variations up to 20% can be observed between samples of the same formulation but from different batches which could smooth in some way the evolution of this curve.

As seen on SEM pictures on figure VI.10, the microstructure of aeropectins is not visibly affected by the amount of calcium added to pectin.
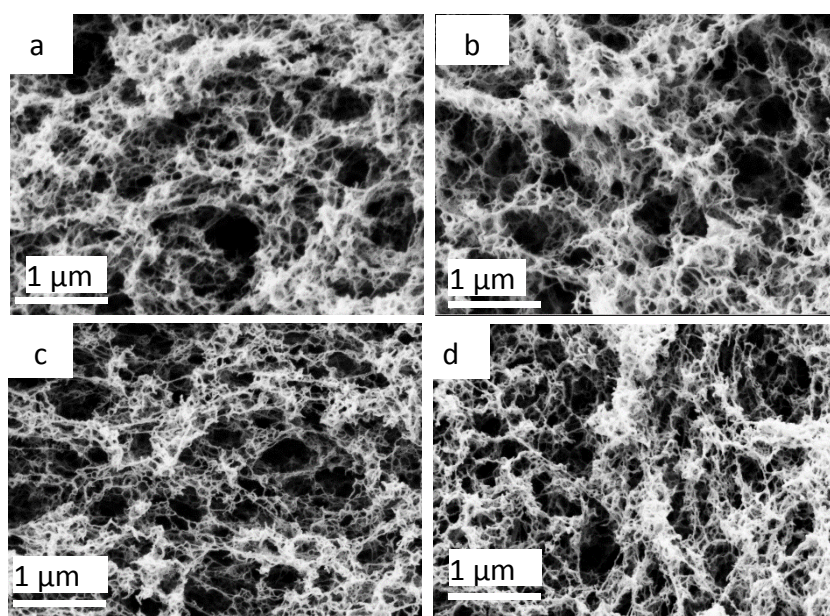


**Figure VI.10: SEM images of the microstructure of CR, 2 wt% aeropectins with a) R = 0.066; b) R = 0.2; c) R = 0.28 and d) R = 0.36**

The theoretical apparent porosities and specific pore volumes have been calculated for a few selected values of R and pectin concentrations. These values are shown along with specific surface areas in table VI.2. The porosity remains very high (97-98%) independently of the amount of calcium added to the pectins. Specific surface areas does not directly correlate with bulk density, as was previously observed; the higher measured values are obtained for R = 0.2 with 293 $m^2.g^{-1}$ for 2 wt% aeropectin and 301 $m^2.g^{-1}$ for 3 wt% aeropectin. These observations being limited to a small number of different formulations, it is difficult to draw significant conclusions on the effect on calcium to carboxyl molar ratio on the porosity and specific surface areas of reticulated aeropectins.

**Table VI.2: Density, porosity, theoretical pore volume and specific surface area of CR pectins at different calcium-carboxyl ratios.**

| Pectin concentration (wt%) | R (mol/mol) | $\rho$ (g/cm$^3$) | $\varepsilon_{th}$ (%) | V $_{th}$ (cm$^3$.g$^{-1}$) | S$_{BET}$ (m$^2$.g$^{-1}$) |
|---|---|---|---|---|---|
| 2% | 0,11 | 0,031 | 98% | 32,04 | 185 |
| | 0,17 | 0,025 | 98% | 38,73 | 203 |
| | 0,20 | 0,038 | 98% | 25,68 | 293 |
| | 0,36 | 0,036 | 98% | 27,14 | 173 |
| 3% | 0,10 | 0,041 | 97% | 23,75 | 241 |
| | 0,2 | 0,044 | 97% | 22,09 | 301 |

## 2. Thermal and mechanical properties of CR aeropectins

### 2.1. Mechanical compression properties of CR aeropectins

The mechanical properties of CR aeropectins were studied by uniaxial compression tests. Samples were cylinders with a height/diameter ratio of 3/2. The detailed procedure is described in materials and methods section. Two series of measurements were performed to evaluate the mechanical properties: Young modulus was evaluated from stress-strain curves at low deformations ($\varepsilon < 10\%$). Varying the strain from up to 90% gave the complete stress-strain curve from which the densification strain and total absorbed energy at densification were determined.

Figure VI.11 shows the stress-strain compression curves of CR aeropectins at two different densities. The stress-train curves of CR aeropectins are comparable to those of cellulose based aerogels (Chapters IV and V) and acid gelled aeropectins: after elastic deformation at low strains, plastic deformation occurs while the pore walls of the aerogel irreversibly bend under the stress; a plasticity plateau is observed, during which the material absorbs energy. Finally, pore walls collapse under strain and cell walls enter in contact with each other: this is the beginning of the densification, characterized by a steep increase in stress as the sample cannot deform anymore (see Chapter II).
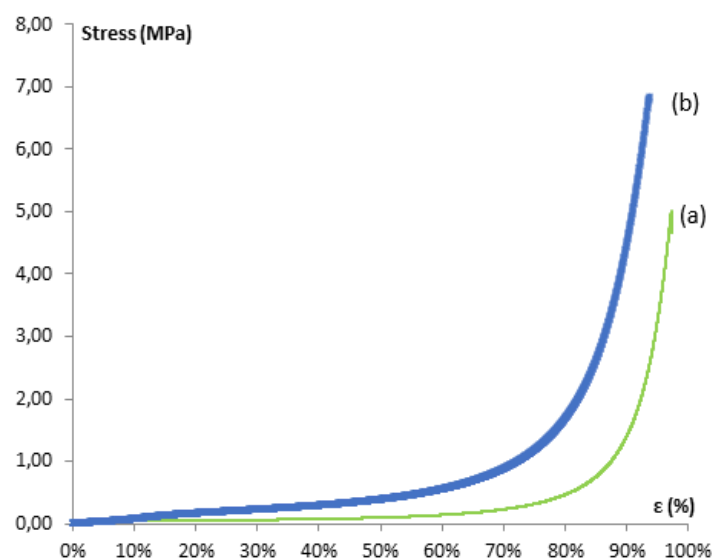
**Figure VI.11 : Stress-strain curves of CR aeropectins with bulk densities of (a) 0.041 g.cm$^{-3}$ and (b) 0.086 g.cm$^{-3}$, R = 0.2, initial pectin concentration in solution 2%wt and 3%wt respectively.**

CR aeropectins are extremely compressible, sustaining deformations up to 90% without breaking. The densification strain is extremely high, being 83% for CR aeropectin with a bulk density of 0.086 g.cm$^{-3}$ and 90% for a CR aeropectin with a density of 0.041 g.cm$^{-3}$. Table VI.3 shows the mechanical properties of CR aeropectins as compared to an acid-gelled sample. The measured values of Young moduli of CR pectin are lower than those of acid gelled aeropectins of comparable densities (0.65 MPa against 4.1 for acid-gelled pectin).

Despite their higher deformation strain, energy absorbed by CR pectin is comparable to that of acid-gelled aeropectins; total absorbed energy at densification increases with sample density.

**Table VI.3 : Mechanical properties of acid gelled (Rudaz, 2013) and CR aeropectins.**

| Pectin formulation | ρ (g.cm-3) | E (MPa) | $\varepsilon_d$ (%) | $W_{\varepsilon d}$ (kJ.m$^{-3}$) |
|---|---|---|---|---|
| 3%wt Acid-gelled | 0.090 | 4.10 | 52% | 217 |
| 2% CR | 0,041 | 0.44 | 90% | 169 |
| 3% CR | 0,086 | 0.65 | 83% | 394 |

We compared Young modulus values of CR aeropectins with those of different aerogels from literature (fig.VI.12). The plot of E against bulk density follows a power law for silica and polysaccharide-based aerogels, according to the models proposed by (Alaoui, 2008, Sescousse et al., 2011, Rudaz, 2014). Because of the very limited number of available samples of CR aeropectins, we cannot reliably derive a value for the scaling exponent for CR aeropectins.
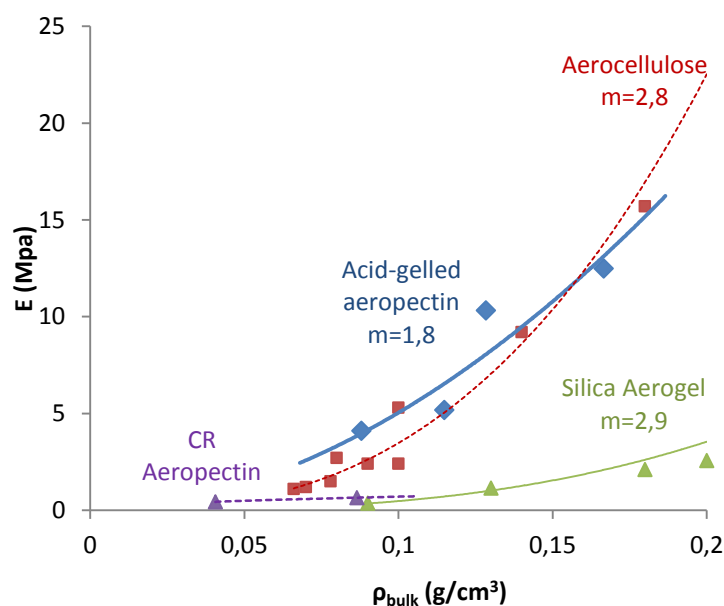
**Figure VI.12 : Comparisons of Young moduli and scaling exponent *m* as a function of bulk density for CR aeropectin; acid-gelled aeropectins (Rudaz, 2013); aerocellulose (data taken from Gavillon, 2007; Sescousse et al., 2011; Sescousse, 2010); and silica aerogel (Alaoui, 2008).**

The calcium-to-carboxylate ratio is known to have an influence on the stiffness of aqueous pectin gels (Capel et al., 2006; Fraeye et al., 2010, Basak and Bandyopadhyay, 2014). We can assume that varying the value of R could have a significant impact on the mechanical properties of supercritically dried CR aeropectins.

## 2.2.   Thermal properties of CR aeropectins

Thermal conductivities of both acid gelled and CR aeropectins were evaluated by Hébert Sallée, CSTB Grenoble, France. A microflowmeter set up was used to allow measuring of small disc-shaped samples with 4 cm diameter. All samples were polished with sand paper before analysis to obtain the even and flat surfaces required for the analysis. The thermal conductivities of CR aeropectin was classically plotted as a function of sample density; figure VI.13 compares their thermal conductivity with that of acid-gelled aeropectins and reference silica aerogels. The thermal conductivity of CR aeropectins was also studied in parallel by hot-wire measurements performed by G. Reichenauer from Bavarian Center for Applied Energy Research, Wurzburg, Germany, within the frame of AEROCOINS, on 2%wt CR aeropectins, for R between 0.11 and 0.22 These results are presented on table VI.4.

**Table VI.4 : Thermal conductivities of CR aeropectins obtained from 2%wt pectin solution, as obtained by hot wire measurements.**

| R | $\rho$ (g.cm$^{-3}$) | $\lambda$ (W.m$^{-1}$.K$^{-1}$) |
|---|---|---|
| **0,11** | 0,031 | 0,0218 |
| **0,15** | 0,031 | 0,0213 |
| **0,17** | 0,025 | 0,0216 |
| **0,22** | 0,044 | 0,0214 |

Samples measured by hot-wire method in Bavarian Center for Applied Energy Research had densities ranging from 0.030 to 0.040 m².g$^{-1}$. It was found that all samples had similar thermal conductivities between 21 and 22 mW.m$^{-1}$.K$^{-1}$. Those values are slightly higher than those obtained in CSTB (see figure VI.13), however, they remain in the super-insulating region. In

the studied range of R, the amount of calcium added to form the gel seems to have a limited effect on the final thermal properties of the material.
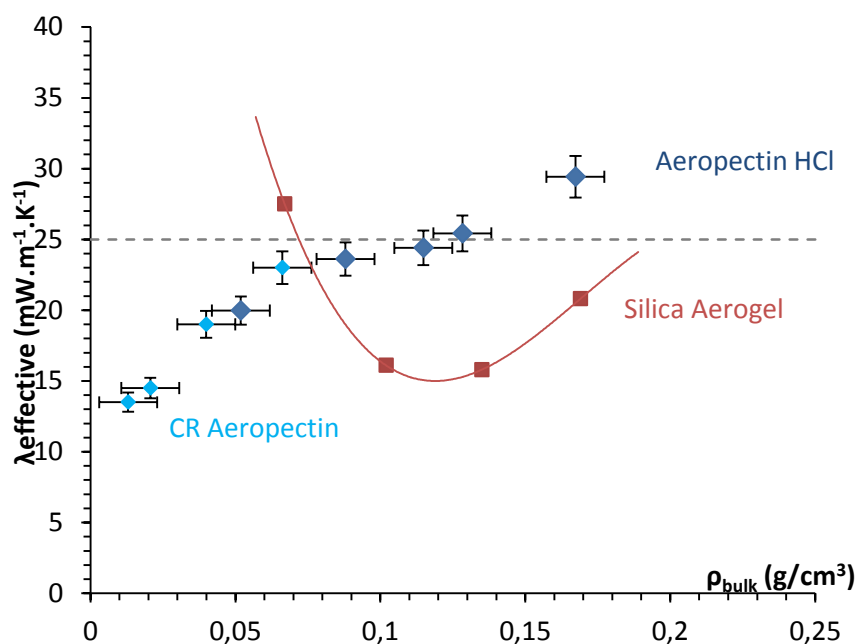


**Figure VI.13: Thermal conductivities, as measured by microflowmetry, of CR aeropectins, compared with those of acid-gelled aeropectins (data taken from Rudaz et al., 2014) and reference silica aerogels (data taken from Bisson et al., 2004).**

The thermal conductivity of pure CR aeropectin is remarkably low, being for all samples lower than 0.025 $W.m^{-1}.K^{-1}$, i.e. in the superinsulating range. The thermal conductivity of CR aeropectins decreases with decreasing aerogel density as measured by microflowmetry. A similar trend was observed for acid gelled aeropectins with the same metrology (Rudaz, 2014). Within the present study, interestingly, the conductivity decrease with the decrease of aerogel density is steady over the density range studied, contrary to the conductivity of reference silica aerogels (Bisson et al., 2004.; Wong et al., 2014) or resorcinol-formaldehyde (Lu et al., 1995) and polyurethane (Diascorn et al., 2015). The latter shows systematically a decrease in conductivity with decreasing density, due to the diminution of solid contribution with density, until a minimum thermal conductivity value is reached at specific densities (generally in the 0.100-0.150 g.cm-3 range). The minimum is followed by an increase of thermal conductivity at extremely low densities. The reason of the increase of thermal conductivity with density decrease at very low density values is the appearance of larger and larger macropores for which Knudsen effect is no longer valid and for which radiative transfer is increasing. Within the frame of the present study, the absence of the minimum on the thermal conductivity-density dependence for aeropectins, obtained for both acid-gelled and Ca-gelled pectins, remains an intriguing question that requires more studies.

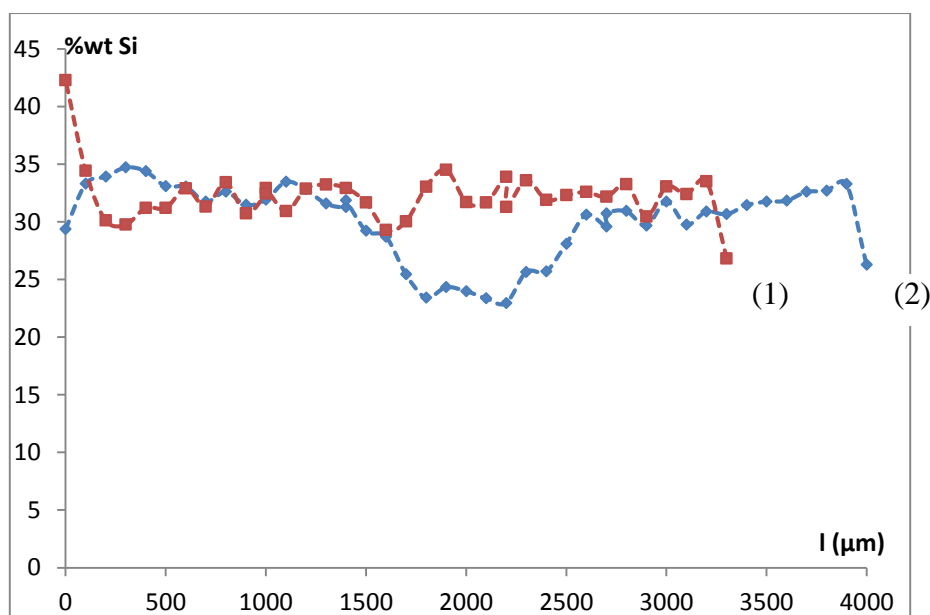## 3. CR aeropectin-silica composites

We showed that using Ca-induced cross-linking of pectin, it is possible to obtain ultra-light weight, ductile and thermal super-insulating aerogels, aeropectin. In order to enlarge the spectrum of porosity, density and specific surface area, we used the approach developed for synthesising organic-inorganic composite aerogels (Chapter IV and V). In the following section

we describe the preparation and properties of pectin-silica aerogels. We also used the known ways of silica hydrophobisation to try to obtain hydrophobic pectin-silica composite aerogels.

### 3.1. Impregnation of pectin matrix with silica

The pectin alcogels were obtained from pectin solutions of concentration between 1-5%, adjusted to a pH of 8, and reticulated with calcium chloride with R = 0.20, as described above. The impregnation of pectin alcogels was performed with 16 wt% PEDS, following the same protocol as for the synthesis of cellulose-silica composites (see chapter IV). Forced-flow (1h processing) and diffusion impregnation (24h immersion in PEDS sol) were tested on a 3 wt% pectin gel, following by 24h immersion in a $NH_4OH$ catalyst solution. It has to be noted that for practical reasons, most of the pectin-silica composite gels studied in the following parts were elaborated using diffusion controlled impregnation, as at lab scale this method allows the preparation of more samples in parallel.

The spatial distribution of the silica in the pectin matrix after sc drying was checked by means of EDS spectroscopy performed on a transversal cut. The wt% in silicium was derived from the intensity of the $K_\alpha$ silicium peak at 1.71 keV. Figure VI.14 shows the silica content as a function of distance from the upper surface for forced-flow and diffusion impregnated samples of 4-5mm thickness.



**Figure VI.14: Distribution of silica (expressed in silicium wt%) in aeropectin-silica composite aerogel from 3 %wt pectin solution, in the case of (1) 1h forced-flow impregnation and (2) 24h diffusion controlled impregnation, measured by EDS spectroscopy on 4-5mm thickness samples.**

The forced flow impregnated sample shows a relatively uniform distribution of silica over the sample cross-section. In the case of diffusion impregnation, the middle part of the sample is less rich in silica, with wt% of Si dropping from ~35%wt to ~20%wt. The impregnation time was 24h, the same as for cellulose samples from chapter IV and V for the sake of comparison. Because pectin gels possess smaller pore size than cellulose ones, the diffusion of PEDS in the pectin matrix is very probably slowed down as compared to cellulose. Longer impregnation times (by at least a few hours) shold be required to uniformly impregnate pectin gels samples by diffusion-controlled impregnation.

Although EDS-X is a surface analysis and thus gives only approximate values, we can see that very similar values of silica content are obtained for both processes. EDS results show that it is possible to obtain, in a similar way to aerocellulose composites, a comparable homogeneous filling of the pectin network with silica aerogel with both forced-flow and diffusion processes.

### 3.2. Morphology and density

Volume contraction upon supercritical drying of aeropectin-silica composites prepared from 3 wt% pectin solution and reference aeropectin are respectively shown in figure VI.15a and VI.15b. Before drying the dimensions of both plates were 9 cm × 9 cm × 1cm; the composite have shrunk by 30% while the pure aeropectin sample shrank by 50%. As noted in part 1.1.2., organic aerogels tend to shrink significantly more than silica aerogels due to higher chain flexibility and lower chemical affinity for supercritical $CO_2$. The addition of the silica phase to the pectin matrix makes it more rigid, limiting the volume contraction of silica-impregnated aeropectin.
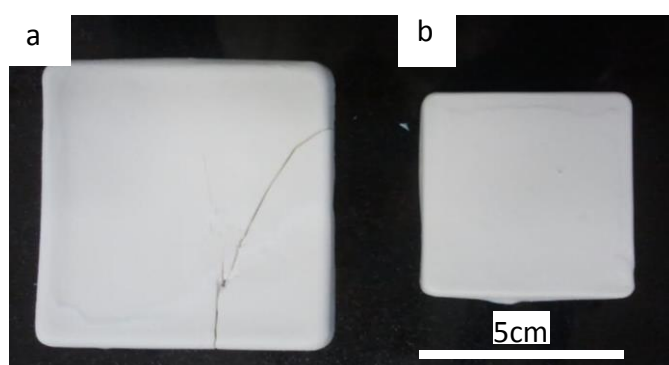


**Figure VI.15: Pictures of (a) silica-impregnated aeropectin (right) and (b) reference aeropectin, both from 3 wt% pectin solution. (NB : Crack on silica-pectin composite aerogel occurred during sample transportation after supercritical drying.)**

The macroscopic aspect of pectin-silica composites for different pectin concentrations is shown on figure VI.16. Aeropectin-silica composites are white, monolithic solids. No powder release can be seen by visual examination. Surface irregularities and small holes are present, as is the case for pure CR aeropectins.
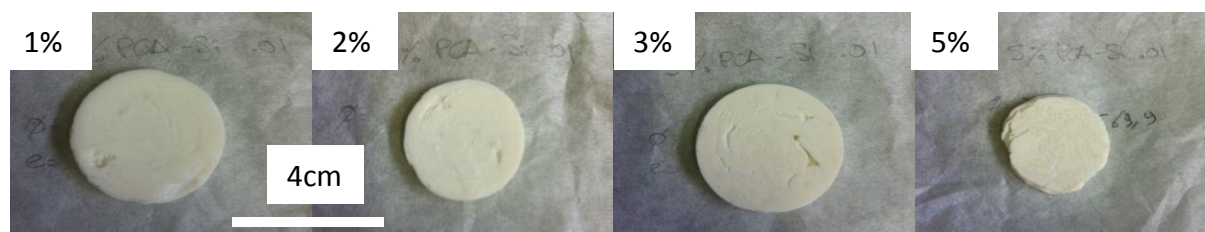


**Figure VI.16: CR aeropectin-silica composites from different initial pectin concentrations in solution.**

The bulk densities of aeropectin-silica composite aerogels is shown along with the densities of aeropectins of the corresponding concentrations on figure VI.17. Pectin-silica composites densities range from 0.114 to 0.156 g.cm$^{-3}$, increasing as pectin concentration increases. Thanks to the extremely low density of the pectin matrix, silica-pectin composites are 1.5 to 2 times lighter than the untreated cellulose-silica composites described in chapter IV. Low densities together with reduction of mean pore size (by impregnation of macroporosity of the organic matrix by silica) are particularly interesting as we are targeting thermal insulation applications.

For pure silica aerogels from PEDS, optimal thermal conductivities are obtained in the 0.100-0.150 $g/cm^3$ density range (Wong et al., 2014).
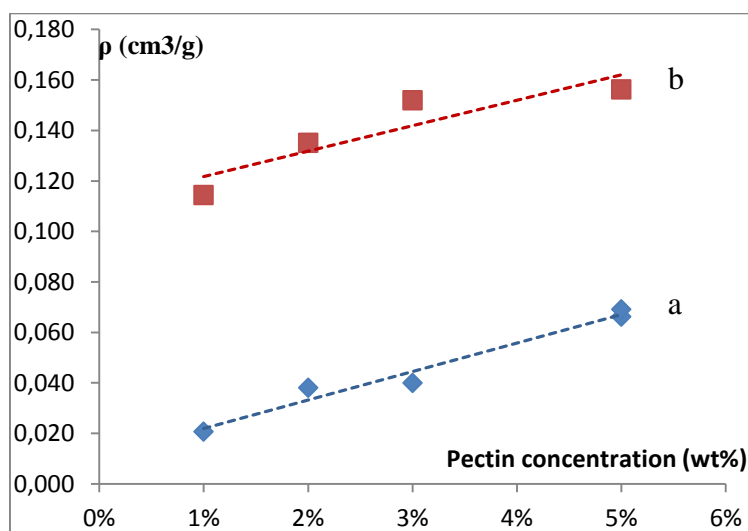


**Figure VI.17: Density of a) CR aeropectins and b) CR pectin-silica composite aerogels for different values of pectin concentration.**

The microstructure of aeropectin-silica composites as observed by SEM is shown on figure VI.18.
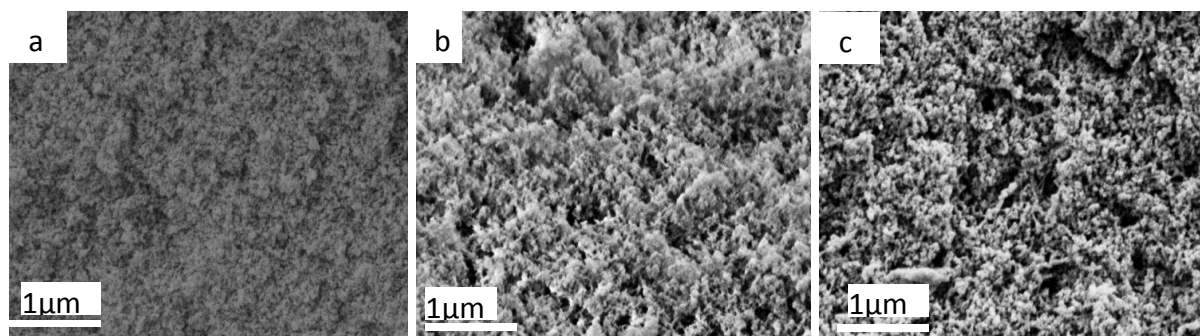


**Figure VI.18: SEM micrograph of the structure of (a) reference silica aerogel from 8%wt PEDS solution; (b) 2%wt and (c) 3%wt diffusion-impregnated CR pectin-silica hybrid aerogels.**

SEM pictures of silica-impregnated CR aeropectins show that the pectin backbone is covered with a finely nanostructured network made of aggregated silica particles. The morphology of silica in the composites (fig. VI.18 b and c) is in good accordance with what is observed on the reference silica aerogel (fig. VI.18 a). Most of the larger pores in aeropectins are filled with silica aerogel. However some macroporosity, only partially filled with silica, can also be seen. SEM observations show that the silica is homogeneously distributed within the composites, consistent with EDS measurements.

Specific surface areas, porosity and theoretical specific pore volume were measured for two formulations of 2%wt aeropectin-silica composites (table VI.4) with different cross-linking ratio. The specific surface area for these samples reaches 845-855 $m^2.g^{-1}$ which confirms the presence of the nanostructured $SiO_2$ aerogel network within the pectin matrix. The composites keep more than 90% porosity. Theoretical pore volume was estimated with the skeletal density taken as 1.57 for pectin and 2.0 for silica (Ayral et al. 1992). $V_{th}$ is of course lowered as compared to pure materials, as silica aerogel fills the pores of aeropectins.

**Table VI.4 : Porosities, theoretical specific pore volume and specific surface areas of 2%wt aeropectin-silica composites.**

| Pectin concentration (wt%) | R (mol/mol) | density (g.cm⁻³) | ε(%) | V$_{pore, th}$ (cm³.g⁻¹) | S$_{BET}$ (m².g⁻¹) |
|---|---|---|---|---|---|
| SiO₂ aerogel | - | 0.130 | 94% | 3.29 | 975 |
| 2% | 0,03 | 0,143 | 91% | 6,36 | 845 |
| | 0,20 | 0,135 | 94% | 9,34 | 855 |

### 3.3. Thermal conductivity of CR pectin-silica composite aerogels

Thermal conductivities of CR aeropectin-silica composites were evaluated by Hébert Sallée, CSTB Grenoble, France. The same procedure as described in section 2.2. was used. The thermal conductivities of CR aeropectin-silica composites was plotted as a function of sample bulk density; figure VI.19 compares their thermal conductivity with that of pure CR aeropectins and reference silica aerogels.
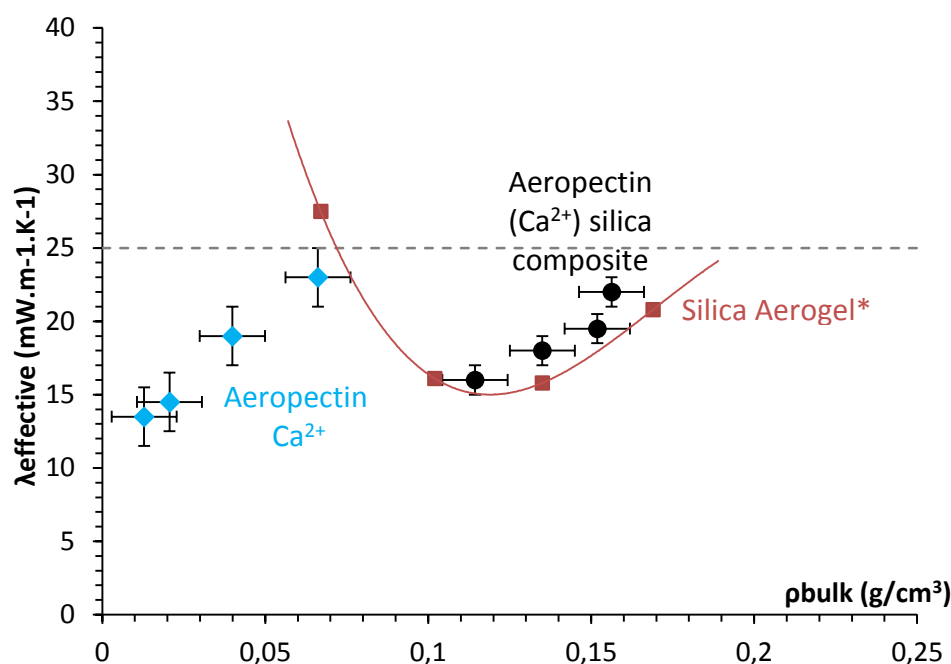


**Figure VI.19: Thermal conductivities, as measured by microflowmetry, plotted as a function of bulk density for CR aeropectins and CR aeropectin-silica composites as compared to silica aerogels (data taken from Bisson et al., 2004). Dotted line at 25 mW.m⁻¹.K⁻¹ corresponds to the thermal conductivity of free air.**

CR aeropectin-silica composites are superinsulating materials with conductivities of 15-23 mW.m⁻¹.K⁻¹. The conductivity values of composites are close to those of reference silica aerogels of corresponding densities albeit slightly higher, probably because the percolating pectin network has an impact on solid contribution to conductivity. However, the thermal conductivity of CR aeropectin-silica composites is not improved as compared to pure CR aeropectins because of the increase in density which leads to an increase in the conductive input coming from the global solid network.

In CR aeropectins, the silica formulation used is the same as the one used for the preparation of cellulose-silica composite by impregnation of a cellulose matrix (see chapters IV and V). As discussed in those chapters, the measured density of the composite aerogels is higher than the theoretical maximal density calculated from the bulk density of each phase. It is known that synthesis conditions strongly influence the structure and final density of silica aerogels. Because the reaction is occurring within the small pores in which the catalyst has to slowly spread through molecular diffusion, the structure and properties of the silica gel formed within the organic matrix may be different as compared to reference silica aerogels. In the case of pectin the acidity of the chain can also affect the sol-gel process. Thus silica aerogel with higher density, and likely of higher thermal conductivity, could be formed within the polymer pores. Silica-pectin composite aerogels conductivities could be improved by adapting the formulation of PEDS sol-gel system to the particular conditions of the synthesis within an impregnated organic matrix.

### 3.4. Hydrophobization of the silica phase of aeropectin-silica composites

As discussed in chapter V, hydrophobization of polysaccharide-silica composites is required for these materials to avoid densification due to humidity adsorption and keep good thermal properties in time. This is particularly crucial as materials used for building insulation are constantly exposed to humidity. A long term development perspective of hydrophobic aeropectins and aeropectin-silica composites would be the development of ambient-dried samples: bypassing the supercritical drying steps would prove extremely interesting for the large scale development of such materials. In this part we first focused on the hydrophobization of the silica phase in aeropectin-silica composites.

Hydrophobization of silica aerogels have been performed using a large variety of methods. In its section concerning the synthesis of hydrophobic silica aerogels, the Aerogels Handbook lists more than 100 chemical agents that can be used for making hydrophobic silica aerogels (Anderson and Caroll, 2011). To hydrophobize the silica phase of aeropectin-silica aerogels, we have tested three hydrophobization agents: Hexamethyldisilazane (HMDZ), Methyltrimethoxysilane (MTMS) and Hexamethyldisiloxane (HMDSO). Coagulated pectin from 3 wt% acid-gelled pectin solution were impregnated with PEDS, followed by gelation of the silica phase in $NH_4OH$. The resulting wet composite was placed in an ethanol solution of the hydrophobization agent during 8h at 65°C. The volume of added solution was equal to that of the gel. The concentration of hydrophobizing agents were calculated relatively to the mass of silica in the sample; they were respectively 36%wt for HMDZ, 32.5%wt for MTMS, and 33.7%wt for HMDSO. The reaction of MTMS and HMDSO with silica was done in the presence of 0.1M hydrochloric acid (HCl). All samples were then dried in supercritical $CO_2$. Ambient pressure drying overnight at 60 °C was attempted in laboratory oven for pectin-silica composites treated with HMDZ, however the samples densified dramatically and cracked upon evaporative drying.

The quantity of each hydrophobization agent, expressed in weight percentage towards the silica phase, is presented on table VI.5, along with composite densities and contact angle with water characterized after drying.

**Table VI.5: Quantities of hydrophobization agents used (expressed in mass percentage relative to silica), bulk densities and water contact angles $\theta_{H2O}$ for hydrophobized silica impregnated 3 wt% acid gelled aeropectins and dried with sc $CO_2$.**

| Hydrophobization agent | Quantity of hydrophobizing reagent (relative to silica) | density (g.cm$^{-3}$) | $\theta_{H2O}$ |
|---|---|---|---|
| Reference aeropectin | - | 0,070 | Drop absorbed |
| Reference aeropectin-silica composite | - | 0.150 | Drop absorbed |
| HMDZ | 36.0% | 0,136 | 135° |
| MTMS | 32.5% | 0,194 | 138° |
| HMDSO | 33.7% | 0,172 | 132° |

Higher bulk densities are obtained for samples treated in MTMS (0.194 g.cm$^{-3}$) and HMDSO (0.172 g.cm$^{-3}$) than for reference composite aerogels (i.e. untreated ones); HMDZ-treated composite sample had a density similar to the reference pectin-silica aerogel. MTMS and HMDSO react with silica in the presence of an acid (here, HCl). The acidic media can influence pectin, partially de-esterifying the pectin chains and disrupting the balance of hydrogen bonds that maintain pectin chains linked together. In this partial degradation scenario, during the hydrophobization treatment the microstructure of coagulated pectin can be modified, possibly leading to a partial densification. This confirm the necessity to follow sylilation routes in a basic environment.

All composite aerogels treated with hydrophobizing agents have contact angles with water superior to 130°, showing their high surface hydrophobicity. The difference in contact angle between the three chemical modification process is low showing that all three procedures were efficient in hydrophobizing the silica phase. On reference aeropectin and aeropectin-silica composites, the water dropled was absorbed by the sample, leaving a hole in its surface (Figure VI.20a) while with hydrophobised samples water drop has high contact angle Figure VI.20b).
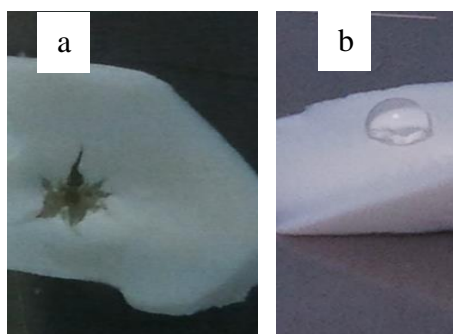


**Figure VI.20: Top (a) and side (b) view of water droplet on the surface of pectin-silica composites aerogels: a) non-hydrophobised and b) HMDSO-treated, both samples coming from 3 wt% pectin solution.**

Water uptake of hydrophobically treated aeropectin-silica composites was measured by letting samples (that were first put in dry conditions 20 °C and 20 %RH) for 48 h at 80%RH and 30 °C. The mass uptake $H_m$ after 48 h was calculated according to eq. VI.8 and is shown VI.21.

$$(VI.8)$$

$$H_m(\%) = \frac{m_{48h} - m_0}{m_0} * 100$$

With $m_{48h}$ the mass of the sample after 48h at 85% humidity and $m_0$ the mass of the sample before the water uptake test.
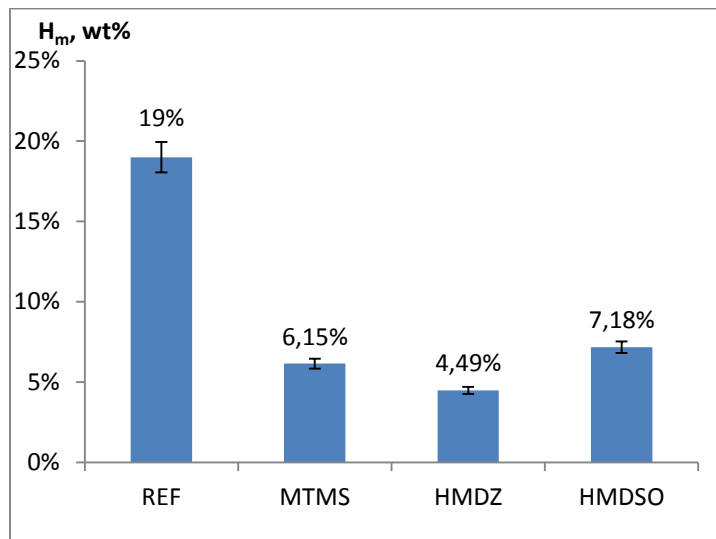


**Figure VI.21: Water vapour uptake $H_m$ at 30 °C and 80 %RH (in wt%) of reference aeropectin and silica-impregnated aeropectin hydrophobized with different silylating agents.**

The reference aeropectin from 3 wt% solution shows 19 wt% humidity uptake in our experimental conditions, accompanied by spectacular volume contraction. The water vapour uptake for hydrophobized composites is 3 to 4 times lower, and their volume contraction is limited. In composite aerogels most of the pectin backbone is covered with layers of nanostructured silica that are hydrophobized by the chemical treatment. The lowest water uptake value is obtained with HMDZ treated sample with $H_m$ being around 4.5 wt%; HMDSO-treated sample has the highest water uptake among partly hydrophobized composites. As seen in chapter V, pure silica aerogel hydrophobized by HMDZ or HMDSO have very low water uptake inferior to 1 wt%. This means that despite the well distributed hydrophobized silica phase in the composites, the hydrophilic pectin backbone remains reachable by water vapour and is probably mostly unaffected by the hydrophobization treatment. The water uptake of pure aeropectins submitted to the same hydrophobization treatments was checked to verify this hypothesis: water uptake of these treated aeropectins are in the 17-25%wt range, confirming that the hydrophilic character of pectins is unaffected by any of the hydrophobization treatment used on the composites.

Pectins are known to be extremely hydrophilic materials (as far as pectin is water-soluble). As a consequence, aeropectins are extremely sensitive to the ambient humidity: like aerocellulose (see chapter V), aeropectins densify during storage in room conditions; this densification is accompanied by a loss of porosity and increase of thermal conductivity. Almost no reports exist in literature about the hydrophobization of pectins; grafting of organic functions giving a certain

hydrophobicity to the pectin chains have been performed by thiolation (Perera et al., 2010) or amidation (Synytsya et al., 2000; Synystya et al., 2004; Zouambi et al., 2009); however the purpose of these studies was generally making of sorbents sensitive to specific organic molecules, and not the preparation of fully water-resistant pectins. Future developpements of aeropectin-silica composites will require an in-depth study of hydrophobization methods for pectin molecules.

## Conclusions

In this chapter the preparation and properties of aeropectin based on calcium-gelled pectin and their composite aerogels with silica were presented and discussed.

A calcium-carboxyl group ratio around 0.11 and a pH of 6-8 resulted in aeropectins with the very low bulk densities ($0.02 - 0.05$ g/cm$^3$). Aeropectin morphology is a porous network made of "nanofibers" with diameters around 10-30 nm. The pore sizes of aeropectins tend to decrease as the material concentration increases; for all calcium-reticulated aeropectins pore with 10-500 nm diameters were observed by SEM.

The morphology of the aeropectin-silica composite aerogels observed by SEM was a fine network of nanostructured pectin fibers covered with silica aerogel. Pectin-silica composite aerogels showed an increase of specific surface area from 200-300 m$^2$.g$^{-1}$ for the pure aeropectins to 800-850 m$^2$.g$^{-1}$ for the composites, confirming the in-situ nanostructuration of the silica phase.

Aeropectins are able to sustain up to 80-90% strain without breaking; their low elastic modulus is consistent with their extremely low bulk densities. More characterization is needed to reliably evaluate the influence of formulation parameters on the final aerogels mechanical properties; silica-pectin composites need to be mechanically characterized as well to see how associated densification impacts mechanics.

In the case of acid gelled and calcium-reticulated aeropectin, we observed by microflowmetry an unexpected linear dependence of the thermal conductivity with density, with values from 0.013 to 0.022 W.m$^{-1}$.K$^{-1}$ for bulk densities in the 0.03-0.10 g.cm$^{-3}$ range. Further studies are necessary to study why the theoretical increase of conductivity at very low densities was not observed experimentally. The conductivity of the pectin-silica composites was in the 0.015-0.022 W.m$^{-1}$.K$^{-1}$ range, slightly higher than that of silica aerogel based on the same formulation of the silica-sol, indicating that the silica formulation should be optimized to further reduce the composite density if necessary.

Finally, the surface hydrophobization of the silica phase of the composites was attempted using three different hydrophobization reagents able to silylate the silica phase. Contact angles with water of 135° and reduced humidity uptake from 19%wt for pure aeropectin to 5-6%wt for composites were obtained. However it appears necessary to hydrophobize also the pectin part to synthesize an hydrophobic composite.

Calcium-reticulated aeropectins are entirely biobased, ultra-light aerogel materials. Their thermal conductivities are the lowest of all polysaccharide-based aerogels known so far. While further characterization of these materials is needed to better understand how optimize their formulation to control their nanostructure and obtain more homogeneous samples, calcium reticulated aeropectins and their composites with silica are extremely promising materials for super-insulating applications.

## References

Anderson, A. M., & Carroll, M. K. (2011). Hydrophobic silica aerogels: Review of synthesis, properties and applications. In *Aerogels Handbook* (pp. 47-77). Springer New York.

Alaoui, A. H., Woignier, T., Scherer, G. W., & Phalippou, J. (2008). Comparison between flexural and uniaxial compression tests to measure the elastic modulus of silica aerogel. *Journal of Non Crystalline Solids*, *354*(40-41), 4556–4561.

Ayral, A., Phalippou, J., & Woignier, T. (1992). Skeletal density of silica aerogels determined by helium pycnometry. *Journal of materials science*, *27*(5), 1166-1170.

Basak, R., & Bandyopadhyay, R. (2014). Formation and rupture of Ca 2+ induced pectin biopolymer gels. *Soft matter*, *10*(37), 7225-7233.

Bisson, A., Rigacci, A., Lecomte, D., & Achard, P. (2004). Effective thermal conductivity of divided silica xerogel beds. *Journal of Non-Crystalline Solids*, *350*, 379–384.

Capel, F., Nicolai, T., Durand, D., Boulenguer, P., & Langendorff, V. (2006). Calcium and acid induced gelation of (amidated) low methoxyl pectin. *Food Hydrocolloids*, *20*(6), 901–907.

Diascorn, N. (2014), PhD thesis, MinesParisTech.

Diascorn, N., Calas S., Sallée, H., Achard,P., Rigacci, A. (2015); Polyurethane aerogels for thermal insulation – textural, thermal and mechanical properties, *The Journal of Supercritical Fluids* (in press) DOI 10.1016/supflu.2015.05.12

Fischer, F., Rigacci, A., Pirard, R., Berthon-Fabry, S., & Achard, P. (2006). Cellulose-based aerogels. *Polymer*, *47*(22), 7636-7645.

Fraeye, I., Colle, I., Vandevenne, E., Duvetter, T., Van Buggenhout, S., Moldenaers, P., Van Loey, A., et al. (2010). Influence of pectin structure on texture of pectin–calcium gels. *Innovative Food Science & Emerging Technologies*, *11*(2), 401–409.

Gavillon, R. (2007). Préparation et caractérisation de matériaux cellulosiques ultra poreux, *PhD thesis*, Ecole des Mines de Paris.

Gibson, L. J., & Ashby, M. F. (1999). *Cellular solids: structure and properties*. Cambridge university press.

Grant, G. T., Morris, E. R., Rees, D. A., Smith, P. J. C., & Thom, D. (1973). Biological interactions between polysaccharides and divalent cations: The egg-box model. *FEBS Letters*, *32*(1), 195–198.

Stephen E. Harding, Gisela Berth, Abigail Ball, John R. Mitchell, Jose Garcia de la Torre (1991), The Molecular Weight Distribution and Conformation of Citrus Pectins in Solution Studied by Hydrodynamics, *Carbohydrate Polymers* 16, 1-15.

Kohn, R., & Kovac, P. (1978). Dissociation constants of D-galacturonic and D-glucuronic acid and their O-methyl derivatives. *Chem. zvesti*, *32*, 478-485.

Lu, X., Caps, R., Fricke, J., Alviso, C. T., & Pekala, R. W. (1995). Correlation between structure and thermal conductivity of organic aerogels. *Journal of Non-Crystalline Solids*, *188*(3), 226–234.

Perera, G., Hombach, J., & Bernkop-Schnürch, A. (2010). Hydrophobic thiolation of pectin with 4-aminothiophenol: synthesis and in vitro characterization. *Aaps Pharmscitech*, *11*(1), 174-180.

Ralet, M. C., Dronnet, V., Buchholt, H. C., & Thibault, J. F. (2001). Enzymatically and chemically de-esterified lime pectins: characterisation, polyelectrolyte behaviour and calcium binding properties. *Carbohydrate Research*, *336*(2), 117-125.

Rudaz, C. PhD thesis, MINES ParisTech 2013.

Rudaz, C., Courson, R., Bonnet, L., Calas-Etienne, S., Salee, H., & Budtova, T. (2014). Aeropectin: fully biomass-based mechanically strong and thermal super-insulating aerogel. *Biomacromolecules,* 15, 2188−2195.

Sescousse, R. (2010). Nouveaux matériaux cellulosiques ultra-poreux et leurs carbones à partir de solvants verts., *PhD thesis,* Mines ParisTech.

Sescousse, R., Gavillon, R., & Budtova, T. (2011). Aerocellulose from cellulose–ionic liquid solutions: Preparation, properties and comparison with cellulose–NaOH and cellulose–NMMO routes. *Carbohydrate Polymers*, *83*(4), 1766–1774.

Synytsya, A., Čopíková, J., Prutyanov, V., Skoblya, S., & Machovič, V. (2000). Amidation of highly methoxylated citrus pectin with primary amines. *Carbohydrate Polymers*, *42*(4), 359-368.

Synytsya, A., Čopíková, J., Marounek, M., Mlčochová, P., Sihelníková, L., Skoblya, S., & Machovič, V. (2004). N-octadecylpectinamide, a hydrophobic sorbent based on modification of highly methoxylated citrus pectin. *Carbohydrate polymers*, *56*(2), 169-179.

Tibbits, C. W., MacDougall, A. J., & Ring, S. G. (1998). Calcium binding and swelling behaviour of a high methoxyl pectin gel.; *Carbohydrate Research*, 310(1), 101-107.

Tilly, G. (2010). Pectines. *Techniques de l'ingénieur* (ref. article : f5000), 0–12.

Wong, J. C., Kaymak, H., Brunner, S., & Koebel, M. M. (2014). Mechanical properties of monolithic silica aerogels made from polyethoxydisiloxanes. *Microporous and mesoporous materials*, *183*, 23-29.

Zouambia, Y., Moulai-Mostefa, N., & Krea, M. (2009). Structural characterization and surface activity of hydrophobically functionalized extracted pectins. *Carbohydrate polymers*, *78*(4), 841-846.

# General Conclusions

The main goal of this thesis was to synthesize and characterize thermal superinsulating and mechanically strong polysaccharide-silica composite aerogels.

In Chapter 3 and 4 we studied two methods to obtain such composites from cellulose gels: i) "one-pot" mixing of cellulose solution in alkaline media with sodium silicate, followed by simultaneous coagulation of each phase in acid media, and ii) impregnation of a wet porous cellulose matrix by a polyethoxydisiloxane (PEDS)-ethanol solution, followed by base-catalyzed sol-gel synthesis of silica within the cellulose porosity. In the case of "one-pot" synthesis, rheological measurements show that the addition of sodium silicate on the cellulose-NaOH system has a strong "destabilizing" effect on cellulose, inducing rapid association of polymer chains which in turn leads to a microphase separation because of the competition for the solvent between silicate and cellulose. Supercritical $CO_2$ drying of the wet "one-pot" gels gave the composite aerogels: a cellulose matrix with dispersed (dense) silica beads.

The materials obtained showed densities between 0.10 and 0.25 $g.cm^{-3}$. Scanning electron microscopy (SEM) revealed the presence of micron-size silica particles, embedded in the pores of Aerocellulose. The specific surface area was lowered, proving that those silica particles are non-porous. Thermal conductivity was increased from 0.035-0.040 $W.m^{-1}.K^{-1}$ for pure Aerocellulose to 0.045-0.050 $W.m^{-1}.K^{-1}$ for the composites, due to the silica particles increasing the solid contribution of the aerogels backbone to the thermal tranfser. Finally, the Young modulus is increased from 20 MPa for pure Aerocellulose to 30-40 MPa for the composites, showing that the silica particles act in parallel as a reinforcing additive for the cellulose matrix.

The morphology and thermal conductivity of freeze-dried "one-pot" samples was also studied. Freeze-dried samples presented low specific surface areas and large pores because the formation of ice crystals during the freezing step. The thermal conductivity of freeze-dried composites is similar to that of supercritically dried samples.

These results showed that "one-pot" cellulose-silica approach is not leading to nanostructuration and thus does not improve the thermal properties of the aerogels obtained.

In the case of impregnation of a wet cellulose matrix, two impregnation methods were tested: simple molecular diffusion, and forcing the penetration of the PEDS solution inside cellulose porosity by a pressure gradient. Thanks to forced-flow process, impregnation times were reduced from ~ 7 hours to less than 30 minutes for a sample with the same geometry. Energy diffractive spectroscopy and SEM analysis were performed to compare silica spatial distribution in both series of samples. The morphology of diffusion impregnated and forced-flow impregnated samples was similar: the cellulose matrix is filled with the nanostructured silica aerogel.

BET analysis confirms the formation of nanostructured silica inside cellulose matrix: specific surface area increases from ≈ 300 $m^2.g^{-1}$ for Aerocellulose to 750-800 $m^2.g^{-1}$ for composite aerogel. The thermal conductivity in room conditions is reduced from 0.033 $W.m^{-1}.K^{-1}$ for aerocellulose to 0.027 $W.m^{-1}.K^{-1}$ ± 0.001 for composite aerogels due to the superinsulating properties of silica aerogel itself, demonstrating that the concept of impregnation works for decreasing the total thermal conductivity of a porous matrix with large macropores. Finally, composite aerogels are strongly reinforced as compared with the reference aerogels still keeping high ductility characteristic to Aerocellulose: Young modulus increases in 3-4 times as

compared to pure silica aerogel, and fracture strain remains very high, about 60% for the composite against 4-10% for the reference silica aerogels.

The impregnation of a porous wet cellulose matrix by PEDS followed by base-catalyzed sol-gel synthesis of silica aerogel within the polysaccharide porosity appeared to be a well suited method to obtain finely structured composite polysaccharide-silica aerogels; this technique was thus used for the preparation of all composites studied in the following parts of the work.

An important requirement for aerogels destined to thermal insulation application is their ability to sustain ambient humidity without losing their thermal and mechanical properties. As cellulose and silica aerogels are hydrophilic, we proceeded to elaborate hydrophobized composite aerogels, synthesizing a chemically modified cellulose (tritylcellulose) as impregnation matrix for PEDS. After impregnation, the silica phase was hydrophobized by silylation in basic conditions.

The resulting aerogels are resistant towards humidity, water mass uptake is reduced from 10%wt for the untreated material to 1-3%wt for "fully" hydrophobised composites, and contact angles with water of 133° are obtained. The obtained organic-inorganic aerogels are finely nanostructured, with high specific surface areas between 600 and 800 $m^2.g^{-1}$. The morphology of the hydrophobized composites was similar to that of aerogels based on non-hydrophobized components. Composite aerogels were stiffer than pure tritylcellulose aerogels with Young moduli ranging around 2-4 MPa vs 0.3 to 1 MPa for tritylcellulose and 1.9 MPa for silica aerogels. Thermally superinsulating composite aerogels were obtained, showing a minimal thermal conductivity of 0.021 $W.m^{-1}.K^{-1}$. This is an important result showing the potential of synthesis of organic-inorganic monolithic and strong aerogels.

The bulk densitiy of xerogels from subcritically dried tritylcellulose and tritylcellulose-silica composites was much higher than that of the corresponding aerogels due to strong volume contraction during evaporative drying. However, the presence of the cellulose phase within the composite allowed the xerogels to remain monolithic after drying, despite the presence of macroscopic cracks. The important densification implies that the xerogels from tritylcellulose are not yet suitable for thermal insulation implications. However, the hydrophobicity of the xerogels was maintained, as assessed by contact angle values of 120°-148°.

In the last chapter we studied an alternative nanostructured polysaccharide matrix for the reinforcement of silica aerogels: aeropectin. Aeropectins were shown in a previous work to have the best thermal insulating properties of the known polysaccharide aerogels. In the sixth chapter we studied aeropectin from calcium-reticulated (CR) pectins and their composites with silica.

A calcium-to-carboxyl group molar ratio around 0.2 and a pH of 6-8 gave the aeropectins with the lowest density. The observed dependence of the thermal conductivity with density was, unusually for porous materials, linear, with values from 0.013 to 0.022 $W.m^{-1}.K^{-1}$ for bulk densities in the 0.03-0.10 $g.cm^{-3}$ range. Moreover aeropectins are able to sustain up to 80% deformation without breaking.

Pectin-silica composites were prepared using the impregnation strategy as developed for cellulose-silica route. The morphology of the composite aerogel observed by SEM was a fine

network of nanostructured pectin fibers filled and covered with silica aerogel. Pectin-silica composite aerogels showed an increase of specific surface area from 200-300 $m^2.g^{-1}$ to 800-850 $m^2.g^{-1}$ for the composites. However, the conductivity of the pectin-silica composites remained in the 0.015-0.022 $W.m^{-1}.K^{-1}$ range as compared to pure aeropectin despite certain increase in bulk density, indicating that further optimization of the silica formulation is required to synthesize the composites. The surface hydrophobization of the silica phase of the composites gave contact angles with water of 135° and reduced the water mass uptake to 5-6%wt as compared to 20%wt for the pure aeropectin studied in the same conditions.

## Prospects and future work

Polysaccharide-silica composite aerogels are promising nanostructured materials for thermal insulation applications. While this work mainly aimed at creating innovative insulation materials for the building industry, superinsulation combined with good mechanical properties and stability against humidity can be extremely useful for other domains, such as food refrigeration appliances or transport industry.

These composite aerogels can be suitable for some other domains, thanks to their high porosity and very high specific surface area: storage of active drug molecules within the porosity and controlled release in the organism is particularly useful for many bio-medical applications.

The hydrophobized aerogels may show increased chemical affinity for organic solvents, allowing them to be used as adsorbents to collect oil spills and help disposing of liquid chemical waste.

The mechanical properties of composite aerogels could be further improved in case of creating chemical bonds between cellulose and silica phase. The same could be said about pure tritylcellulose aerogels, which could be easier to handle in coagulated form and have better mechanical resistance with cross-linking of cellulose chains themselves.

In parallel, pectin-silica composite aerogels should be characterized in more details (particularly in terms of mechanical properties), to better understand the overall properties and potential uses of this new category of composite aerogels. Using pectin with lower degree of esterification might allow a better control of cross-linked aeropectins morphology and bulk density.

Finally an open question which requires more experimental work and also modelling of thermal transfer is the linear dependence of aeropectin thermal conductivity as a function of bulk density.

Of course, the hydrophobization of pectin also has to be studied in depth for these aerogels to become, for instance, efficient insulation materials.

# Synthèse et caractérisation d'aérogels composites à base de polysaccharides et de silice pour la superisolation thermique

**RESUME :** L'amélioration des propriétés des matériaux pour l'isolation thermique est un défi clé pour la réduction de la consommation énergétique et de l'émission de gaz à effets de serre. Cette thèse a pour objectif l'élaboration de matériaux composites nanostructurés, combinant les bonnes propriétés mécaniques des bio-aérogels avec les excellentes propriétés d'isolation thermique des aérogels de silice. Deux polysaccharides ont été étudiés comme source de bio-aérogels : la cellulose et la pectine. Deux stratégies pour l'élaboration des composites ont été considérées : un procédé « one-pot »; et l'imprégnation d'une matrice polysaccharide poreuse. Les aérogels composites ont été obtenus par séchage au $CO_2$ supercritique. Alors que la méthode « one-pot » génère des particules de silice micrométriques au sein d'un réseau poreux, le procédé d'imprégnation a permis d'obtenir un réseau nanostructuré interpénétré. La surface spécifique atteint 700-800 $cm^2.g^{-1}$, les propriétés mécaniques sont améliorées par rapport aux aérogels de silice et la conductivité thermique est réduite comparée à l'Aerocellulose pure. Utiliser une cellulose hydrophobisée chimiquement, la tritylcellulose, comme matrice d'imprégnation, a permis d'obtenir des composites hydrophobes ayant un angle de contact avec l'eau de 133° et des conductivités thermiques de 0.021-0.022 $W.m^{-1}.K^{-1}$. Les aérogels à base de pectine réticulée et leurs composites avec la silice présentent des densités extrêmement basses (0.05 $g.cm^3$) et des conductivités thermiques de 0.013-0.022 $W.m^{-1}.K^{-1}$.

**Mots clés :** Aerogels, cellulose, pectine, bio-aerogels, aerogels de silice, composites, materiaux nanostructurés, superisolation thermique.

## Synthesis and characterization of polysaccharide-silica composite aerogels for thermal superinsulation

**ABSTRACT :** Improving the thermal insulation of materials is a key challenge to lower global energy consumption and greenhouse effect gas emissions in the coming decades. This thesis focuses on the preparation and characterization of nanostructured composite materials combining the good mechanical properties of bio-aerogels with the excellent thermal insulation properties of silica aerogels. Two polysaccharides were used to make bio-aerogels: cellulose and pectin. Two strategies aiming to elaborate composite materials were investigated: "one-pot" process and impregnation of a porous "wet" polysaccharide matrix by polyethoxydisiloxane. Drying with supercritical $CO_2$ yields the composite aerogels. While the one-pot method gave micron-sized silica particles embedded in a porous cellulose network, impregnation process allowed obtaining a nanostructured interpenetrated network of cellulose and silica. The specific surface area was 700-800 $cm^2.g^{-1}$, the mechanical properties improved as compared to neat silica aerogels and thermal conductivity lower than that of cellulose aerogels. Using a chemically hydrophobized cellulose, tritylcellulose, as the impregnation matrix, hydrophobic composites were obtained showing a contact angle with water of 133° and thermal conductivities of 0.021 $W.m^{-1}.K^{-1}$. Aerogels from cross-linked pectin and their composites with silica show extremely low densities (around 0.05 $g/cm^3$ for the neat pectin aerogels) and thermal conductivities in the 0.013-0.022 $W.m^{-1}.K^{-1}$ range.

**Keywords** : Aerogels, cellulose, pectin, bio-aerogels, silica aerogels, composites, nanostructured materials, thermal superinsulation.

MINES
ParisTech

ParisTech
INSTITUT DES SCIENCES ET TECHNOLOGIES
PARIS INSTITUTE OF TECHNOLOGY